COMPARING FAILURE MECHANISMS OF ULTRA-THIN CONTINUOUSLY REINFORCED CONCRETE PAVEMENTS (UTCRCP) UNDER CYCLIC AND MONOTONIC LOADING

LOUIS GELDENHUYS

A dissertation submitted in partial fulfilment of the requirements for the degree of

MASTER OF ENGINEERING (GEOTECHNICAL ENGINEERING)

in the

FACULTY OF ENGINEERING, BUILT-ENVIRONMENT AND INFORMATION TECHNOLOGY

University of Pretoria

APRIL 2018

ABSTRACT

Comparing failure mechanisms under cyclic and monotonic loading of Ultra-Thin Continuously Reinforced Concrete Pavements (UTCRCP)

by

Louis Wimpie Geldenhuys

Conventional concrete road pavements are widely used and their behaviour is reasonably well understood and readily predictable, generally by means of semi-empirical design methods. An alternative pavement type, referred to as Ultra-Thin Contentiously Reinforced Concrete Pavement (UTCRCP), comprises a conventional concrete pavement substructure with a 50 mm thick high-strength concrete overlay, heavily reinforced with steel mesh and fibres. In contrast to conventional road concrete road pavements, the thin and heavily reinforced overlay behaves in a flexible manner. Several uncertainties remain regarding this system's behaviour and analysis in the context of pavement design and scope exists for the improvement of design methods of UTCRCP. These uncertainties include (but are not limited to) the bond and possible debonding between the concrete overlay and the material below, the build-up of pore pressure within the soil during cyclic loading and the behaviour of the structure after a load higher than the assumed design load has been applied. Improvements can be affected when behavioural data from such pavements is available, but relevant data from the literature is limited.

UTCRCP have recently been studied at the University of Pretoria using 1:10 scale physical models. Data from such studies have the potential to contribute to UTCRCP design methods. However, the amount of data currently available from these studies are limited and a need for further work exists. To add to the data base of UTCRCP behaviour in models, experiments were conducted in which 1:10 scale UTCRC pavement models were tested under cyclic and monotonic loading. Two parallel strip loads were used to represent the wheel loads of a single axle,

modelling pavement behaviour idealised to plane-strain conditions. Tests were carried out using UTCRCP model pavements with layerworks constructed from a fine silica sand and a graded gravel respectively. Experiments were conducted at optimum moisture content and under saturated conditions. The fine silica sand was used for the observation of typical failure mechanisms while the gravel was used as a more realistic road pavement material. The settlement under load application at the surface of the pavement was monitored with an LVDT and Digital Image Correlation was used to track deformation fields within the pavement surface during testing.

Monotonic load tests were first carried out to determine upper bounds of the failure loads for each pavement model type. Thereafter, various percentages of the upper bound loads were applied to the road pavements under cyclic loading until excessive deformation had occurred or until deformation had stabilised. Deformation mechanisms from the monotonic and cyclic load tests were then compared at several settlement magnitudes. ("Settlement" refers to the settlement of the strip load bogey and can be also be viewed as the depth of imposed rutting.) This was done to determine whether a load applied monotonically to cause a certain amount of settlement (rutting), would result in a deformation mechanism in the road layers that would be similar to that from cyclic loading, given the same amount of settlement (rutting).

It was found that settlements remained small until a certain number of load cycles had been imposed. The settlement trend was found to be linear when plotted against the logarithm of the number of load cycles, matching the way in which creep movement proceeds. However, once a certain number of load cycles had been imposed, the settlement trend accelerated. The number of load cycles at which the settlement accelerated was strongly dependent on the applied load magnitude. This behaviour is typical of the deterioration of a road pavement which demonstrates that the models have value in simulating actual road behaviour and that they are therefore suitable to be used to study elements of pavement behaviour.

When the deformation mechanisms were compared between cyclic and monotonic tests at the same settlement values, it was found that the mechanisms were different. Although slip mechanisms developed for both monotonic and cyclic loading at higher load magnitudes, the strain distribution resulting from cyclic loading was found to be more gradual and generally extended wider and deeper than the failure zone which resulted from a monotonically applied load. Under monotonically applied load, failure generally occurred along well-defined shear surfaces with little straining of the materials contained within the shear bands. This could be due to particle reorientation happening within each load cycle as load is relaxed, causing the slip plane to be disrupted during cyclic loading. Slip planes were constantly changing, resulting in slip bands over a wider and often deeper extent in the cyclic tests. An exception to this were the tests conducted on the fine silica sand under saturated conditions. Due to the more incompressible nature of the

saturated material, the slip mechanisms in the monotonic and cyclic tests were similar in shape and size. The model studies suggest that monotonic testing (i.e. an accelerated test) can replace cyclic testing in pavements that are fully saturated, but such accelerated testing is not suitable when considering pavements under normal partially saturated conditions. It must be noted that most road pavements are unsaturated and therefore need to be tested under cyclic loading if realistic behaviour is to be expected.

DECLARATION

I, the undersigned hereby declare that:

I understand what plagiarism is and I am aware of the University's policy in this regard;

The work contained in this project report is my own original work;

I did not refer to work of current or previous students, lecture notes, handbooks or any other study material without proper referencing;

I have not allowed anyone to copy any part of my project report;

I have not previously in its entirety or in part submitted this project report at any university for a degree.

Louis Geldenhuys

11308886

24 APRIL 2018

ACKNOWLEDGEMENTS

TABLE OF CONTENTS

LIST OF TABLES

LIST OF FIGURES

1 INTRODUCTION

1.1 BACKGROUND

Pavement engineering and the field of soil mechanics have both developed separately over many years (Brown, 1996). This has resulted in separate testing procedures and analysis tools being applied in the two fields.

The behaviour of conventional concrete pavements is reasonably well understood. Ultra-Thin Contentiously Reinforced Concrete Pavement (UTCRCP) is an alternative pavement type that comprises a conventional concrete pavement substructure with a 50 mm thick high-strength concrete overlay, heavily reinforced with steel mesh and fibres. In contrast to conventional road concrete road pavements, the thin and heavily reinforced overlay behaves in a flexible manner. Several uncertainties remain regarding this system's behaviour and analysis in the context of pavement design and scope exists for the improvement of design methods of UTCRCP. These uncertainties include (but are not limited to) the bond and possible debonding between the concrete overlay and the material below, the build-up of pore pressure within the soil during cyclic loading and the behaviour of the structure after a load higher than the assumed design load has been applied. Improvements can be affected when behavioural data from such pavements is available, but relevant data from the literature is limited.

UTCRCP have recently been studied at the University of Pretoria with the purpose of defining improved analysis methods. To fully understand the behaviour of the pavement models, deformations, strains and stresses need to be determined and interpreted. Physical modelling is the primary research tool being employed and this allows deformations and strains to be observed. It has been found that instrumentation used to measure stresses during these experiments interfere with the model behaviour. Stresses can be determined from numerical models in which the appropriate material models are applied. This is very complex for a moving wheel load and would have to be determined in stages.

The current UTCRCP research program at the University of Pretoria proposes the following stages:

1. Physical modelling of cyclic loading on UTCRCP using plane strain strip load tests are to be conducted on various UTCRCP models.

2. The results from the plane strain modelling are to be replicated using numerical modelling in which the appropriate soil models are used.

3. Numerical modelling will then have to be done for UTCRCP in which radial symmetry is maintained for the load application. This would be to replicate the

existing data from physical modelling experiments in which a stationary wheel load was applied cyclically to a scaled UTCRCP model.

4. Physical and numerical modelling for moving wheel loads will then have to be conducted, with the numerical models calibrated to match the results of the physical models.

This research program will allow the behaviour of UTCRCP to be replicated for real roads and will provide information to improve design methods. The research in this study was conducted to accomplish the first stage of the research program in which physical models of cyclic loads in plane strain are done on UTCRCP.

1.2　OBJECTIVES OF THE STUDY

The purpose of this study was to determine whether, and to what extent, plane-strain monotonic loading of a road pavement could be used as an accelerated test method of imposing the damage accumulation that would result under numerous cyclic load applications in model pavements. This was done for Ultra-Thin Continuously Reinforced Concrete Pavements (UTCRCP) road layerworks of two material types and at two degrees of saturation each.

It is hypothesised that an accelerated test, involving only monotonic loading, can be used to replicate the behaviour of UTCRCP for a predetermined degree of rutting.

The following were specific objectives:

1. To observe failure mechanisms of UTCRCP model road pavements under monotonically increasing strip loads at different degrees of saturation of the base materials.

2. To observe failure mechanisms of UTCRCP model road pavements under cyclically applied strip loads of various magnitudes at different degrees of saturation of the base materials.

3. To compare the mechanisms associated with monotonic and cyclic load at the same displacement values to assess their similarity at different degrees of saturation of the base materials. If the mechanisms were found to be similar, it implies that monotonically increasing strip loads can be applied to cause a certain amount of damage, providing a means of accelerated testing of model pavements, thereby proving the hypothesis.

1.3   SCOPE OF THE STUDY

This study investigated the behaviour of model UTCRC pavements under monotonic and cyclic loading using physical models. The model scale was 1:10, and all tests were conducted at normal gravity. The tests were carried out at normal gravity because of the limitations that currently exist for testing at a high cyclic load frequency in the centrifuge. Since in situ road stresses are comparatively low (when compared to stresses imposed during compaction and the stresses due to loading), testing the scaled down model at normal gravity could be expected to result in similar pavement structure behaviour when compared to testing at accelerated gravity. The scaling effect on the effective stress in the soil was therefore not mitigated.

The application of a wheel load was simulated using two strip loads imposed using a loading bogey (modelling a plane-strain situation). Plane-strain strip loads impose a greater stress influence zone than typical wheel loads, which can, for practical purposes, be viewed as point loads. Their use is therefore conservative. However, the cyclic loads applied along a strip do not result in the principal stress rotation as caused by a moving wheel load. It is reported in the literature that repeated principal stress rotation results in more intense straining than simple cyclic load application and the use of the latter is therefore not necessarily conservative. This is a limitation of this study.

A sinusoidal cyclic load was applied during the study. No consideration was made to investigate the influence of rest and load times or to calibrate the loading pattern to realistic traffic loading.

Base layers of two soil types were tested. One was fine silica sand with well-known properties that is often used in centrifuge testing at the University of Pretoria. The other was a scaled-down graded gravel.

Aspects of behaviour considered in the model study included the load settlement response vs number of load cycles for a range of load intensities, the stiffness response vs the number of cycles, as well as the displacement mechanisms that developed during monotonic and cyclic loading. This behaviour was observed for the two material types at different degrees of saturation. Of particular interest was the associated failure mechanisms.

1.4   METHODOLOGY

The following process was followed to complete this study:

- A literature review was conducted. The history of pavement engineering was summarised. The design assumptions and analysis tools typically used in pavement engineering were investigated. Relevant concepts of unsaturated soil mechanics were introduced. The cyclic loading of soils and pavements under both saturated and unsaturated conditions was then reported on. The literature study ended with a discussion on the design and analysis of UTCRCP and experiments that have already been conducted on this pavement type.

- Experiments on scaled-down UTCRCP models were done. This involved determining the soil properties, pre-casting and preliminary testing of the concrete slabs, construction of the model pavement structures as described in the scope above and then testing the pavement. Settlement data were obtained from LVDTs and images taken during the tests were processed to acquire strain data using Digital Image Correlation. The following loading regimes were applied:

  o Monotonic loads, under displacement control, applied to UTCRCP with layerworks constructed of:

    ▪ Silica sand at optimum moisture content

    ▪ Silica sand at saturated moisture content

    ▪ Graded gravel at optimum moisture content

    ▪ Graded gravel at saturated moisture content

  o Cyclic load of 20 kN applied to UTCRCP with layerworks constructed of graded gravel at optimum moisture content

  o Cyclic load of 14 kN applied to:

    ▪ Silica sand at optimum moisture content

    ▪ Silica sand at saturated moisture content

    ▪ Graded gravel at optimum moisture content

  o Cyclic load of 10 kN applied to:

    ▪ Silica sand at optimum moisture content

    ▪ Silica sand at saturated moisture content

    ▪ Graded gravel at optimum moisture content

    o Cyclic load of 3 kN applied to:

      ▪ Silica sand at optimum moisture content

      ▪ Silica sand at saturated moisture content

      ▪ Graded gravel at optimum moisture content

- The results from the experiments were processed and analysed. Conclusions were drawn according to the objectives of the study.

1.5 ORGANISATION OF THE REPORT

The report consists of the following chapters and appendices:

- The introduction to the report is given in Chapter 1.

- In Chapter 2 a review is given of literature that is applicable to the study.

- Chapter 3 describes the experimental methodology that was followed. The model setup, equipment used, as well as the test parameters are given in this chapter.

- The results of the experiments and the analysis thereof are given in Chapter 4.

- Chapter 5 contains the conclusions and recommendations based on the findings of this study.

- The list of references is given at the end of the report.

2 LITERATURE STUDY

2.1 INTRODUCTION

In this chapter a study of literature related to ultra-thin continuously reinforced concrete pavement (UTCRCP) is done. It also includes some of the pioneering work done on UTCRCP by pavement engineers as well as geotechnical engineers.

Firstly, a broad introduction to pavement engineering is given as UTCRCP is ultimately a pavement type. The pavement is described in its structural form. A brief history and the development of pavements is given. Developments in the analysis of pavements are summarised.

Next, the concept of UTCRCP is introduced. The merits and implications of the use of this type of pavement are given. The various components of UTCRCP are described. The first is the ultra-high strength concrete that is used in the pavement. Work that has already been done on the testing of this concrete is summarised. The scaling down of this concrete for small scale tests is mentioned discussed. The current design practice for UTCRCP is given, together with research that indicates the shortcomings of the methods currently used. This section is concluded with a summary of research done on UTCRCP, including full-scale tests and centrifuge tests.

As a road pavement can essentially be viewed as a geotechnical structures it is important that the advances made in the field of knowledge in soil mechanics be applied to pavement engineering (Brown, 1996). It is therefore important to link the two fields (soil mechanics and pavement engineering). An overview of the ways in which soil mechanics has been applied successfully to the field of pavement design and evaluation is mentioned. The overriding theme of unsaturated soil mechanics, a fundamental part of geotechnical engineering, is discussed with regard to its part in the performance of a road pavement. The concept of cyclic loading, particularly of soils, is introduced and expounded on. The general theory of repetitive loading is also discussed in terms of road pavements. The influence of principal stress rotation on soils is discussed together with its implications for tests done on road pavement materials.

2.2 PAVEMENT ENGINEERING

According to the conventional definition of pavements, the function of a pavement is to provide a safe, economic and comfortable ride for vehicles (Ioannides, 2006). Brown (1996) also defines pavements as civil engineering structures that provide a surface for vehicles to operate safely and economically. It is more useful to define and analyse a pavement as an

engineering system in which all the components play a role in its performance and longevity. To analyse and design a pavement, it is important to consider the following components (Ioannides, 1991):

- The natural in-situ soil layers (including the subgrade)

- The constructed layerworks (selected layer, subgrade, base layer and surfacing)

- The geometry of the applied loads

2.2.1 The history of pavement engineering

The pioneer in modern pavement engineering would be Westergaard. Many of the developments in pavement engineering, particularly concrete pavements, can be attributed to his work in the 1920s (Ioannides, 2006). His work focused predominantly on concrete pavements. He evaluated the pavement structure as a rigid plate supported by springs. His findings were influenced by the work of Arthur Newell Talbot, who analysed railways as a beam on a Winkler medium. The work of Burmister (1895-1981) influenced research in asphalt-surfaced pavements. Later, road tests were done because of the frustration of pavement engineers at the slow rate at which mechanistic design was developing and the lack of practical advice stemming from it (Ioannides, 2006). This resulted in a greater focus on empirical derivations from full scale tests rather than a mechanistic approach to design that would incorporate soil mechanics and failure mechanisms. Later, it was Westergaard (1926) who suggested that the stiffness values for pavements on grade be back calculated from existing trial sections, until it was realised that the assumption of an elastic solid foundation is unsuitable (Ioannides, 1991).

2.2.2 Analysis and design of pavements

2.2.2.1 Empirical methods

The analysis and design of road pavements has mostly been empirical (Brown, 1996). More focus has been on the response and behaviour of pavements, rather than the geometry of the applied loads (Ioannides, 2006).

One such empirical design method is the use and application of the California Bearing Ratio (CBR). Although the CBR method for pavement design was phased out in California, it was widely adopted elsewhere. It is regarded as a shear test (Turnbull, 1950) that indicates the layer thickness required to resist shear. The CBR method was also adopted in the UK and remains the recommended method for characterising pavement materials (Brown, 1996).

Powell et al. (1984) reported that the stiffness (Young's Modulus) of the subgrade (in MPa) can be estimated from the CBR using the following empirical relationship

$$E = 17.6CBR^{0.64}$$

Analysis of data from studies using finite elements showed that materials with very different stress-strain relationships could still have the same CBR value (Hight & Stevens, 1982). It was also noted that in the CBR test there is no control over drainage, and that the effective stress state within the sample remained unknown. The horizontal stresses developed in compacted samples greatly influence the CBR value for unsaturated soils. The CBR value can therefore not be simply related to the stiffness of the soil (Nutt, 1982).

2.2.2.2 Elasticity theory

The theory of elasticity has frequently been used in the analysis of road pavements. Burmister (1943) is credited with the development of the early equations for the application of elasticity theory to the layered pavement structure. Early computer programs that were developed for pavement analysis assumed linear elastic values for stress, strain and deflection in the pavement layers. These did not account for the transient wheel loads in real pavements. It had, however, already been shown that the stress-strain relationship in soils was non-linear. Figure 2-1 shows the results from dynamic plate load tests on soil that clearly illustrate the non-linear behaviour of soil (Brown & Bush, 1972).
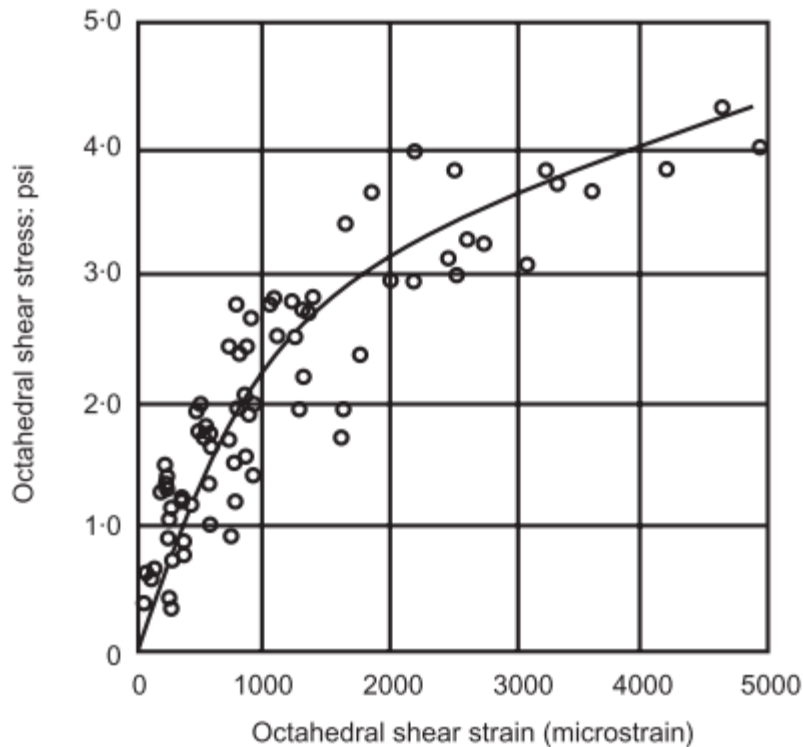
Figure 2-1: The non-linear stress-strain relationship for soils (after Brown & Bush, 1972)

The application of linear elastic theory is only justified for monotonic loading of a soil below its shear strength or for pavements with thick concrete or bituminous layers (Brown, 1996). In this case, the pavement will respond in a resilient manner and the irrecoverable strains will be much smaller than the resilient strains. For non-surfaced or thinly surfaced pavements, non-linear behaviour has to be taken into account. This is because the response of thinly-surfaced pavements, unlike pavements with thick surfacing, is dominated by the resilient properties of the soil in the layerworks.

2.2.2.3 Experimental work

Numerous full-scale experiments have been conducted on pavements. Unfortunately, most of them have not had much instrumentation and yet the data from these experiments are still been used for the empirical design methods in pavements at the end of the 20th century (Brown, 1996). Such experiments, in which only superficial measurements are made, lead to what is referred to as the "black box" approach (Werkmeister et al., 2004). This refers to when empirical relationships are formed that may be reasonably accurate in predicting deformation behaviour of pavements, but are restricted to the materials and test conditions under which the experiments were conducted. These methods have been adopted due to a lack of understanding of the exact mechanisms and micromechanical behaviour at play within

pavements over numerous loading cycles over the pavement's lifetime. This in turn is partly a result of difficulty of instrumenting and monitoring a pavement in sufficient detail over many its lifetime.

Accelerated loading of full scale pavements is one way in which pavements can be tested to examine the long-term behaviour of pavements. The Heavy Vehicle Simulator (HVS) is one example of accelerated pavement testing. This device can apply increased wheel loads to an existing pavement or a trial section over a period of weeks and thus simulate the traffic loads on a pavement that is equivalent to a number of years. In this way, the test accelerates the loading and subsequent damage accumulation of the pavement, hence the name. Data from an HVS programme (Walker, 1985) formed the basis of the South African pavement design (Brown, 1996). Deformation and failure mechanism could be monitored by instrumentation and trenching. The data obtained was used in theoretical models to design pavements.

2.2.2.4 The Resilient Modulus

The resilient modulus (M_R) was initially recommended in the AASHTO (1986) pavement design guide and is a key property in the mechanistic design of pavements (Han & Vanapalli, 2016). According to Seed et al. (1962), this modulus, can be related to the stiffness of a soil under repetitive loading, and is described in the following equation:

$$M_R = \frac{\sigma_d}{\varepsilon_r}$$

Where:

σ_d is the cyclic deviator stress

ε_r is the resilient strain for a particular cycle

This relationship is illustrated in Figure 2-2.
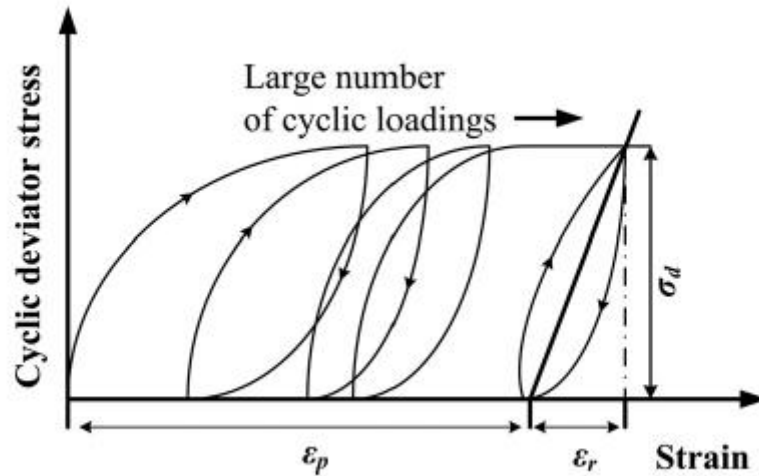
Figure 2-2: Illustration of applied stress and associated strains during cyclic loading of a soil (Han and Vanapalli, 2016)

2.2.2.5 Mechanisms

According to Han and Vanapalli (2016), two criteria are used in the design of the pavement layers. The first is the fatigue cracking that occurs at the bottom of the surfacing. The second is the cumulative permanent deformation of the subgrade soils which is measured at the surface of the soil. These two criteria are illustrated for a typical asphalt pavement in Figure 2-3. The fatigue cracking is related to the resilient response of the pavement subjected to numerous cycles of traffic loading (Seed et al., 1962).
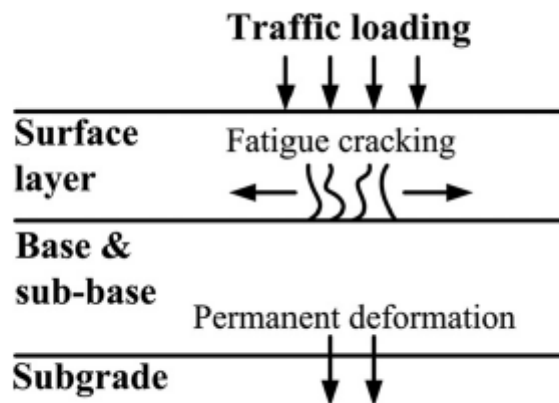
Figure 2-3: Fatigue cracking and permanent deformation illustrated for a typical asphalt pavement structure (Han and Vanapalli, 2016)

Failure mechanisms in pavements are dependent on the pavement structure and the type of loading. In terms of structure, the thickness of the surfacing plays a role in the failure mechanism that will occur.

One such mechanism is cracking on the surfacing. This is due to pavement fatigue (Brown, 1996). A study done by Hveem (1955) found that, for thin bituminous layers, tensile cracks due to repeated loading occurred outside of the wheel path. The stiffness contribution of thin flexible pavements is mostly attributed to the stiffness properties of the granular layers in the pavement structure (Salour et al., 2014).

This is illustrated in Figure 2-4. The maximum tensile strain occurred on the top of the layer outside of the wheel path.
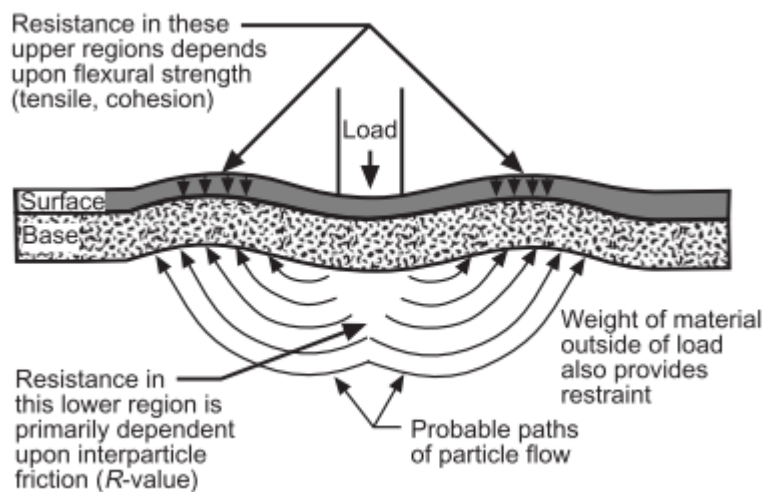
Figure 2-4: Illustration of possible failure mechanism in pavement with thin surfacing layer (after Hveem & Sherman, 1962)

For thicker bituminous layers, it was found that the maximum tensile stress in the surface layer occurred directly below the wheel path (Klomp & Neisman, 1967). The resilient modulus of the supporting soil layers has an influence on the tensile stresses and strains in the surfacing layer of the pavement (Dawson & Plaistow, 1993). Other research also found that the rate of crack propagation in an asphalt layer is inversely related to the stiffness of the surfacing (Ramsamooj et al., 1972).

A further mechanism that develops in pavements under repeated loading is rutting. This is the permanent vertical deformation of the pavement. Although only visible on the surface, the rut depth is the sum of the vertical deformation of all the layers in the pavement. This is shown in Figure 2-5. The degree to which the granular layers of the pavement contribute to the total rut depth is dependent on the thickness of the surfacing layer in the case of bituminous

pavements. For thicker bituminous layers, most of the rut depth is contributed by the permanent deformation in the bituminous layer (Lister, 1972). In pavements with thin bituminous layers the permanent deformation in the granular layers, as well as the subgrade, will probably cause most of the rutting. It must be noted that permanent deformations will occur wherever there is a weakness in the pavement (Brown, 1996).
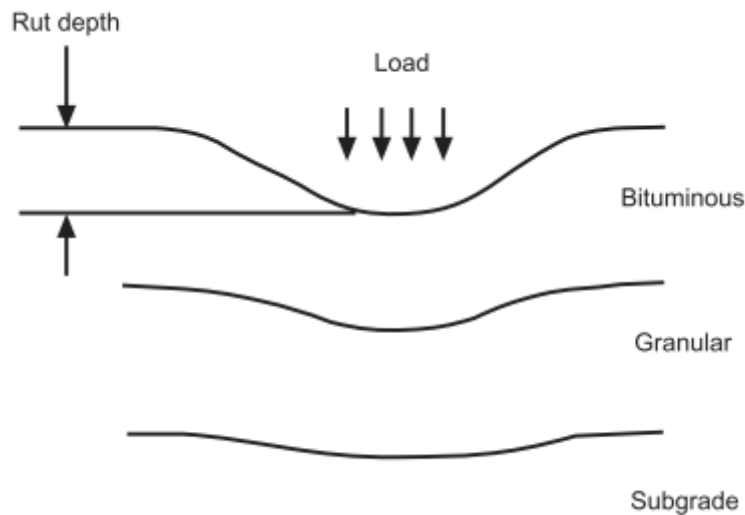
Figure 2-5: Rutting throughout the layerworks of a pavement (Brown, 1996)

2.2.3 South African Pavement Design Method

The South African mechanistic design method (SAMDM) has been under development since the 1970s (Thyse et al., 1996). The following flow diagram (Figure 2-6) shows the sequence of steps of the design process. Should the material properties not be available, it is suggested that laboratory and field testing be done (Thyse et al., 1996). A linear elastic static analysis is then done for the multilayer system under an applied load. Transfer functions, with the pavement response calculated from the abovementioned static analysis as an input, are used to determine the fatigue life of the individual layers in the pavement and are then combined to estimate the overall life of the pavement.
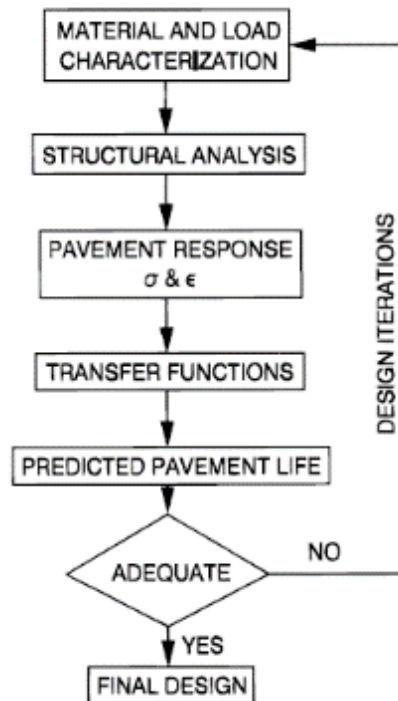
Figure 2-6: Flow diagram for mechanistic design analysis procedure (Thyse et al., 1996)

Transfer functions generally have to be determined empirically. Initially, transfer functions were only made available for thin asphalt pavements (Freeme & Marais, 1974). Thereafter, transfer functions were supplied for asphalt pavements with thick surfacing and then also for cemented material (Otte, 1972, 1974, 1977).

Maree (1978) helped introduce the concept of a safety factor that would provide a limit to the permanent deformation in the layerworks of the pavement. Much of the development that occurred on the SAMDM was a result of accelerated testing that was done using heavy vehicle simulators (HVS) (Maree & Freeme, 1981 and Freeme, 1983). Various revisions were subsequently undertaken (TRH4, 1985 and Thyse et al., 1995).

The material characterisation in the design method relies heavily on the stiffness moduli. Initial suggested stiffness values, which were calculated from laboratory measurement, were updated to effected moduli from data collected from multidepth deflectometer measurements. This resulted in a drastic reduction in the magnitude of stiffness values used as material properties (Jordaan, 1993).

In the SA design method the structural analysis is based on an assumption of a uniform contact pressure of 520 kPa for a wheel load. The fatigue life is determined according to the horizontal strain at the bottom of the asphalt and cemented layers. However, the maximum tensile strain in a layer may not necessarily be at the bottom of a layer (De Beer, 1994), but it

is the assumption used in the transfer functions. Another assumption is that the granular layers within the pavement cannot sustain any tensile stress (Thyse et al., 1996).

For concrete pavements, it is suggested that a mechanistic and risk-based approach be used (Strauss et al., 2001). It was argued that the design of concrete pavements in South Africa had followed a "recipe-type" method that resulted in overly conservative estimations and resulted in higher costs for the construction of concrete pavements. The suggestion was that the mechanistic approach would incorporate linear elastic software programs that would estimate pavement performance using a series of transfer functions and performance curves. These functions would be adapted from results from instrumented pavement sections and also test sections where the heavy vehicle simulator was used. The basis of the software programs still relied on early assumptions made by Westergaard where an equivalent stiffness from the soil is assigned and interpreted as a spring support.

2.3   SOIL MECHANICS IN PAVEMENT ENGINEERING

The knowledge accumulated in the field of geotechnical engineering and the principles of soil mechanics could be used in the design and analysis of road pavements as these are essentially geotechnical foundations or structures. The application of these principles has lagged behind the gains made in research. The soil mechanics for pavement engineering has developed separately from geotechnics (Brown, 1996).

The various pavement types include gravel roads, sealed gravel roads, asphalt pavements, concrete pavements, composite pavements, block pavements and railways. The base consists of one or more compacted layers of material that could be stabilised with cement or bitumen. The sub-base is usually layers of compacted material with the subgrade being the in-situ material that has been compacted. This configuration would be adapted for cuttings, fills and embankments. The typical layout of a road pavement is given in Figure 2-7.
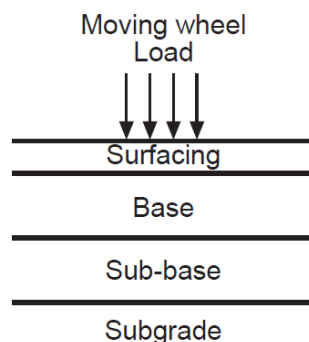
Figure 2-7: Structural layout of a typical road pavement

The importance of soil mechanics is evident since all pavements are built on the ground and consist of layers of unbound granular material. According to Brown (1996), soil mechanics for road pavements does not feature prominently in geotechnical journals and conferences. The research that has been done in pavement engineering has concentrated on the bituminous and concrete layers. Potential scope to integrate the field of soil mechanics into pavement engineering and design is clearly evident.

The soil below a pavement exists (mostly) above the water table but below a sealed surface. The soil is therefore in a state of partial saturation. According to Brown (1996), the influence of partial saturation on the effective stress below a pavement should be further researched and this could be the basis of improvements in the field of pavement engineering. When pavements are constructed, the soil layers which form part of the pavement structure are compacted as near as possible to the optimum moisture content for compaction (Zaman et al., 2010). This allows for the optimisation of compactive energy, allowing for the best compaction with the least amount of effort applied. For pavement material, the optimum moisture content is at a degree of saturation which is well below a state of total saturation. This means that a pavement should be analysed as unsaturated material (Brown, 1996). The influence of the moisture content of the soil in a pavement structure on the behaviour of the pavement should therefore be considered in the design and modelling of pavements (Zapata et al., 2007 and Cary and Zapata, 2010). This is because a change in the moisture content in a fine-grained soil is known to result in a change in the stress state of the soil (Salour et al., 2014).

Even though the partially saturated nature of granular layers in pavements has been recognised, analysis and modelling of the material behaviour in pavement engineering is usually done from a total stress approach. In this way, the effect of pore pressures on the material behaviour during loading is not considered (Salour et al., 2014).

2.3.1 Unsaturated soil mechanics and its implications for pavement response

All soils contain a solid portion (comprising of the soil particles) and voids (the space between the solid particles). A soil is can exist as a two-phase or a three-phase material. A completely dry soil is a two-phase material in which the voids are completely filled with air. A completely saturated soil is a two-phase material in which all the void space is filled with pore water. A partially saturated soil, also known as an unsaturated soil, is a three-phase material in which the voids are partially filled with water and the rest of the void space is filled with air (Knappet and Craig, 2012). The saturated and unsaturated zones within the hydrological cycle are shown in Figure 2-8. It should be remembered that the soil within the

unsaturated zone, shown in Figure 2-8 as the area above the phreatic surface, can still have a degree of saturation (S_R) of 1 due to capillary rise (Sheng et al., 2004).
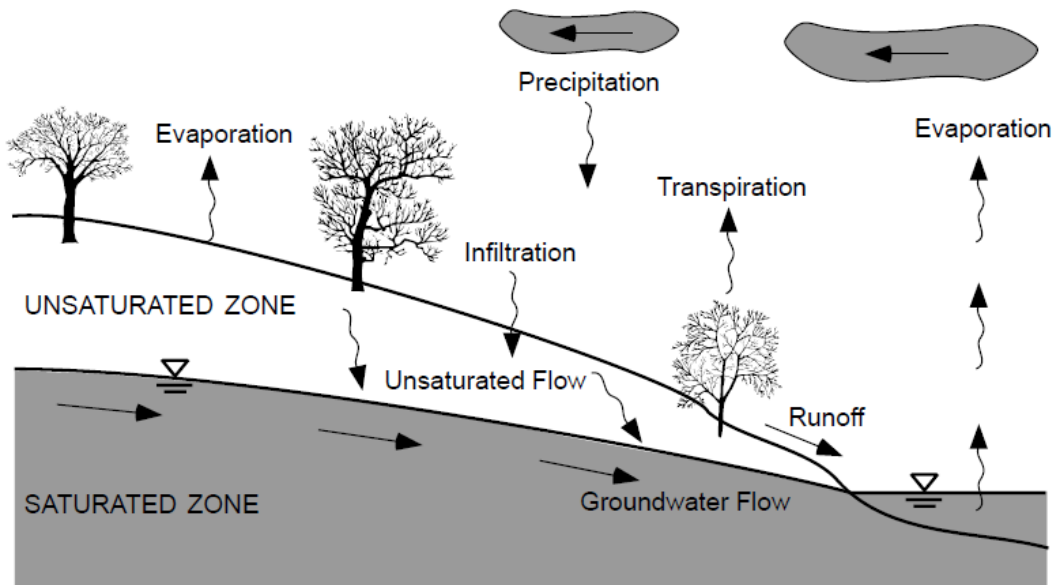
Figure 2-8: Saturated and unsaturated zones within the hydrological cycle (Lu & Likos, 2004)

A conceptual illustration of the degree of saturation, total head and the pore pressure across the saturated and unsaturated zones of a soil mass is shown in Figure 2-9. It can be seen that 100 % saturation is possible above the phreatic surface within the unsaturated zone. Negative pore pressures in the unsaturated zone cause capillary rise into the unsaturated zone. This causes a saturated state just above the phreatic surface.
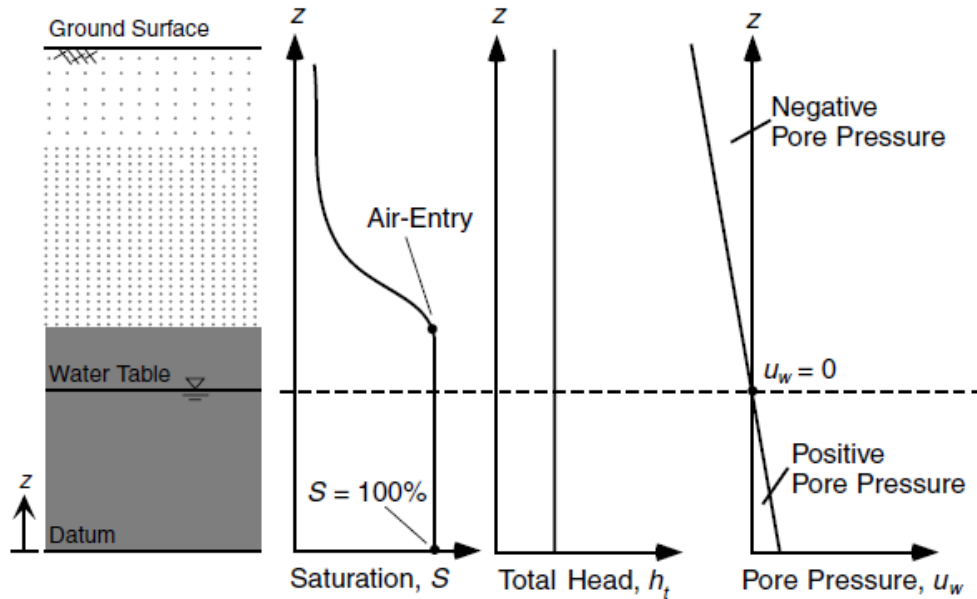
Figure 2-9: Conceptual illustration of saturation, total head and pore pressure within the saturated and unsaturated zones (Lu & Likos, 2004)

The analysis of a saturated material follows Terzaghi's principal of effective stress (Knappet & Craig, 2012 and Lu & Likos, 2004). This is given in the following equation:

$$\sigma = \sigma' + u$$

Where:

σ is the total stress

σ' is the effective stress

u is the pore water pressure

The components (soil particles and water) of a saturated soil are assumed to be incompressible. Volume change is partially dependent on the rate at which water can move into and out of the soil (also known as hydraulic conductivity), with the rate at which the water can move into or out of the soil determining whether the material behaves in an undrained or drained manner (Lu & Likos, 2004). The soil skeleton also partially influences the compressibility of the soil.

For unsaturated soils, the solid particles and water are assumed to be incompressible, but the air retains a degree of compressibility. The behaviour of the soil is now dependent on the soil skeleton, the rate at which air and water can pass into and out of the soil, as well as the capillary forces generated by the water within the voids in the soil. These capillary forces, also called suctions, are dependent on the particle size and distribution within the soil matrix as well as the liquid bridges between particles in an unsaturated soil. These liquid bridges

change in size and shape, depending on the degree of saturation of the soil (Lu & Likos, 2004).

The suctions within an unsaturated soil can be explained by surface tension. In an air-water interface, the water molecules close to the surface do not experience an equal cohesive force in all directions. Figure 2-10 shows the change in the distribution in cohesive forces within water. Closer to the air-water interface, the cohesive forces are imbalanced. For mechanical equilibrium to remain, a resultant force, which acts in tension across the surface of the water, is needed (Lu & Likos, 2004). This force is called surface tension.
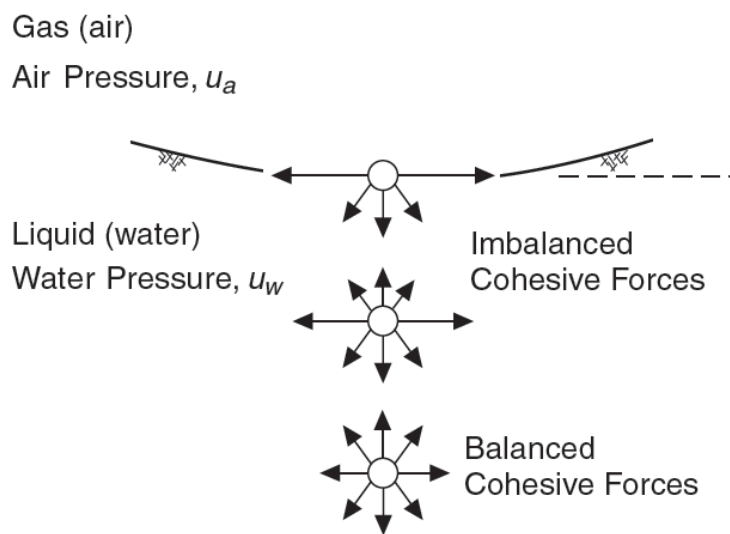
Figure 2-10: Cohesive forces within water (Lu & Likos, 2004)

A curved interfacial surface will occur if there is a difference in pressure across the air-water interface. This is when the air pressure is not the same as the water pressure. The phase with the smaller pressure tends to expand. Figure 2-11 illustrates the inter-particle forces due to suction and external stress. As with a saturated soil, normal and tangential forces exist between particles due to external stresses. For an unsaturated soil, the surface tension on the surface of the liquid bridge that forms across the gap between two particles tends to pull the two particles together.
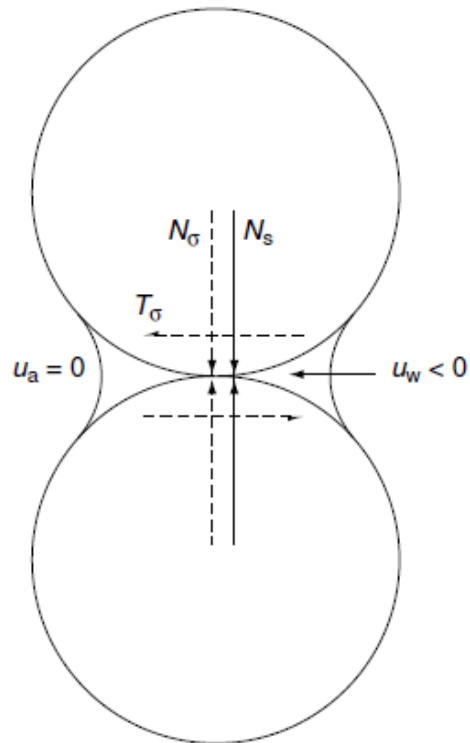
N_σ = normal component of inter-granular force due to external stress
T_σ = tangential component of inter-granular force due to external stress
N_s = inter-granular force due to suction

Figure 2-11: Inter-particle forces due to suctions and external stress (Ng & Mendez, 2007)

Figure 2-12 shows the surface tension acting across the water surface and between the two particles (F_t) along with the negative pore pressure within the liquid bridge.
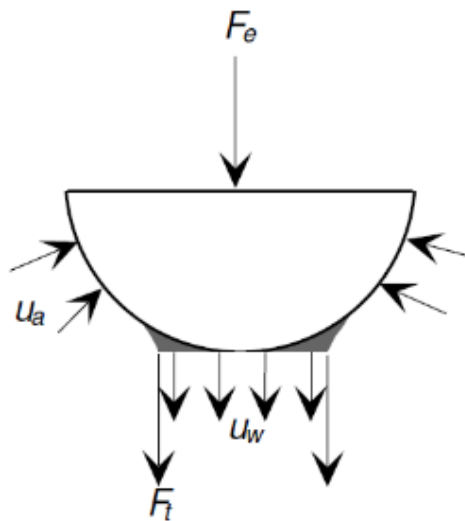
Figure 2-12: Inter-particle forces free body diagram (Lu & Likos, 2004)

Figure 2-13 shows the radius of curvature of the meniscus that forms in a water bridge across two solid particles. For mechanical equilibrium, the smaller this radius is, the greater the surface tension has to be (Lu & Likos, 2004). This radius is dependent on a few soil-water relationships. A smaller radius will occur when particles are closer together, or when there is less water in the bridge between the particles, or if the particles are smaller, or if the pressure difference (u_a-u_w) across the air-water interface is greater. All these contribute to the meniscus radius, hence the magnitude of the surface tension between the particles and thus the suction that pulls the two particles together. It is therefore evident that finer grained, materials with a lower degree of saturation and more highly compacted materials will experience greater suctions in the pore water.
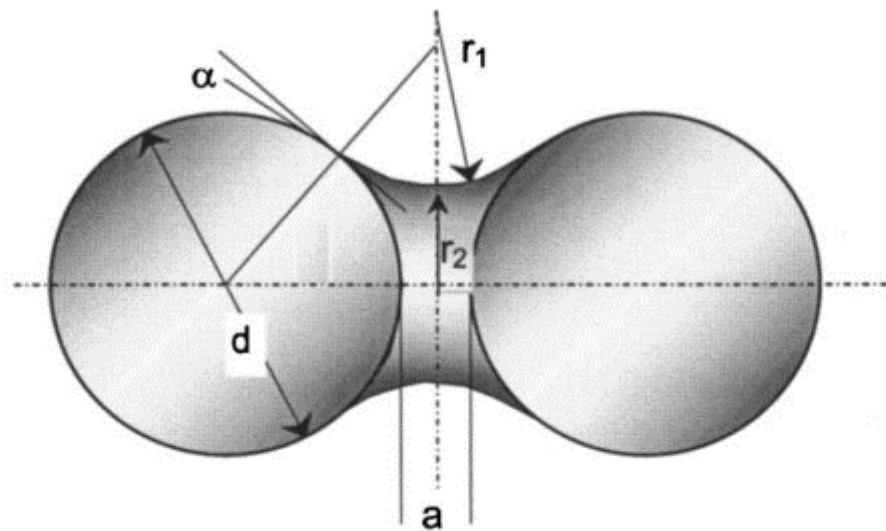
Figure 2-13: Radius of meniscus of water bridge between two solid particles (Lu et al., 2007)

As the degree of saturation within a soil changes, the distribution of pore water is affected. The change in suctions within a soil due to a change in saturation is material dependent and dependent on the level of compaction. Thus, the soil water retention curve (SWRC) is a useful tool used to describe and predict suctions within a soil across a spectrum of saturation levels. Various methods are available to measure the suctions in a sample, including the use of tensiometers and the filter paper method (Toll, 2012). A typical soil water retention curve, expressing the volumetric water content as a function of the matric suction, is given in Figure 2-14. The difference between the water content-suction relationship for drying and wetting is highlighted.
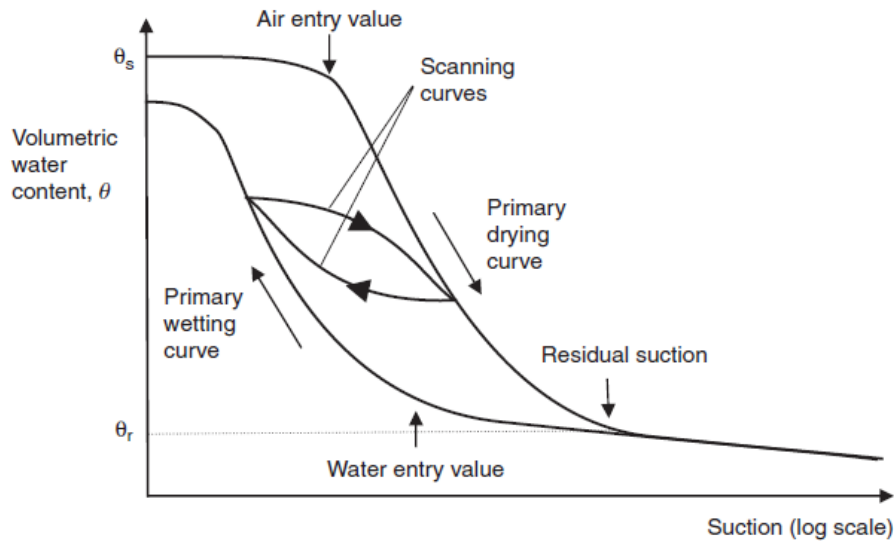
Figure 2-14: A typical soil water retention curve (Toll, 2012)

Although it is apparent that, as the degree of saturation drops, the negative pressure within the unsaturated soil will also increase, this increase in suction does not continue to contribute to the tensile strength of the soil indefinitely. This can be explained by the various water regimes that exist within a soil at different degrees of saturation. In Figure 2-15, a soil water retention curve is shown with degree of saturation on the horizontal axis and suction on the vertical axis. Suction increases as the degree of saturation drops. The conceptualised tensile strength is also depicted. As the degree of saturation drops, the tensile strength increases up to the pendular regime where it drops. This is because, as the degree of saturation drops, the suction stress within the liquid bridge between particles increases. However, at the same time, the area over which this stress acts decreases and the interconnectivity of pore water throughout the soil mass begins to break. The increase in suction increases the tensile force, while the decrease in area over which this suction stress acts decreases this tensile force. Eventually, the area becomes so small that, even though the suction stresses become enormous, the force is reduced. The interconnectivity between pore water begins to break and the suction acts in isolation and not throughout the soil mass.
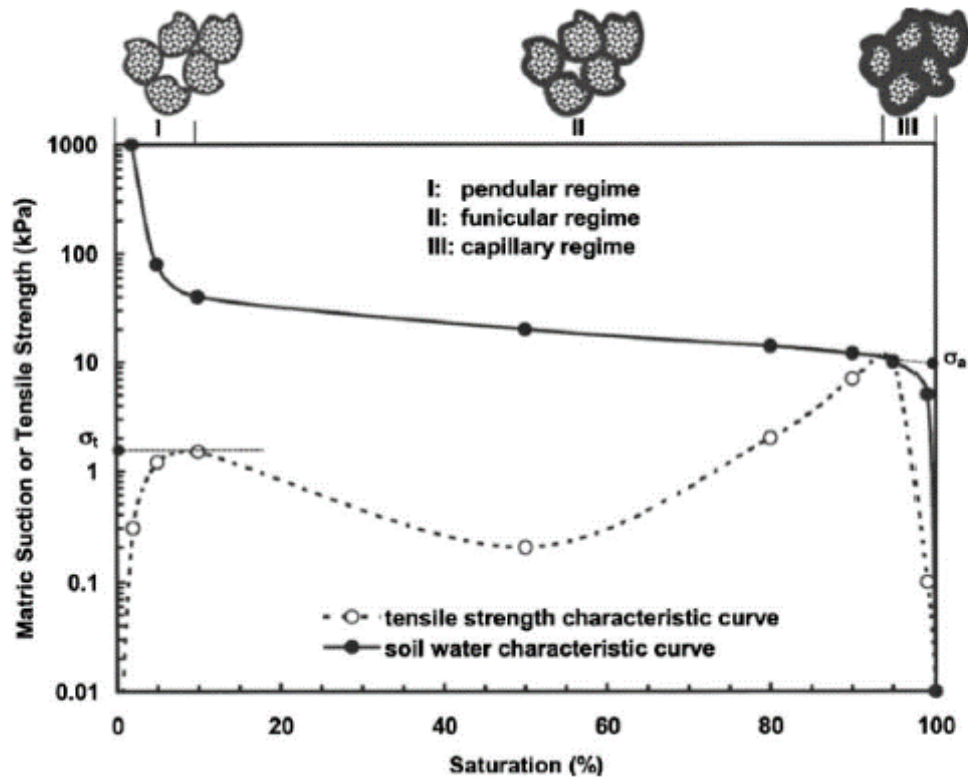
Figure 2-15: Water regimes at various levels of saturation (Lu et al., 2007)

The effective stress in an unsaturated soil, unlike a saturated soil, need to be calculated with the effect of the suctions taken into account. The following equation for calculating the effective stress in a partially saturated soil was proposed by Bishop (1959):

$$\sigma = \sigma' - \chi(u_a - u_w)$$

Where:

σ is the total stress

σ' is the effective stress

$u_a - u_w$ is the matric suction (the difference between the air pressure (u_a) and the pore water pressure (u_w)

χ is a parameter related to the degree of saturation of the soil

Lambe (1960), Jennings (1960), Aitchison (1961) and Richards (1966) are some of the researchers who have since suggested modifications and alternatives to the original equation suggested by Bishop. These account for complexities involving moisture regimes, volume changes, wetting and collapse. Because the suctions within the pores and the external stresses acting on the boundary of the soil element act in different ways in the soil skeleton, it is effectively impossible to combine the two in a single effective stress equation for unsaturated

soils (Jennings & Burland, 1962 and Ng & Menzies, 2007). The various proposed equations are merely estimations of the behaviour of unsaturated soils at this stage.

The moisture content within a pavement structure can be influenced by environmental effects. These could include temperature changes and seasonal wetting and drying periods. These changes in turn influence the soil suction within the pavement. The behaviour of the granular layers in a pavement is largely affected by the moisture content in the soil (Salour et al., 2014 and Erlingsson, 2010). A change in soil suction will influence the stiffness of the pavement (Han & Vanapalli, 2016). The influence of suction change in a pavement on the stiffness, and therefore the resilient modulus, is an important point for consideration. This is discussed in the next section.

Most problems in pavement maintenance and improvement have been related to excess moisture in the pavement structure (Saarenketo and Aho, 2005 and Charlier et al., 2008). Early work was done by Croney & Coleman (1948) to investigate moisture conditions in subgrades. Because the subgrade of a road soil is above the water table, it was decided that conditions were similar to those of interest to the agricultural sciences. Their work was therefore influenced more by agricultural soil physics than by the field of soil mechanics. Research into the moisture conditions below sealed surfaces did not link to the development in soil mechanics at the time. This led to differences in definitions and philosophies between pavement and geotechnical engineering with regard to moisture in pavements (Brown, 1996).

Tests have been done in which the performance of pavements was determined for varying moisture content in the soil below the surfacing. Freeme & Servas (1985) did tests in which water was injected into the pavement during HVS testing. The permanent deformation was measured at the surface of the pavement. The results from these simulations are shown in Figure 2-16. It can be seen that the saturation level of the granular layers in the pavement has a significant influence on the permanent deformation and therefore the performance and durability of pavements. It is therefore important that appropriate instrumentation is used to monitor the pore pressure and suctions in such experiments in which the influence of moisture content is investigated. This is because the effective stress in the soil needs to be known in order to analyse the pavement from a soil mechanics point of view.
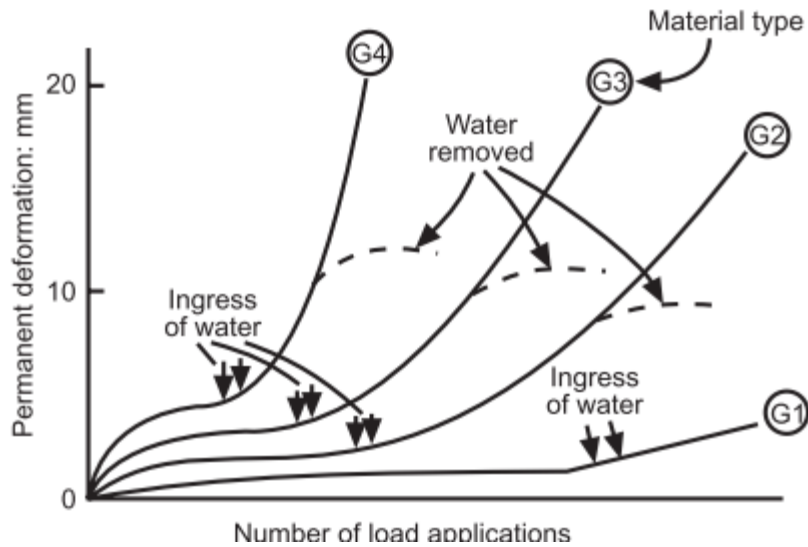
Figure 2-16: Observations made of the influence of water ingress on permanent deformations for various base layer materials (after Freeme & Servas, 1985)

In an investigation into the resilient behaviour of soils (Loach, 1987), cyclic triaxial tests were done on clays with varying degrees of saturation. The deviator stress at which the rate of permanent deformation began to increase was recorded. It was found that there was a distinct relationship between the suctions in the soil (which change with a change in the degree of saturation) and the deviator stress at which the permanent strain rate began to increase. This can be seen in Figure 2-17.
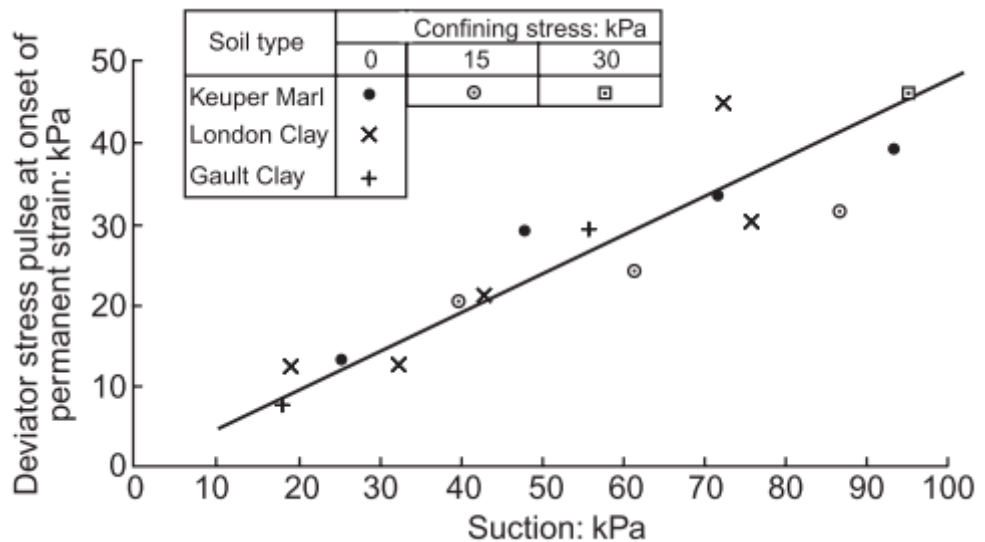
Figure 2-17: Threshold deviator stress as a function of suction (after Loach, 1987)

Heath et al (2004) found that, for tests done on unsaturated granular pavement material, the soil matric suction can even be greater than the applied confining pressure in typical road

pavements. This highlights the importance of the recognition of the role of soil suction and unsaturated soil mechanics as a whole in the field of pavement engineering.

In an unsaturated soil that contains clay, the clay can act as a form of cementation. This is also dependent on the degree of saturation of the soil. An increase in suction results in an increase in bond and overall matrix stiffness. These bonds have an energy threshold that limit the energy that can be stored in these bonds before damage can occur (Yang et al., 2008). A certain load magnitude is required to break these bonds which plays a role in the load than a pavement can withstand.

In view of the above, a road pavement can be viewed as a highly complex unsaturated soil structure from a soil mechanics perspective.

2.3.2 Cyclic and monotonic loading of soils and pavements

Advanced methods of research have been used to perform cyclic loading of soils and other granular materials. The road pavement, and thus the granular material that would be part of the pavement, is loaded repeatedly over its lifespan. The understanding of the behaviour of soils under cyclic loading is therefore of importance to pavement design and evaluation. The applied load magnitude associated with the high number of load applications must be below the shear strength of the soil (Brunton & Akroyde, 1990). The recoverable deformations in a pavement dictate the resilient modulus and the irrecoverable deformations cause the rutting.

2.3.2.1 The Resilient Modulus

Under monotonic loading, a pavement will respond in a resilient manner (Brown, 1996). The resilient modulus is an important parameter of pavement design (Cary & Zapata., 2016) and has been described in Section 2.2.2. It describes the stiffness of the soil during cyclic or dynamic loading. The resilient modulus of a pavement structure, which is important in flexible pavement design, has been shown to depend on, among other factors, soil grading, applied stress, compaction, density, number of load cycles and moisture content (Lekarp et al., 2000). It is important to note, however, that the resilient modulus is only a stiffness measurement and does not represent the actual strength of a material (Buchanan, 2007). In pavement design, correlations using the California Bearing Ratio (CBR) have been used to estimate the resilient modulus of a pavement material (NCHRP, 2004). Research has also been done to measure the resilient behaviour of soil under repeated loading. It has been suggested by Ng et al. (2013) that an increasing linear correlation exists between the resilient modulus of a soil and the applied confining pressure for soils typically used in pavements. Cyclic triaxial tests, in which samples were loaded by varying repeated deviatoric stresses,

were done on a silty clay (Seed et al., 1962). The resilient modulus was determined for each sample after 100 000 cycles. The results in Figure 2-18 show the influence of the repeated deviatoric stress application on the resilient modulus. It can be seen that the resilient modulus initially decreases with increasing cyclic deviator stress, whereafter it remains approximately constant as deviator stress is further increased.
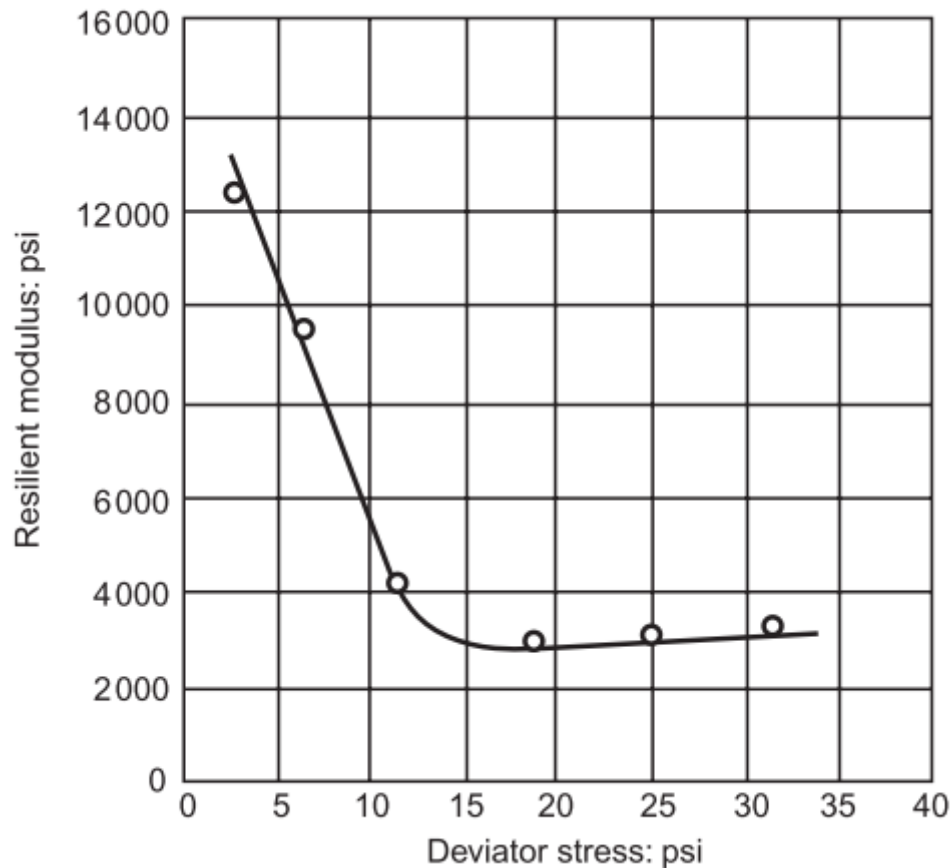
Figure 2-18: Relationship between the resilient modulus and repeated deviator stress for a silty clay after 10^5 cycles (after Seed et al., 1962)

2.3.2.2 Cyclic loading research in other civil engineering fields

Relevant research in this regard has already been done in the geotechnical engineering fields of earthquake engineering, machine foundation design and off-shore foundation design. It is of interest that the work done by Professor Harry Seed (Seed et al., 1955) in the field of earthquake engineering originated from his interest in cyclic loading of pavements.

In the analysis of cyclic loads on offshore piles, Peralta (2010) attempted to develop a criterion that would differentiate cyclic from dynamic loading. This was done on the basis of the loading frequency and is shown in Table 2-1.

Table 2-1: Different cyclic and dynamic loading regimes (after Peralta, 2010)

	Cyclic	Cyclic-Dynamic	Dynamic
Frequency	0 to 1 Hz	1 to 10Hz	> 10 Hz
Inertia	Negligible	Relevant	Relevant
Strain accumulation	Predominantly plastic	Plastic and elastic	Predominantly elastic

When examining the degradation of offshore pile shaft capacity under cyclic loading due to wave loads, De Jong et al. (2003) did modified direct shear tests to study interface shearing using image capturing. These tests were conducted on various cemented and uncemented sands. Under cyclic loading, it was found that the shear modulus at the interface would increase in the first few cycles and then remain fairly constant throughout the test. Dilation would occur in the shear zone with volume contraction in the rest of the sample. This dilation was more prominent for tests with small induced displacements or normal loads. The contraction of the samples was consistently greater than the dilation. This resulted in a net contraction in sample size. On a microscale level, the continuing slip with the number of cycles was attributed to particle rearrangement and crushing. It was also found that the magnitude of shear strain in the zone of shearing decreased with the number of cycles.

2.3.2.3 Cyclic triaxial tests

Brown et al. (1987) did an experiment in which a cyclic load regime was imposed on reconstituted clay samples in triaxials. Not only was it found that the rate of plastic deformation accumulation was highly sensitive to the overconsolidation ratio, but also that there appeared to be an asymptotic imposed stress level, which, if exceeded, caused large plastic deformations, but if kept below this level, the plastic deformation was almost negligible. This also holds true for granular material. Data from Boyce (1976) and Pappin (1979) showed that plastic strains remained insignificant if the cyclic load on granular materials remained below 70 % of the monotonic failure load. The influence of the overconsolidation ratio highlights the effect that the stress history of the soil has on its cyclic behaviour. Work by Cheung (1994) also demonstrates the sensitivity of permanent deformations to the magnitude of the deviator stress. Cyclic triaxial tests were done on two types of clay in which the samples were axially loaded at 2 Hz. The results, shown in Figure

2-19, indicate that permanent deformations increase with an increasing cyclic deviator stress but, once the deviator stress increases beyond a specific value, the increase in permanent strains become much larger. The stress at which this happens is dependent on the material type and the effective stress in the soil.
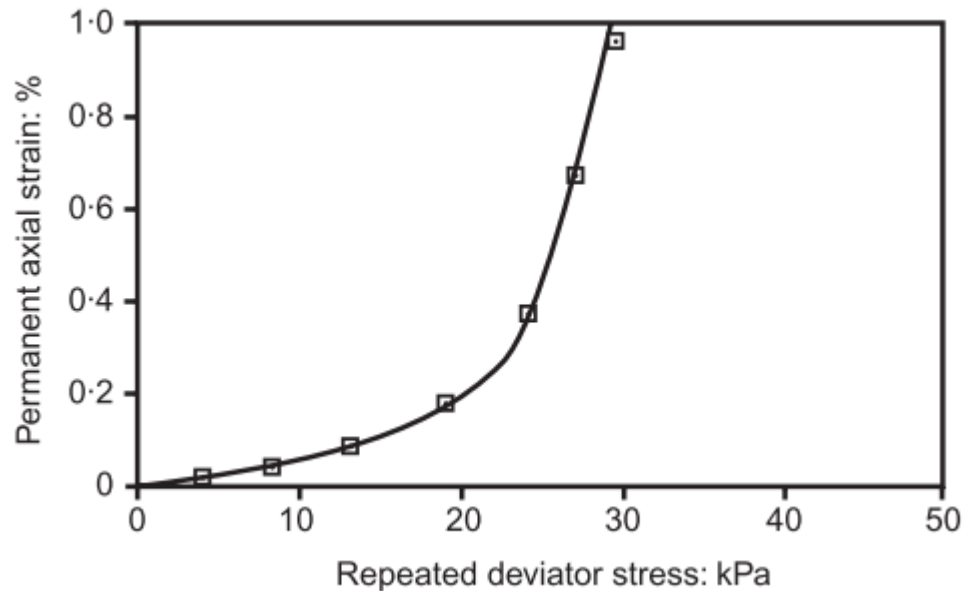
Figure 2-19: Plastic strain against repeated deviator stress for compacted silty clay (after Cheung, 1994)

Repeated load triaxial tests were done on crushed rock aggregate (Werkmeister et al., 2004). This was done for various confining pressures and deviator stress magnitudes. The tests were done under load control and the deviator stress was kept constant during a test. The results from three tests are depicted in Figure 2-20. Sample A was loaded with a cyclic deviator stress of 70 kPa, Sample B with 280 kPa and Sample C with 840 kPa. At the lowest applied cyclic load (Sample A), the permanent vertical strain development remained stable indefinitely. At an intermediate load (Sample B), the strain appeared to be stable until a threshold number of cycles was reached. The permanent strain then increased rapidly to the onset of the failure of the sample. At a relatively high applied cyclic load (Sample C), the permanent strains were unstable from the start of the tests and the sample failed rapidly.
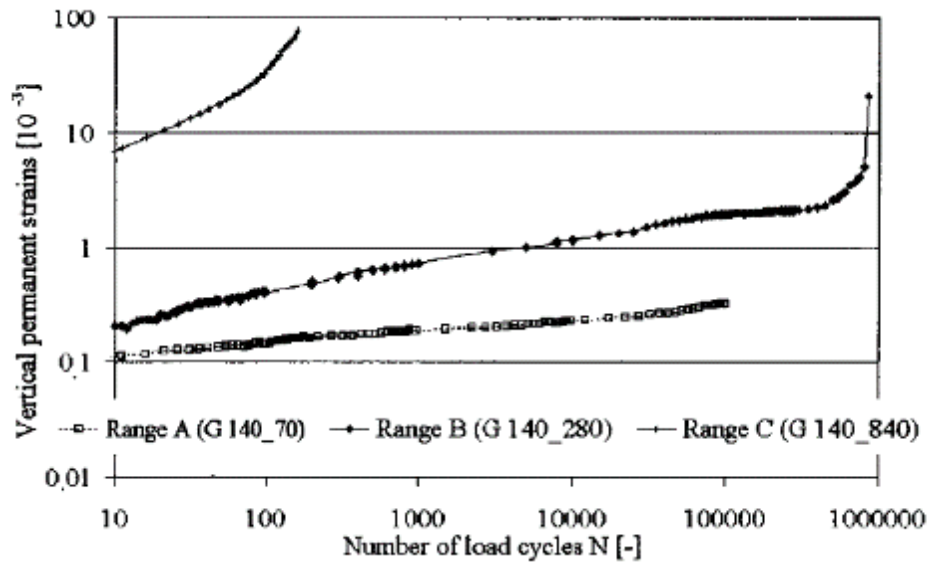
Figure 2-20: Permanent strain for three samples under cyclic loading (Werkmeister et al., 2004)

It was assumed that shakedown was being achieved for Sample A. (Shakedown is defined as a reduction in plastic strain with increasing number of load applications). At very low stress levels, the small level of plastic strain was only due to particle reorientation (Werkmeister et al., 2004). Once the individual soil grains had reoriented into the densest possible state for the applied load, plastic strain reduced and ceased. Any elastic strain at this point would be the elastic deformation of the soil skeleton. For Sample B, it was assumed that slip between particles and recoverable plastic particle rotations occurred. The higher imposed cyclic load resulted in at higher effective stress which limited the permanent particle rotations. The increased contact force between particles resulted in a polishing effect during recoverable slip and rotations. With increased number of cycles, this polishing effect resulted in a reduction in internal friction which, once a critical point was reached, resulted in the eventual collapse of the sample. Another possible explanation for the sudden increase in deformation is that repeated cyclic loading would result in abrasion of particles, causing pieces to chip off. These would end up in the voids between particles. The chipping off would result in stress drop between particles that were in firm contact associated with a drop in strength also explaining the sudden increase in deformation. For Sample C, the high applied load caused crushing of the particles and the threshold shear stress for slip to occur was reached almost immediately. In this case, large plastic strains, which resulted in the rapid failure of the sample, were achieved under a relatively small number of cycles. This material behaviour was also seen by Erlingsson & Rahman (2013). This is idealised in Figure 2-21 from multistage repeated triaxial tests done on unbound granular materials, similar to what was later researched by Salour & Erlingsson (2017).
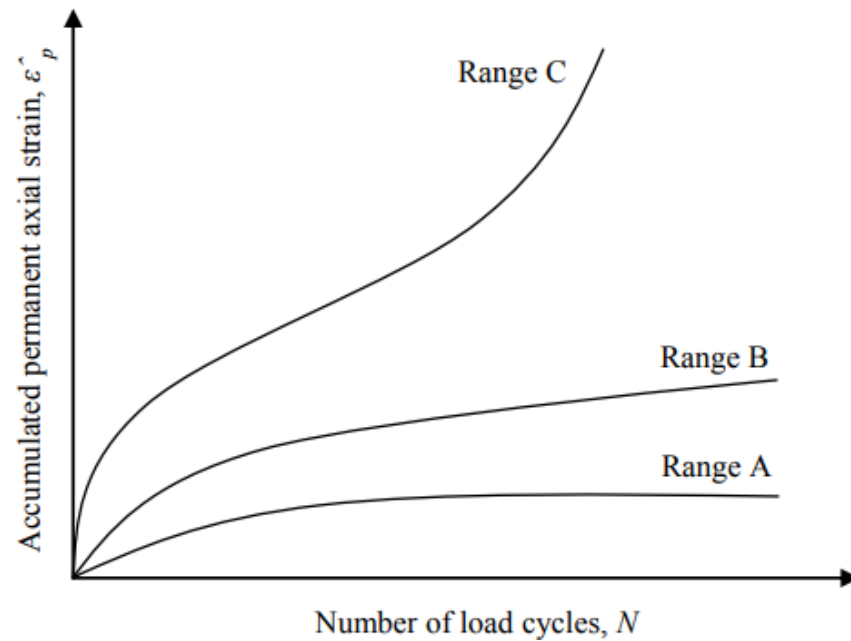
Figure 2-21: Idealised behaviour of granular pavement materials under various magnitudes of applied deviator stress (Erlinsson & Rahman, 2013)

2.3.2.4 Full scale cyclic tests

Experiments in which fibre reinforced beams, which were placed on three soil or foundation types, were loaded monotonically and cyclically were conducted by Briggs et al. (2015). The subgrades tested were a loose granular base, a dense granular base as well as a polystyrene base. The polystyrene was used to replicate the material behaviour in a Winkler model, but it was found that the subsequent deformations for this material was not representative of the behaviour of a natural granular material. Beams were tested with and without restrains at the ends. It was found that there was no difference in the behaviour of the restrained and unrestrained beams under cyclic and monotonic loading. The modulus of subgrade reaction (k_s in MN/m³) was evaluated at intervals during testing. It was found that this modulus, which is representative of the subgrade stiffness in a Winkler model, would increase during the first few cycles and then remain fairly constant throughout the rest of the cyclic test. Dilation was observed in the initial stages of loading during which load magnitudes were still relatively low. During cyclic load testing, the load would be applied and then kept constant for a short period of time (called the relaxation time) and then released again during each cycle. It was found that an increase in resting time resulted in an increase in beam settlement. The cyclic load frequency, apart from just the resting time, was also found to influence the measured deflections. A higher cyclic load frequency resulted in a lower cumulative deflection.

2.3.2.5 Unsaturated cyclic tests

Work that links cyclic loading of soils to unsaturated soil mechanics has also been done. Yang et al. (2008) and Kalil et al. (2008) developed such models to simulate soil degradation and liquefaction. Zhou and Ng (2016) took a step further and looked at the behaviour of unsaturated soils under cyclic loading while also looking at the effect of temperature. This new model coupled thermal, hydraulic and the mechanical behaviour of the soil under unsaturated conditions (Zhou & Ng, 2016). This model allowed plastic strains within the bounding surface (unlike many other models that only allow plastic strain once the surface that bounds elastic behaviour has been exceeded). This was done to allow more realistic cyclic stress-strain relations. The model was validated by conducting cyclic triaxial tests on compacted silt in which temperature and degree of saturation was varied. The influence of temperature on deviatoric strain for unsaturated silt is shown in Figure 2-22. It shows that, for a given number of cycles, the accumulated strain would be larger for a higher temperature. This is because soil suctions decreased as temperature increased for a given moisture content. The decrease in suction resulted in a decrease in stiffness of the soil.
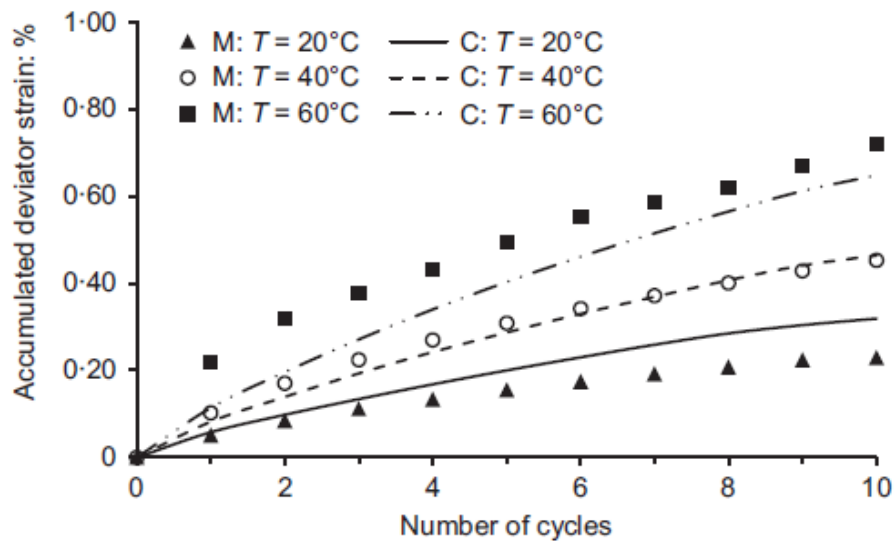
Figure 2-22: Predicted and measured strain of compacted silt under cyclic loading for various temperatures (Zhou & Ng, 2016)

Work was done by Yang et al. (2008) to develop a constitutive model for unsaturated cemented soils under cyclic loading. Suction effects were considered using the Barcelona Basic Model (Alonso et al., 1990) and inter-particle bonding due to cementation was also considered to describe the bond degradation in the soil framework. The possibility of the soil stiffness changing due to the possible change in shape of the yield surface of the model was

also examined. The damage to the soil structure was linked to the strain magnitude in the soil. The model was then compared to results from cyclic triaxial tests on an unsaturated material with cementation. The samples for these tests were prepared at different moisture contents. A typical result for a test on cemented loess is shown in Figure 2-23. It was concluded that more work was required to incorporate the hysteretic behaviour of soils subjected to cyclic loading into the constitutive model.
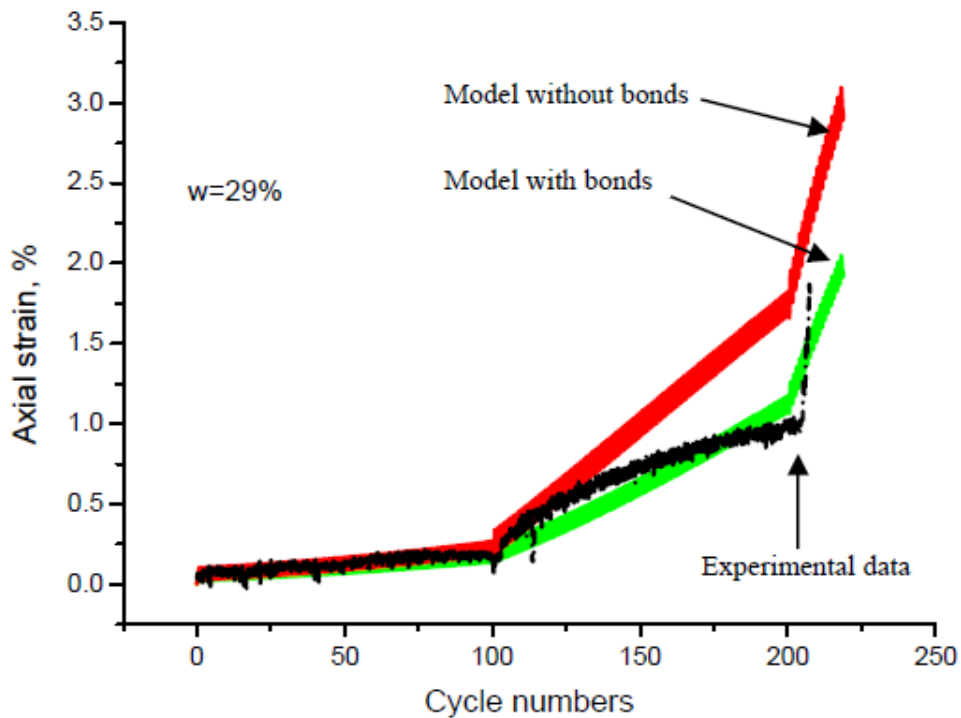
Figure 2-23: Unsaturated cyclic triaxial test data compared to predicted data from constitutive model for cemented soil at 29 % moisture (Yang et al., 2008)

Various researchers have investigated the relationship between the mechanical properties of soils and soil suction. Fredlund et al. (1978), Alonso et al. (1990), Vanapalli et al. (1996) and Ng and Zhou (2014) are some examples. Han and Vanapalli (2016) set out to compare various predictive methods to actual laboratory results for the influence of soil suction on the resilient modulus of the soil. The predictive methods included various empirical relationships along with constitutive models that incorporated soil suction in the calculation of stresses within the soil. The predicted results were compared to results obtained from repeated load triaxial tests. It was found that the stress to which the samples were subjected to influenced the suction magnitude in the soil. This made any predictions complicated. The relationship between suctions and the resilient modulus was also found to be highly dependent on the soil type. This presented difficulties in using empirical relationships to predict the outcome of any

of the cyclic tests conducted because they are limited to the test conditions for which the empirical relationship was developed. The results from the experimental work showed an increasing non-linear correlation between resilient modulus and suction in the lower suction range. Further increases in suction, also observed by Edil and Motan (1979) and Ceratti et al. (2004) did not result in a significant increase in the resilient modulus. In some cases, the resilient modulus even decreased with an increase in suction in the higher suction range. This can be explained when considering the moisture regime within a soil (Vanapalli et al., 1996). In the higher suction range, also known as the residual zone in terms of moisture regime, the wetted contact areas between adjacent soil particles becomes smaller with increasing suction. This can result in a breaking of the capillary menisci which in turn reduces or completely ceases the influence of soil suction towards the strength and stiffness of the soil (Caicedo et al., 2009). It was therefore concluded, in this study, that the influence of soil suction on the resilient modulus of the soil should be investigated in conjunction with the related moisture regime of the soil. This is highly soil dependent and requires the soil water retention characteristics of the soil to be known. This further reduces the applicability of empirical relationships for predicting the influence of soil suction on the resilient modulus. It was also found that an inverse correlation existed between the resilient modulus and the applied shearing stress. This reduction in resilient modulus with increasing shear stress was also observed by Ng et al. (2013) and Sivakumar et al. (2013) for fine grained soils. The relationship between resilient modulus (M_R) and soil suction and between resilient modulus (M_R) applied cyclic stress is shown in Figure 2-24.
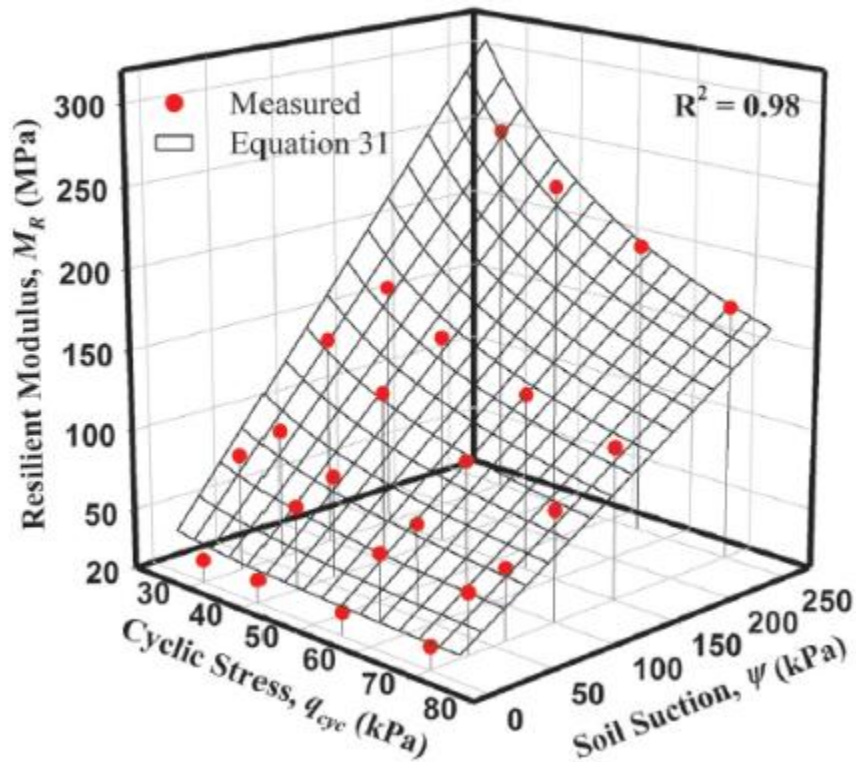
Figure 2-24: Relationship between resilient modulus (M_R) and soil suction and between resilient modulus (M_R) applied cyclic stress (Han and Vanapalli, 2016)

The influence of cyclic loading on pore pressure response in a soil also has to be understood. Due to the inherent plasticity of soils below many pavements, it is expected that the soil stiffness will reduce under cyclic loading due to an accumulation of excess pore water pressure (Cary & Zapata, 2016). Work on the influence of cyclic loading on pore pressure response for saturated soils has been largely investigated, particularly in the field of railway engineering (Li & Selig, 1996; Grabe & Clayton, 2009). Studies have also been done to show that the change in pore water pressure for unsaturated samples is mainly, from the various factors considered, influenced by the magnitude of the matric suction at the start of the test in unsaturated soils which are subjected to cyclic loading (Minh Thu et al., 2006 and Yang et al., 2008). Cary & Zapata (2016) did research to measure the increase in pore water pressure during cyclic loading of saturated and unsaturated soils. The measurement of negative pore pressures in an unsaturated soil during cyclic loading is a very challenging task and not all tests were completed successfully. Triaxial test equipment was used which allowed dynamic loading and pressure measurements, including the air pressure in the cell for unsaturated tests. It was found that pore water pressure did increase for saturated and unsaturated samples. This can be seen in Figure 2-25.
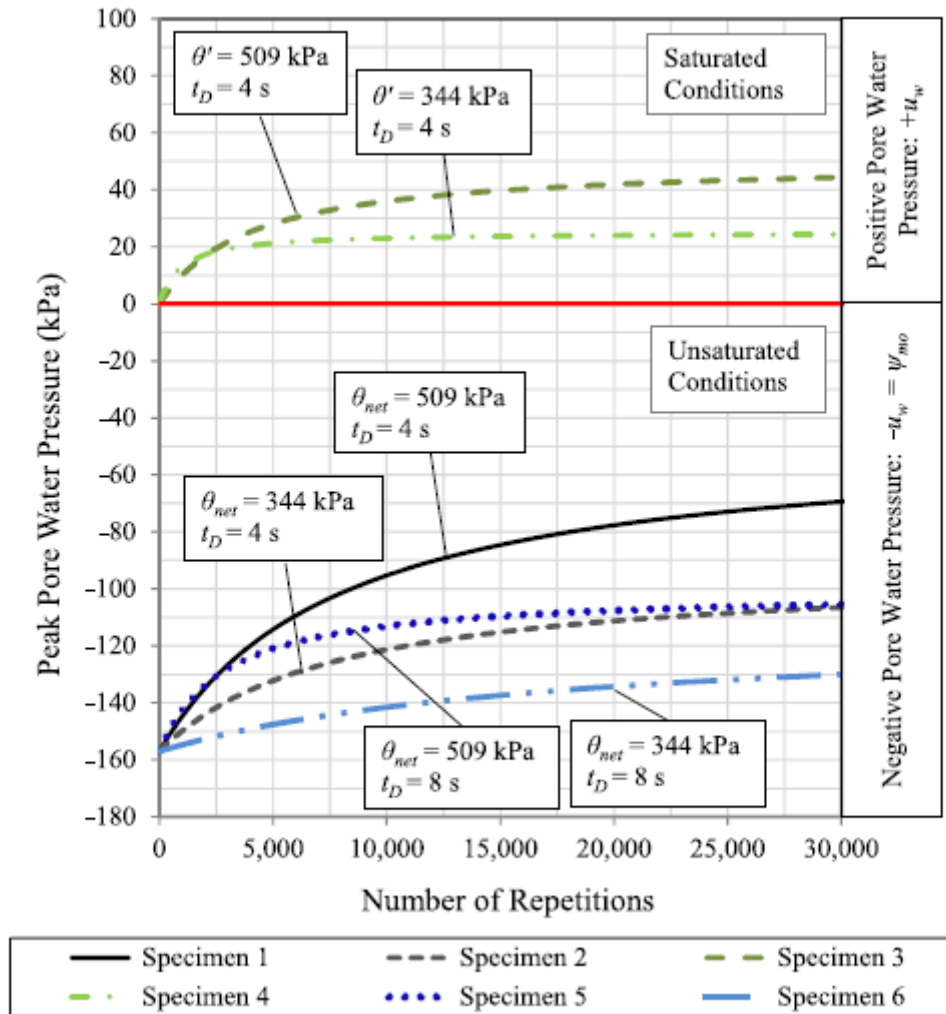
Figure 2-25: Pore pressure buildup for saturated and unsaturated samples tested under cyclic loading (Cary & Zapata, 2016)

It is evident that the pore pressure build-up (or loss of suctions) for the unsaturated samples was greater than for the saturated samples. With each cycle, there was only a slight difference in pore pressure, but the accumulation of these differences resulted in a large pressure build-up for many cycles. This is particularly important for unsaturated soils under traffic loading, as a loss in suction will result in a loss in tensile strength in the soil and stiffness degradation. Cary & Zapata (2016) argued that the pore pressure increase in the unsaturated samples was greater than for the saturated samples and was possibly due to the following factors:

- Air, which becomes pressurised as the sample contracts within the voids of unsaturated samples, exerts pressure on the water in the voids.

- Unsaturated samples have a lower hydraulic conductivity than saturated samples and therefore limit the rate at which excess pore pressures can be dissipated, resulting in a small residual excess pore pressure at the end of each cycle.

It was found that, for the tests conducted, the pressure build-up in the unsaturated samples never exceeded the suctions at the start. The pore water pressure therefore remained negative at the end of the tests. Another aspect that was considered in the tests was the loading time (t_L) and the dwelling time (t_D). This can be seen in Figure 2-26. For the tests, the loading time was not changed as it was assumed to have no influence on the pore pressure build-up in the soil (Lashine, 1971). It was, however, found that the dwelling time influenced the pore pressure build-up. A shorter dwelling time resulted in a greater increase in pore pressure for the duration of the test. This was explained by relating it to the dissipation of excess pore pressures in the soil. This dissipation could only occur during the rest period (dwelling time) between cycles. With a shortening of the dissipation time, the remaining excess pore pressures at the end of each cycle would be higher.
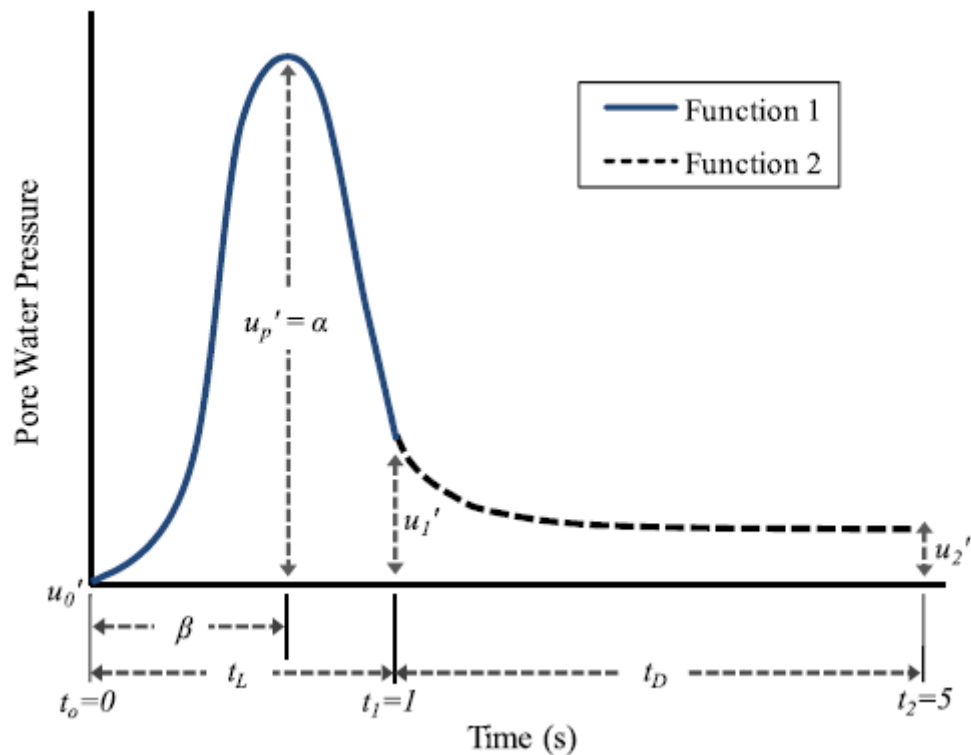
Figure 2-26: Pore pressure during a single loading cycle (Cary & Zapata, 2016)

2.3.2.6 Seasonal effects

The moisture content in a soil is often seasonal. Although the pavement layers are compacted at optimum moisture content, the moisture content will with time equilibrate to the natural state. In many cases, this results in an increase in moisture content. The resilient modulus of compacted subgrades, with matric suction control, was modelled to reflect the seasonal

variations in moisture content of the soil (Salour et al., 2014). Modified tests were done using the axis translation technique using triaxial equipment in which pore air and pore water could be measured and controlled. This involved increasing both the air and pore water pressure, while still maintaining the same matric suction (which is the difference in pore air and pore water pressure), so as to avoid cavitation. Under conditions of higher matric suction it was found that the soil behaved stiffer under cyclic loading. For example, for one of the materials tested (Torpsbruk subgrade), an increase in the degree of saturation of 30% resulted in a complete loss of matric suction (which had been over 300 kPa before the increase in the moisture content). This resulted in a decrease in the resilient modulus by over 50%.

2.3.2.7 Effects of principal stress rotation

The cyclic loading of pavements is due to a moving wheel load. A phenomenon that occurs in pavements under a moving wheel load is the rotation of the principal stress planes. The vertical stress in a soil element is caused by a load applied to the surface of the pavement by a wheel. The horizontal stress is due to the confinement caused by compaction along with the overburden of the wheel load on adjacent soil elements. The vertical and horizontal stresses increase as the wheel approaches and reaches a maximum when the wheel is directly above the soil element and decrease again as the wheel starts moving away. In addition to this, a double pulse of shear stress is applied to the soil element as the wheel passes over it. This behaviour of the reversal of the shear stress can be observed in Figure 2-27.
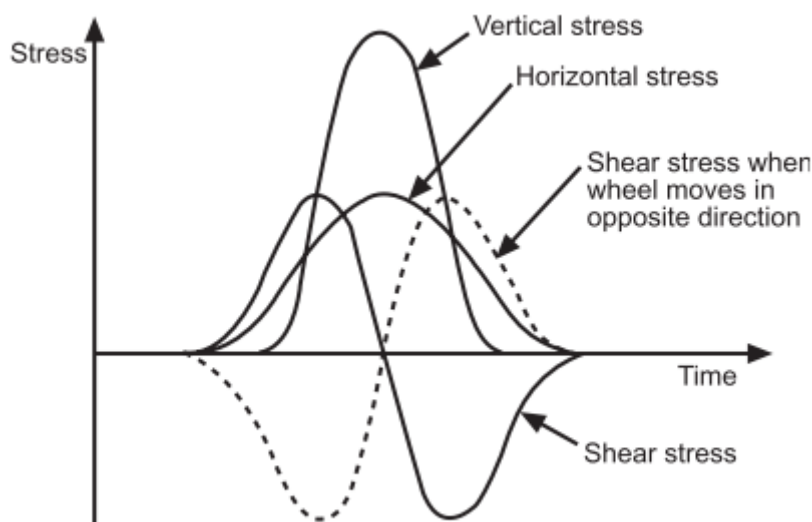
Figure 2-27: Vertical, horizontal and shear stress in an element within a pavement as a wheel passes over (after Brown, 1996)

This behaviour needs to be understood when evaluating the long term behaviour of pavements due to passing wheel loads. The shear stresses due to traffic loading are influenced by the rotation of the principal stress directions (Ishihara and Towhata, 1983). Traffic loading applied to pavement sections resulted in higher permanent deformations than when the same load was applied repeatedly using plate loads (Brown & Brodrick, 1999). This is due to the influence of the rotation of the principal stress directions. Cyclic triaxial tests do not account for this behaviour as they can only simulate the change in the ratio between the vertical and horizontal stresses but not the double shear pulse with sign reversal as caused by a moving wheel. The Hollow Cylinder Apparatus can, however, allow the control of the normal and shear stresses in such a way that field conditions can be recreated. Chan & Brown (1994) found that the principle of shear reversal was of significance when plastic strain accumulation in soils is being investigated, while the resilient strains were not affected by this (Chan, 1990). Since it is the development of plastic strain which causes rutting in pavements, shear reversal in pavement testing should be considered.

Figure 2-28 shows that permanent strain is influenced by the phenomenon of stress reversal and that resilient strains remain largely unchanged.
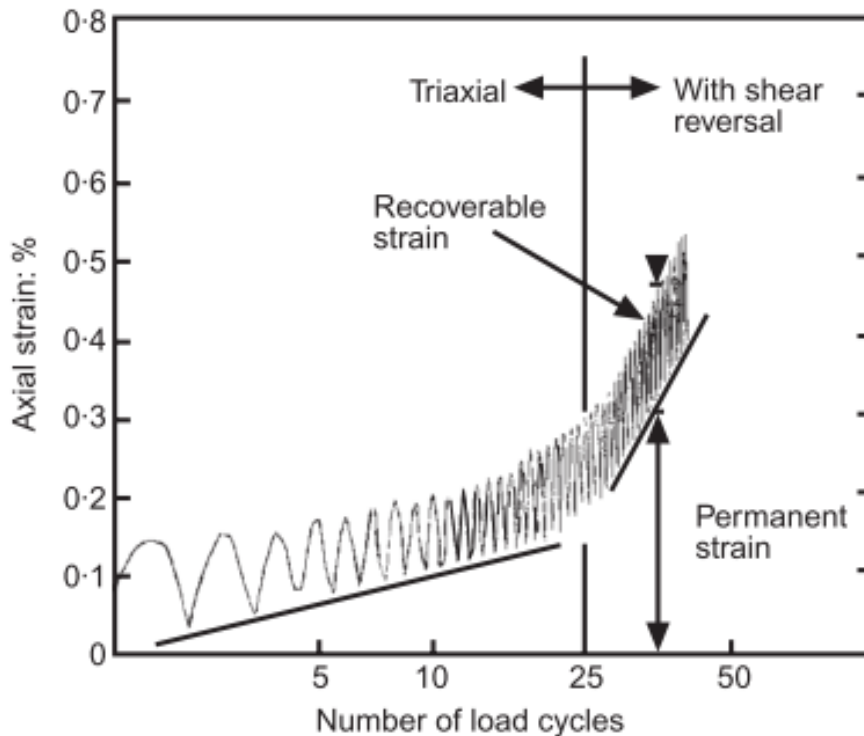
Figure 2-28: Influence of shear stress reversal on accumulation of plastic strain in a dry crushed rock (after Chan & Brown, 1994)

Tests done on sand showed that, when cyclic rotation of the principal stress is included, the cyclic shear strength of the sand is reduced compared to sand tested in conventional cyclic triaxial tests that do not allow for the application of principal stress rotation (Ishihara and Towhata, 1983). These tests were done to replicate the cyclic loading of soil on the seabed under wave loads. It was also found that when the cyclic load amplitude was kept constant, there was a buildup of pore water pressure when principal stress axis rotation was performed. This resulted in a predominantly elastic response in the deformation of the soil until the pore pressure buildup caused liquefaction to occur. At this point the soil began to deform plastically.

2.3.2.8 Effects of drainage

The behaviour of soil under cyclic loading for different drainage conditions was investigated by Mamou et al. (2017). This was done using the hollow cylinder apparatus that allows for principal stress rotation. It was found that the resilient behaviour of the material (a railway track foundation material) depended on a threshold value of shear stress. When the threshold stress was exceeded, a sudden reduction in material stiffness would occur and strains would accumulate rapidly. Below this threshold of shear stress, the pore pressure increase and strain accumulation would remain insignificant. Figure 2-29 shows the shear stress approaching a critical value with increasing number of cycles.
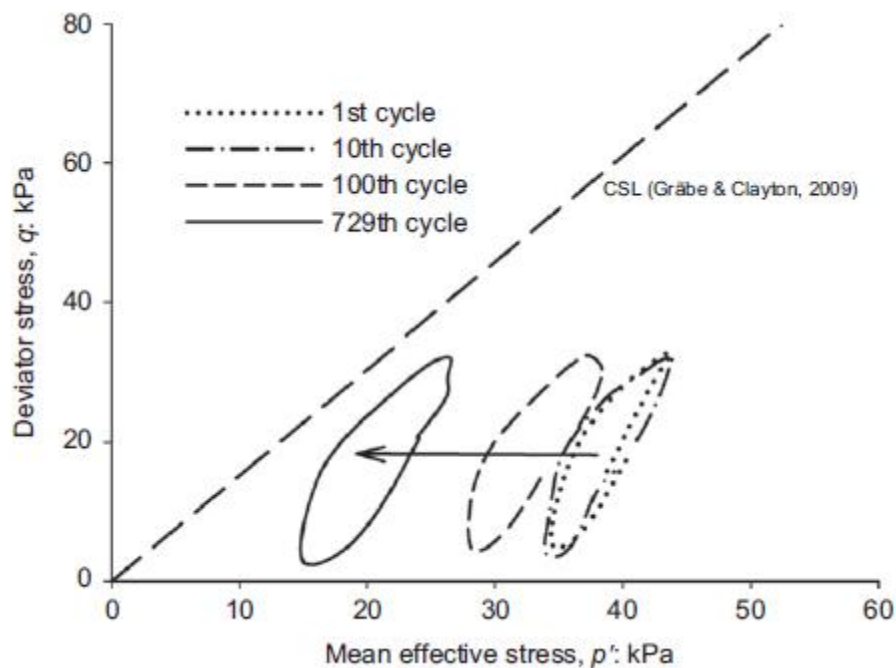
Figure 2-29: Stress cycles approach critical state line with increasing number of cycles (Mamou et al., 2017)

In Figure 2-30, it can be seen that the resilient modulus decreased rapidly once the shear stress threshold was reached.
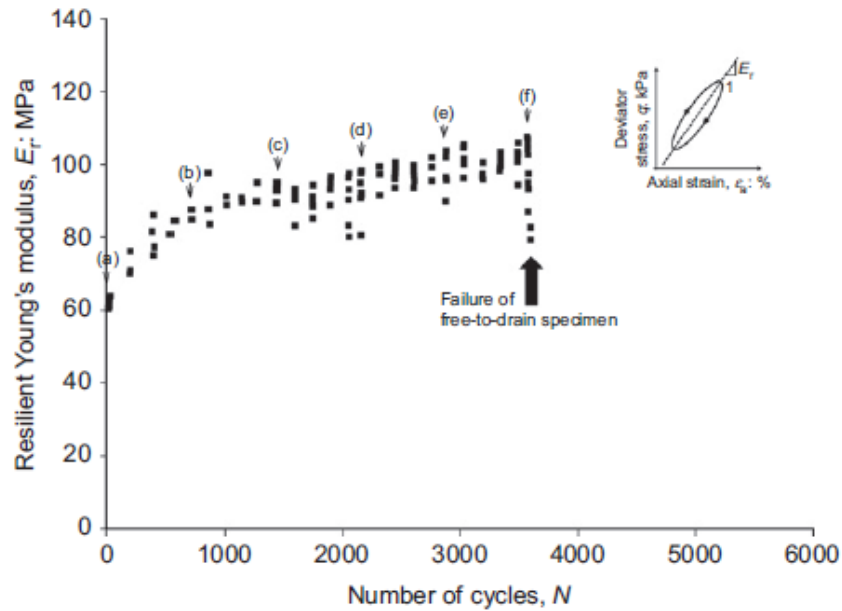
Figure 2-30: Rapid reduction in resilient modulus once critical shear stress is achieved (Mamou et al., 2017)

Figure 2-31 shows the strain accumulation with increasing number of cycles. Once the threshold shear stress was reached, the sample failed as volumetric strain suddenly increased. This coincided with the rapid reduction in the resilient modulus (Figure 2-30).
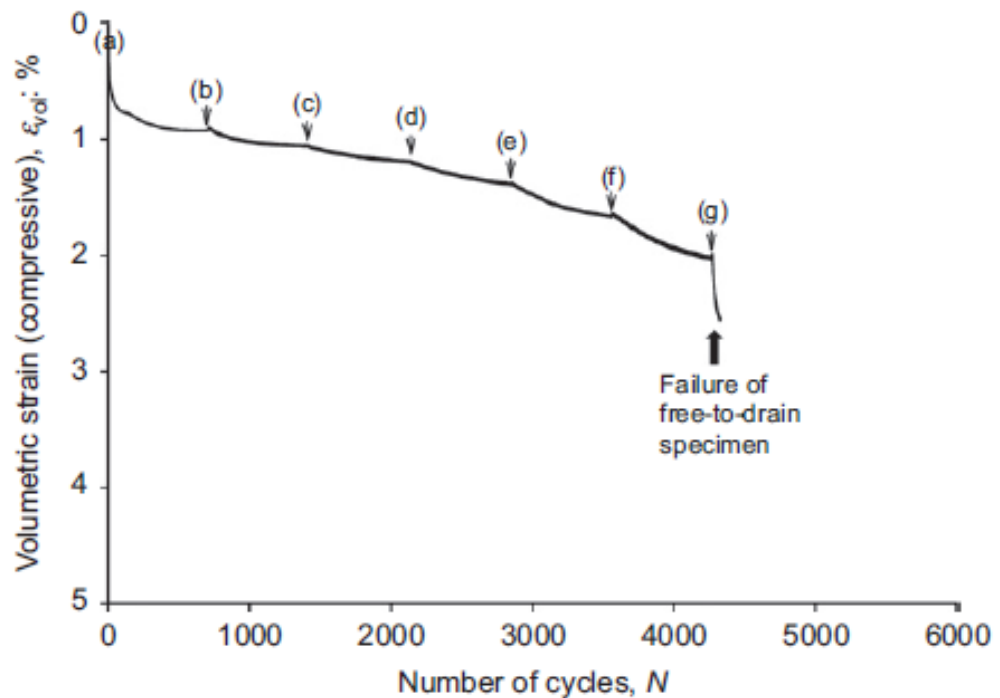
Figure 2-31: Sudden increase in strain once critical shear stress threshold is achieved (Mamou et al., 2017)

The study found that undrained samples which were tested failed under fewer number of load applications than the samples which were free to drain. This is because the generation of excess pore pressures occurs more rapidly in undrained tests. Under cyclic loading, even in a drained sample, excess pore pressures are eventually generated. The resilient modulus of free to drain samples also increased with increasing number of cycles below the threshold shear stress.

Repeated load triaxial tests were performed using equipment at Nottingham University (Brown et al., 1980 and Raybould, 1992). In these tests, instead of applying a confining fluid pressure, confinement was applied using a partial vacuum through the top and bottom porous disks of the triaxial. This made it easier to attach strain measurement instrumentation directly to the membrane on the sample since the triaxial cell was no longer required to contain the confining fluid. These tests showed that the resilient behaviour of the soil was not sensitive to the loading rate. The limitation of this observation is that it the sample could only be tested to a limited number of cycles due to the limitations in the test control equipment (Brown, 1996).

Field tests of soil response to repeated loading have also been performed. One such test, initially used to test the California Bearing Ratio (CBR) of a compacted soil, is the static plate load test. This method has its limitation in that it cannot reproduce the time-dependent loading

associated with wheel load (Brown, 1996). The load pulses generated in quick succession by wheels on a pavement result in the soil being loaded in an undrained manner. The time between successive loads in the plate load test allows the excess pore pressures in the soil to dissipate, resulting in drained conditions. This difference is less evident in granular materials than in material with high clay content.

2.4 ULTRA-THIN CONTINUOUSLY REINFORCED CONCRETE PAVEMENTS

A conventional concrete pavement is topped by a rigid concrete slab that could be up to 300 mm thick. The behaviour of this pavement structure can be adequately predicted using the beam on an elastic foundation model. An alternative pavement method is the ultra-thin continuously reinforced concrete pavement (abbreviated to UTCRCP). This method entails the use of a very thin (as thin as 50 mm) reinforced 90 MPa concrete slab that is cast over the layerworks. This concrete layer is heavily reinforced (with a steel mesh and steel fibres) and behaves in a flexible manner.

This pavement type has been used in rural and township roads (Jansen van Rensburg, 2013). It was originally developed by the CSIR to provide surfaced roads in rural areas (CSIR, 2011).

2.4.1 Ultra-high strength concrete

Experimental research on fibre-reinforced slabs on grade has been done by Falkner et al. (1995), Irving (1999) and Roesler et al. (2004), amongst others. The added benefit of fibre contributing to flexural capacity is not always taken into consideration for design (Briggs et al., 2015). The increase in flexural capacity, which is provided by the steel fibres, results in slabs that are thinner. Thin, highly reinforced slabs were initially used in industrial floors and the rehabilitation of bridge decks in Europe (Kannemeyer et al., 2007).

This project investigates the behaviour of UTCRCP using scaled models. For scaled-down testing of UTCRCP, the concrete layer also has to be scaled-down. Research by Kearsley & Mostert (2009) was done to try and reproduce the behaviour of the flexible concrete used in UTCRCP, but using concrete that was scaled-down. It has been shown by Denneman et al. (2010) that the size of a concrete sample plays a role in its behaviour. The aim of the research was to achieve the same load-deformation behaviour in a scaled-down concrete sample as in the full scale sample. Various concrete tests were done. These included the Brazilian disc tests to find the cracking strength of the concrete, direct tensile tests as well as the flat disc punch test to determine the energy absorption potential of the concrete. Trial-and-error was used to eventually propose a concrete mix design for the scaled-down concrete that would

satisfactorily reproduce the behaviour of the full-sized concrete. Consideration had to be given to the particle size distribution of the aggregate as well as the steel reinforcing used in the concrete. The final mix design by Kearsley & Mostert (2009) is given in Table 2-2.

Table 2-2: Mix composition for UTCRCP scaled models (Kearsley & Mostert, 2009)

Material	kg/m^3
Cement (Cem II 42.5 R)	450
Condensed silica fume	50
Water	210
Dolomite sand (<2.36 mm)	1850
High range water reducing agent (litres)	16
Micro steel fibre	80
Polypropylene fibre	2

2.4.2 Current UTCRCP design method

Conventional rigid concrete pavements fail in a brittle manner and so the design and analysis thereof can be simply reduced to a rigid slab on an elastic foundation. Modelling of the flexible concrete typically used in UTCRCP has also been successfully done. To model the combined behaviour of the flexible slab on the supporting layers has proven to be difficult. The research that has been done using the HVS has revealed that the previously used models did not accurately predict the load distribution and failure mechanisms (Kearsley et al., 2014).

Table 2-3: Mix composition for UTCRCP (not scaled) (Kearsley et al., 2014)

Material	kg/m³
Cement (Cem I 42.5 R)	480
Pulverised fuel ash	87
Condensed silica fume	72
Water	170
6.7 mm stone	972
Sand	689
High range water reducing agent (litres)	6.4
Hook-ended steel fibre	100
Polypropylene fibre	2

In the design of UTCRCP, the stress in the pavement is assessed using CBR design curves (CSIR, 2011).

2.4.3 Research on UTCRCP

Experimental sections of UTCRCP were initially tested in South Africa using specifications for the rehabilitation of bridge decks in Europe (Kannemeyer et al., Buitelaar, 2004). These tests were conducted using the heavy vehicle simulator (HVS). It was found the introduction of surface water which infiltrated the cracks in the concrete caused the failure of the pavement. It was also concluded that curling of the concrete did not influence the overall performance of the pavement. Issues with the debonding of the concrete from the soil below were identified. It was assumed that this was caused by water that had infiltrated the cracks in the concrete (Kannemeyer et al., 2007).

UTCRCP was tested by means of full-scale experimental trial sections during the National Highway Renewal Programme in South Africa. Full-scale testing with the Heavy Vehicle Simulator (HVS) has also been done (Du Plessis et al., 2006). Further testing using the HVS was done on trial sections in Mamelodi and Soshanguve (Denneman & Du Plessis, 2012).

Analysis was done in which the pavement was modelled using the assumptions of Westergaard (1926) of a plate on springs (Winkler spring model). It was concluded that the design guidelines, as advised by the CSIR, which used the CBR design curves, did not work satisfactorily for the design of UTCRCP.

Research has been conducted on UTCRCP at the University of Pretoria since 2006 (Kannemeyer et al., 2007). By way of scaled-down testing, the high costs associated with full-scale testing, including material and time-related costs, are reduced. Because the depth of a pavement is low relative to most other geotechnical foundations, the self-weigh induced stress in the soil is largely negligible. The need to test at accelerated gravity is therefore not as great as it is for deeper foundations (Kearsley et al., 2014). One such experiment involved a scaled-down UTCRCP pavement with a stabilised base layer. A loading cart with four wheel loads applied load to the pavement. It was found that cracking tended to initiate at the centreline of the road (between the wheel loads) and that the scaled deflections were similar to those recorded in full-scale tests (Kearsley et al., 2014).

Research on the constructability of UTCRCP was done by Mukandila et al. (2009). This was for a trial section built at the Heidelberg traffic control centre. The aim of the research was to find a suitable method of construction that would be efficient when used in full-scale projects.

2.5   SUMMARY

The literature review considered aspects of pavement engineering, soil mechanics and specifically UTCRCP.

The section on pavement engineering includes a brief history of pavement engineering and then the analysis and design of pavements. It is evident that many assumptions regarding the design of pavements are based on empirical research. It appears attractive to attempt to incorporate more elements of soil mechanics in pavements design, but this is hampered by the fact that a road pavement under traffic load is a highly complex geotechnical structure.

Unsaturated soil mechanics is important for pavement engineering since a pavement is constructed from materials at or below optimum moisture for reasons of compaction. Research on the behaviour of pavements and soils under partially saturated conditions was summarised. Literature on the cyclic loading of soils and pavements was briefly summarised. Important aspects highlighted include the observation that road deflection seem to remain resilient (small) until the applied load exceed a certain threshold value and the role of stress rotation associated with wheel load application that results in more rapid strain development compared to simple cyclic load application.

3   METHODOLOGY

3.1   EXPERIMENTAL SETUP

It was shown that design methods applied to conventional concrete pavements are not generally applicable to the design of Ultra-Thin Continuously Reinforced Concrete Pavements (UTCRCP). Further work on the refinement of design methods for UTCRCP is therefore still required. In order to study the behaviour of UTCRCP under load it is attractive to make use of model studies. In testing the models the application of numerous cyclic loads is required to allow pavement response to be studied. This is a time consuming process. This study investigates whether it is possible to carry out realistic accelerated load testing to study the behaviour of UTCRCP under loading. The effect of the magnitude of the applied load and the corresponding number of cycles required to cause a certain amount of rutting was investigated. The resulting deformation of the layerworks under the different cyclic load magnitudes were compared and, in turn, compared to the deformation of a model pavement caused by a monotonic load application imposing the same amount of rutting. The purpose was to assess whether the test can be accelerated by simply applying a monotonic load to impose a given amount of rutting.

The tests should preferably be carried out in a geotechnical centrifuge so that stresses in the model are identical to that in the full scale prototype, but because the in situ stresses in a road pavement are low and because of equipment limitations the tests described here were carried out at normal gravity.

In addition tests should be carried out by applying a running wheel load to impose principal stress rotation. However, this study considers the simple application and removal of strip loads, modelling the pavement in plane-strain. In terms of road layers two material types placed at a range of moisture contents and densities were considered.

This chapter presents a description of the experimental equipment. During development a number of tests had to be carried out to validate procedures. The results of these tests are also presented in this chapter as they are seen as part of the development and validation process of the equipment. The results of the main research study are presented in Chapter 4.

3.1.1   Model properties and dimensions

The model was constructed in a centrifuge strongbox. This box has very stiff sides and a bottom panel with a thick glass front. It is constructed in such a way that it will not deflect significantly when a load is applied to the model it contains. With the glass front, the

behaviour of the model could be observed in profile. It also allowed for photos of the model to be taken during testing. Digital Image Correlation, using PIV software, could be used to study in-plane deformations. Figure 3-1 shows the top view of the strongbox and its dimensions. The box is 600 mm long by 400 mm wide, but a compartment divider was inserted to reduce the width to 130 mm to reduce the amount of material required and loads applied during testing. The depth of the model was also restricted to 130 mm. Figure 3-2 subsequently shows the front view of the strongbox. The box was 400 mm deep.
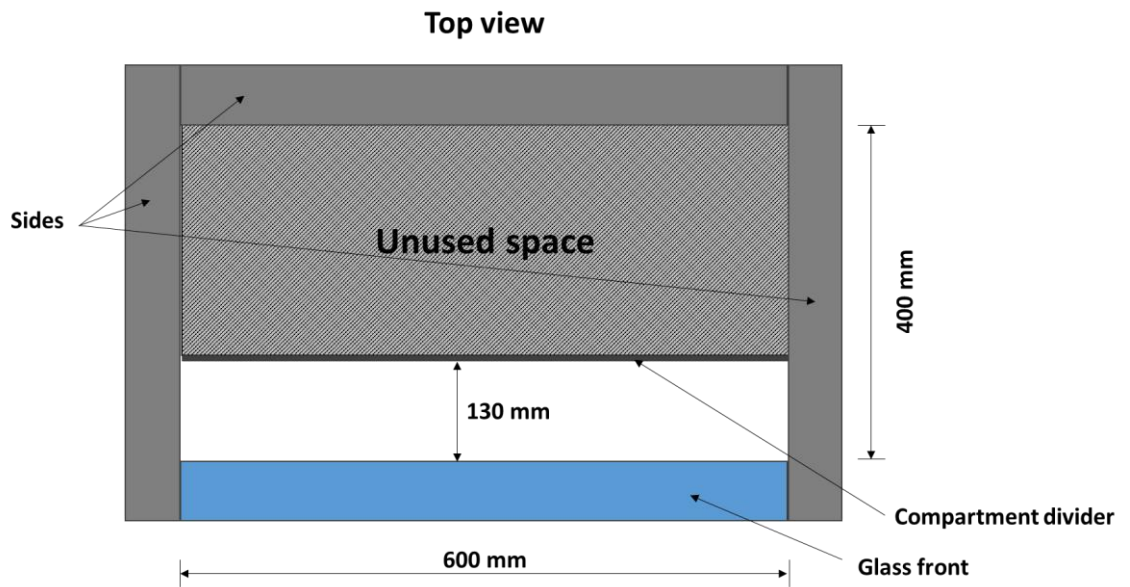
Figure 3-1: Top view of strongbox
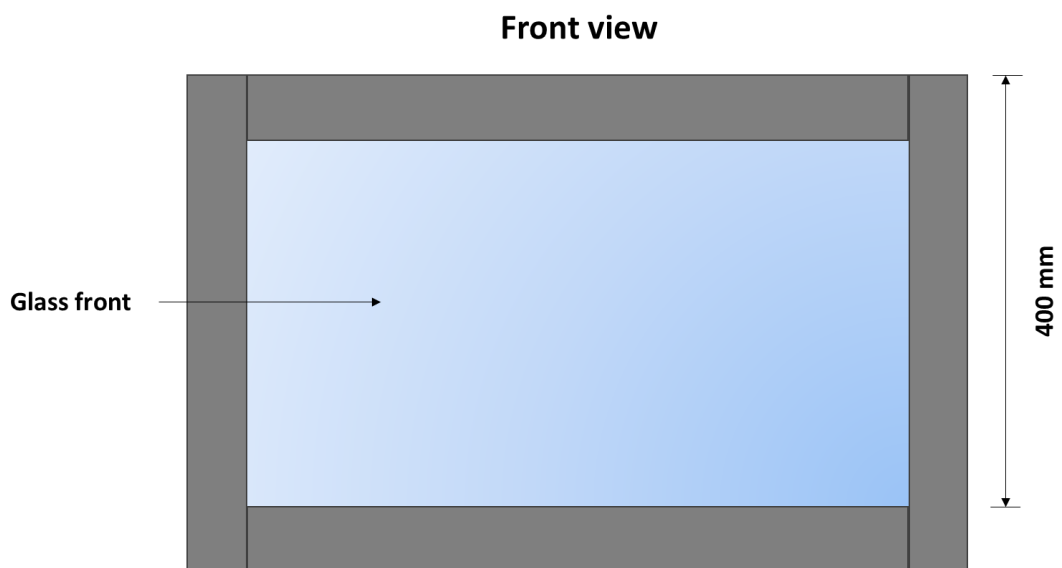
Figure 3-2: Front view of strongbox

The 1:10 scale model was constructed in the front 130 mm wide compartment of the strongbox. A 100 mm subgrade layer was constructed out of fine silica sand that we the same in every test. The sand was prepared to optimum moisture content and compacted to 90 % of its maximum dry density (Mod AASHTO compaction). This was compacted in a single layer. Four base layers of 15 mm each were then placed above the subgrade. Each layer was compacted at optimum moisture content to 95 % of its maximum dry density (Mod AASHTO compaction). The material for the base layers varied for the tests. The variables are given later in this chapter. Figure 3-3 shows the setup of the model in the centrifuge strongbox.

Front view
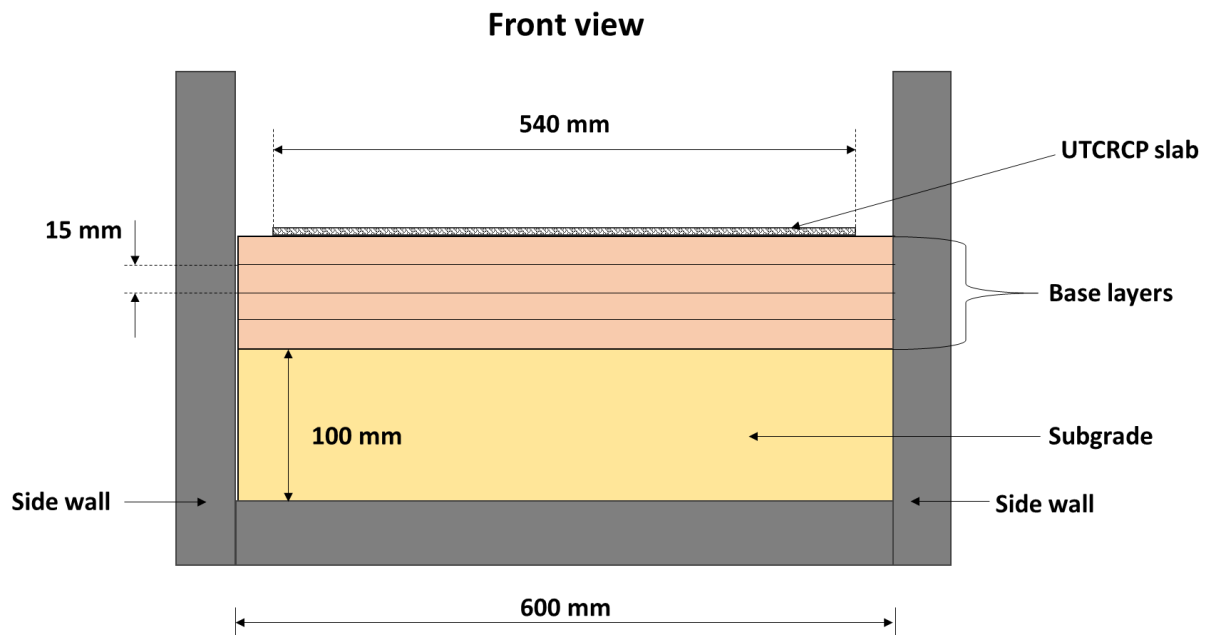
Figure 3-3: Model setup in strongbox

The load was applied to the pavement using a loading bogey that simulated a wheel load in plane strain. A piston, controlled by the hydraulic load actuator, applied the load to the loading bogey which transferred the load on to the pavement stricture. A load cell recorded the load in the piston. Two rubber strips were placed between the bogey and the concrete pavement. The setup used to apply the load to the pavement is shown in Figure 3-4. The loading bogey details are shown in Figure 3-5. An image is shown of the actual loading setup in Figure 3-6.

Front view
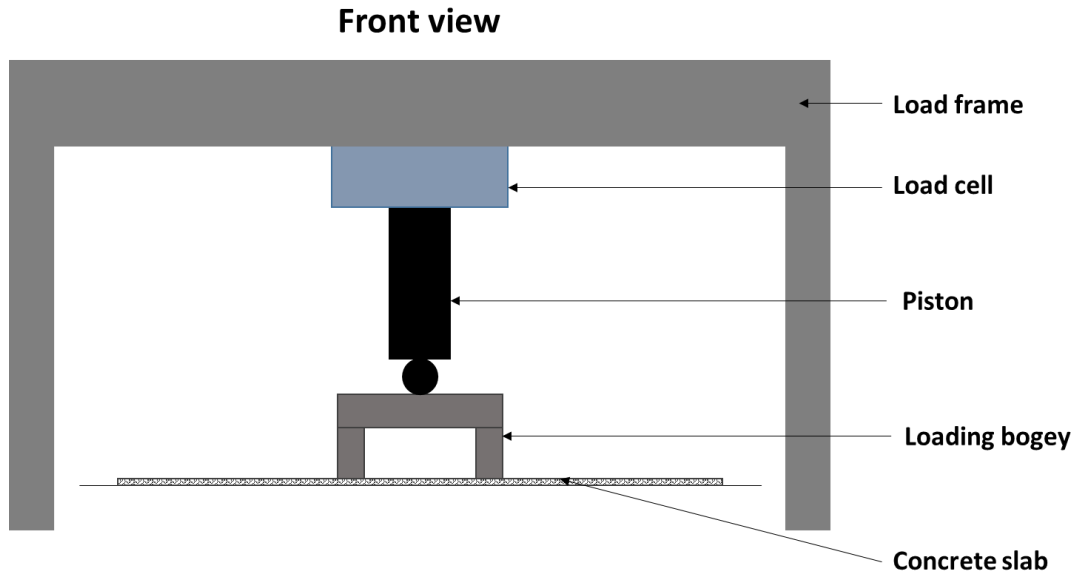
Figure 3-4: Setup used to apply load to the pavement

Top view

Front view
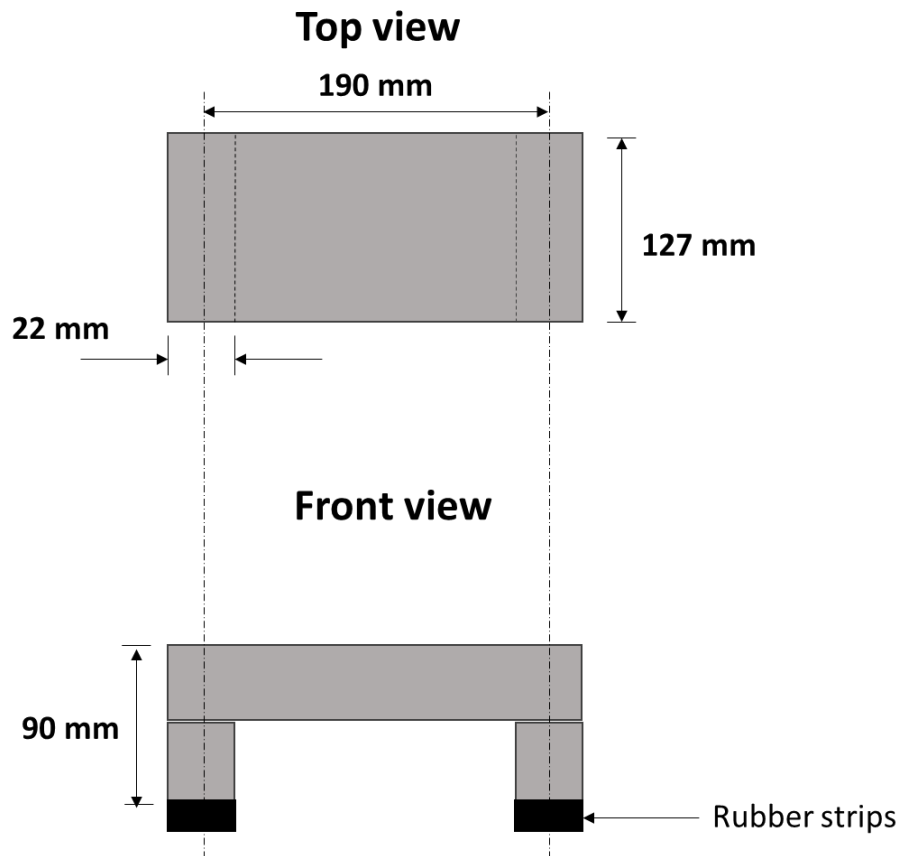
Figure 3-5: Dimensions of loading bogey
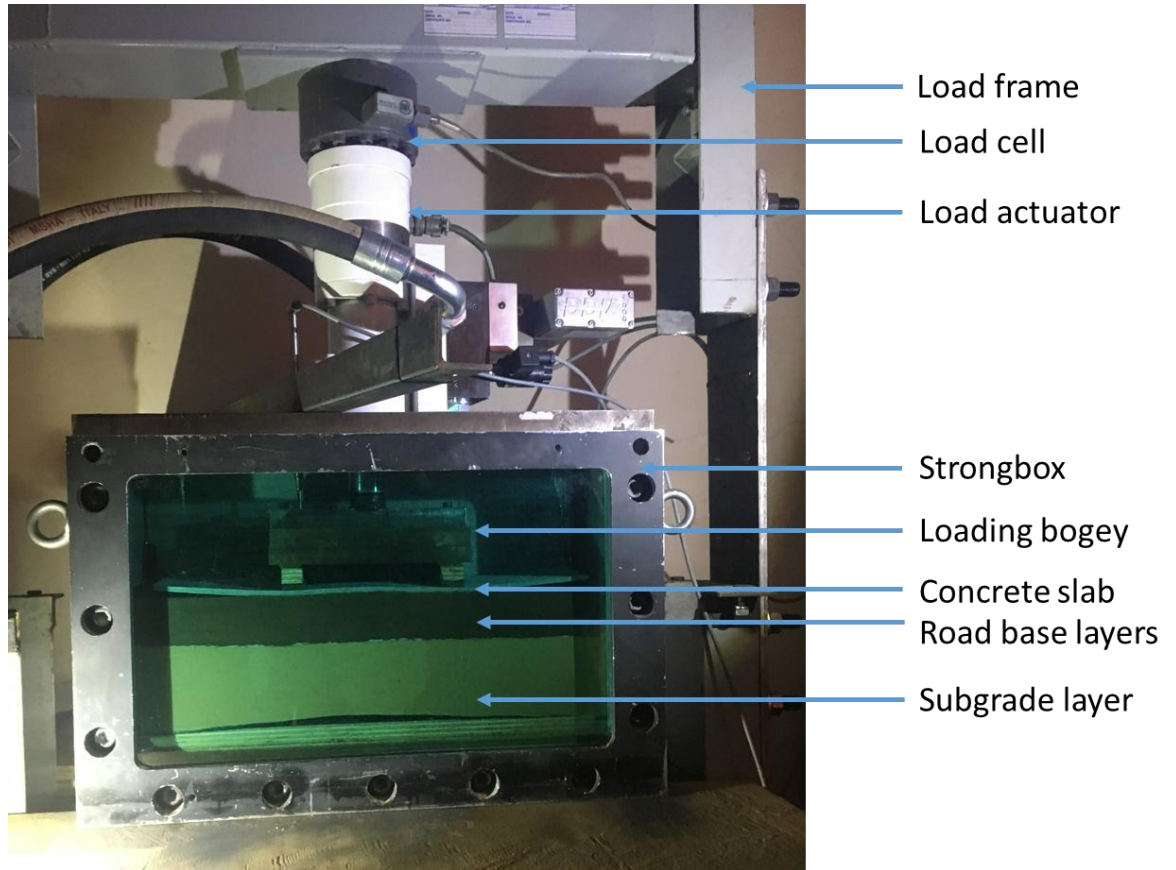
Figure 3-6: Labelled image of loading setup

3.1.2 Hydraulic load actuator

The hydraulic load actuator consisted of a hydraulic piston which was under constant hydraulic pressure supplied by a pump. An image of this actuator is shown in Figure 3-7. The extension and retraction of this piston was controlled by servo valves on either side of the piston. These valves could open and close with the flow direction of the hydraulic fluid determining whether the piston rod would extend or retract. Under displacement control, the reading from an LVDT in the piston rod would be used to control the action of the servo valves. Under load control, the measured load on the load cell would determine the action of the servo valves. The loading capacity of the setup used was 100 kN.
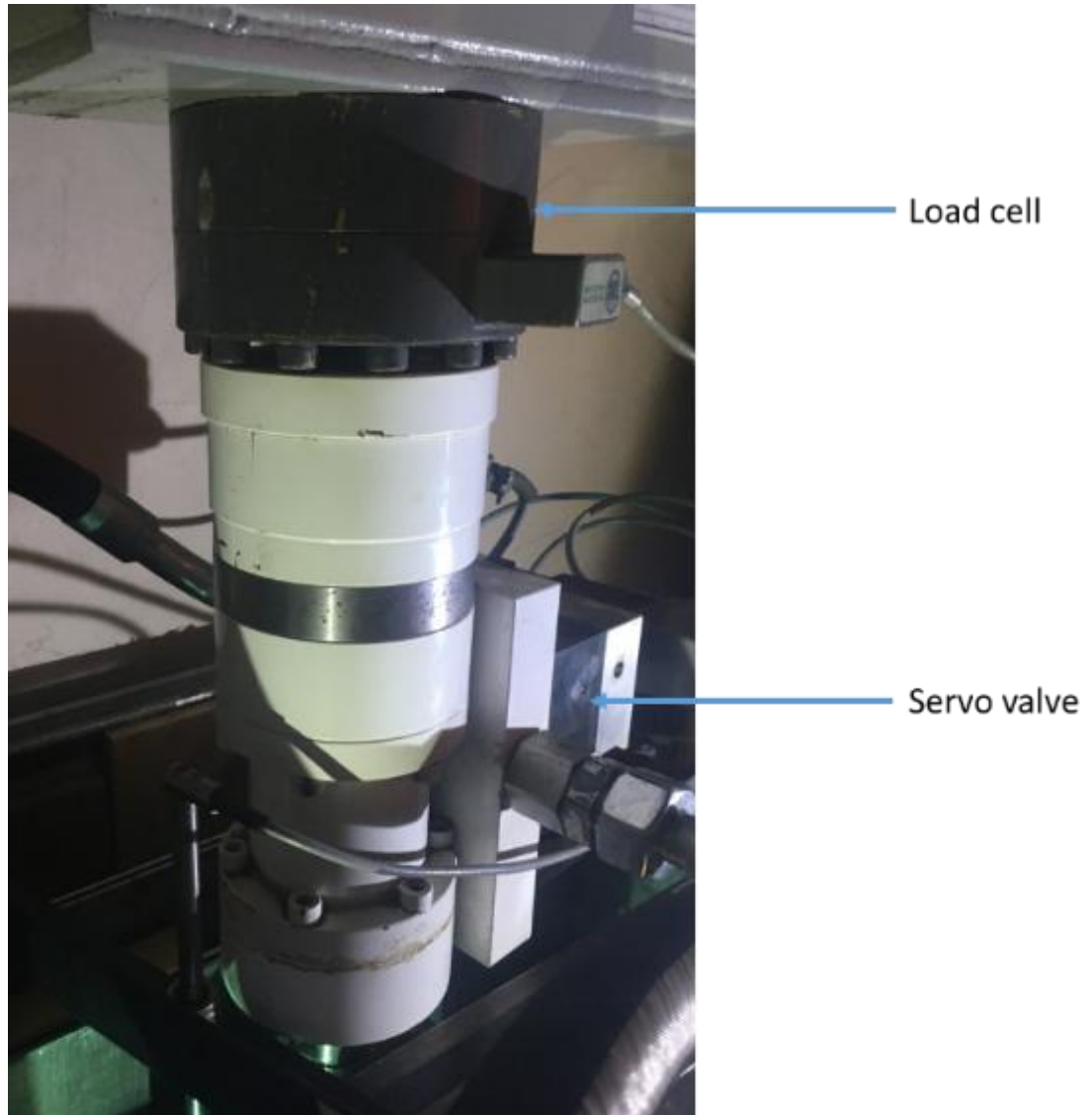
Figure 3-7: Hydraulic load actuator with load cell and servo valve

3.1.3 Precasting of reinforced concrete slab

The thin concrete slab could either be cast on the layerworks of the model (in situ) or it could be precast and then placed on top of the layerworks when a test had to be conducted. Casting it in situ would allow bonding between the slab and the soil below. Precasting the slab would allow better control of curing. Preparing precast slabs means that many slab could be prepared before testing, allowing for a shorter turnaround time between tests. An example of a 1:10 scale precast slab under preparation can be seen in Figure 3-8.
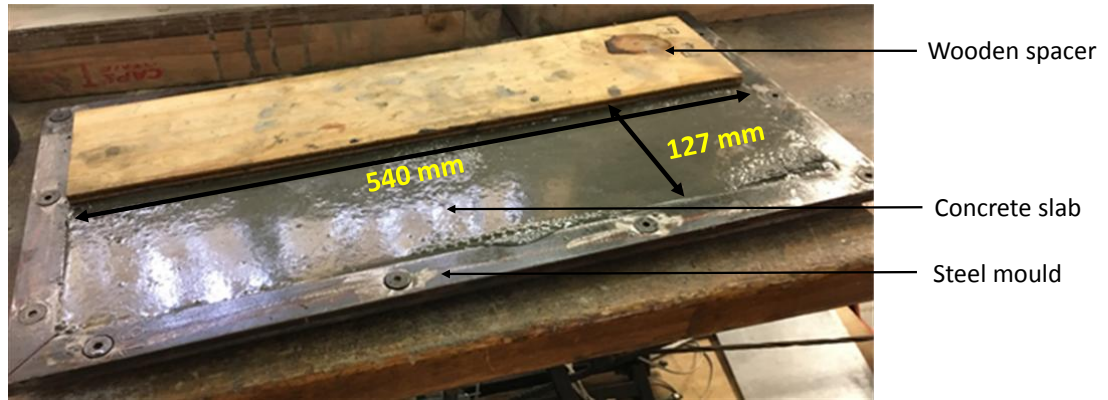
Figure 3-8: Thin concrete slab in precast mould

An experiment was conducted to assess whether the behaviour of a pavement with a precast slab would differ significantly from that with a slab cast in situ. Two 1:10 scale models of UTCRCP were constructed. The models each consisted of a subgrade layer that was 100 mm deep and four base layers that were each 15 mm thick. The subgrade was made of fine silica sand compacted to 90 % of the maximum dry density (mod AASHTO). The base layers were compacted to 95 % of the maximum dry density (mod AASTHO). The concrete slab was cast in situ for the first test and precast and placed on the layerworks for the second test. The model setup can be seen in Figure 3-9.
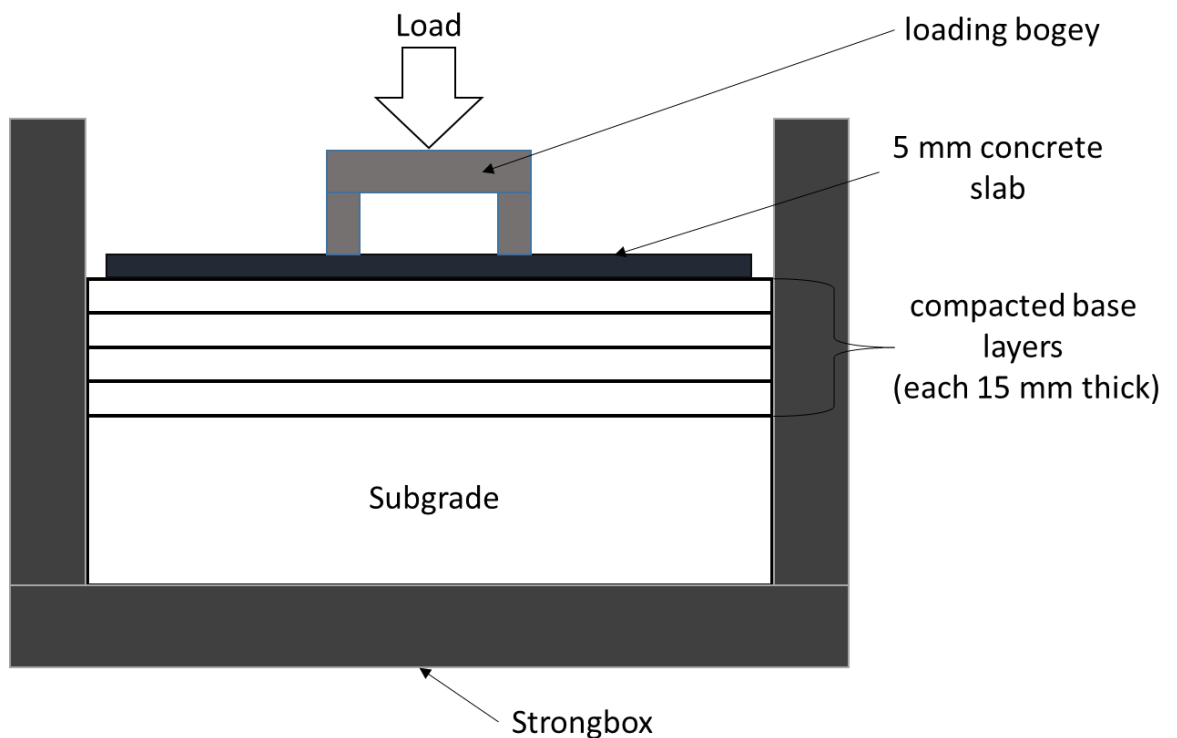
Figure 3-9: 1:10 scale model configuration

Both pavements, one with the slab cast in situ and the other with a precast slab placed in position prior to testing, were tested in the centrifuge at 10g. A double strip load was placed on the pavement to resemble wheel loads using the loading bogey described above. Ten cycles of 3 kN were applied to the pavement. Thereafter, ten cycles of 6 kN were applied. Finally, each pavement was loaded until it was deemed to have failed when large deformations were observed. The loading sequence applied during both tests is shown in Figure 3-10.
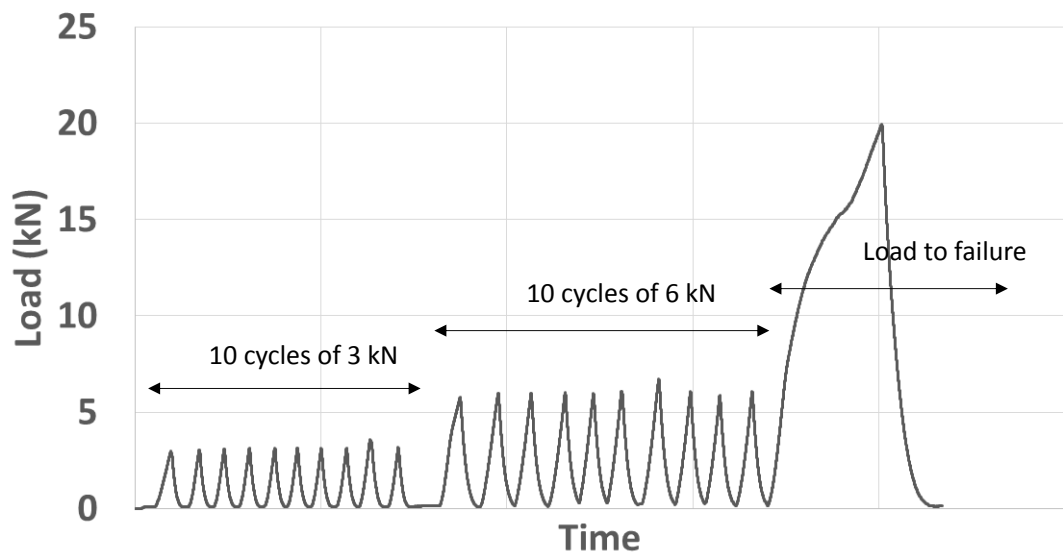
Figure 3-10: Loading cycles imposed

Figure 3-11 shows the load-displacement behaviour of the two pavements, i.e. the cast in situ and precast slabs. Both pavements had a similar stiffness during the first cycle of 3 kN. By the tenth cycle of 3 kN, the pavement with the cast in situ slab had accumulated a slightly higher total displacement than the pavement with the precast slab. It is also evident that the stiffness, indicated by the slope of the linear portion on the load-deformation curve, of the pavement with the precast slab was higher during the tenth cycle of 3 kN than the pavement with the cast in situ slab.

The first and tenth 6 kN load cycle for both pavements is also shown. Again, the load-displacement behaviour for both pavements followed a very similar path during the first 6 kN load cycle. This behaviour was almost identical during the tenth 6 kN cycle. The total accumulated displacement for the two pavements was the same at the end of the tenth 6 kN cycle.

The load-displacement curves for the two pavements, during which load was applied until visible failure of the pavement structure, is also shown. The curves were practically identical

during the first 7 kN. Thereafter, there was only a slight difference in the load-displacement behaviour. The loading of the pavement with the precast slab was ended at a load of 17 kN while the pavement with the cast in situ slab was tested to a load of 20 kN. The difference is because the test was stopped based on visual observation of damage to the pavement which was somewhat subjective. It can be noted that the stiffness during the various cycles reduced once the applied load exceeded the previous highest load experienced by the pavement. This is similar to a virgin compression curve.

The results show that there was no significant evidence from this experiment to indicate that precasting the slab and placing it on the layerworks would result in a significant difference in behaviour to casting the slab in situ. If casting the slab in situ resulted in better bonding between the layerworks and the concrete slab, this had no noticeable effect on the load-displacement behaviour when compared to a pavement where a precast slab was placed on top of the layerworks. For ease of model preparation it was therefore decided that the UTCRCP would be constructed using slabs that were precast and placed on top of the layerworks. This allowed better control of the casting and curing process. It also allowed the slabs to be manufactured concurrently to the pavement tests which were being conducted.
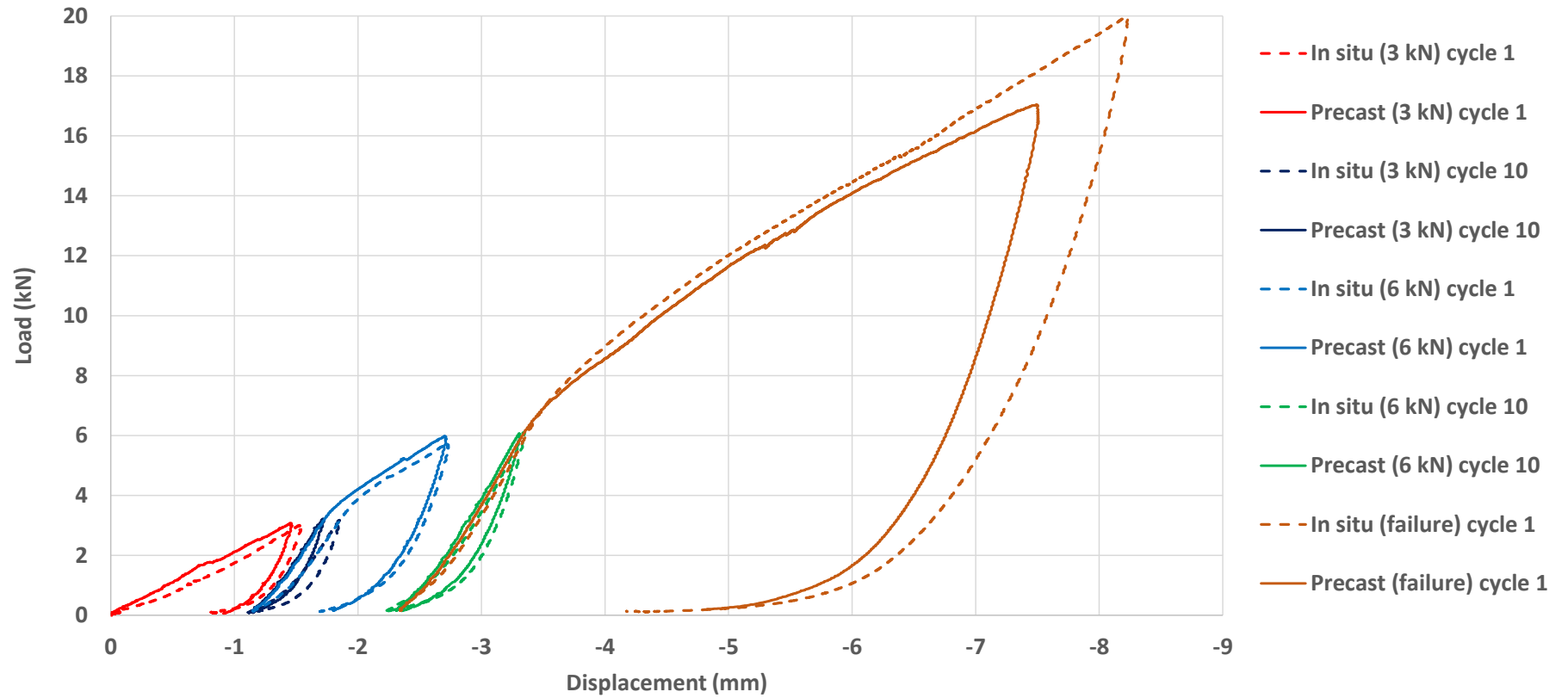
Figure 3-11: First and tenth cycles at 3 kN for slab cast in situ and precast slab

3.1.4 Model pavement response at normal gravity

Self-weight is an important factor to consider when modelling geotechnical problems using physical models (Schofield, 1980). This is because the behaviour of geotechnical materials is heavily dependent on their stress state imposed on the soil. The stress level is an intrinsic property of model size. If the model is scaled down, the stresses in the soil become unrealistically low. It is therefore necessary to keep the stress state in the soil the same by increasing the self-weight of the model. This can be done in a centrifuge.

Due to the cyclic nature of the tests that had to be done for this research and the equipment available in the Geotechnical Centrifuge at the University of Pretoria, tests had to be done to explore the possibility of conducting experiments at normal acceleration. This was because equipment capable of performing large numbers of cyclic loads at varying frequencies was not available on the centrifuge. Testing in the centrifuge would severely limit the number of load cycles that could be applied. The effect of testing at normal gravity therefore had to be considered.

An experiment was conducted in which two UTCRCP models were prepared, with one tested at normal gravity and the other at 10g. Each model consisted of four layers of silica sand compacted at optimum moisture content to 95 % of the maximum dry density (Mod AASHTO). A scaled-down reinforced slab was placed on top of the layerworks. A monotonic load test, under displacement control, was done on each model. Figure 3-12 shows the load-displacement curves for these two tests.
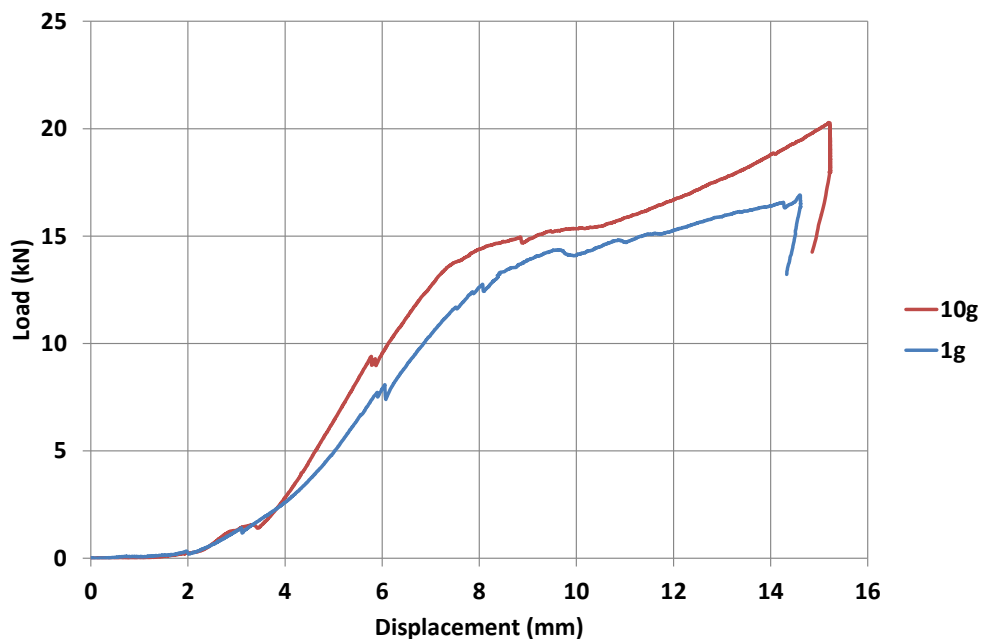
Figure 3-12: Load-displacement data for tests conducted at 10g and at 1g

It can be seen that the load-displacement behaviour for the two tests was similar. The general shape of the curves was the same. The model tested at 10g had a slightly stiffer response than the one tested at 1g. For the same load, there is approximately a 5 % difference in in the linear portion of the load-displacement curves.

There are various factors that influence the effective stress in the granular medium within a pavement structure. There is the effective stress caused by the self-weight of the material which increases with depth. There is also the effective stress caused by confinement. The confining stress can be due to compaction which causes horizontal confinement. Then there are the effective stresses caused by loading the pavement. The stresses in a pavement granular medium that are caused by compaction and loading are higher than the stress induced by self-weight. The stress due to self-weight is low because of the shallow depth of the pavement layers below the ground surface. The small different between the load displacement curves in Figure 3-12 indicates that testing a scaled-down model at 1g would still reasonably reflect the behaviour of the full-scale pavement without the need to test at 10g in a centrifuge. The test described in this report were therefore carried out at normal gravity.

3.2   MATERIAL PROPERTIES

In this section the material properties of the pavement models are given. This includes the soil properties along with those of the concrete. Various preliminary tests are described done to determine material properties and the model setup.

3.2.1 Soil properties

3.2.1.1 Soil types

In this section, the three soils used in the model study are discussed. One is a fine silica sand which is often used in scaled-down and centrifuge modelling at the University of Pretoria. The properties of this fine silica sand are well understood. The other material is a typical road building material which is used in various layerworks of road pavement. The grading of this material ranges from larger cobbles down to finer material, i.e. silts and even a small amount of clay. This material, a weathered dolerite gravel, was acquired from a road construction site on the N1 highway near Trompsburg in the Free State, South Africa. It was classified on site as a G7 base material. This means that it is a natural material (soil, sand or gravel) with a plasticity index of less than 12 and a grading modulus between 0.75 and 2.7 (COLTO, 1998). The MOD AASHTO density was 2385 kg/m^3 and the optimum moisture content was 5.3%. The third material described in this section is a graded gravel. This was obtained from scaling

down the material obtained from site by truncating all the material larger than 4.75 mm. The scaling down of the material obtained from the road construction site to produce the graded gravel is discussed in more detail in Section 3.2.2. Only the graded gravel and the fine silica sand were used in the experimental work of this research. The two soil types that were used can be seen in Figure 3-13.

Figure 3-13: Fine silica sand (left) and graded gravel (right)

3.2.1.2 Particle size distributions

Figure 3-14 shows the grading curves of both the material obtained from the road building site as well as the graded gravel obtained from truncating the site material at 4.75 mm.
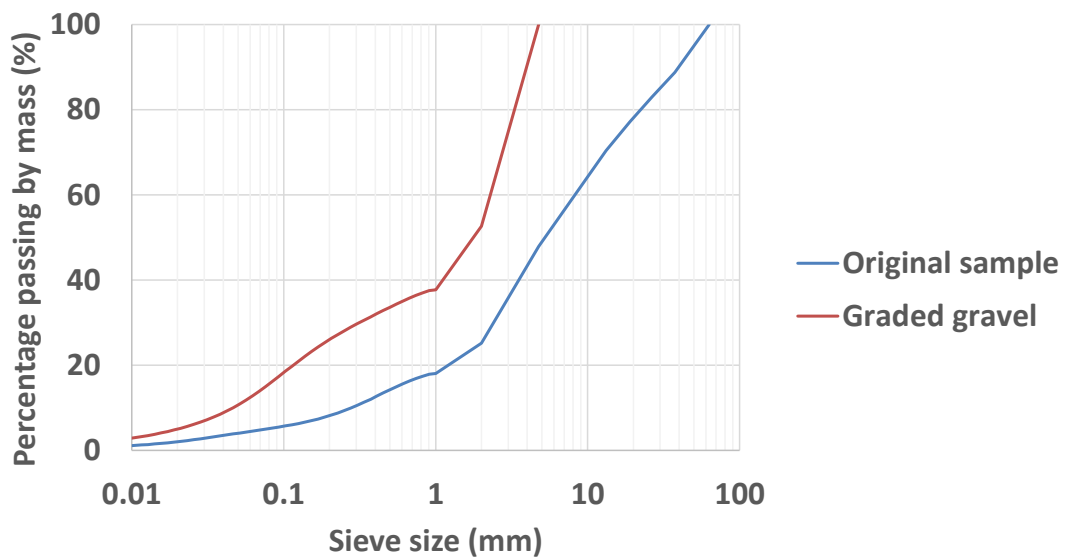
Figure 3-14: Particle size distribution of original sample as well as the scaled-down sample

In Figure 3-15, the grading curves for the fine silica sand and the graded gravel can be seen. The fine silica sand had a maximum particle size of 1 mm. The sand was used to construct the subgrade layers in the experiments to identify the mechanisms at play under ultra-thin pavements. The behaviour of this sand is well understood and has been used frequently in scaled-down centrifuge testing at the University of Pretoria. This allowed comparison to previous tests done on UTCRCP using this material. The graded gravel was used to investigate the difference in behaviour when using a more realistic road construction material.
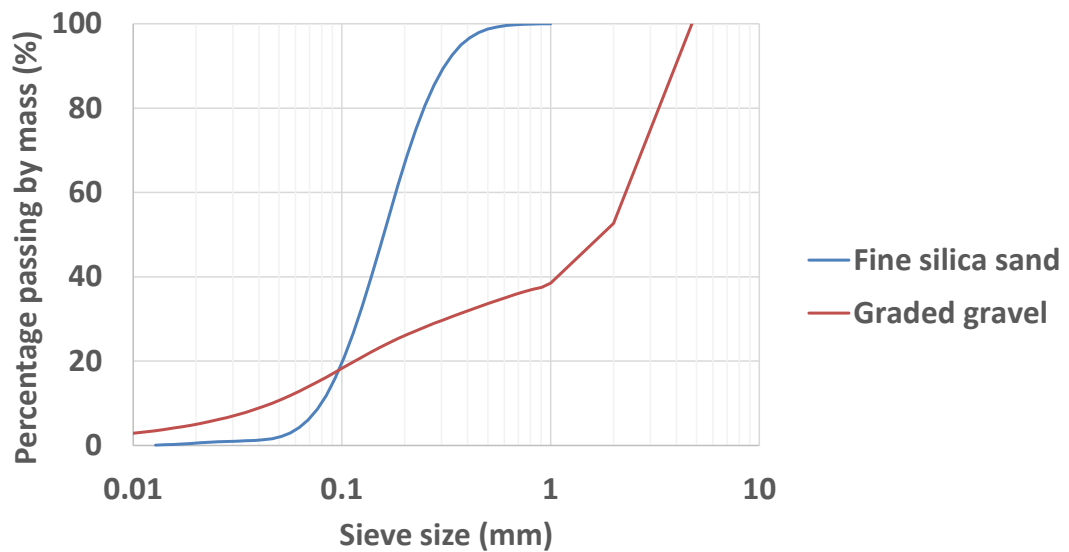
Figure 3-15: Particle size distribution of the fine silica sand and the graded gravel

3.2.1.3 Compaction properties

Since the original material obtained from site was not used at all in the experiments conducted, it is not discussed further. The properties of the materials used in the experimental work are given in Table 3-1. The particle density was derived from data obtained using a gas pycnometer.

Table 3-1: Material properties of the fine silica sand and the graded gravel

Material	Fine silica sand	Graded gravel
Maximum dry density (kg/m^3) (Mod AASHTO)	1714	2238
Density at 95 % of maximum dry density (kg/m^3)	1628	2126
Optimum moisture content (OMC) (%)	8.7	5.8
Degree of saturation (S_r) at OMC at 95 % of maximum dry density	0.363	0.507
Particle density (S_G)	2.67	2.81

The maximum dry density and optimum moisture content of the material was determined in accordance to TMH1 (A7). This was for a gravel truncated to 4.75 mm. The scaling of the material is discussed in detail in Section 3.2.2. Five layers of approximately 1 kg each were compacted with 56 blows per layer in a 152.4 mm diameter mould by a 4.536 kg hammer falling through a height of 457.2 mm. Each layer was between 25 and 30 mm thick. The results of the Mod AASHTO density test for the fine silica sand are given in Figure 3-16 and the results for the graded gravel are given in Figure 3-17.
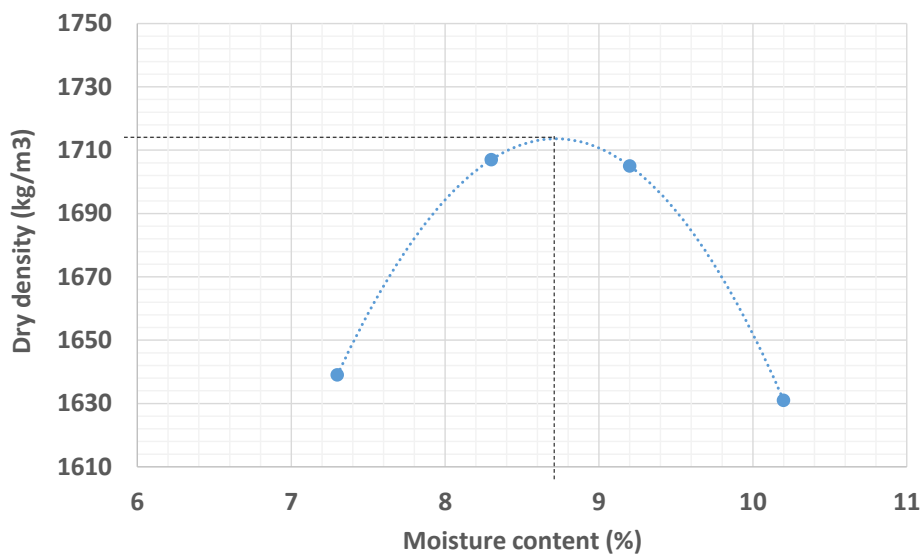
Figure 3-16: Results from Mod AASTHO compaction density test for fine silica sand
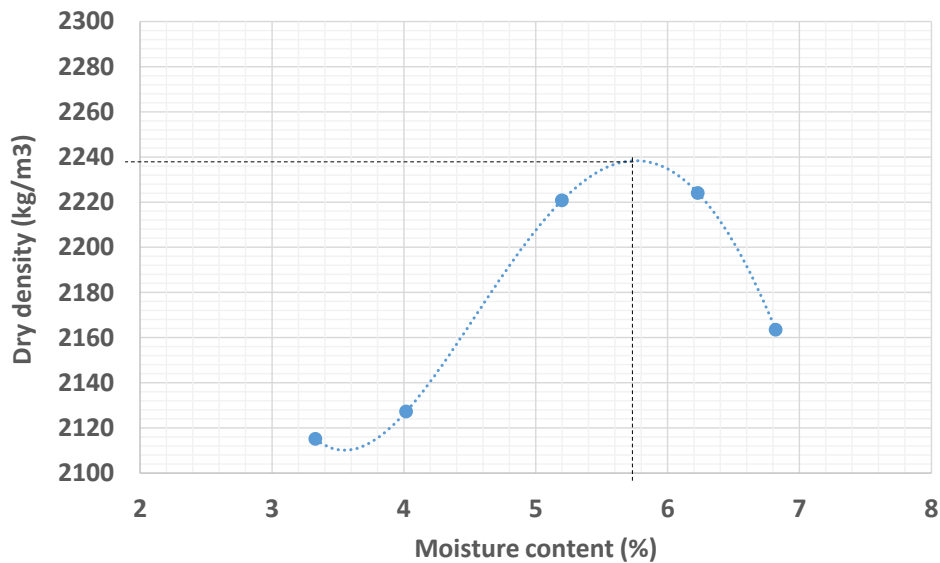
Figure 3-17: Results from Mod AASTHO compaction density test for graded gravel

3.2.1.4 Soil water retention curves

Understanding the water retention behaviour of a soil, as well as the associated change in suctions, is important in the analysis of unsaturated soils. The soil water retention curves (SWRC) were obtained for the two soil types during a drying cycle. This was done by preparing a sample of each soil at its maximum dry density (Mod AASHTO), applying sufficient moisture to saturate it and then drying it out while measuring pore pressures with tensiometers embedded in the sample. Tensiometers are piezometers capable of measuring negative pore water pressure in a soil (they will also register positive pore pressure, if present). All this was done while continuously measuring the mass of the sample so that the change in moisture content could be known. As a check, another data point was obtained using the filter paper method of suction measurement (Hamblin, 1981 and Chandler & Gutierrez, 1986) for the graded gravel. That the single data point from the filter paper method plots close to the dry out curve for the graded gravel, this gives confidence in the result obtained from the tensiometers for the soil water retention behaviour of the graded gravel. Figure 3-18 shows the SWRC for both materials along with the single data point obtained from the filter paper method for the graded gravel.
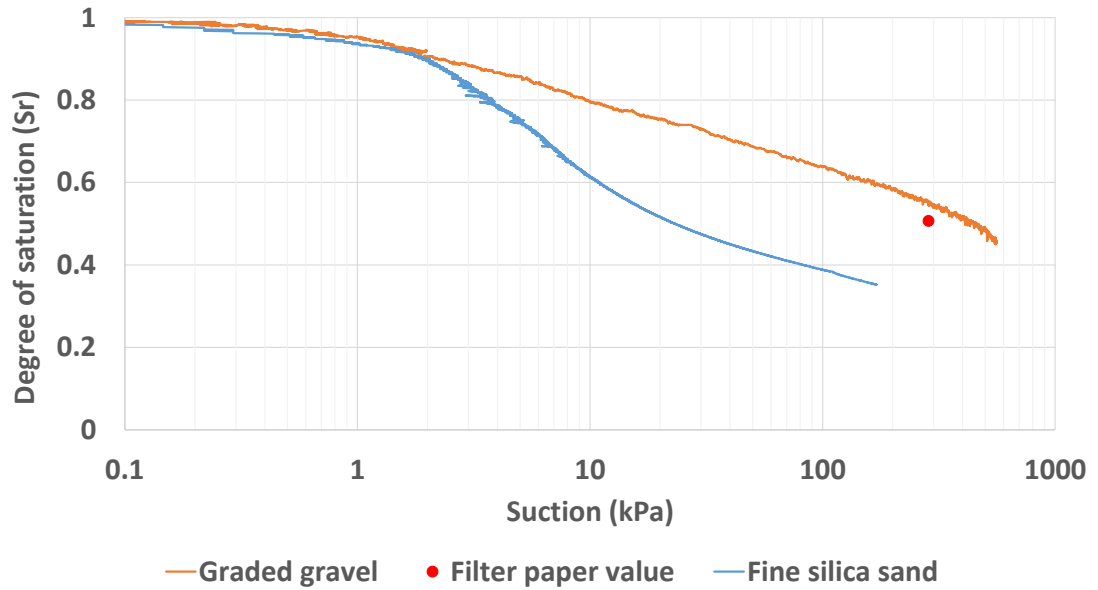
Figure 3-18: Soil water retention behaviour for the fine silica sand and the graded gravel

It is evident that the graded gravel generates higher suctions in the range of lower moisture contents than the fine silica sand. This is to be expected as the graded gravel contains a larger portion of fine material passing the 0.1 mm sieve (Figure 3-15). The graded gravel has a smaller volume of voids at the density to which it was compacted. This also contributes to the higher suctions that were generated.

3.2.2 Scaling down of the PSD

The particle size distribution (PSD) of the graded gravel, obtained from a road construction site near Trompsburg in the Free State, is given in 3.2.1. For compaction purposes, the maximum particle diameter of the material in road pavement layerworks should be restricted to not more than two thirds of the layer thickness (COLTO, 1998). For the 1:10 scale model with layerworks 15 mm thick, the maximum particle size would have to be restricted to 10 mm. For the original material, almost 40 % of the material was retained on the 10 mm sieve. The typical size of the largest portion of the material obtained from site is shown in Figure 3-19.

Figure 3-19: Cobble from material obtained from road building site

There are two commonly used methods which can be used to change the grading of a material in such a way so as to limit the maximum particle size that are often used in centrifuge testing. The "truncated" scaling method involves removing all the material over a certain particle size and the "parallel" scaling method that results in a PSD curve that is parallel to the PSD of the original field sample. The sequence of grain sizes is maintained and the result thereof is a true scaling of the material (Lee, 1986 and Verdugo & Gesche, 2003).

When down-scaling the grading of a material, it is important to realise that the various portions of the material in the grading curve do not all have equal contribution on the behaviour of the material. This can be illustrated with clay. A small change in the amount of clay in a material can have a significant change in the behaviour of that material. When using the parallel grading technique, the fine material is changed from silt to clay size. This is a disadvantage of using this method for scaling down materials as the behaviour of clays are completely different from that of a silt.

An experiment was conducted to investigate the influence on the strength and stiffness of the material when truncating the grading curve by limiting the maximum particle size. This was done by preparing three samples, each one from the original material obtained from site, but truncated to various maximum particle sizes. Sample A was truncated to 6.35 mm, Sample B

to 2.00 mm and Sample C was truncated to 1.18 mm. The grading curve of the original sample, as well as the grading curves of the truncated samples are shown in Figure 3-20.
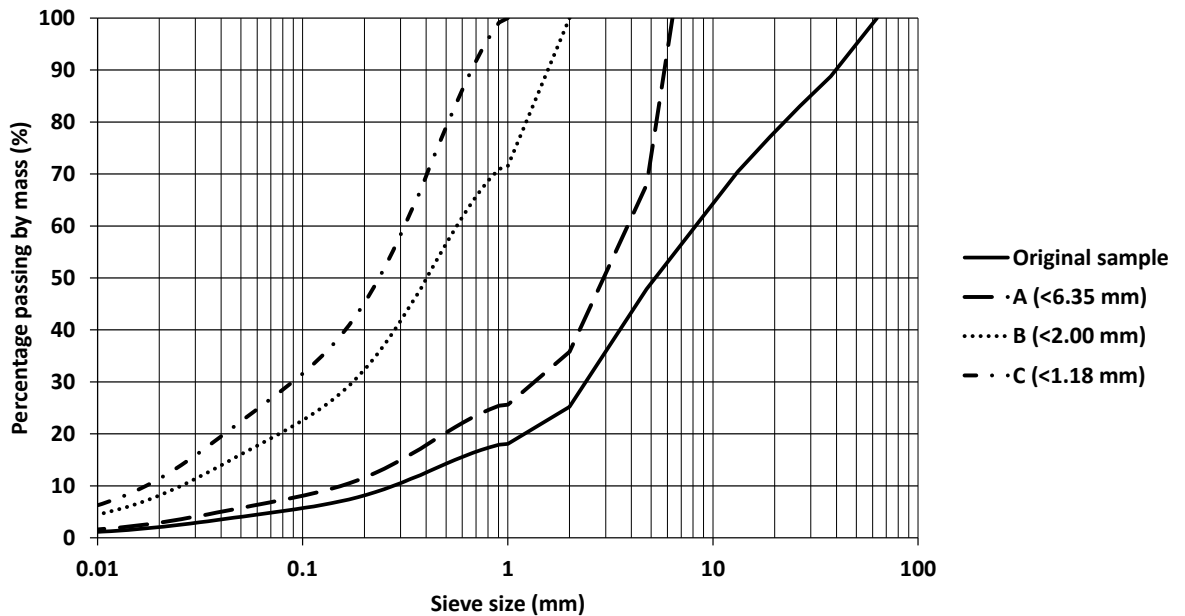
Figure 3-20: Grading curves of original sample along with truncated samples

Consolidated undrained triaxial tests were done on cylindrical samples, measuring 50 mm in diameter and 100 mm high, with the measurement of pore pressures to allow effective stress parameters to be measured. Specimens were prepared to a target density of 2000 kg/m^3. The specimen details are given in Table 3-2. The specimens were saturated until a *B*-value of at least 0.96 was obtained and then consolidated to effective stresses of 100, 300 and 500 kPa. The specimens were sheared at a rate of 0.1 mm/min. This rate was determined based on the time taken to consolidate so as to be slow enough to allow pore pressure equalisation during shearing. The load, axial displacement and pore pressures were recorded.

Table 3-2: Properties of prepared specimens

Sample	Dry density of prepared sample (kg/m³)	Compaction moisture content (%)
A_300 kPa	2009	4.8
A_500 kPa	2015	4.8
B_100 kPa	1980	7.4
B_300 kPa	1964	7.4
B_500 kPa	1975	7.4
C_300 kPa	1997	6.6
C_500 kPa	1997	6.3

Two parameters were considered important in this investigation to determine the effect of scaling and the soil properties. The shear strength of the soil, which determines the load carrying capacity of the soil, as well as the failure mechanism that will develop within the soil, was the first parameter. The second important parameter was the stiffness of the soil. This determines the deformability and compressibility of the soil. This is important because road pavements experience recoverable and irrecoverable deformations which depend partly on the stiffness of the soil.

The shear strength was determined by plotting the stress paths of each triaxial test in s'-t invariant space and calculating the friction angle (ϕ). In s'-t space the friction angle is calculated as follows:

$$\phi' = \sin^{-1}(\alpha)$$

Where α is the slope of the failure envelope in s'-t space.

Figure 3-21 shows the stress paths of the two specimens tested of Sample A. One was tested at a confining pressure of 300 kPa and the other at 500 kPa. The Mohr-Coulomb line was fitted through the estimated failure points. Sample A showed evidence of contractive behaviour at shear failure (stress paths turning towards the left).
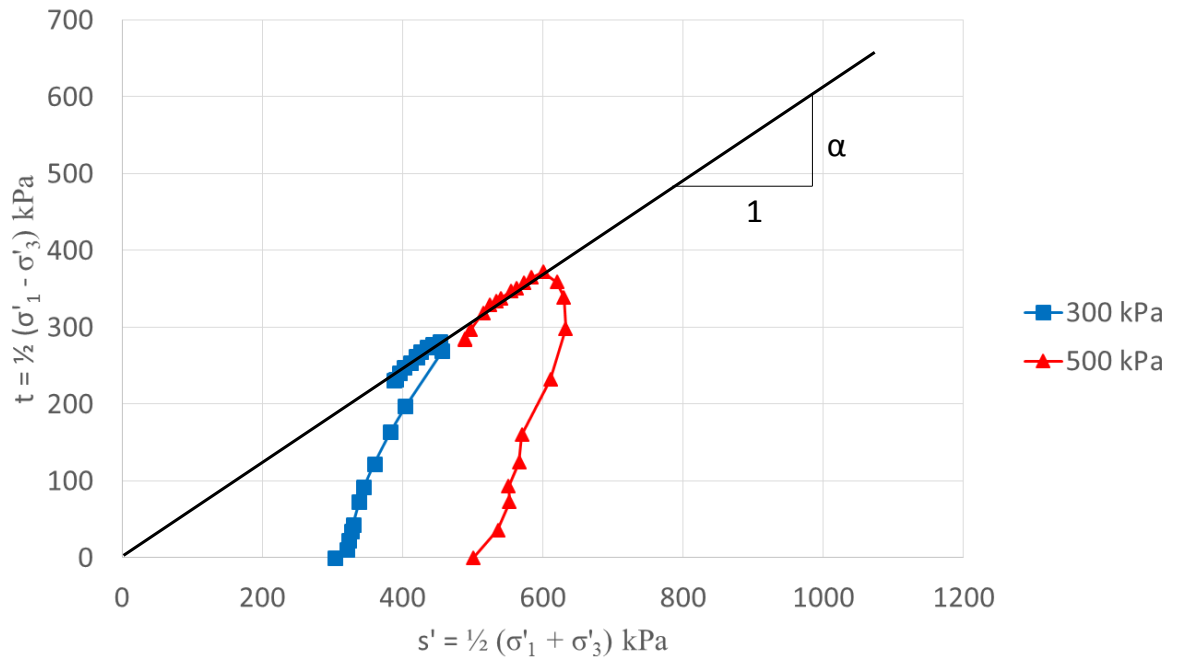
Figure 3-21: Stress paths for Sample A

Figure 3-22 shows the stress paths and estimated Mohr-Coulomb failure envelope for Sample B. For Sample B, specimens were tested at confining pressures of 100, 300 and 500 kPa. Sample B displayed dilative behaviour at shear failure (stress paths turning towards the right).
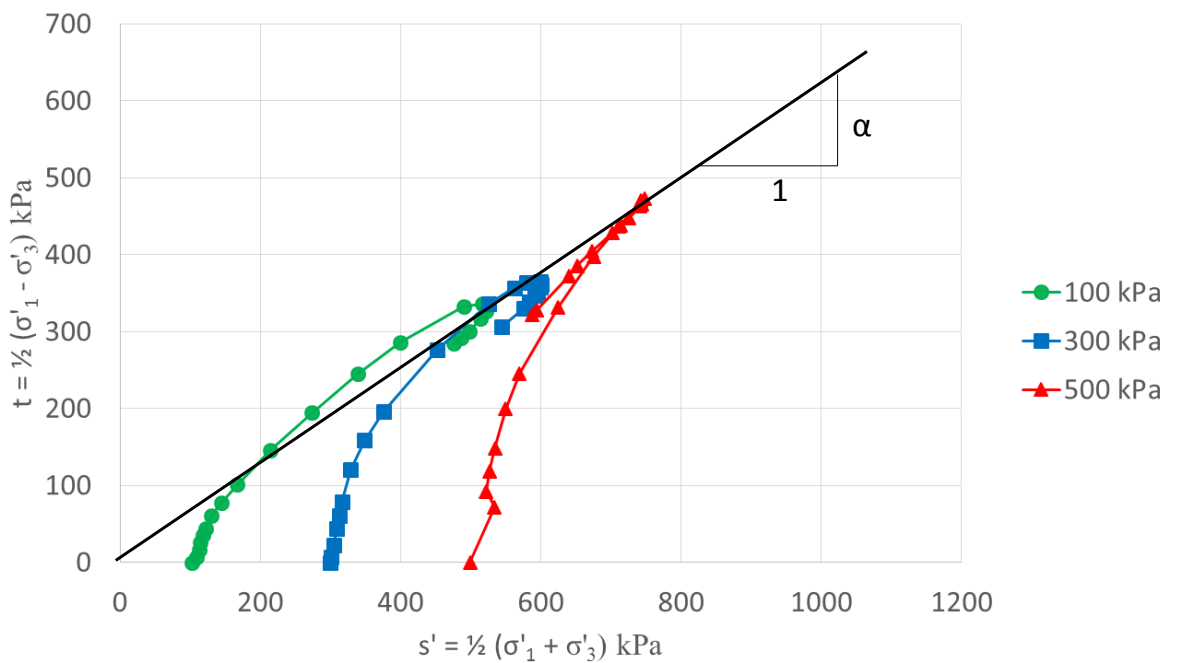
Figure 3-22: Stress paths for Sample B

Figure 3-23 shows the stress paths of two specimens of Sample C tested at confining pressures of 300 and 500 kPa. Sample C, like Sample B, showed evidence of dilative behaviour during shearing failure.
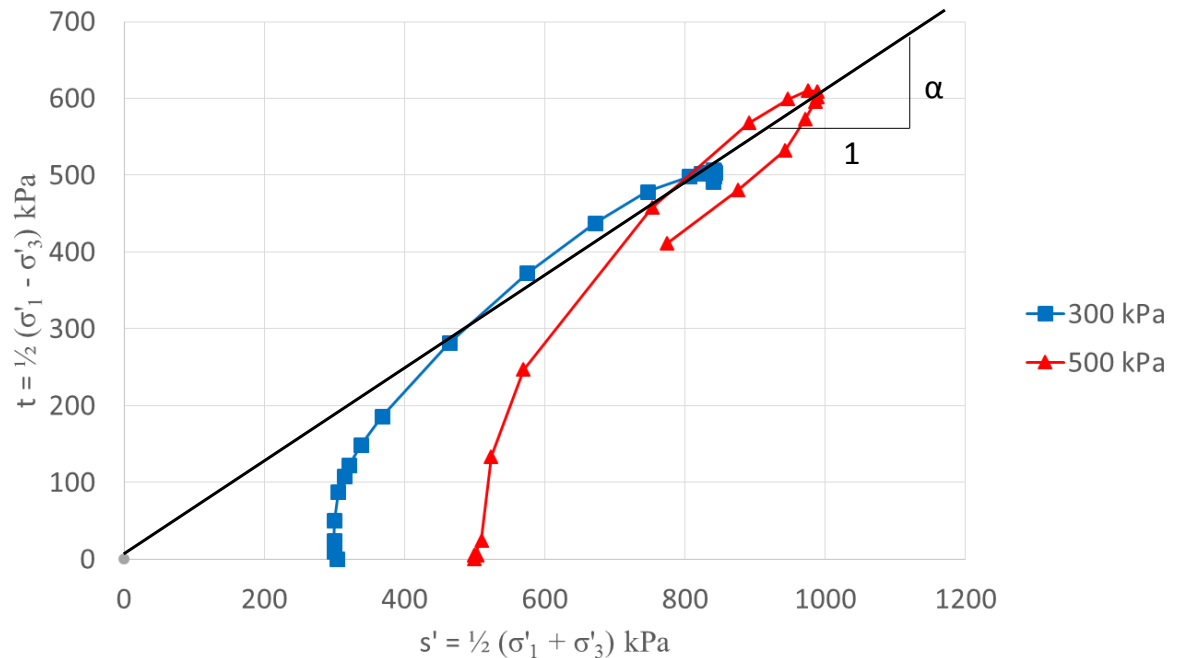
Figure 3-23: Stress paths for Sample C

Although some samples dilated while the other contracted, the friction angles were calculated for the three samples and were all found to be within a narrow range of 38.5° and 39.5°. This indicates that truncating the particle size distributions of the materials did not significant influence the friction angle.

The stiffness of the specimens was calculated from the axial strain and deviatoric stress data obtained during the triaxial tests. Because the stiffness of a soil is inherently dependent on the confinement of the soil, the results of the triaxial tests were grouped according to confining pressure. The Young's modulus could then be calculated as the slope of the linear portion of the stress-strain curves. Figure 3-24 shows the calculation of the Young's modulus from the slope of the linear portion of the stress-strain curves of the three samples. This is shown for the three specimens sheared at a confining pressure of 500 kPa. Figure 3-25 shows the calculation of the Young's modulus from the slope of the stress-strain curves of the specimens tested at a confining pressure of 300 kPa. Figure 3-26 shows the same for the one specimen tested at a confining pressure of 100 kPa.
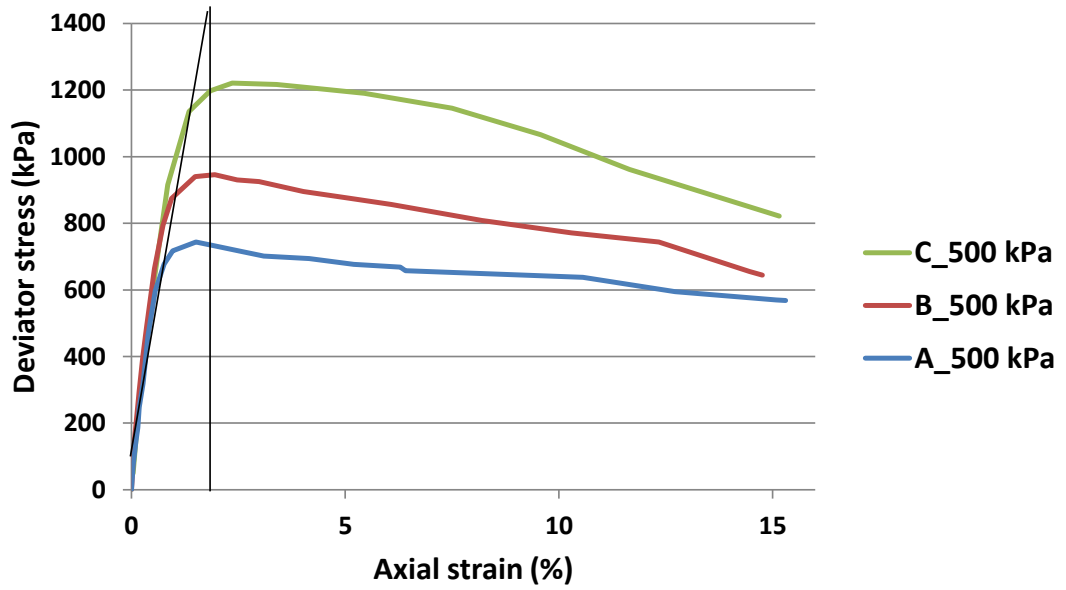
Figure 3-24: Stiffness of three specimens with different grading at a confining stress of 500 kPa
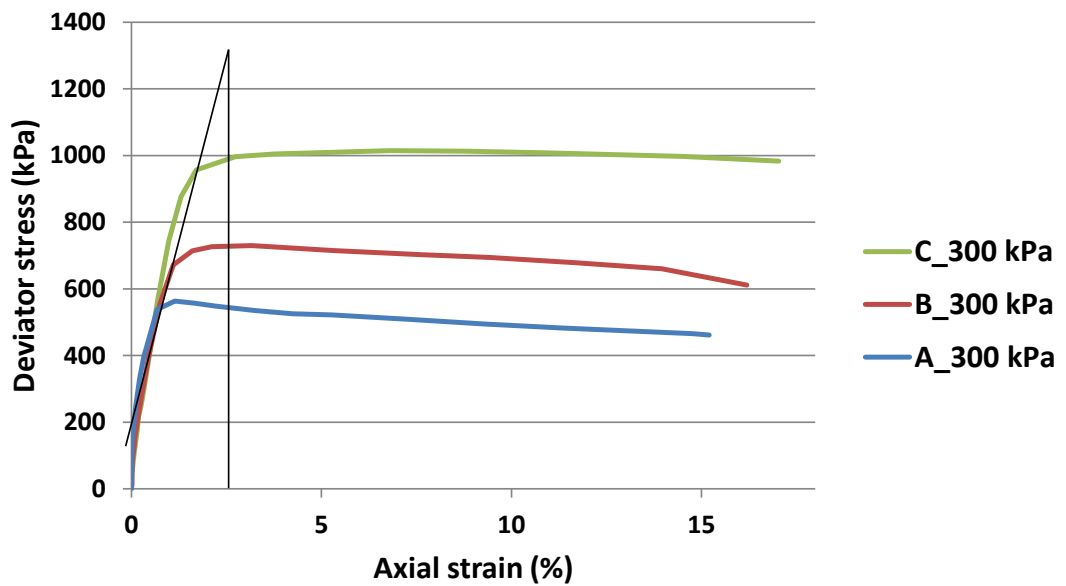
Figure 3-25: Stiffness of three specimens with different grading at a confining stress of 300 kPa
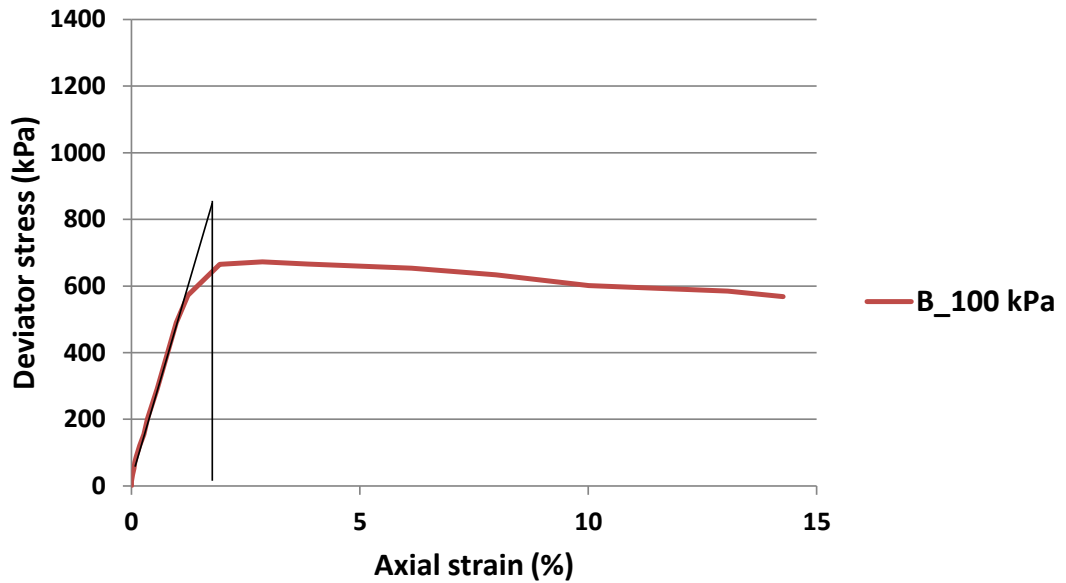
Figure 3-26: Stiffness of the specimen tested at a confining stress of 100 kPa

There was a clear relationship between confining pressure and the Young's modulus of the samples, as seen in Figure 3-27. However, at the same confining pressure, the samples all had a very similar Young's modulus.
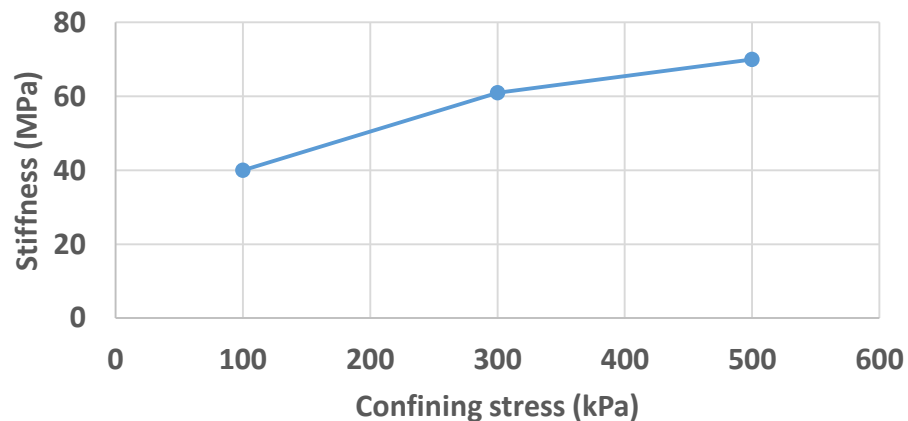
Figure 3-27: Relationship between stiffness and confining pressure

In addition to the triaxial test, a cobble (75 mm in diameter) as well as a portion of the finest material from the material obtained from site was taken for X-ray diffraction to determine their mineralogy. This was done to determine to what extent the mineralogy of the material was changed if the portion with the larger particles was removed. A road building material, such as the G7 used in this test, is often a blended material in which gravels, sands and finer material are mixed together. These may not necessarily all come from the same source and may therefore have different mineralogy. The coarser particles could compose of a different

mineralogical composition to the fines. Removing some of the coarse material could therefore change the overall mineral composition of the mixed material. This would be of particular interest if the material would be used in a chemically stabilised base layer. The results of the XRD analysis are shown in Figure 3-28. Of the minerals listed the one with the greatest proportional change was smectite. This mineral represents the clay portion of the material. The portion of clay mineral in the fine material was almost 8 % higher than the stone.
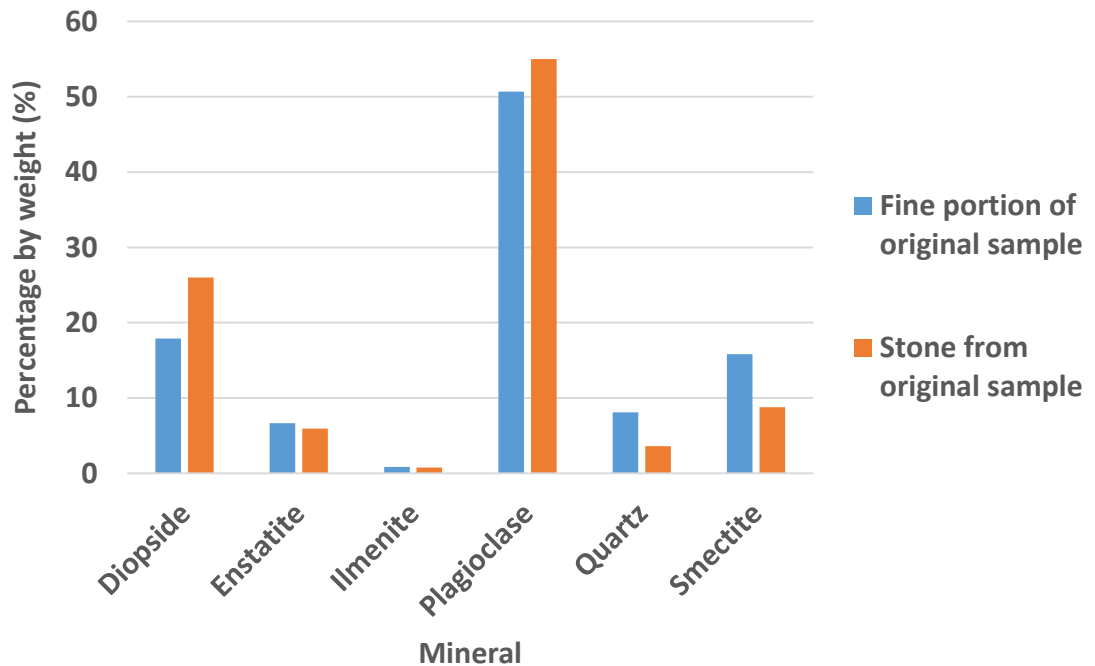
Figure 3-28: XRD results for the finest and coarsest portion of the material obtained from site

The following could be concluded from this study:

1. The friction angle (ϕ) of the material measured in undrained triaxial tests was not influenced by the maximum particle size for the range of particle grading considered.

2. The stiffness of the material was independent of the maximum particle size, but directly proportional to the confining stress.

3. The clay portion, which can often determine the behaviour of a material, will increase proportionally as the larger grains are removed to scale-down the material.

It was therefore decided that the grading of the original material obtained from site could be truncated so that the maximum particle size would be small enough to allow adequate compaction in the base layers of the 1:10 scale model base layers. The maximum dry density

(Mod AASHTO) and the optimum moisture content of the truncated material would have to be determined.

3.2.3 Reinforced concrete slab

Table 3-3 gives the concrete mix design that was used for the slabs.

Table 3-3: Mix design for concrete slab (Kearsley et al., 2014)

Material	Quantity (kg/m³)
Cement (CEM II 42.5 R)	450
CSF (silica fume)	50
Water	210
Dolomite sand (<1.18 mm)	1850
Micro steel fibre	80
Chryso Premia (plasticizer)	10
Chryso Optima (plasticizer)	10

As discussed earlier, the slabs were precast in a mould. This was done in the following steps:

1. The materials in Table 3-3 were mixed in a concrete mixer

2. Half the mix was placed in the prepared mould which was then vibrated on a vibrating table to ensure an even spread

3. The steel mesh, which had been soaked in diluted acid for an hour, was then placed in the mould on top of the concrete

4. The second half of the concrete mix was then placed in the mould on top of the mesh and vibrated to ensure an even spread

5. The mould with the wet concrete was covered with a plastic sheet and left to harden for 24 hours

6. After 24 hours, the slab was removed from the mould and placed in a curing bath at 25 °C for 27 days and then removed

The dimensions of the slab and the steel mesh are given in Figure 3-29. The steel mesh was 0.5 mm thick spaced at 5 mm intervals. Due to there being a concern of poor bonding between the concrete and the smooth surface of the steel mesh, the mesh was placed overnight in a diluted acid to allow for the slight corrosion of the smooth steel surface. The roughening effect of this acid treatment is shown in Figure 3-30.
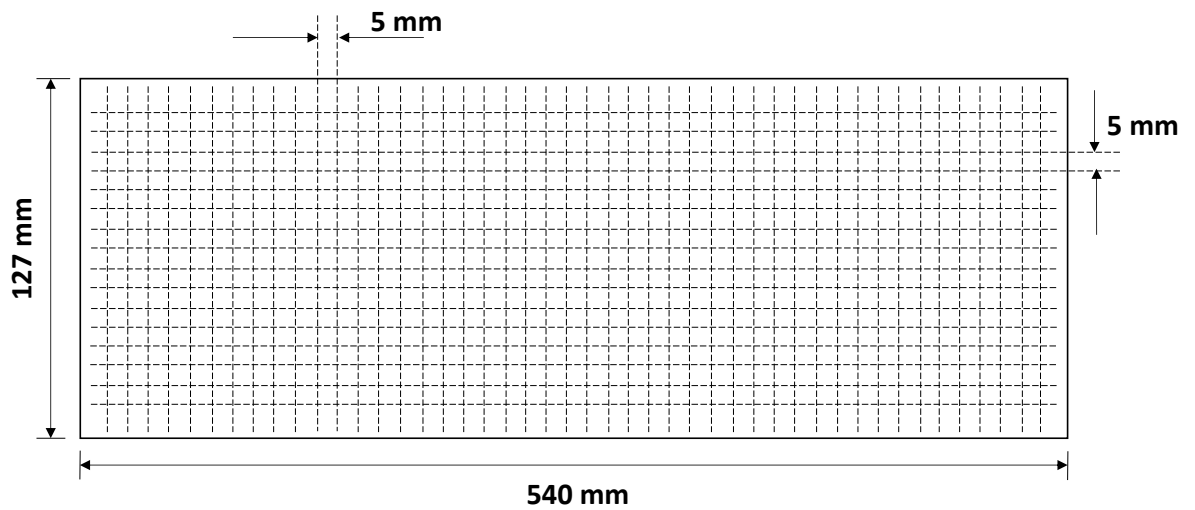
Figure 3-29: Dimensions (in plan view) of reinforced concrete slab and steel mesh
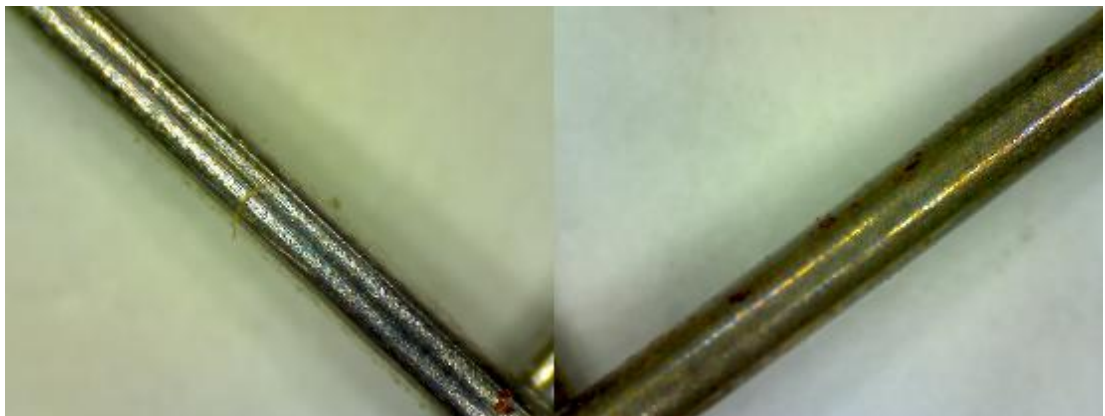
Figure 3-30: Steel mesh prior to acid treatment (left) and after acid treatment (right)

The slabs had to be tested for quality control purposes. A non-destructive bending test was done on each slab after 28 days of curing. This was done by pin supporting the slab at a 500 mm spacing and then loading it at midspan. The load was applied by placing weights on a hanger. Increments of 50 g were placed on the hanger up to a total mass of 250 g and then

removed in the same increments. The deflection at midspan was measured using an LVDT. Using the deflection data, slab dimensions as well as the magnitude of the applied load, a characteristic stiffness (EI) (N.m^2) could be calculated. If the characteristic stiffness fell outside of a range of 160 to 200, the slab would not be used in the experiments. Figure 3-31 shows the loading configuration for the non-destructive bending tests. In addition, the thickness of the slabs were measured with a calibre to check that they fell within a narrow range.
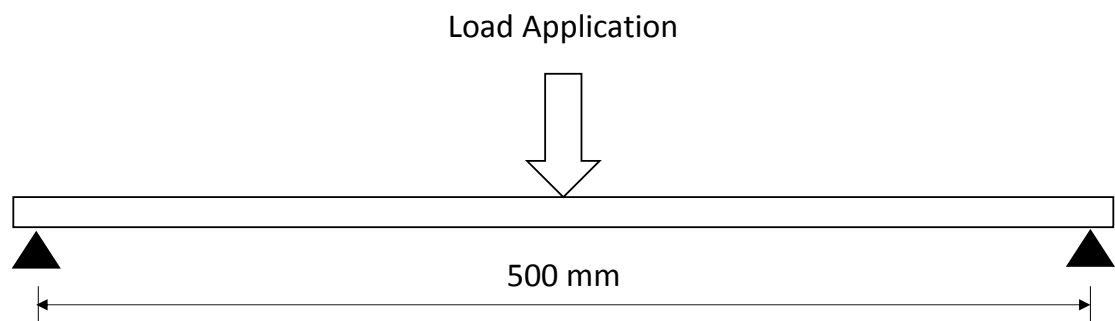
Figure 3-31: Loading configuration for non-destructive bending tests on slabs

The spread in thickness is presented in Figure 3-32 together with the resultant Young's Modulus (E) and cross-sectional stiffness (EI).
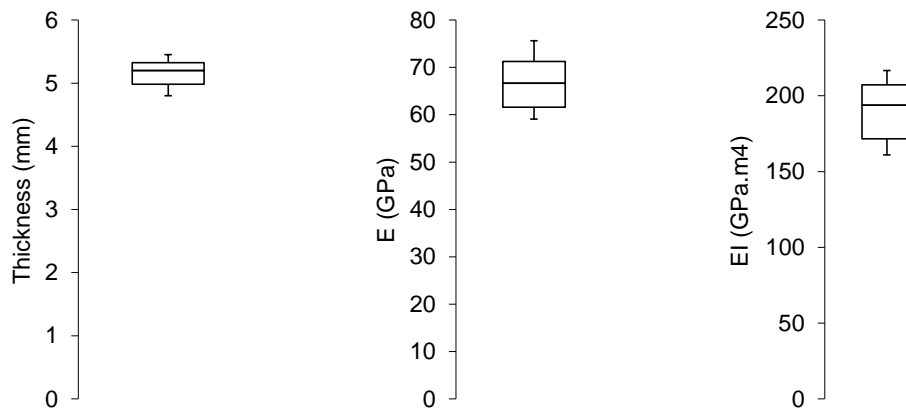
Figure 3-32: Box-and-whisker plots of the slab thickness, Young's modulus (E) and the characteristic stiffness (EI)

Since the slabs were all cast 240 mm wide, a strip 113 mm wide was cut off to produce a slab of the required width. The cut-off sections were then used in a four point bending test. A typical result from one of these tests is shown in Figure 3-33.
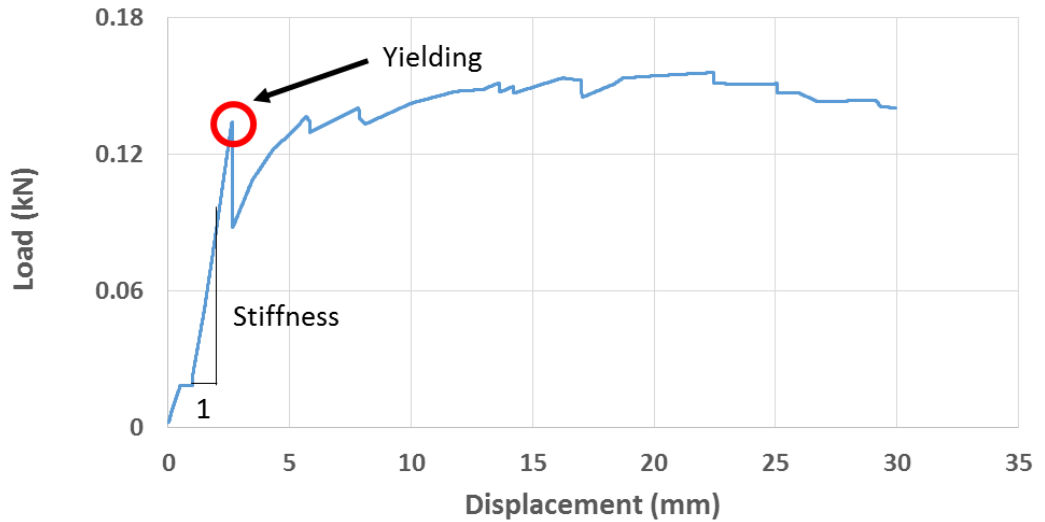
Figure 3-33: Typical load-displacement result from four-point bending test

The results for all the Yielding points and characteristic stiffness are shown in the box-and-whisker plots in Figure 3-34.
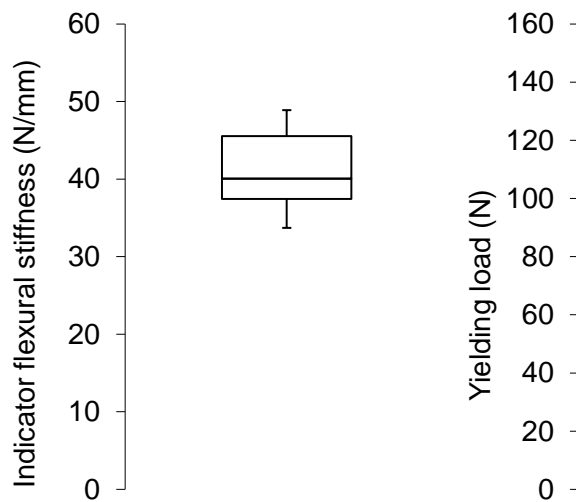
Figure 3-34: Box-and-whisker plots of yield points and calculated characteristic stiffness

3.3 VARIABLES INVESTIGATED IN THE STUDY

The following model properties were varied in the experiments conducted:

- Material type

- Degree of saturation of the base layers

- Magnitude of the applied load

Table 3-4 gives a summary of the variables relevant to the various experiments. Two material types were used for the construction of the layerworks and the experiments were repeated for each material. One was a fine silica sand that is often used in centrifuge testing at the University of Pretoria. The other was a graded gravel obtained from the road construction site mentioned. The graded gravel had to be scaled-down as discussed. The degree of saturation of the base layers was also varied. Some tests were conducted in which the base layers were at optimum moisture for compaction while others were tested in which the soil was fully saturated. The magnitude of the applied load was varied in the experiments. For each material type and degree of saturation, a monotonic failure load was applied. After measuring the monotonic failure load, cyclic loads of respectively 20 kN, 14 kN 10 kN and 3 kN were then applied to the pavements (all smaller than monotonic load).

Tests were named according to the variables of each test. The letter S or G refers to fine silica sand or graded gravel respectively. "Opt" or "sat" refers to the degree of saturation of the base layers for that specific experiment. The magnitude of the applied load is referred to as "mon" for monotonic loading or a numerical value of the actual load that was cycled. "S_opt_mon" therefore is the name of a test in which the base layers were constructed from fine silica sand, the degree of saturation was at optimum for compaction and a monotonic load was applied to failure.

Table 3-4: List of experiments conducted

Variables			Test name
Material Type	**Load magnitude (kN)**	**Degree of saturation (S_r)**	
Fine silica sand	Monotonic to failure	0.375 (OMC)	S_opt_mon
		1	S_sat_mon
	14	0.375 (OMC)	S_opt_14
		1	S_sat_14
	10	0.375 (OMC)	S_opt_10
		1	S_sat_10
	3	0.375 (OMC)	S_opt_3
		1	S_sat_3
Graded gravel (G7)	Monotonic to failure	0.496 (OMC)	G_opt_mon
		1	G_sat_mon
	20	0.496 (OMC)	G_opt_20
	14	0.496 (OMC)	G_opt_14
	10	0.496 (OMC)	G_opt_10
	3	0.496 (OMC)	G_opt_3

Throughout testing, there was an attempt to keep certain variables constant. The properties of the concrete slab had to always be the same. This was done by using a consistent mix design and curing regime. The bending tests were conducted to single out any slabs that would behave differently from the rest. A consistent methodology for model preparation was followed. To ensure that the densities of the soil were constant, the same approach was used to compact the soil each time. The moisture readings of the soil were taken prior to compaction. After each test, moisture readings were taken from soil samples again.

Due to the poor contrast in saturated image under Digital Image Correlation (a technique used to track patches in image, described in more detail in Section 4.1.2), the deformation mechanisms of saturated gravel could not be studied. The gravel tests were done to model a realistic pavement under typical conditions. Saturation does not represent typical conditions, but rather an exception.

3.4   LOADING REGIMES

Loading of the pavement was done under displacement control for the monotonic tests. The displacement used to control the load was measured by an LVDT within the piston of the actuator that measured the displacement of the piston. Displacement control was used because the failure load and load-deformation characteristics of the pavement model were not yet known. A large displacement was specified which would ensure that the pavement model would fail or reach unacceptable deformation. This displacement was applied to the pavement at rate of 0.025 mm/s. This was slow enough to allow photos to be taken of the deformations taking place throughout the pavement structure. The maximum displacement, once reached, was maintained for ten seconds and then the load was removed completely by retracting the loading piston at a rate of 1 mm/s until it was no longer in contact with the loading bogey.

Ten cycles were first applied manually at about 20 seconds per cycle (0.05 Hz). This allowed images to be taken of the deformation during each cycle. Thereafter, 100 cycles were applied automatically at 3 Hz. A single manual cycle of 20 seconds was then applied for the purpose of taking images during the cycle and then 1000 cycles were then applied at 3 Hz. This pattern of alternating between single manual cycles and multiple automatic cycles was continued until the end of each test. The number of automatic cycles were done in stages of 1000, 5000 or 10 000 cycles, depending on the observed deformation rate. Implications of the slower load cycles with regard to the influence of load rate on the deformations and pore pressure build up and dissipation have to be considered. This is discussed in the Results chapter of this report (Chapter 4).

Loading of the pavement was done under load control for the cyclic tests. A load cell between the hydraulic actuator and the frame of the hydraulic actuator monitored the load applied by the hydraulic piston. This load was used to control the loading of the pavement. Figure 3-35 shows an example of the cyclic loading for a 20 kN load. The cyclic load was applied as a sine wave with a specified frequency, average load (which is the midpoint of the sine wave) and a load amplitude. The hydraulic actuator would first extend until the load reached the average load magnitude (preload stage). Thereafter, it would extend and retract to impose the cyclic loading. This movement was controlled by the servo valves in the actuator, using the feedback from the load cell in such a way that the load would follow the specified sine curve. This continued until the specified number of cycles had been applied to the pavement.

A minimum load of 0.2 kN was maintained throughout the cyclic loading to ensure that the piston would never detach from the bogey. In preliminary testing done, it was found that the loading rate of the piston would accelerate once the piston detached from the bogey and result in it reapplying the load very rapidly and causing a large impact load. It was therefore found

to be important to maintain a positive compressive force between the piston and the bogey to prevent this from happening.

Throughout the cyclic loading, precaution had to be taken that the required load would not accidentally be exceeded due to a malfunction of the test equipment. This was done by setting a load limit of 1 kN above the required load. This would ensure that the piston would retract and the hydraulic pump would immediately stop once the feedback from the load cell indicated that this load limit had been reached.

Cyclic load magnitudes which were used, which were derived from the observed monotonic behaviour, are shown in Table 3-5. A load of 3 kN results in a pressure of 525 kPa below each strip under the loading bogey.

Table 3-5: Applied cyclic loads and equivalent wheel pressure

Applied cyclic axle load (kN)	Wheel pressure (kPa)
20	3500
14	2450
10	1750
3	525
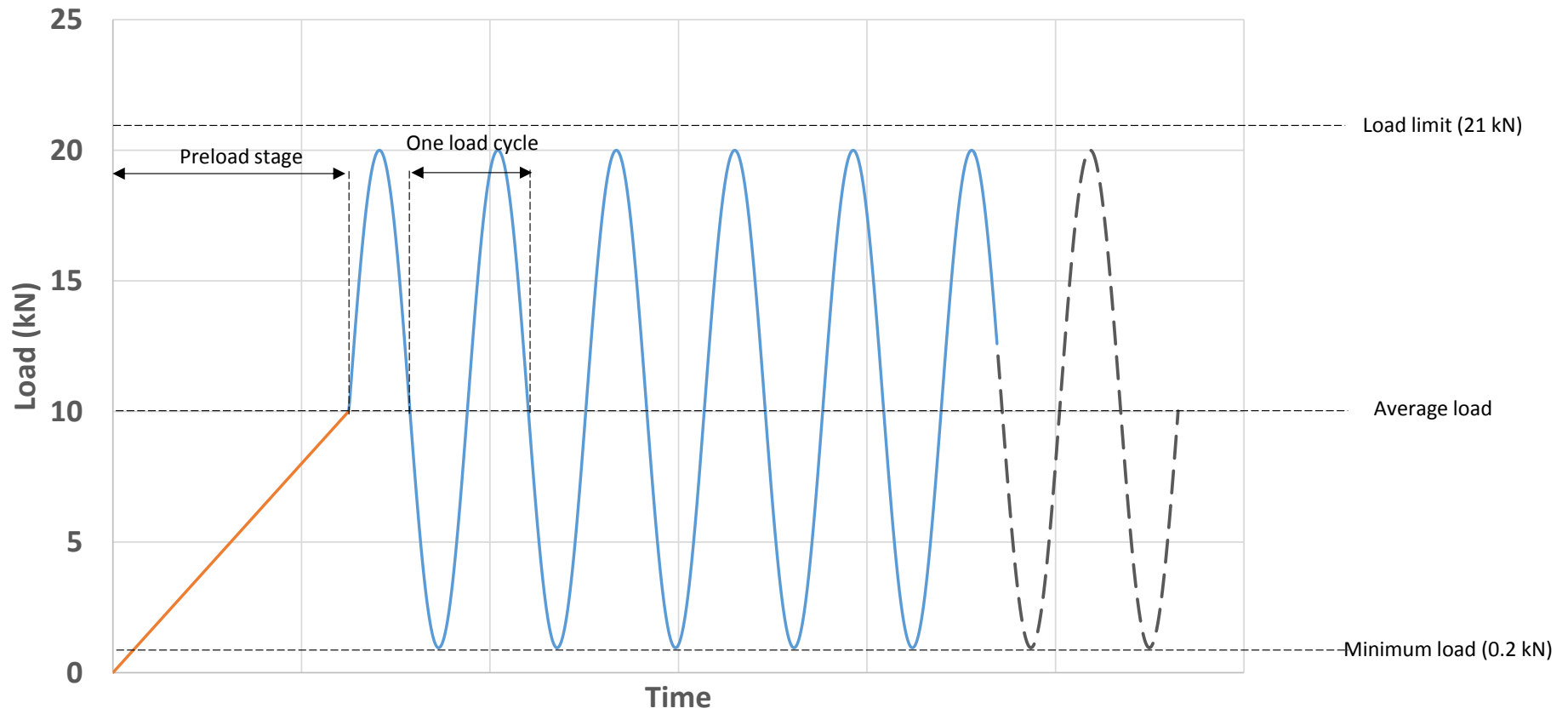
Figure 3-35: Example of a cyclic loading regime imposed for a cyclic load of 20 kN

4 RESULTS

In this section, the results from the experimental work are presented.

First, monotonic loads were applied to a UTCRCP pavement model with base layers of fine silica sand at optimum moisture for compaction (Mod AASHTO compaction standard) and then also with the layerworks fully saturated. This was all then repeated for a model in which the base layers were of a graded gravel.

After the monotonic load, cyclic loads were then applied at various load magnitudes lower than the monotonic failure load. Comparison is made between the model with the fine silica sand layerworks and the graded gravel, which is a more realistic road construction material. The performance of the pavements are also compared for the different degrees of saturation specified earlier. The settlement accumulation with number of cycles is presented. Thereafter, load-settlement characteristics are presented. Finally, the deformation mechanisms are compared for the monotonic load tests to the cyclic load tests.

The nomenclature referring to the various tests is "Material_saturation_loading". This is described in Section 3.3 and the reader is referred to Table 3-4.

4.1 MONOTONIC FAILURE LOADS

The monotonic tests were conducted to determine an upperbound for the failure loads for the pavement types that were tested. The magnitudes of the monotonic loads were then used to determine the cyclic loads that were to be applied to the pavements. The cyclic loads were smaller than the monotonic loads and required different number of load cycles to be applied before causing large deformation of the pavements.

4.1.1 Load-settlement behaviour

Figure 4-1 shows the monotonic load-settlement behaviour of UTCRCP built on layerworks of fine silica sand and the graded gravel at two degrees of saturation. The tests were conducted under displacement control and were stopped once excessive visible settlement had occurred. It can be seen that the models in which the layerworks were at optimum moisture content (S_opt_mon and G_opt_mon) behaved in a stiffer manner than when the layerworks were fully saturated (S_sat_mon and G_sat_mon). The change in slope after the initial, approximately linear, section in both curves occurred at a similar load of 17 kN (for the models constructed with the silica sand (S_opt_mon and S_sat_mon). A load of 17 kN results

in an applied pressure of 2975 kPa below each strip of the bogey. The settlement at this load was, however, higher for the fully saturated model.
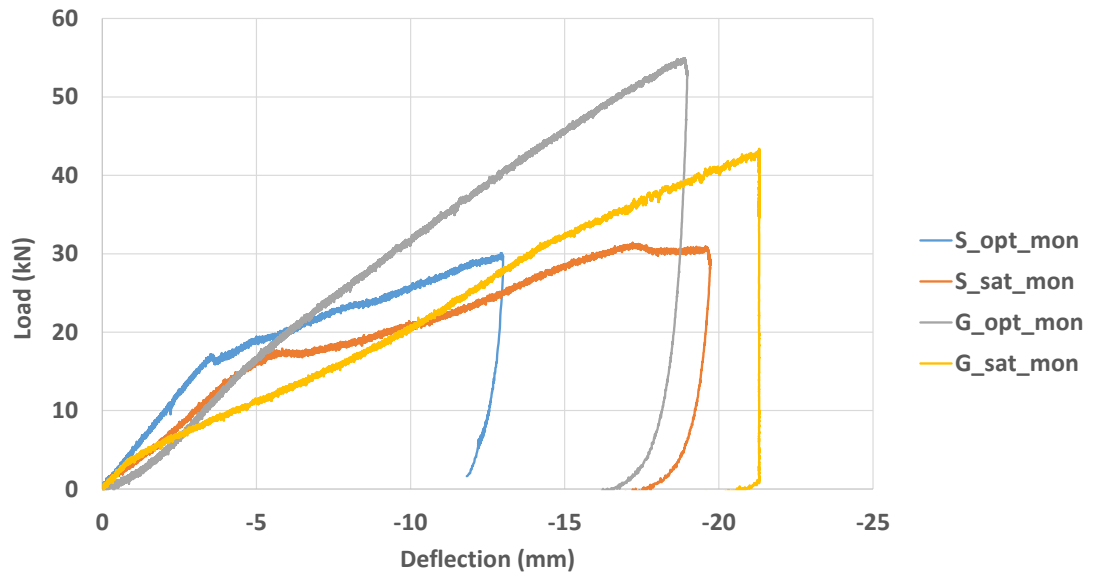
Figure 4-1: Load-settlement of UTCRCP at optimum moisture content and fully saturated

For the gravel, the model at saturated conditions (G_sat_mon) behaved initially slightly stiffer than the model built at optimum moisture content (G_opt_mon). This is somewhat unexpected but could be because of better bedding between the slab and the surface of the compacted layer below in the saturated model. This would result in the load being carried by the entire pavement structure. Poorer bedding-in of the slab on the drier layerworks could result in an initial bedding error in which small contact points first yield under the load until enough strain has developed for the slab to be adequately bedded-in to the soil layer below. Thereafter, the load was carried evenly throughout the pavement structure. Once the load was evenly carried throughout the pavement, the stiffness of the pavement increased. This is evident by an increase in the slope of the load-settlement behaviour curve of the model at optimum moisture content.

When comparing the two material types at optimum moisture content, in both instances, up to the point at which the slope changes the fine silica sand, the pavement built with the gravel was less stiff than the fine silica sand pavement. This was unexpected when considering the absolute densities of the two pavements. Although both are compacted to 95 % of their maximum dry density, the gravel was much denser than the fine silica sand and would be expected to react in a stiffer manner. This could be due to inadequate compaction of the gravel. Since the gravel was underlain by the sand that had a significantly lower compacted density, it is possible that the compactive effort applied to the gravel was absorbed by the

layer below, acting as a cushion. Hence, the perceived degree of compaction of the gravel was actually lower than the true density of the gravel.

4.1.2 Comparison of strain fields

Figure 4-2 shows stages, based on load and displacement, at which images taken during the monotonic tests were analysed to compare deformation fields at different stages during the tests. The first stage was chosen at the start of the tests during the initial loading. This is labelled as A. this was at a low load magnitude and the settlements were still very small. The second stage, labelled as B, was at a load of 17 kN (2975 kPa). This was chosen because of the change in the slope of the load-displacement curves for the models constructed using fine silica sand at this load. Finally, at stage C, the images were analysed at the point where a settlement of 10 mm had been reached. The loads at this point for the different models differed due to the varying stiffness of the models.
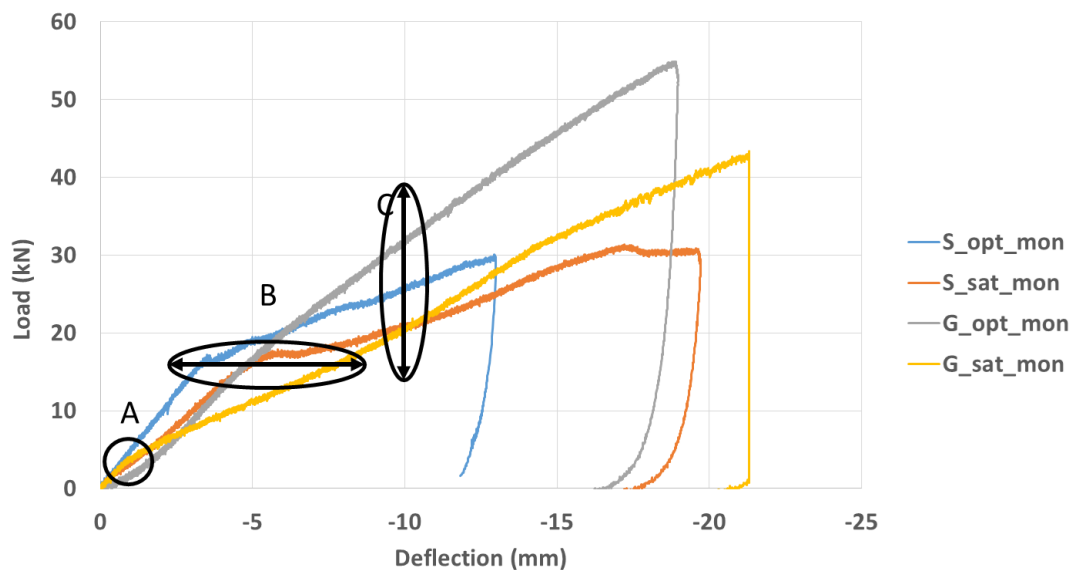
Figure 4-2: Stages for which images were analysed

Figure 4-3 shows the mesh size and positioning of patches for which Digital Image Correlation (DIC) (White et al., 2003 and more recently by Stanier & White, 2013) was performed. The mesh consisted of patches of 48 by 48 pixels that were spaced 16 pixels centre-to-centre. Using DIC, the displacement of each patch could be calculated from photos

taken during the test. Strain fields could be calculated from the displacement of these patches. This allowed deformation mechanisms to be studied and compared at various stages during the tests.
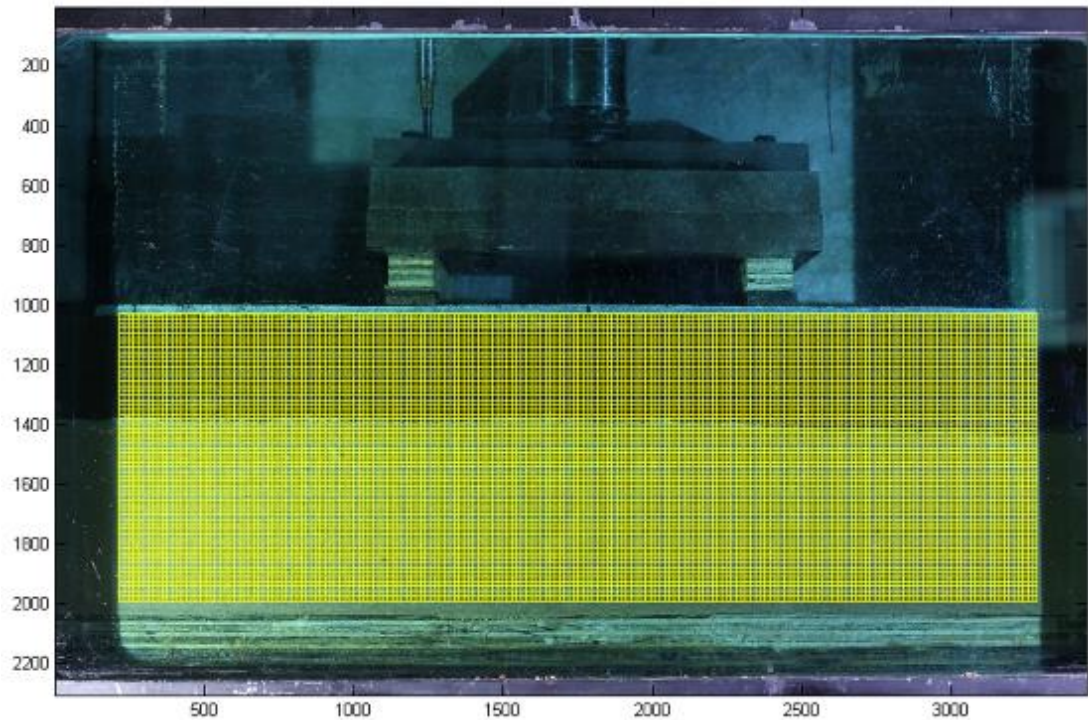
Figure 4-3: Location of mesh for which Digital Image Correlation was performed

4.1.3 Strain development for silica sand at optimum moisture content

The strain development during monotonic loading for the pavement model with base layers constructed from fine silica sand is show in this section. As shown by the mesh (Figure 4-3), the DIC analysis covers only the layerworks and subgrade sections of the pavement structure. The concrete slab was not analysed. Figure 4-4 shows displacement vector plots for the model constructed using fine silica sand layerworks. Vector plots are shown for stage A (the beginning of load application to the pavement structure), stage B (when a load of 17 kN / 2975 kPa was reached) and stage C (when a total settlement of 10 mm was reached). Stages A, B and C are defined in Figure 4-2.
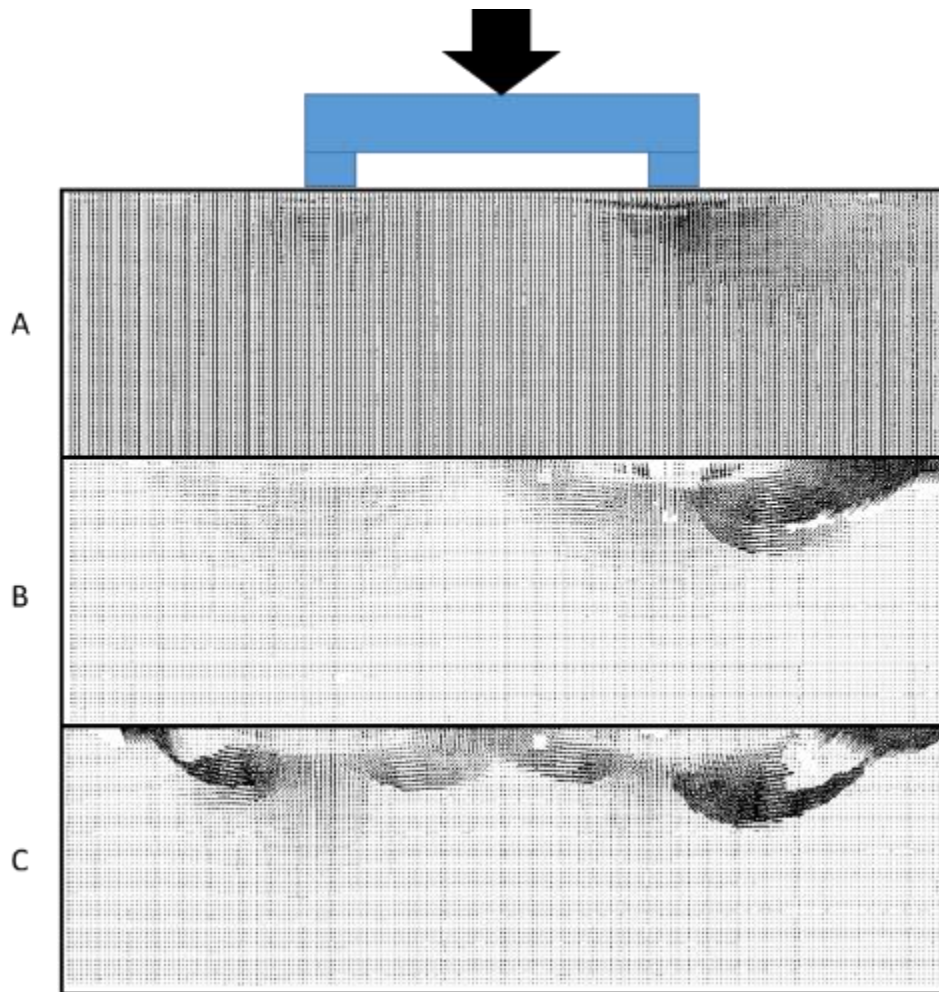
Figure 4-4: Displacement vector plot at stages A, B and C for fine silica sand at optimum moisture content

At stage A, there was only a small amount of displacement evident in the soil immediately below the point of contact of the bogey. The deformation was also not uniform, with more deformation occurring below the right hand of the bogey. There is no evidence of the development of a slip plane in the soil at this stage. At stage B, there was evidence of a rotational slip plane having developed below the right hand side of the bogey. This matches with the reduction in stiffness of the pavement structure at stage B in Figure 4-2. The deformation was still not uniform, with no slip yet occurring below the left hand side of the bogey. At stage C, where 10 mm of settlement had occurred, deformation in the pavement structure was mainly in the form of soil sliding along rotational slip planes originating below the bogey. The rotational slip planes were not the same size on both sides. This could be due to the non-uniformity of the applied load that was evident from stage A and B. The slip planes are not symmetrical about the centres of the footings. This could be due to confinement between the footings. It could also be due to the interference of the two slip mechanisms between the footings. In addition, it is highly unlikely that perfect symmetry will occur,

because as soon as deformation begins to occur on a particular side, deformation will concentrate there due to strain softening, leading to non-symmetric behaviour.

Figure 4-5 shows the shear strain progression in the layerworks of the pavement during loading at the three stages selected. The shadings represent the maximum shear strain percentages (the maximum shear value of the strain Mohr-circle), with intensity indicated by the legend in the image.
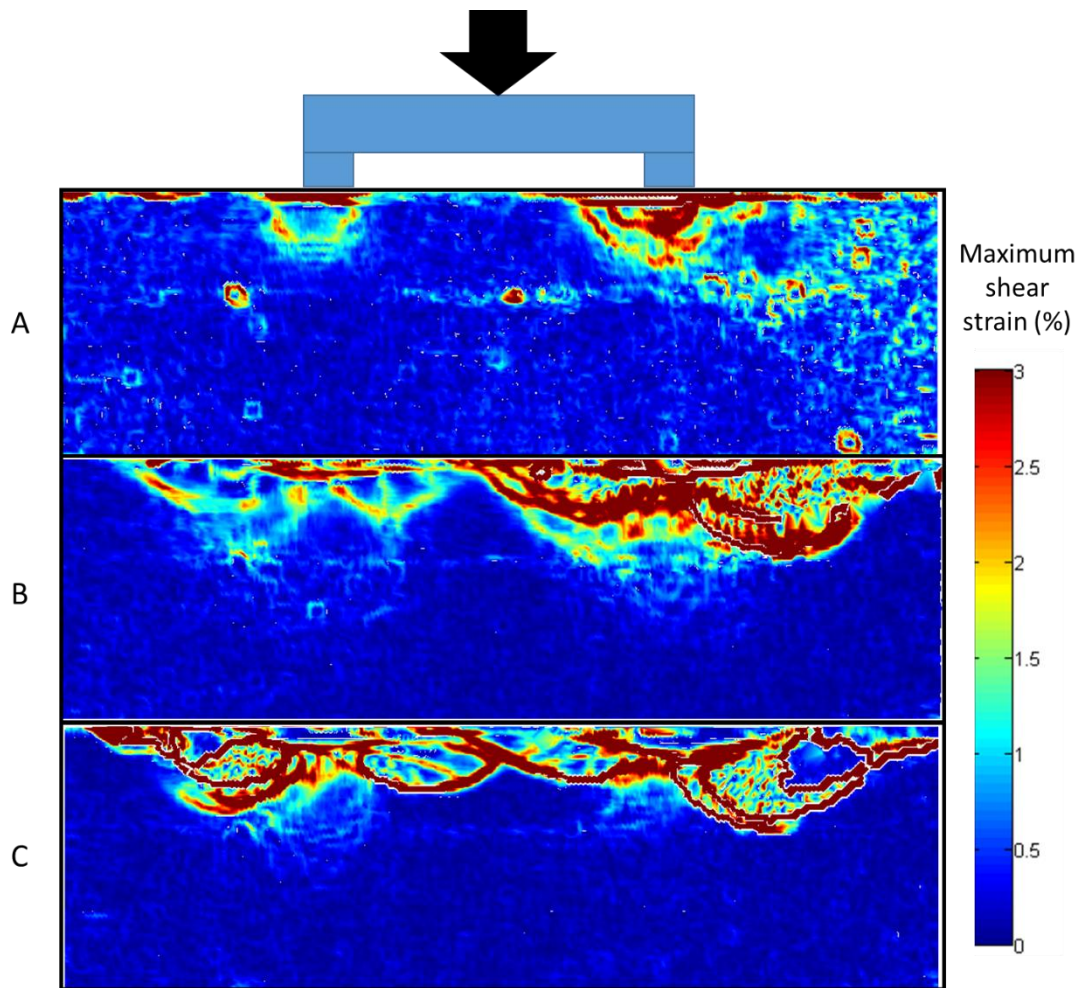
Figure 4-5: Maximum shear strain plot at stages A, B and C for fine silica sand at optimum moisture content

Initially, as indicated in the shear strain diagram at stage A, a small bulb of shear strain developed below each footing. This indicates that compression of the soil is occurring at this stage. These shear bulbs were still very shallow. A low influence depth can be expected under low loads. It can also be seen that the slab was still bedding in, as evident from the strip of intense shear strain along the length of the slab. At stage B, the development of the slip planes is evident. This is indicated by the high shear strain percentages. Although the non-uniformity

of the loading can be seen, the slip planes below the left hand footing had already taken shape. This was not yet evident at this stage in the vector plot. At stage C, the rotational slip planes below both footings had fully developed. Almost all the movement at this point was occurring as shear strain along the slip planes only. Very little shear strain can be seen anywhere else in the diagram.

Figure 4-6 shows the volumetric strain progression in the pavement structure. A positive volumetric strain indicates contraction (volume reduction), while a negative volumetric strain indicates dilation (volume increase).
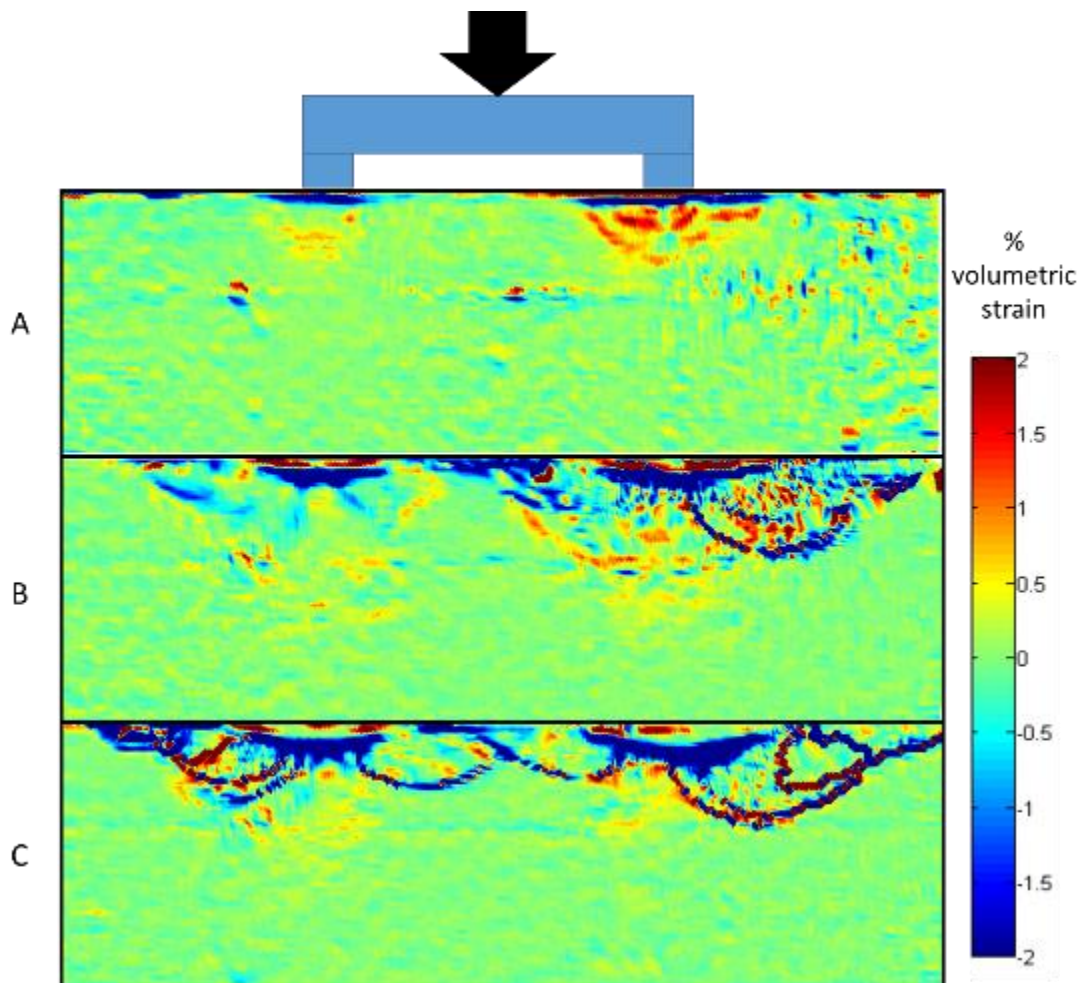
Figure 4-6: Volumetric strain plot at stages A, B and C for fine silica sand at optimum moisture content

Compression below both footings occurred at stage A, as discussed for the shear strain. It can be seen that, as slip occurred in stage B, the soil dilated along the shear bands. A characteristic of a dense material, such as the fine silica sand used in this case, is that it dilates along a shear band. This is again shown in stage C. It can be seen that the mode of

deformation under the applied load was associated with a complex mechanism of shear band formation rather than the compression of material.

4.1.4 Strain development for silica sand under saturated conditions

Figure 4-7 shows the displacement vector plot for the silica sand which was saturated. It can be seen that the deformation field is more equally distributed below both sides of the bogey.
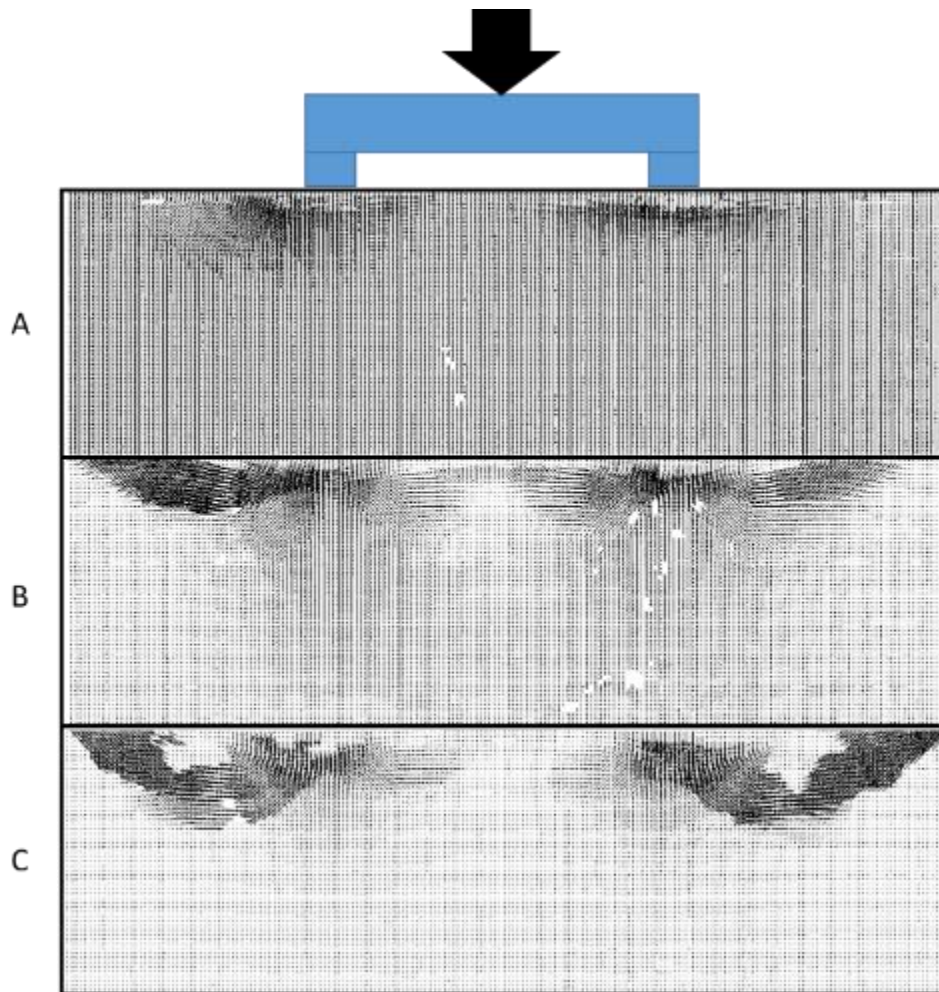
Figure 4-7: Displacement vector plot at stages A, B and C for fine silica sand under saturated conditions

At stage A, the displacement below the footings was mostly in the vertical direction, with very little horizontal movement of the soil. At stage B, rotational deformation of the soil had begun. This matches the point at which the stiffness of the pavement reduced in Figure 4-2. Besides the rotational movement of the soil, there still remained a small component of vertical movement in the soil below the footings but deeper than the slip planes. At stage C, all

movement of the soil was contained within the slip zones. The slip zones were not symmetrical about the centre of each footing. The reason why there is less soil slip between the two footings could be due to confinement or interaction between adjacent deformation mechanisms.

In Figure 4-8, the shear strain development in the pavement structure can be seen. As with the displacement vector diagram in Figure 4-7, the load distribution between the two footings appears to be evenly (symmetrically) distributed.
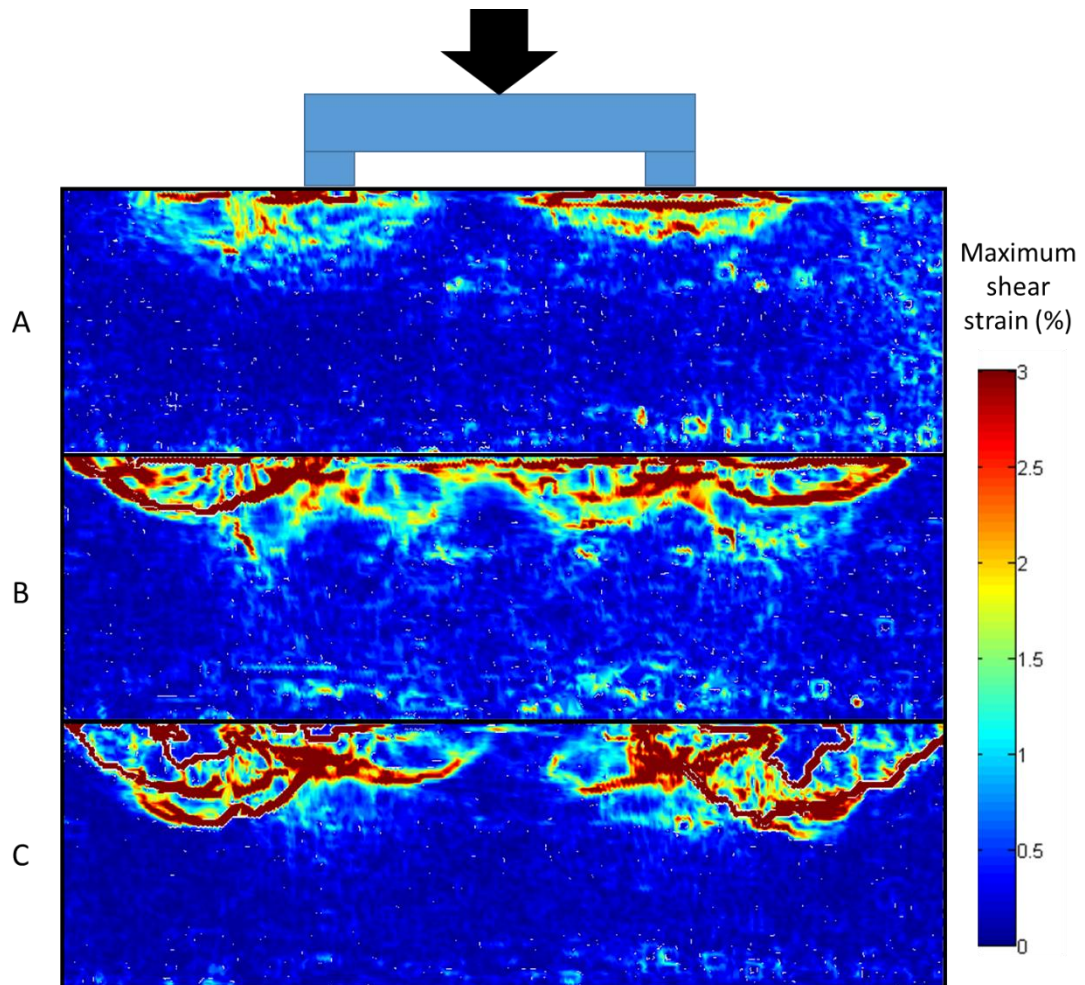
Figure 4-8: Maximum shear strain plot at stages A, B and C for fine silica sand under saturated conditions

For stage A, two wide compression bulbs formed, but the percentage maximum shear strain was low. The compression bulbs were no deeper than the interface between the base layers and the subgrade below. Stage B shows the development of the slip mechanisms with shear strains concentrated about narrow slip planes. As discussed for the vector plots, there exists an area below the slip planes where shear associated with some compression still occurred.

Stage C shows better developed slip mechanisms. Most, if not all, of the shear strain occurred along these slip planes. The slip mechanisms were now deeper than at stage B. These mechanisms are symmetrical about the centre of the model, but not symmetrical about the strips where the load was applied.

The volumetric strain development in the model under monotonic loading, for stages A, B and C in Figure 4-2, can be seen in Figure 4-9. The volumetric strain diagrams are interpreted in conjunction with the shear strain diagrams.
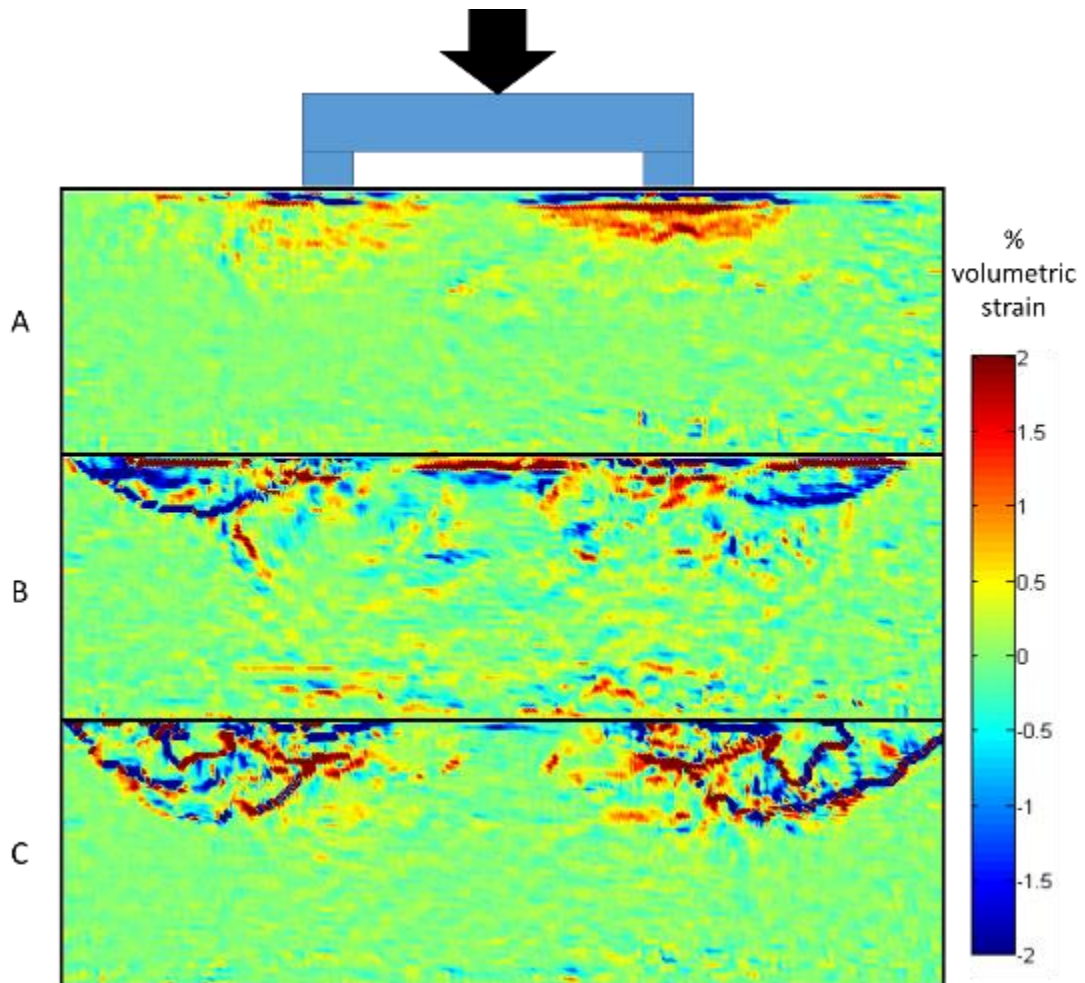
Figure 4-9: Volumetric strain plot at stages A, B and C for fine silica sand under saturated conditions

There was mainly compression (indicated by positive volumetric strains) occurring during the initial loading stage at stage A in Figure 4-2. The low load magnitude allowed this dilation to occur. Bands of dilating material at stage B indicate the presence of slip planes that have developed. This coincides with the reduction in stiffness in the load-settlement graph in Figure 4-1 and Figure 4-2. The bands of dilation at stage C were deeper than at stage B.

Throughout the test, there remained a degree of compression occurring right through the depth of the model, while shear strains were mostly restricted to the upper portion of the model.

4.1.5 Strain development for graded gravel at optimum moisture content

The strain development within the soil of the pavement constructed using a graded gravel for the base layers is shown in the following figures. Figure 4-10 shows the displacement vectors at stages A, B and C which are indicated in Figure 4-2.
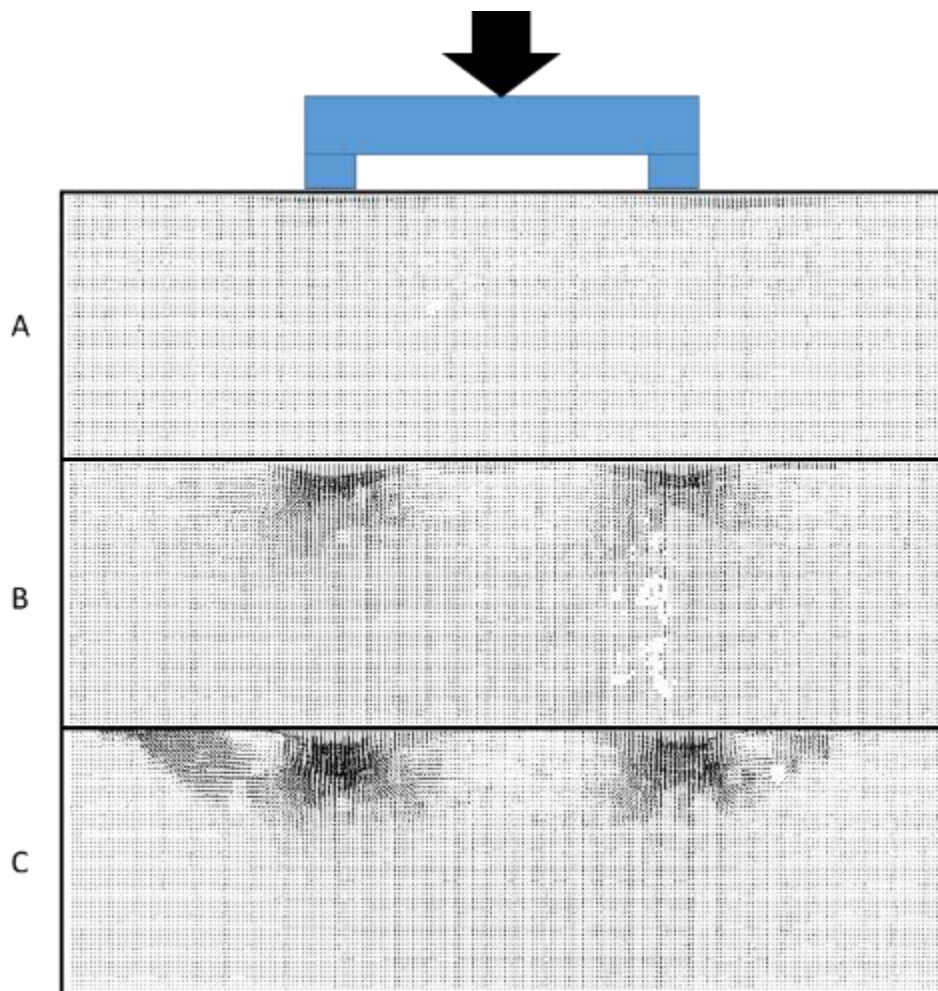
Figure 4-10: Displacement vector plot at stages A, B and C for graded gravel at optimum moisture content

For stage A, there was almost no displacement throughout the pavement structure. The slight vertical displacement below the footings is distributed widely along the length of the slab and could thus still be the bedding-in stage. A deflection bulb had formed at load stage B (17 kN / 2975 kPa), but the magnitude of the deflections was still very small. There was no evidence of any horizontal soil movement at load stage B. The displacement vectors at load

stage C, which is once a total settlement of 10 mm had occurred, indicate that a rotational slip mechanism had begun to form. This is more evident below the left hand footing.

The shear strains during the monotonic loading of the pavement are shown in Figure 4-11.
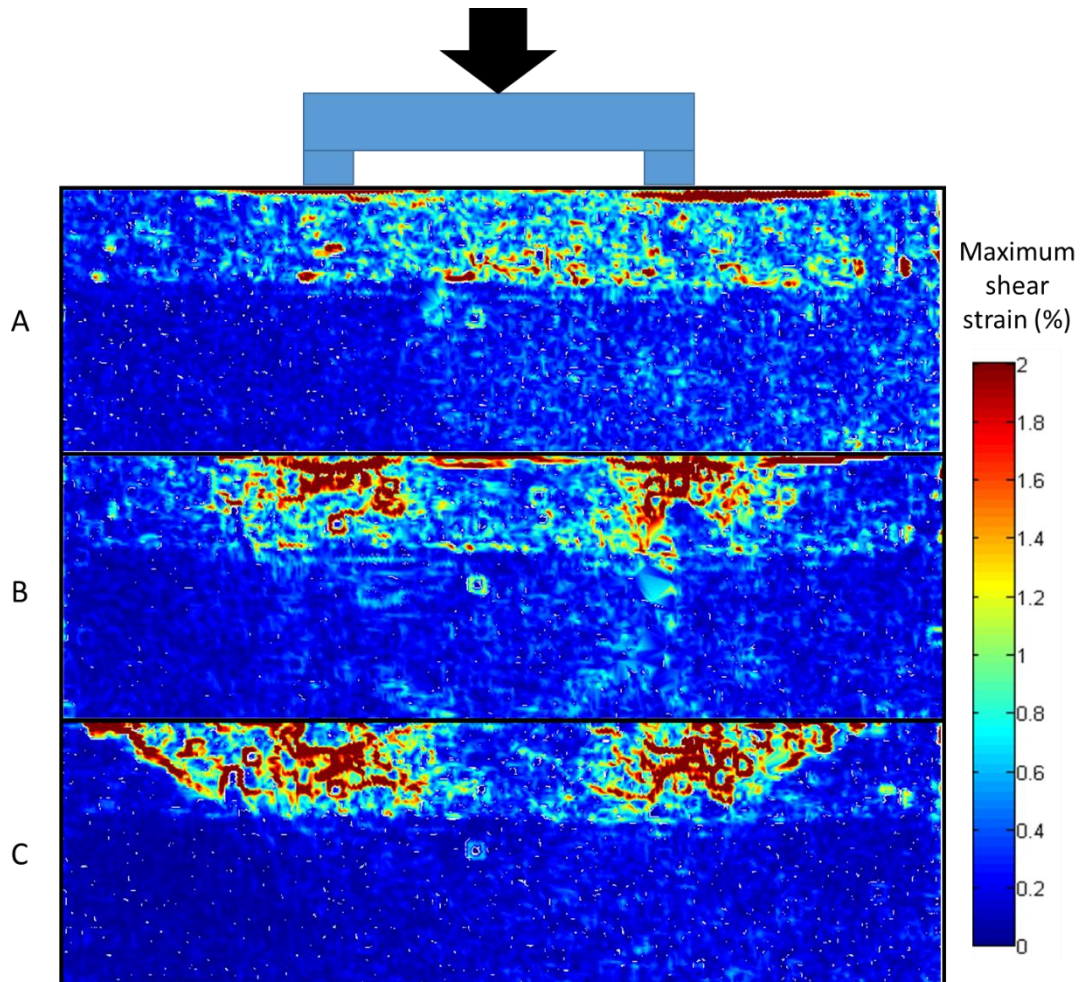
Figure 4-11: Maximum shear strain plot at stages A, B and C for graded gravel at optimum moisture content

For stage A, the shear strains are evenly distributed throughout the base layers of the pavement. There is a clear change in the magnitude of shear strains over the interface between the base and subgrade of the pavement structure. The strips of intense shear strain immediately below the slab may be due to the slab bedding in. Two bulbs of shear strain had developed below the footings at stage B. There was still very little shear strain occurring within the subgrade. The band of shear strain extending diagonally to the surface below the left hand footing confirms that the development of a slip mechanism had begun.

The volumetric strains during loading are shown in Figure 4-12. These indicate areas of compression (positive volumetric strain) and expansion or dilation (negative volumetric strain) within the pavement structure.
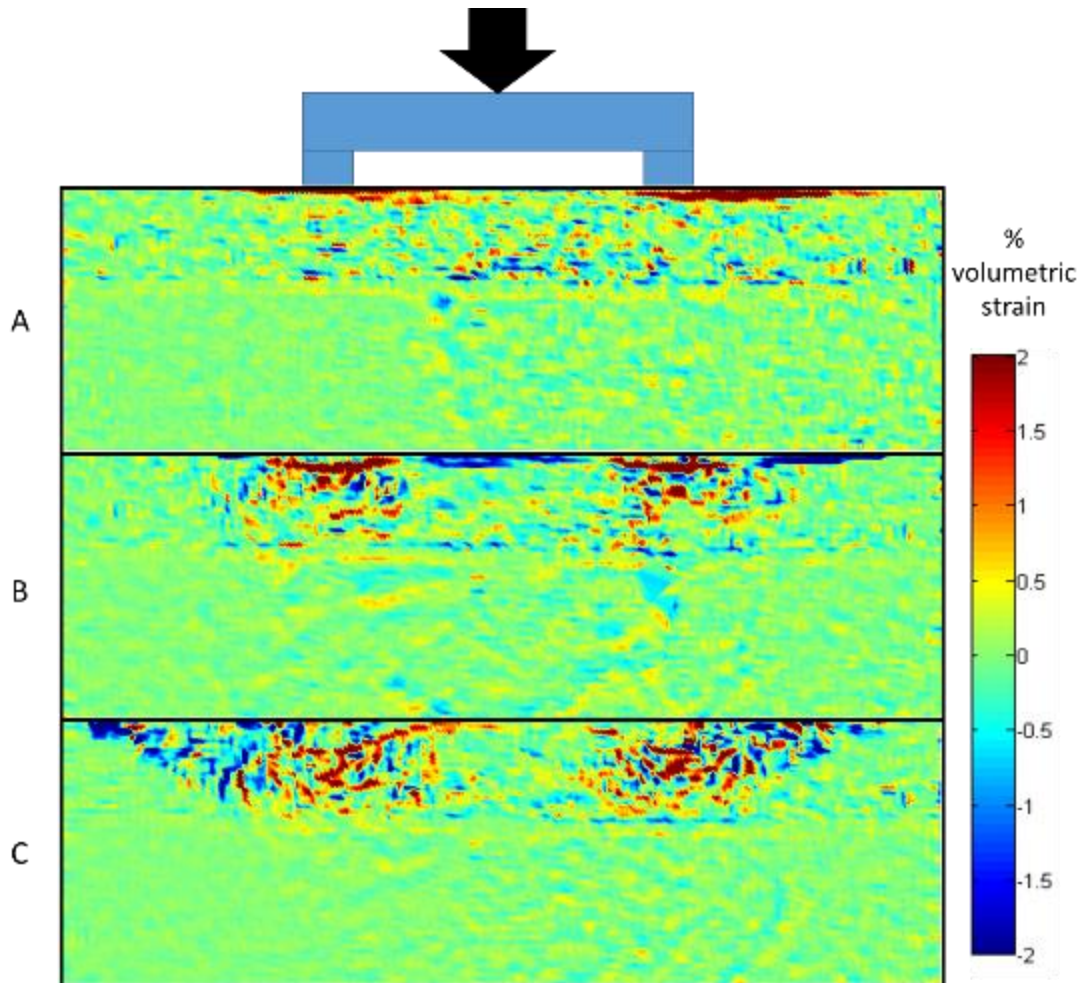
Figure 4-12: Volumetric strain plot at stages A, B and C for graded gravel at optimum moisture content

There were mainly compressive strains occurring at very low load magnitude (stage A), while volumetric expansion occurred directly beneath the slab between the wheel loads and to the right hand side of the right hand footing (for load stage B). At load stage B, dilation occurred along the slip plane below the left hand footing. This confirms the observation of slip failure made for the shear strains at this load stage.

4.1.6 Comparison of strain development during monotonic loading

The loading of the model constructed with fine silica sand and tested at optimum moisture content was not equally distributed between the two footings. This could have been due to initial out-of-straightness of the pavement loading bogey. This was less evident in the two other tests. In the initial loading stage (stage A), shear strain bulbs formed beneath the footings in both tests where fine silica sand was used as the layerworks material. At the same loading stage, the strain was evenly distributed throughout the layerworks for the model in which the layerworks were constructed using the graded gravel. For the two models constructed entirely out of fine silica sand, the shear strain bulbs were wider, but shallower, for the model that was tested under saturated conditions than the one tested at optimum moisture content. Due to the saturated material being less stiff than the unsaturated soil (aided by suctions), the relative stiffness between the slab and the soil was higher for the saturated than for the model at optimum moisture content. This resulted in more settlement and less bending of the slab for the saturated model. This could explain why the compression bulb was shallower and wider for the saturated model than for the model at optimum moisture content. At stage B of the load-settlement behaviour, distinct slip was evident for the two models constructed from silica sand, while no slip was yet shown for the model in which graded gravel was used for the layerworks.

Once 10 mm settlement had been reached (load stage C), the slip mechanisms were well developed for the sand models and started to show in the gravel model. The slip planes extended further towards the outside of the saturated model than for the unsaturated sand model. The slip planes extended from the footings to the centre of the pavement below the loading bogey and outwards and away from the footings in the model constructed of silica sand at optimum moisture content. The slip planes extended outwards and not to the centre of the saturated model. Dilation was evident along the slip planes for the models constructed of silica sand.

The DIC analysis, together with the load-settlement relationships shown in Figure 4-1, shows evidence that the two pavements constructed of sand failed at load stage B (17 kN / 2975 kPa). The fully developed slip planes and the stiffness reduction confirm this. For the gravel pavement model, the overall failure of the pavement was not clear at this point. Only after 10 mm of settlement, and more than 30 kN (5250 kPa) of load, did significant slip become visible in the soil. The 10 mm settlement, and thus a load of over 30 kN, was taken as failure for the gravel model. Any settlement before this load was attributed to compression of the gravel material. Inadequate compaction of the gravel could be the cause of the majority

of the shear strain occurring in the gravel base layers and not being transferred to the subgrade below.

4.2   SETTLEMENT RESPONSE VS NUMBER OF CYCLES

In this section, the settlement of the loading bogey under cyclic loading is presented for the three pavement models. Two models were constructed in which the base and subgrade were constructed using fine silica sand, with one model being at optimum moisture content and the other fully saturated. All graphs are intentionally plotted to the same vertical scale for ease of comparison between the various tests.

4.2.1 Settlement response at optimum moisture content for silica sand pavement

The settlement accumulation under cyclic loading is shown in the following figures. Figure 4-13 shows the accumulated settlement of the loading bogey strips for the fine silica sand at optimum moisture content for loads of 14, 10 and 3 kN. The loads result in a pressure of 2450, 1750 and 525 kPa below the bogey strips, respectively. At 14 kN, the first cycle resulted in a settlement of a little more than 2 mm. The settlement then reaches 10 mm within 5000 cycles. The settlement rate had not yet stabilised after 5000 cycles. For the 10 kN load cycles, the initial settlement was slightly less than 2 mm and then seems to have gradually stabilised. The 3 kN load cycles resulted in a small initial settlement and then stabilised quickly. Very little settlement occurs between 1000 cycles and 75 000 cycles when the test was ended. Boyce (1976) and Pappin (1979) observed that, for granular material, plastic strains remained insignificant if the cyclic load remained below 70 % of the monotonic failure load. The failure load, in this case, was determined to be 17 kN (Section 4.1) and so cyclic loads of 10 and 3 kN are below 70 % of the monotonic failure load. Strictly speaking, the same rule cannot apply in its entirety, since this load distribution and loading conditions of a pavement structure is not the same as the loading of a granular material to failure. It is evident, however, that the cyclic loads of 10 and 3 kN resulted in a stable settlement rate.

It can be seen that there are steps in the data during the initial stages of the test. This occurred due to the loading actuator being stopped at intervals, as explained in Section 3.4. The slower manual loading cycles resulted in more dwelling time of the load. This resulted in a greater deformation as also observed by Lashine (1971), who related the influence of dwelling time on pore pressure dissipation, which influences the settlement. This situation was not ideal, but was done solely for the purpose of being able to take photos for DIC analysis during loading.

A dotted line is also plotted to represent, what can be argued to be, the real trend of the data. This is done for all the subsequent settlement vs number of cycles graphs in this chapter.

4.2.2 Settlement response under saturated conditions for silica sand pavement

Figure 4-14 shows the accumulated settlement for the models with fine silica sand as the layerworks under saturated conditions. A similar trend can be seen as in Figure 4-13 where the 10 kN (1750 kPa) load cycles seem to have resulted in a gradually reducing settlement rate (considering the log scale), while the 14 kN (2450 kPa) load cycles resulted in less stabilisation in the settlement. Compared to Figure 4-13 the settlements were significantly higher under fully saturated conditions for the same cyclic load magnitude than under optimum moisture conditions. The 10 kN load cycles resulted in 8 mm settlement within 1000 cycles when fully saturated, but did not reach this settlement after almost 20 000 cycles when at optimum moisture content. This illustrates the influence of the build-up of excess pore pressures (in fully saturated soil) on the reduction in stiffness of a pavement.

In this case, where the material is saturated, the observation that settlements are insignificant at cyclic loads below 70 % (Boyce, 1976 and Pappin, 1979) of the monotonic failure load does not seem to hold. The settlement rate still continues to increase after numerous cycles for a load of 10 kN, which is below 70 % of the monotonic failure load of 17 kN.
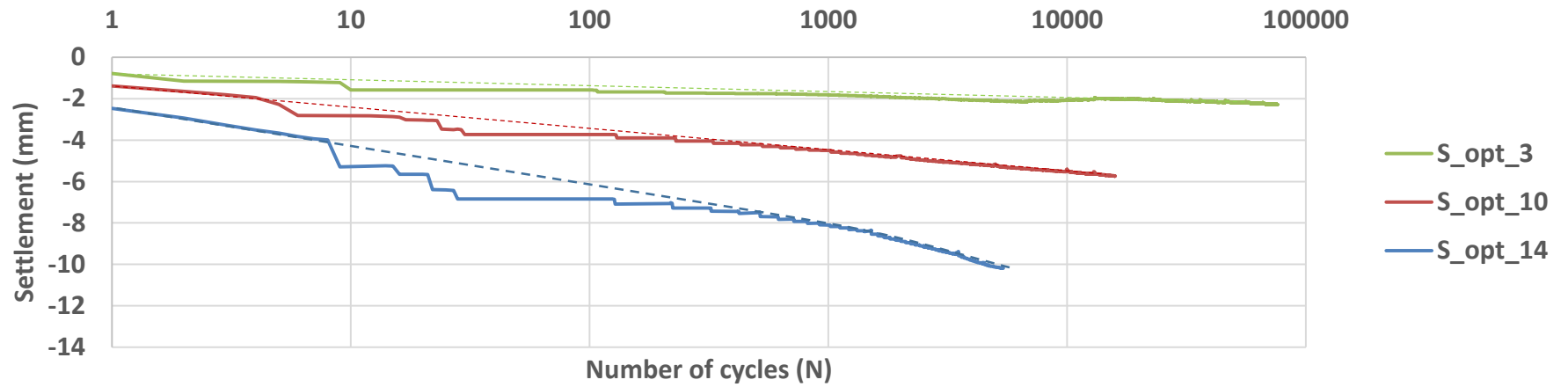
Figure 4-13: Settlement vs number of cycles for fine silica sand at optimum moisture content
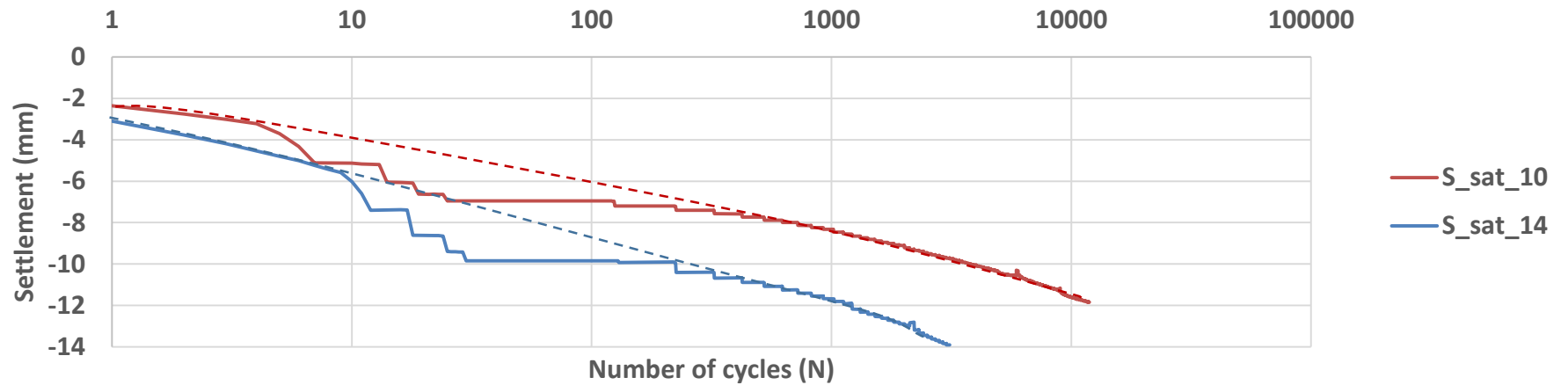
Figure 4-14: Settlement vs number of cycles for fine silica sand that is fully saturated

4.2.3 Comparison between settlement response at optimum moisture and under saturated conditions for silica sand pavement

Figure 4-15 and Figure 4-16 compare accumulated settlement at optimum moisture content and fully saturated conditions at specific loads for the silica sand pavement. In Figure 4-15 it can be seen that the accumulated settlement under 14 kN (2450 kPa) cyclic loads was higher when the soil was fully saturated than when it was at optimum moisture content. A settlement of 8 mm was reached within 20 cycles when the sand was fully saturated and after 1000 cycles when at optimum moisture content.

The settlement under 10 kN (1750 kPa) cyclic loads is shown in Figure 4-16. The saturated model reached 8 mm settlement within 1000 cycles and the settlement did not seem to have stabilised by the time the test was ended after almost 16 000 cycles. The model at optimum moisture content never did not reach the same amount of settlement. From about 6000 cycles the settlement had stabilised for the sand at optimum moisture content.

At optimum moisture content, the degree of saturation of the silica sand is 0.363, resulting in suctions of 100 kPa (Section 3.2.1.4). These suctions, although not very large, contribute to the effective stress in the soil. It is therefore expected that the pavements tested at optimum moisture content would experience less settlement than those tested under saturated conditions where no suctions occur. Additionally, with the dwelling time being very low, it is expected that pore pressure buildup will occur in the saturated material (Cary & Zapata, 2016). This pore pressure buildup reduces the effective stress in the soil and so the strength of the soil decreases. The acceleration in the settlement towards the end of the saturated tests (when plotted on a log scale) could indicate that a threshold stress level is reached (Mamou et al., 2017), not only due to the stress buildup within the soil, but also due to a reduction in effective stress caused by a buildup of excess pore pressure. This buildup of excess pore pressure was even observed in samples that were free to drain during cyclic loading (Mamou et al., 2017).
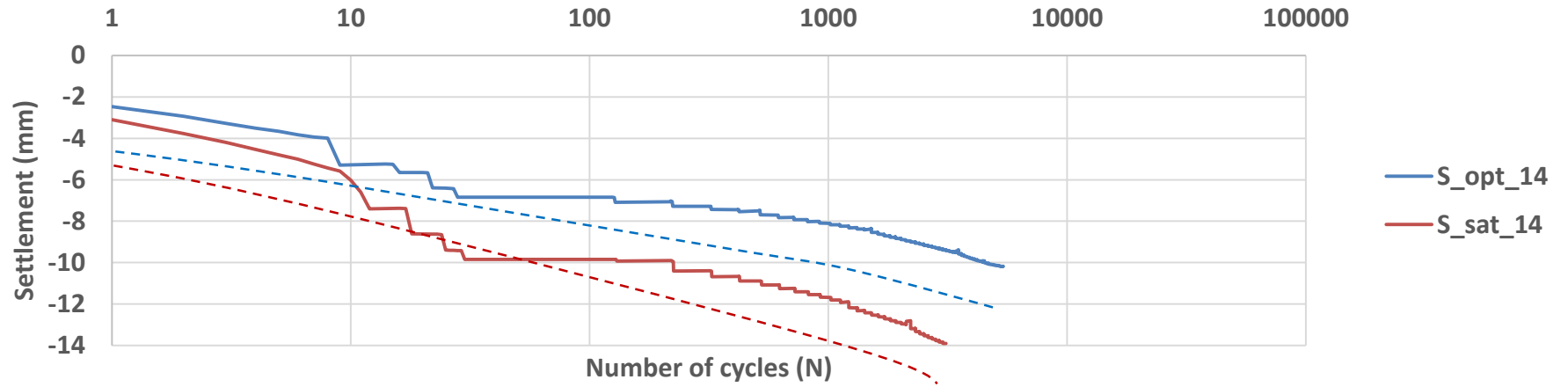
Figure 4-15: Settlement vs number of cycles for fine silica sand at 14 kN (2450 kPa) load at optimum moisture content and fully saturated
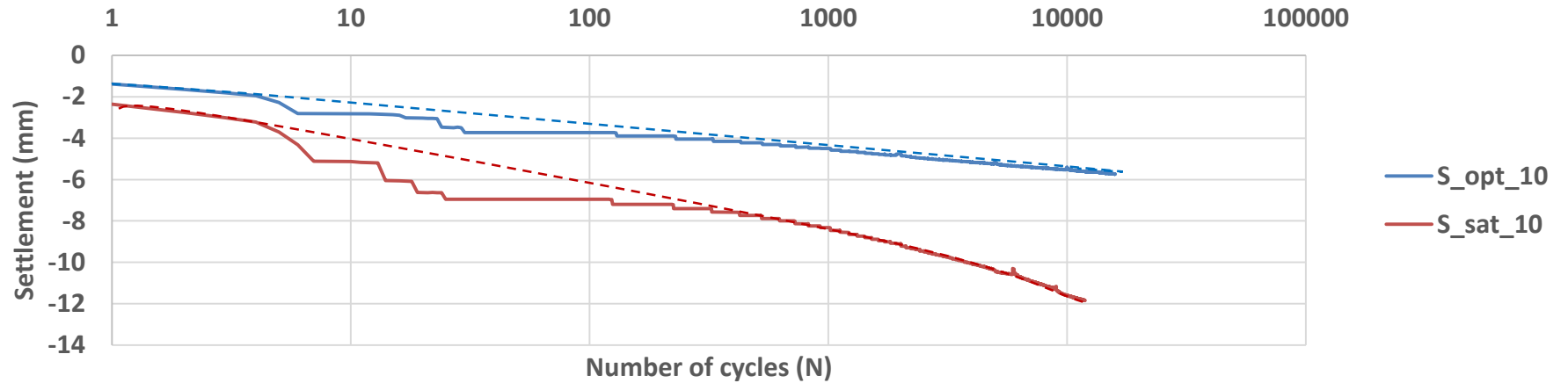
Figure 4-16: Settlement vs number of cycles for fine silica sand at 10 kN (1750 kPa) load at optimum moisture content and fully saturated

4.2.4 Settlement response of graded gravel at optimum moisture content

Figure 4-17 shows the accumulated settlement for the graded gravel at various cyclic load magnitudes at optimum moisture content. At a load of 20 kN (3500 kPa), the settlement was rapid in the initial cycles, accumulating over 6 mm settlement in the first few loading cycles. This did not abate much and the settlement rate was still high when the test was stopped after 14 000 cycles. The test conducted at 14 kN (2450 kPa) also showed a high initial settlement and the rate of settlement then decreased. A settlement of 7 mm was not reached in the 25 000 cycle test period. Extrapolating the data at the same rate, 10 mm settlement would not be reached after 100 000 cycles at a cyclic load magnitude of 14 kN. At 10 kN (1750 kPa) an initial settlement of 4 mm was reached within 10 cycles and then the settlement reduced to a constant rate after about 10 000 cycles until the test ended after 45 000 cycles. The 3 kN (525 kPa) cyclic load resulted in a much smaller initial settlement. The settlement hardly increased between 100 cycles and 75 000 cycles when the test ended. It could be assumed that the settlement will not reach unacceptable levels within the service life of the pavement. This confirms the observation by (Mamou et al., 2017), that if load magnitudes remain below a certain threshold, damage will not occur. There is, however, a slight increase in the settlement rate towards the end of the load cycles, particularly for the higher load magnitudes, when plotted on a log scale.

The spikes in the settlement curves in Figure 4-17 relate to the times when the testing had to be stopped for a short period. This evidently resulted in a small strain recovery. This rebound was not as evident with the tests conducted on the fine silica sand. Once load cycling commenced, the settlement quickly (within 10 cycles) returned to the point at which it was before the rest period, suggesting that the effect of the interruption on the tests results was insignificant.
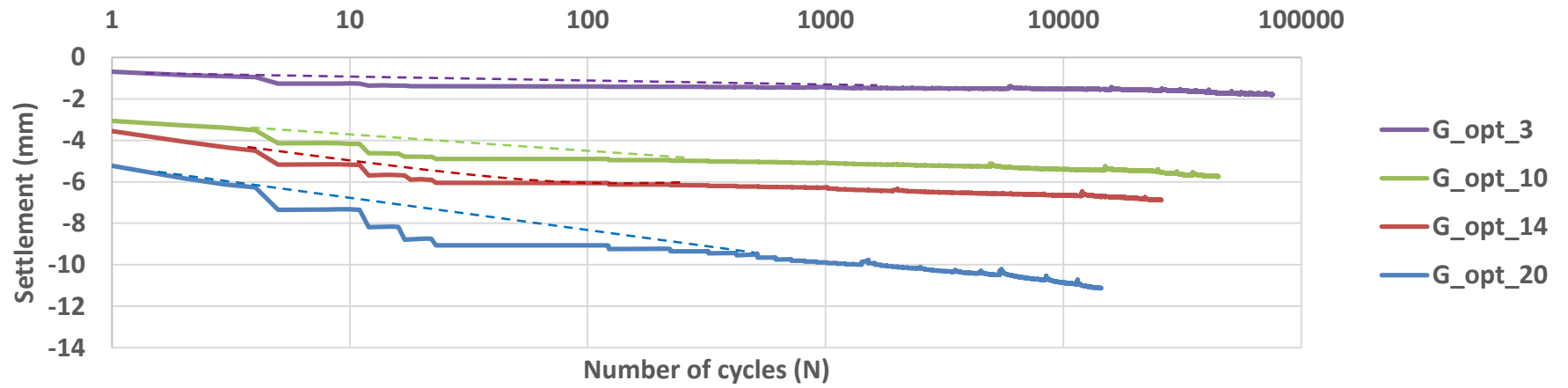
Figure 4-17: Settlement vs. number of cycles for graded gravel at optimum moisture content

4.2.5 Comparison of settlement response between fine silica sand and graded gravel at optimum moisture content

Figure 4-18, Figure 4-19 and Figure 4-20 compare the settlement response of fine silica sand and the graded gravel and various cyclic load magnitudes. All these tests were conducted at optimum moisture content. Figure 4-18 shows that, although the initial settlements were similar, the model constructed with fine silica sand quickly reached large settlements, while the model constructed with the graded gravel reached a more stable settlement rate at a load of 14 kN (2450 kPa).

In Figure 4-19, the settlements for the two materials are compared for a 10 kN (1750 kPa) load magnitude. The initial settlement was unexpectedly higher for the graded gravel than for the fine silica sand. This could be due to better bedding-in of the concrete slab being achieved on the sand than on the gravel or poorer compaction control of the gravel, as already discussed. Once this initial settlement was complete, the model constructed with the graded gravel reacted stiffer with a lower settlement rate than the fine silica sand. The fact that the silica sand settled more during the last cycles than the graded gravel is underemphasised by the use of a log scale. However, what is apparent, is the slope of the settlement curve being steeper for the silica sand than the graded gravel. Had the test continued for more cycles, the difference in the settlement would have been even clearer.

The accumulated settlement under 3 kN (525 kPa) cyclic loading for the two material types at optimum moisture content is given in Figure 4-20. As for the 14 and 10 kN load cycles, the accumulated settlement was lower for the graded gravel than for the fine silica sand under a load of 3 kN. After about 15 000 cycles, the settlement rates seem to have been the same. The fine silica sand responded with decreasing settlement for a period of about 5000 cycles between 7000 cycles and 12 000 cycles. When plotted with an enlarged vertical axis, as in Figure 4-21, the difference in the settlement becomes more evident. Within 10 cycles, the settlement of the silica sand was already greater than that of the graded gravel.
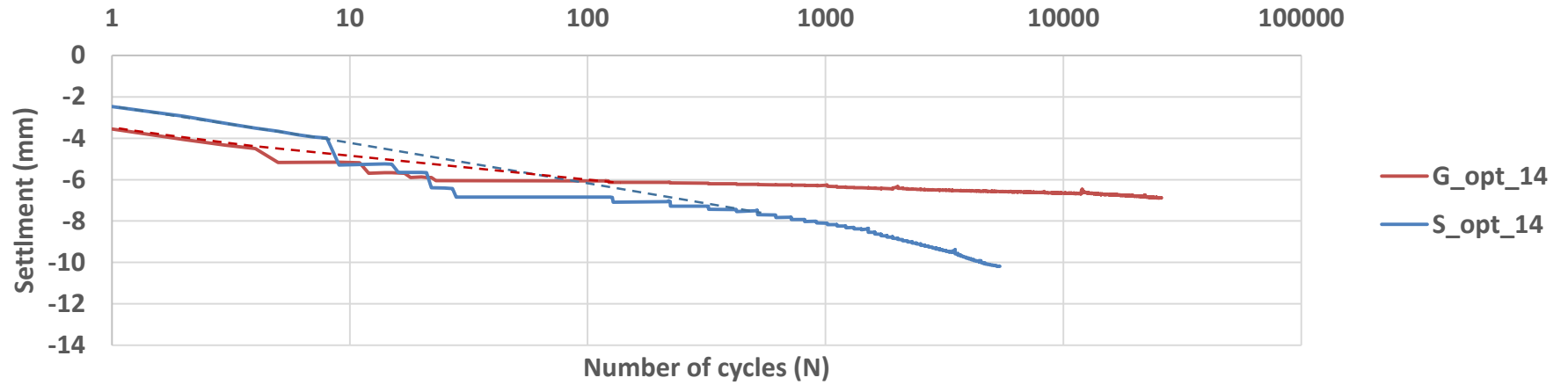
Figure 4-18: Settlement vs. number of cycles at 14 kN (2450 kPa) for graded gravel and fine silica sand at optimum moisture content
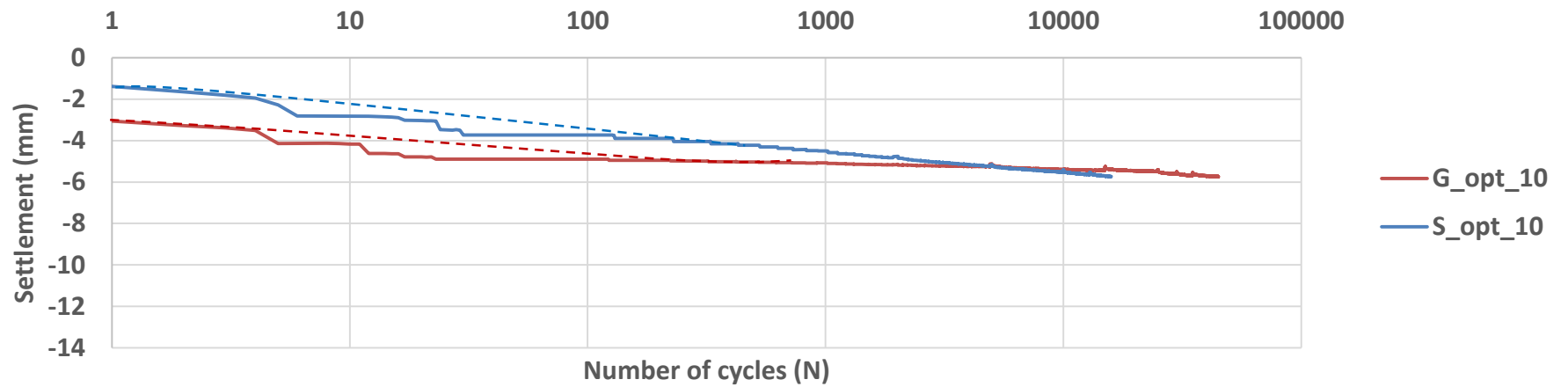
Figure 4-19: Settlement vs. number of cycles at 10 kN (1750 kPa) for graded gravel and fine silica sand at optimum moisture content
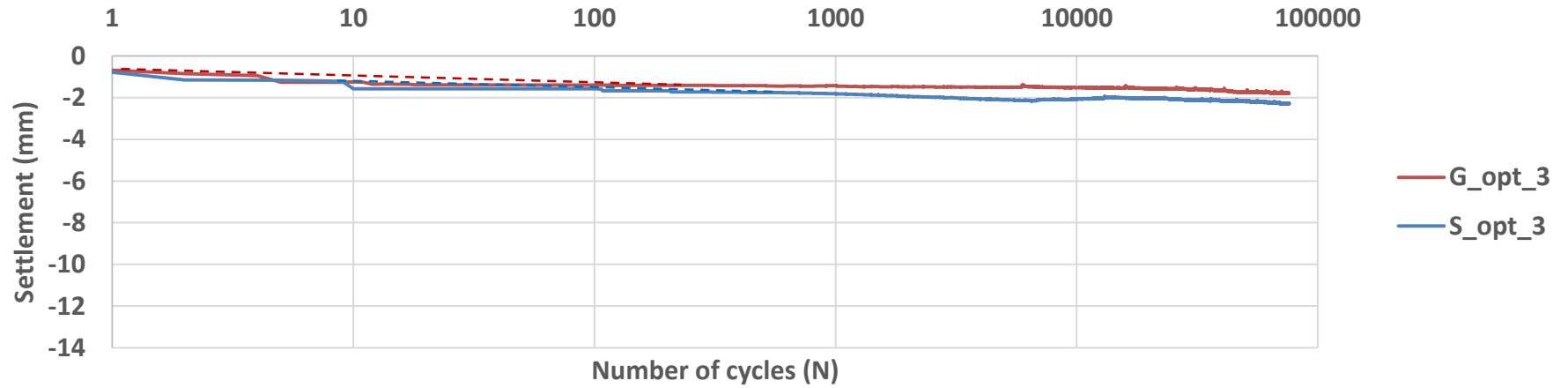
Figure 4-20: Settlement vs. number of cycles at 3 kN (525 kPa) for graded gravel and fine silica sand at optimum moisture content
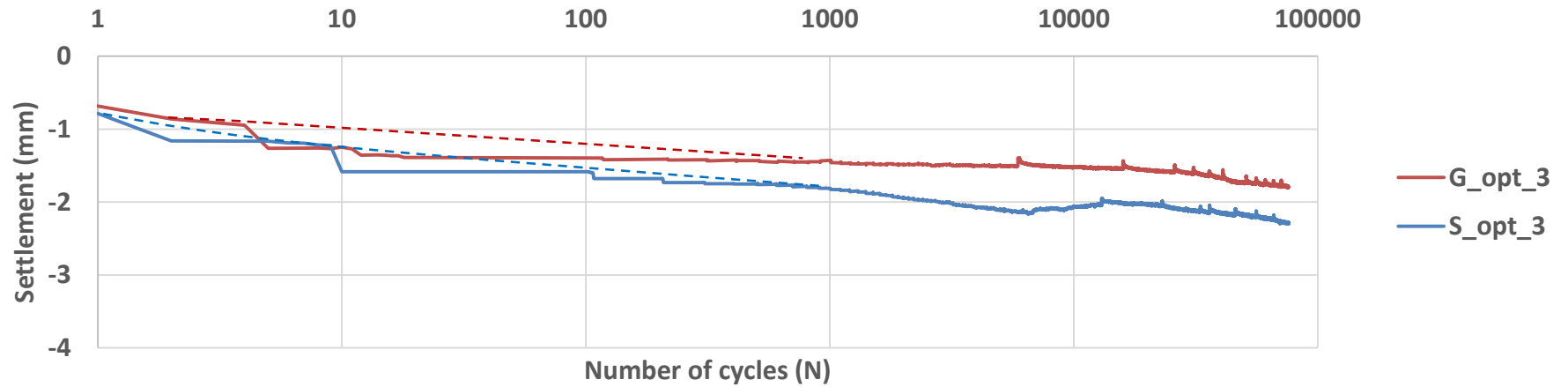
Figure 4-21: Settlement vs. number of cycles at 3 kN (525 kPa) for graded gravel and fine silica sand at optimum moisture content with enlarged vertical axis

4.3   PAVEMENT LOAD-SETTLEMENT RESPONSE

The load-settlement behaviour of all pavements during the cyclic tests is presented in this section. Besides confirming the observations made by considering the settlement behaviour in the previous section, examining the load-deflection allows the changes in the stiffness of the pavement to be observed under cyclic load application.

4.3.1   Silica sand layerworks at optimum moisture content

Figure 4-22, Figure 4-23 and Figure 4-24 show the load settlement response of the pavements constructed with fine silica sand at optimum moisture content subjected to cyclic load magnitudes of 14 kN (Figure 4-22), 10 kN (Figure 4-23) and 3 kN (Figure 4-24) respectively. For clarity, only a few load-displacement cycles, corresponding to the numbers in the figure legends, were extracted to allow comparison between data sets.   For all three loading conditions, the settlement during the first cycle was the largest. Also, the slope of the loading stage of the first cycle was flatter for the first cycle in all three tests. The lower stiffness and high settlement indicates that the slab was bedding in at the start of the test. It can also be argued that the first load application is on the virgin compression curve. Thereafter, each load application is on the rebound line.

At the higher cyclic load magnitudes, the load-settlement cycles crept constantly with increasing number of cycles. This is evident in Figure 4-22. The pavement structure becomes stiffer as is seen by the secant slopes of the hysteresis loops which become steeper.

In Figure 4-23, it can be noted that the hysteresis loops became wider from 10 cycles to 100 cycles. Thereafter the width of the hysteresis loops remained relatively constant. The secant slopes of the hysteresis loops were constant, as was the deformation per log cycle. This is also reflected in Figure 4-13 for 10 kN, where the settlement became linear on a log scale.

Figure 4-24 shows the load-settlement behaviour at 3 kN. The plotted load–settlement cycles appear to be evenly spaced. The hysteresis loops are very narrow and remain constantly so, indicating low energy loss per cycle.
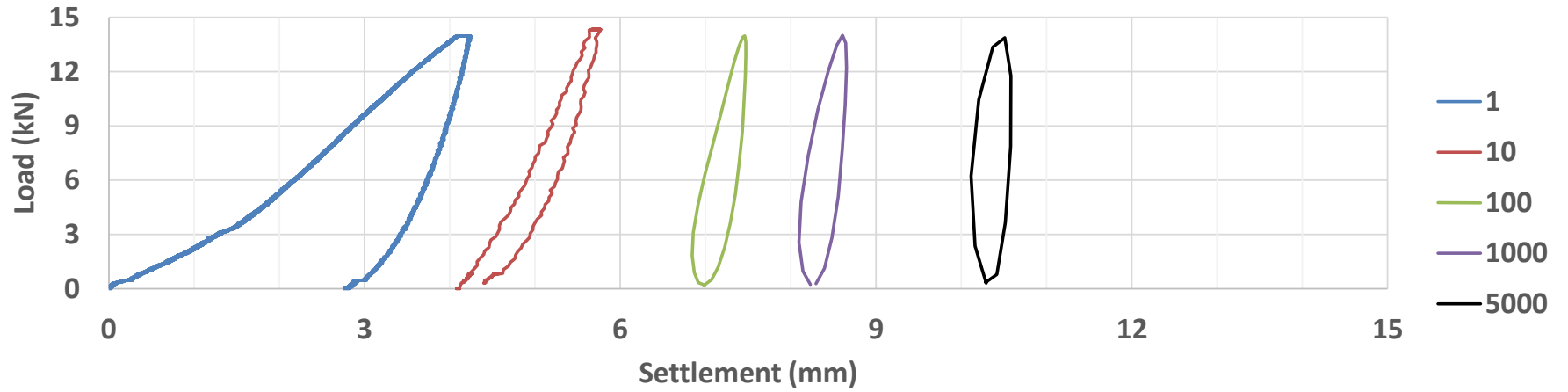
Figure 4-22: 14 kN (2450 kPa) load cycles for fine silica sand at optimum moisture content
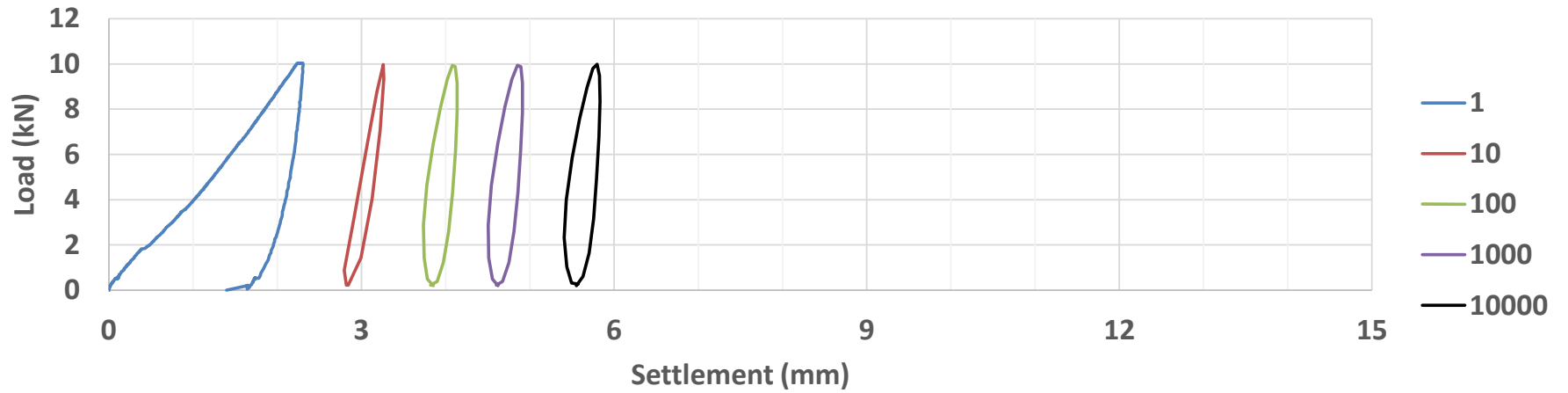
Figure 4-23: 10 kN (1750 kPa) load cycles for fine silica sand at optimum moisture content
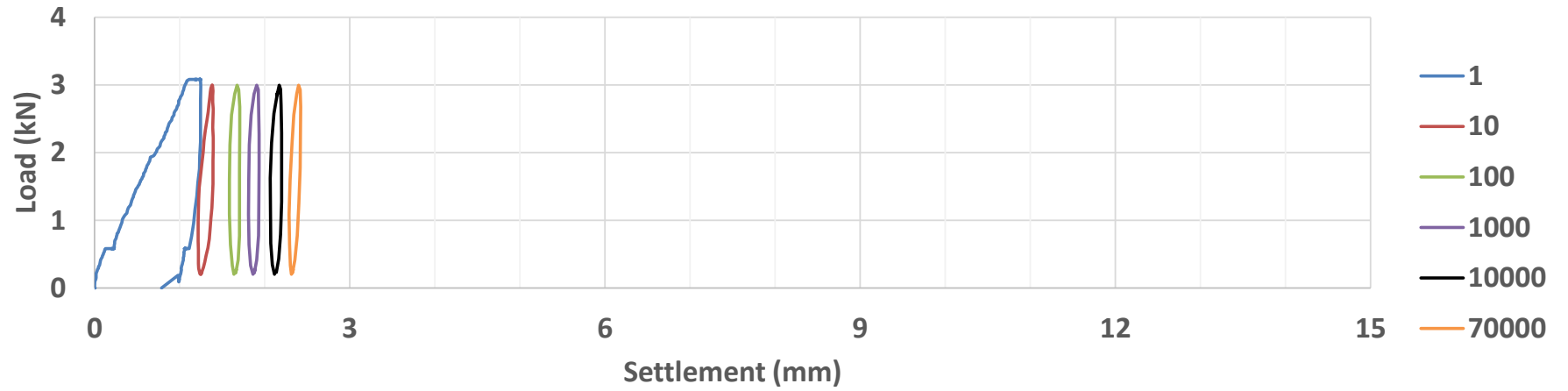
Figure 4-24: 3 kN (525 kPa) load cycles for fine silica sand at optimum moisture content

4.3.2 Silica sand layerworks under saturated conditions

In Figure 4-25, the load settlement behaviour is shown for cycles 1, 10, 100, 1000 and 3000 for the test conducted at 14 kN on fine silica sand under saturated conditions. A substantial settlement occurred in the first cycle, whereafter the hysteresis loops became narrower. The settlement per log cycle was high, particularly between the 10th and 100th loop and between the 1000th and 3000th loop. Cycle 1000 to 3000 is only a part of a log cycle. The settlement per log cycle was therefore particularly high at this stage. This indicates that substantial plastic strains were occurring in the pavement and very little resilient behaviour was evident. This was matched by the settlement profile in Figure 4-14. The spacing between the hysteresis loops is greater than for the test conducted at optimum moisture content Figure 4-22 indicating more rapid settlement with increasing load.

The hysteresis loops for the test conducted at 10 kN on fine silica sand under saturated conditions is shown in Figure 4-26. A large initial settlement occurred in the first cycle. The settlement per log cycle, as indicated by the spacing between the hysteresis loops, increased substantially towards the end of the test. This shows that the pavement response was not reaching a stable equilibrium but tended towards failure. This is also indicated in Figure 4-14, where the slope of the settlement curve is increasing on a log scale. The spacing between the hysteresis loops is greater than for the test conducted at optimum moisture content Figure 4-23. This was due to the presence of excess pore pressure generated in the saturated material causing more rapid deterioration than in the case of sand at optimum moisture content.
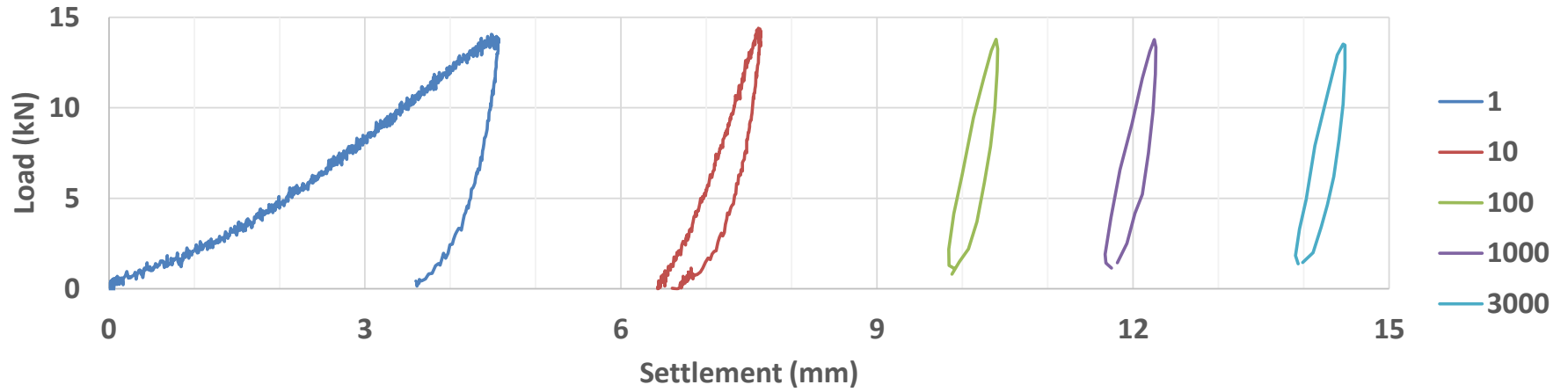
Figure 4-25: 14 kN (2450 kPa) load cycles for fine silica sand layerworks under saturated conditions
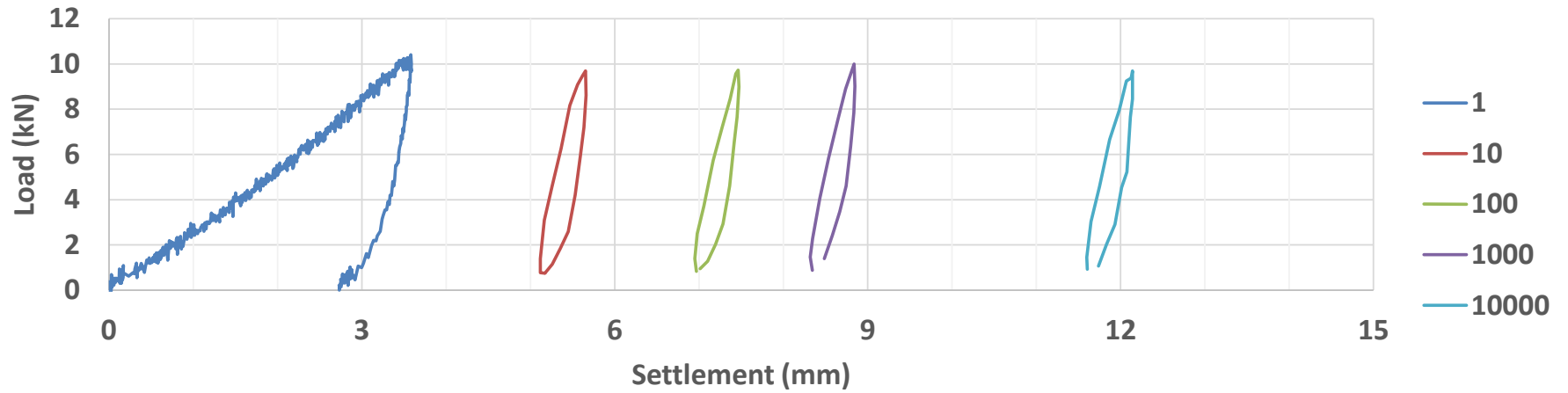
Figure 4-26: 10 kN (1750 kPa) load cycles for fine silica sand under saturated conditions

4.3.3 Graded gravel layerworks at optimum moisture content

Figure 4-27, Figure 4-28, Figure 4-29 and Figure 4-30 show the behaviour of the graded gravel at optimum moisture content at various cyclic load magnitudes.

Figure 4-27 shows this behaviour under a cyclic load magnitude of 20 kN. The first load cycle shows a large initial settlement. Thereafter, the hysteresis loops at 10, 100, 1000 and 10 000 become narrower. The settlement between 10 and 100 cycles is comparatively large, whereafter the settlement per log cycle becomes constant. The pavement passes 10 mm of settlement within 1000 cycles.

Figure 4-28 shows a similar behaviour for a cyclic load magnitude of 14 kN, where the settlement per log cycle is initially high but becomes constant after the 100th cycle. The load cycles at 100, 1000, 10 000 and 20 000 plot very close together and have a very similar hysteresis loop width and secant slope. This shows that the stiffness remains constant after a certain number of load applications. This could indicate that the pavement is approaching a stable equilibrium. This is even more evident in Figure 4-29 for a cyclic load magnitude of 10 kN where, apart from the first cycle, the cycles plot very close together for 10 to 40 000 cycles. There is a large gap between the first and tenth cycle, when compared to the gap between the tenth and subsequent cycles. This could mean that the bedding-in has not finished until the tenth cycle. The bedding error is higher for the test conducted at 10 kN than the one conducted at 14 kN, up to the 10th cycle, whereafter the settlement per log cycle is higher for the test conducted at 14 kN.

Figure 4-30 shows the load-settlement cycles at 3 kN cyclic load magnitude. The initial cycle only results in 1 mm permanent settlement. The width of the hysteresis loops gradually decrease as the number of cycles increase. This indicates that the energy loss in each cycle is decreasing and that the pavement is reaching a stable equilibrium, also known as 'shakedown' (Werkmeister et al., 2004). The slopes of the hysteresis loops remains constant after the first cycle. The permanent settlement from the tenth to the last cycle is less than 1 mm. It is apparent that under a small applied load, the pavement life extends indefinitely, as stated by Mamou et al. (2017).
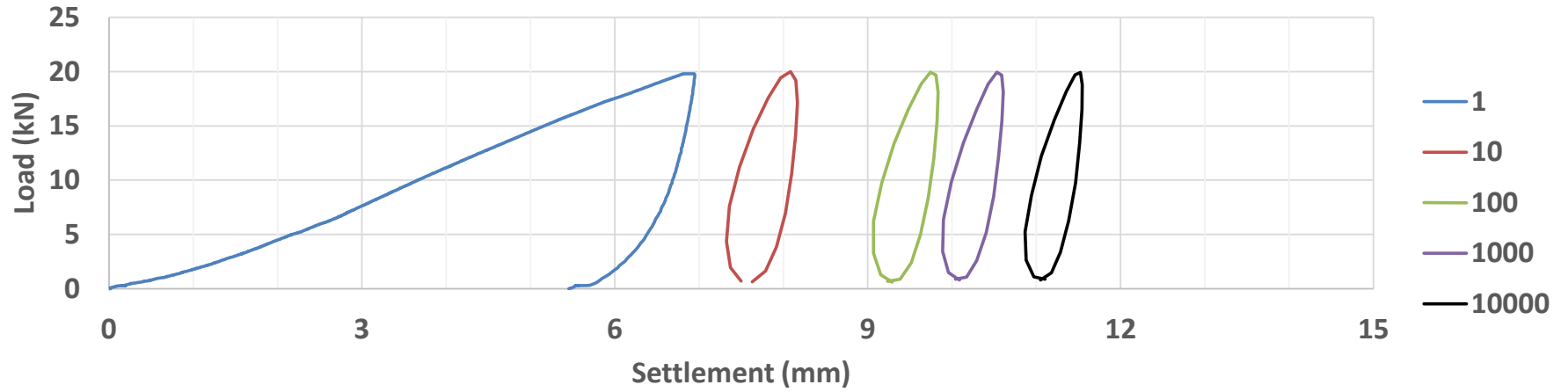
Figure 4-27: 20 kN (3500 kPa) load cycles for graded gravel at optimum moisture content
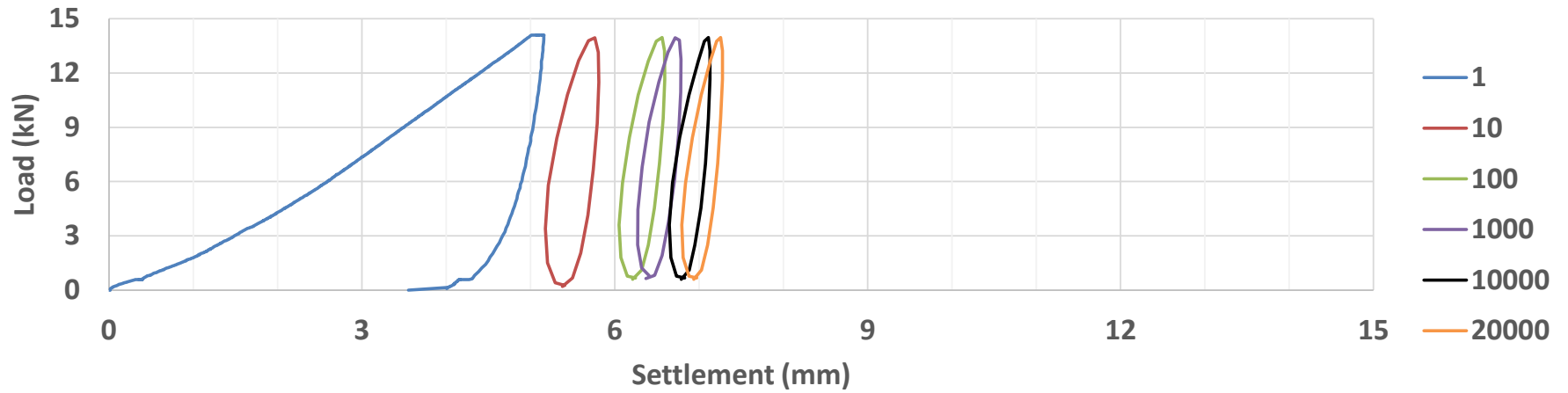
Figure 4-28: 14 kN (2450 kPa) load cycles for graded gravel at optimum moisture content
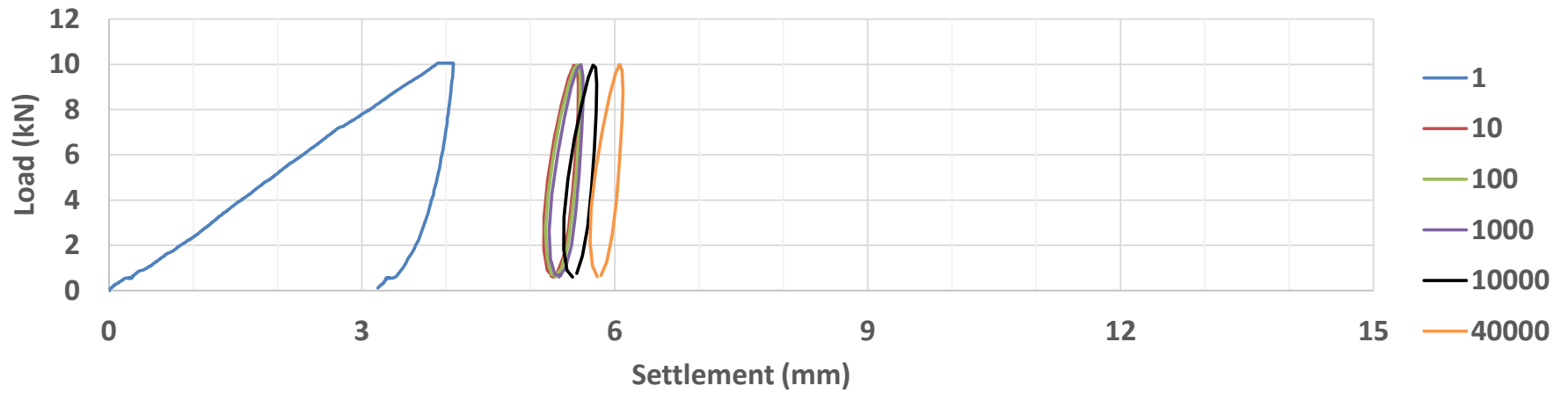
Figure 4-29: 10 kN (1750 kPa) load cycles for graded gravel at optimum moisture content
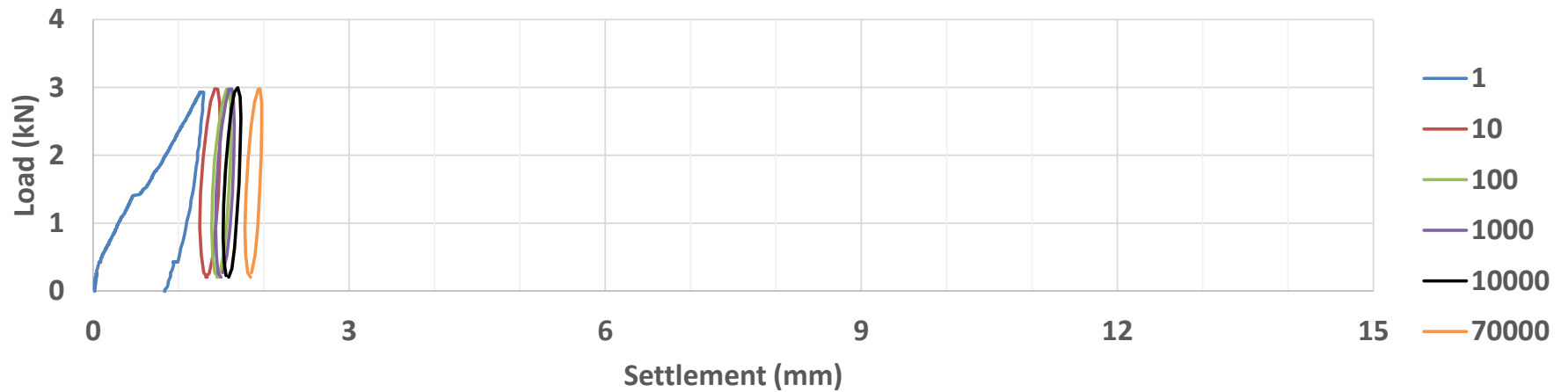
Figure 4-30: 3 kN (525 kPa) load cycles for graded gravel at optimum moisture content

4.4   STIFFNESS RESPONSE AND DAMAGE ACCUMULATION

In this section, the stiffness response and the damage accumulated during cyclic loading is shown. The stiffness is calculated from each hysteresis loop as shown in Figure 4-31. It should be emphasised that this stiffness cannot be called a resilient modulus, as the deformation due to the applied load cannot be simply quantified from the settlement measured on the surface. Deformation occurs throughout the pavement structure in various directions. The calculated stiffness (S_I) is therefore indicative, but not equal to, of the resilient modulus of the pavement. The units were calculated as kilo-Newton per millimetre (kN/mm).
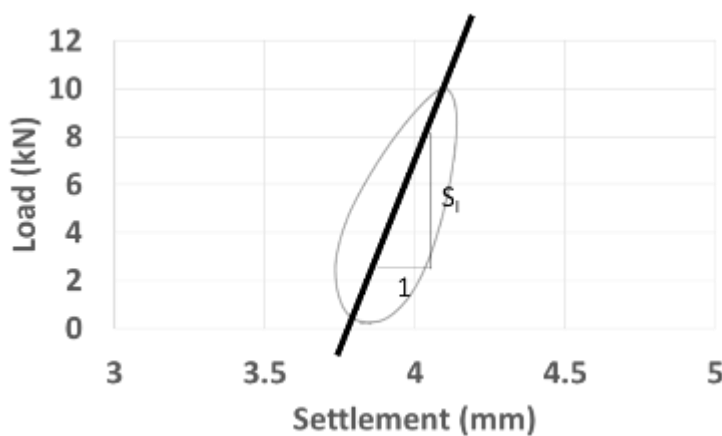
Figure 4-31: Determination of indicator stiffness (S_I) for each cycle

Apart from calculating the stiffness during cyclic loading, the work done on the pavement during each cycle was calculated. According to Werkmeister et al. (2004), the area of each hysteresis loop corresponds to the deformation work done on the soil. The size of the hysteresis loop indicates the energy loss per cycle of loading. Energy loss is also indicative of the damage done to the pavement during a single loading cycle. This energy loss can be calculated as the area of each hysteresis loop. The calculated units for the energy loss per cycle are in Joules (N.m). This principle is illustrated in Figure 4-32.
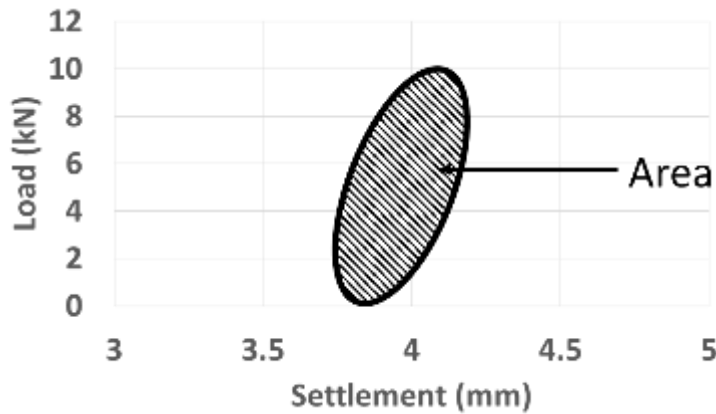
Figure 4-32: Area of hysteresis loop indicates energy loss during cycle (After Werkmeister et al., 2004)

4.4.1 Pavement stiffness during cyclic loading

As explained in Figure 4-31, the indicator stiffness was calculated for cycles 1, 100 and 1000. From cycle 1000 up to the end of testing, for each test, the indicator S_I remained relatively constant. For ease of portrayal, it was decided to only show results for the aforementioned cycles as after these cycles, the value remained approximately constant. Figure 4-33 shows S_I for fine silica sand at optimum moisture content. The stiffness is low during the first cycle for the three tests. Thereafter, the stiffness increases with an increase in the number of cycles. The stiffness of the pavement for the test performed at 3 kN (525 kPa) repeated load is the highest. The stiffness for all three tests shown is inversely proportional to the applied load. This is to be expected given the small-strain stiffness of soils which reduces with strain level as demonstrated by Clayton & Heymann (2001) as shown by the soil stiffness degradation curves in Figure 4-33. For road pavement it would be advantageous if small strain stiffness can be applied. This superior stiffness is available at small strains, i.e. at lower loads. This illustrates the importance of not overloading road pavements.
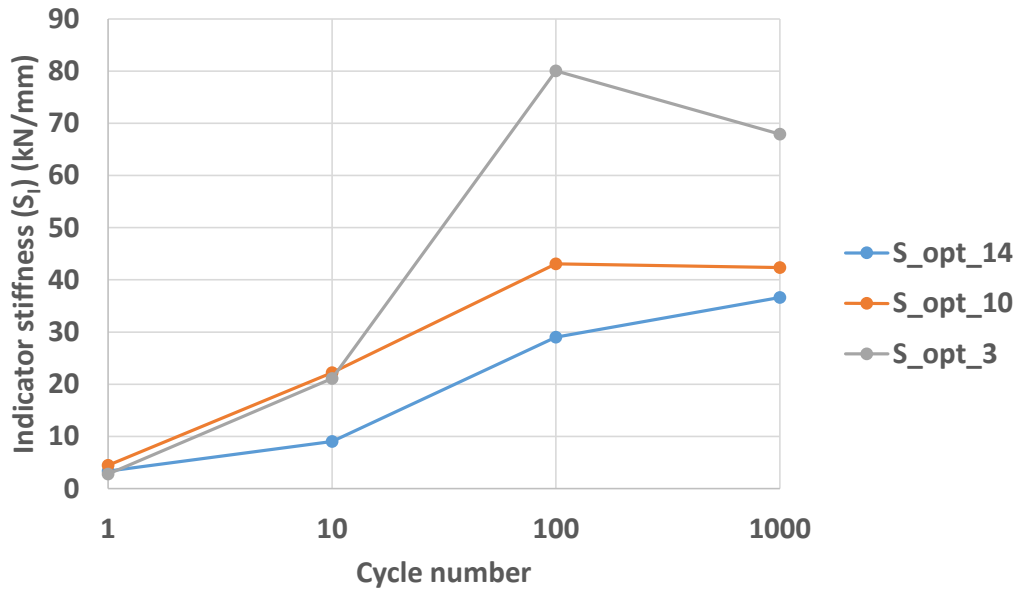
Figure 4-33: Indicator stiffness for cyclic tests done on fine silica sand pavement at optimum moisture content

In Figure 4-34, the indicator stiffness is shown for the tests performed on the saturated silica sand pavement. Again, the stiffness is very low initially and then increases with an increase in the number of load applications. The two loading conditions exhibit very similar stiffness response. This stiffness is lower when compared to the same loading cycles at optimum moisture content (Figure 4-33).
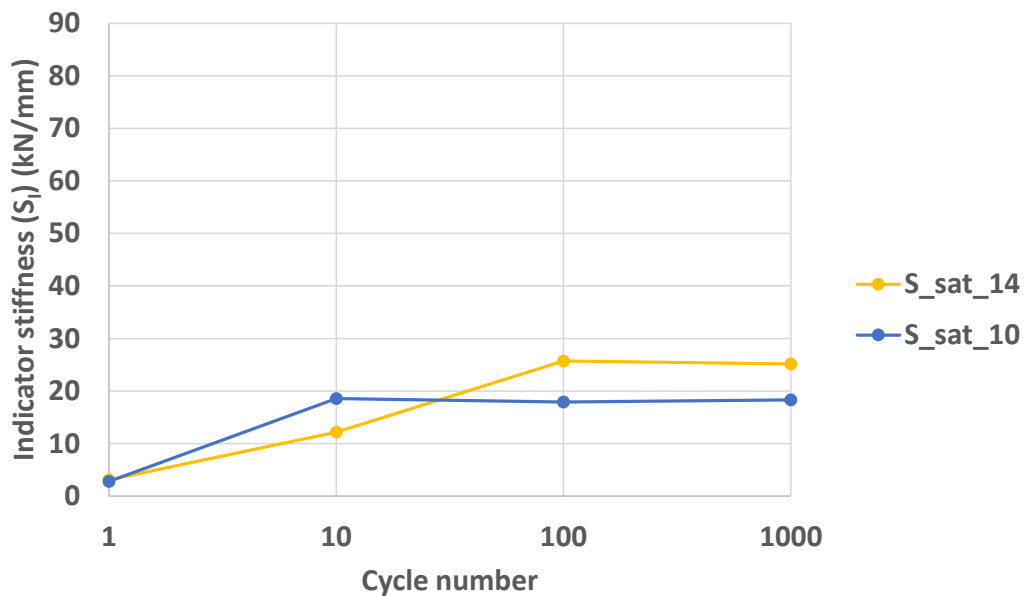
Figure 4-34: Indicator stiffness for cyclic tests done on fine silica sand pavement under saturated conditions

Figure 4-35 shows the indicator stiffness for the cyclic tests done on the pavements which were constructed with graded gravel at optimum moisture content. As with the other tests, the pavements had a very low stiffness during the first load cycle. Thereafter, the stiffness was higher for the pavements tested under a cyclic load of 10, 14 and 20 kN or respective pressures of 1750, 2450 and 3500 kPa. The stiffness reduces marginally for the test conducted at 3 kN. The overall stiffness for the tests conducted on the graded gravel are lower than for those on fine silica sand at optimum moisture content. This could be due to poorer bedding in the tests on the gravel as the gravel is a less compliant material causing difficulty to bed the slabs properly. This would have resulted in more stiffness contribution from the concrete slab and less from the soil as the slab first had to deflect before loading the underlying soil, as compared to the pavement constructed on fine silica sand, a more compliant material which would have offered better support to the slab.
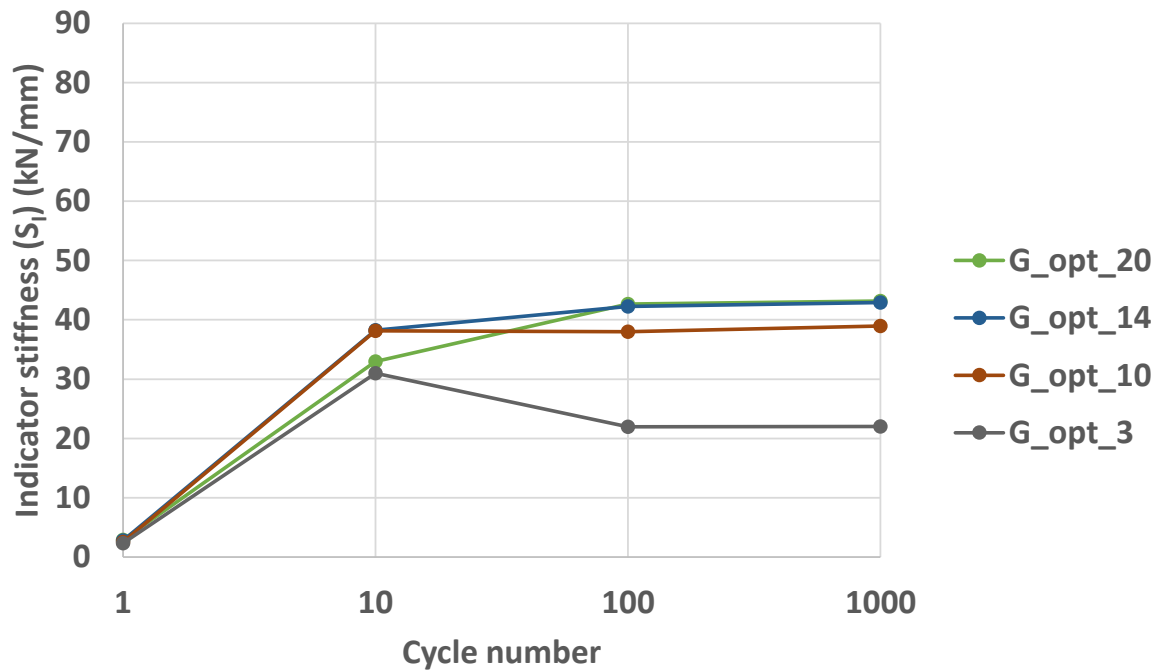
Figure 4-35: Indicator stiffness for cyclic tests done on graded gravel at optimum moisture content

4.4.2 Damage accumulation during cyclic loading

The energy loss, as an indicator of damage to the pavement, was also calculated for cycles 1, 100 and 1000. All results are plotted on the same vertical scale to allow comparison. The results for the tests conducted on fine silica sand at optimum moisture content are shown in

Figure 4-36. The greatest energy loss occurred during the first cycle and then reduced as the number of cycles increased. This complements the stiffness response for the same sequence of tests, with a low stiffness matching a large energy loss and a higher stiffness matching a lower energy loss. In this case, the energy loss per cycle is proportional to the applied load. This indicates that more internal damage occurs to the pavement at higher loads. The very low energy loss per cycle for the test conducted at 3 kN indicates that the pavement response is purely resilient and is due to generally elastic deformation of single grains and the slab and limited recoverable particle reorientation (Werkmeister et al., 2004).
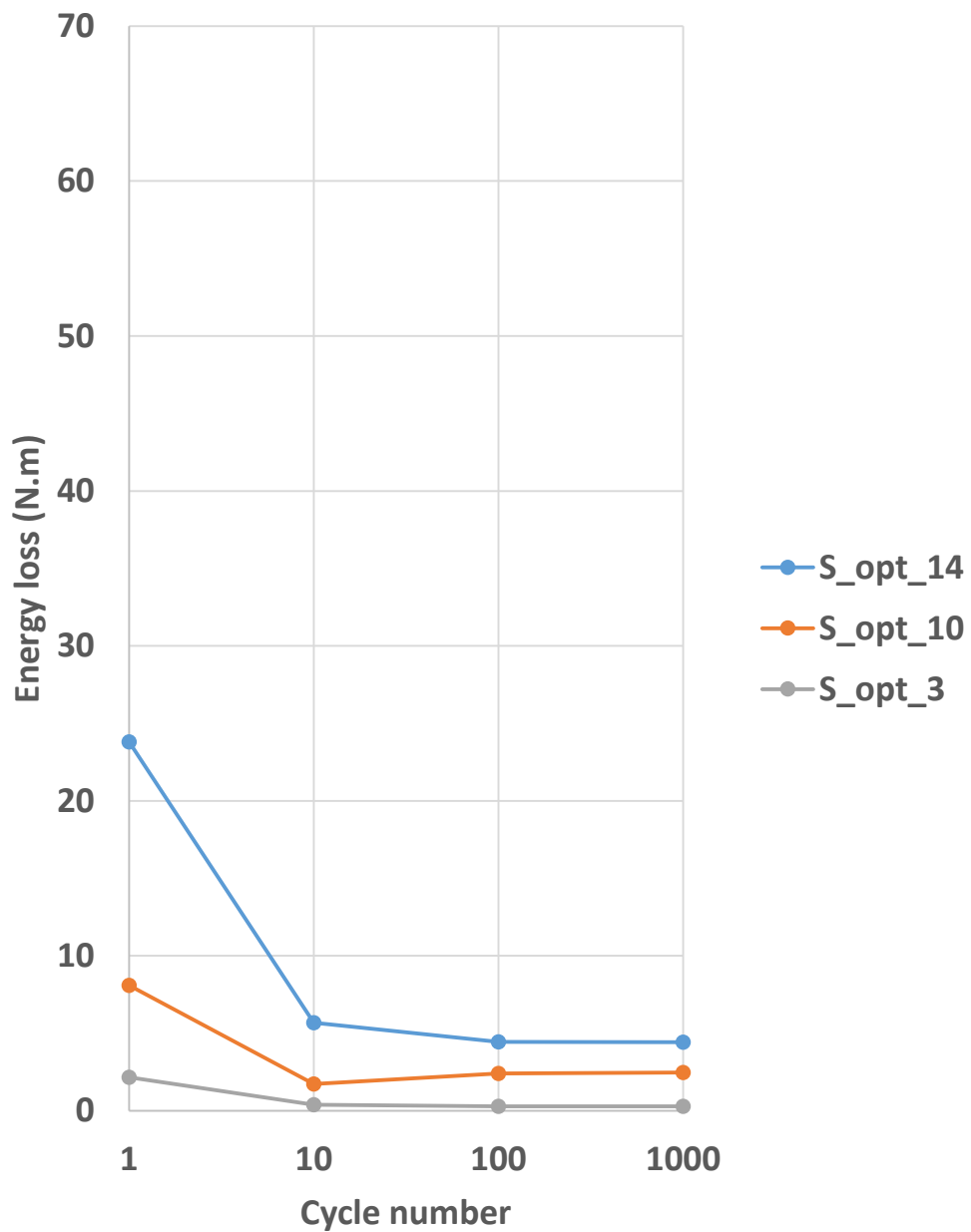
Figure 4-36: Energy loss during cyclic loading for tests conducted on fine silica sand at optimum moisture content

Figure 4-37 shows the energy loss per cycle for the tests conducted on fine silica sand under saturated conditions. Apart from the energy loss being highest during the first cycle, the energy loss per cycle is higher than for the tests conducted at optimum moisture content (Figure 4-36).
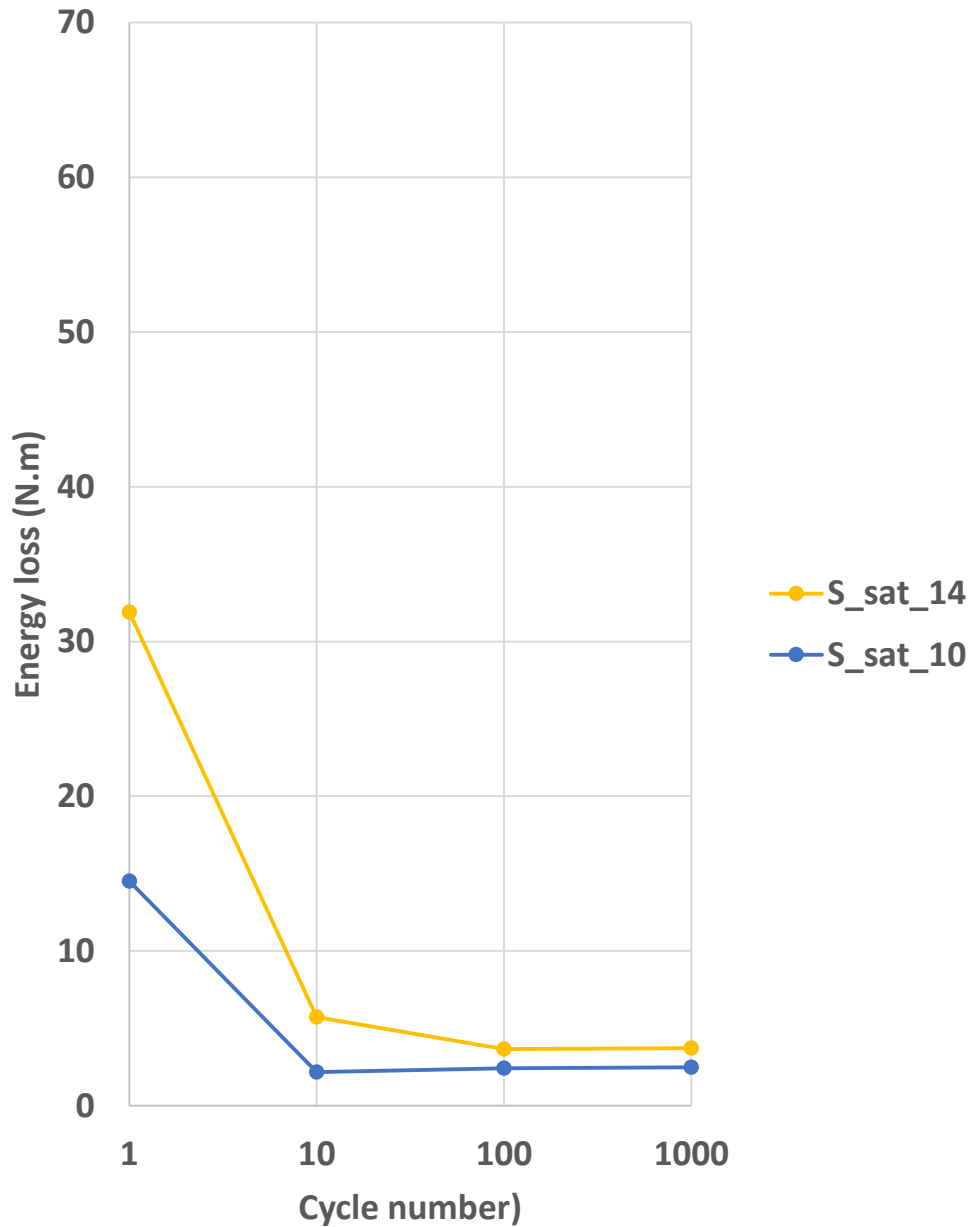
Figure 4-37: Energy loss during cyclic loading for tests conducted on fine silica sand under saturated conditions

The same pattern of high energy loss during the first cycle can be seen in Figure 4-38 for tests conducted on the graded gravel at optimum moisture content.
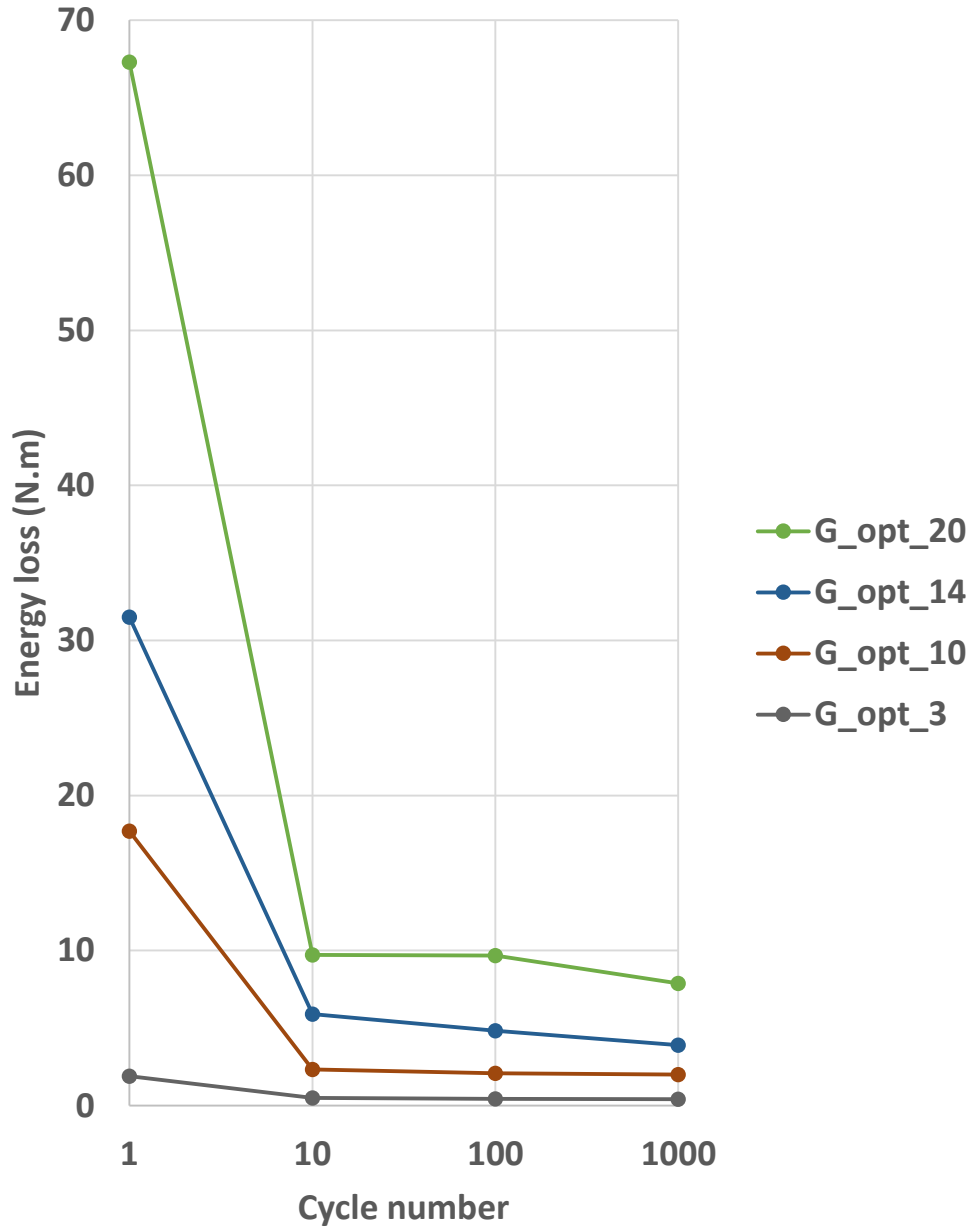
Figure 4-38: Energy loss during cyclic loading for tests conducted on fine silica sand at optimum moisture content

4.5 COMPARING CYCLIC VS MONOTONIC DEFORMATION MECHANISMS

Under cyclic loading, pavements settled as strains accumulated under the repeated applied load. This settlement was measured by the LVDT on the loading bogey as well as the LVDT within the piston of the hydraulic load jack. Besides these measured settlements, which were only surface measurements, it is also necessary to observe the strains occurring within the pavement structure throughout its depth. This was done using Digital Image Correlation (DIC) using a series of images taken during the loading of the pavement.

For each magnitude of settlement reached during the cyclic tests, the same settlement, albeit at different loads, was reached at some stage during the monotonic tests. It was of interest to compare the deformation mechanisms in the pavement at given settlements reached respectively under monotonic and cyclic loading. If these deformation mechanisms at given displacements were similar, it could be argued that the cyclic testing can be simulated by simply applying monotonic loading to cause the amount of displacement associated with the degree of damage under consideration. For example, suppose that the application of 100 000 load cycles of 10 kN (1750 kPa) resulted in 8 mm of settlement of the bogey on the model pavement. It was desired to investigate whether the associated pavement damage can simply be imposed by applying a monotonic load to cause 8 mm of settlement. Should the two deformation mechanisms be similar, the application of monotonic load represents an accelerated test method, saving the time to impose a large number of load cycles.

Although such deductions could be made by comparing the settlement results from the cyclic and monotonic tests, the pavement deformation mechanisms involved should also be investigated. During the settlement under wheel loads (rutting) and failure of a road pavement, the mechanism by which it settles and fails should be understood to inform the design and analysis of similar pavements.

In this section, results from cyclic and monotonic tests are compared at the same settlement values examining the results from the DIC. Images taken during the monotonic and cyclic tests are analysed to compare the deformation mechanisms that developed during the loading of the pavement. For this purpose, the strain development at specific magnitudes of settlement from the cyclic and monotonic tests were compared.

4.5.1 Silica sand layerworks at optimum moisture content

A monotonic load test was done on a pavement in which the layerworks were constructed of fine silica sand which was compacted at optimum moisture content to 95% MOD AASHTO dry density. Cyclic load tests to 14 kN (2450 kPa), 10 kN (1750 kPa) and 3 kN (525 kPa) were performed on models with the same specifications as the model used in the monotonic test. At various stages within each cyclic load test, settlement magnitudes were identified that match up to the same settlement at a specific load during the monotonic test. (The monotonic tests were performed under displacement control while the cyclic tests were conducted under load control.)

4.5.1.1 Cyclic load of 14 kN (2450 kPa)

Figure 4-39 shows the record of settlement experienced by the bogey under a repetitive cyclic load of 14 kN (primary vertical axis). The settlement plotted for the cyclic loading is the idealised settlement, as explained in Section 4.2.1. Also plotted, for the same range of settlement during the cyclic loading, is the settlement under monotonic loading (secondary vertical axis). The settlement during the monotonic test at a load of 14 kN (2450 kPa) is slightly higher than the settlement during the first application of 14 kN during the cyclic load test. This could be due to the rate at which the load was applied. Cyclic tests occur at a higher loading rate than the monotonic test. A more gradual rate of loading can result in higher displacement than a higher rate of loading. The cyclic test was concluded after 5400 cycles of 14 kN had been applied to the pavement. The settlement after 5400 cycles of 14 kN corresponds to the settlement caused by a monotonic load of 26 kN (4550 kPa). Settlement appeared to increase approximately linearly with the logarithm of the number of load cycles but showed an acceleration beyond approximately 1100 cycles.

Figure 4-39: Cyclic load test performed at 14 kN (2450 kPa) on fine silica sand layerworks at optimum moisture content with identified settlements

Three points on the settlement curve were identified for which DIC was performed. Images were analysed for settlements of 3.51, 9.63 and 10.2 mm for both the cyclic and monotonic tests. These are indicated by the vertical blue lines in Figure 4-39. Therefore, the mechanisms at play during the settlement could be compared for the cyclic and monotonic tests for the specific settlements for the identified points.

Figure 4-40 shows the maximum shear strain development during the cyclic load test (on the left) and the monotonic test (on the right) at the same settlement values. The first row shows the shear strain experienced during the 5th cycle on the left and at a load of 17 kN (2975 kPa) during the monotonic loading of the model on the right. Both correspond to the same settlement value of 3.51 mm. The second row shows the shear strain experienced during the 3500th cycle during cyclic loading and a load of 25 kN (4375 kPa) during the monotonic load test on the left and right respectively. The same pattern is followed for the rows that follow and in the rest of the figures in this section. Symmetry was assumed and therefore only the right half of the model are presented from the DIC analysis.

Figure 4-40: Comparison of shear strain development for 14 kN (2450 kPa) cyclic load against result from monotonic test at specific settlement magnitudes for fine silica sand layerworks at optimum moisture (legend shows maximum shear strain percentage)

Although the settlement magnitudes are the same for each image in the left and right-hand columns, the deformation mechanisms are not entirely the same. For 3.51 mm settlement (5 cycles / 17 kN monotonic load), the mechanism during the cyclic loading shows deeper shear strain zones than for the same settlement during the monotonic loading. The slip planes are also more pronounced during the monotonic loading. During monotonic loading, once a slip plane had developed, all the strain was concentrated on this slip surface as the load was increased. During cyclic loading a slip plane formed initially. However, with the removal of the load, particles could reorientate under the lower effective stress into a state of lower contact stress. This reorientation disturbed the slip plane development. Once load was reapplied, the slip did not occur on exactly the same surface as the cycle before. This pattern continued for each loading cycle. Because of this, the shear band in which slip occurred was wider for the cyclic loading than for the monotonic loading.

4.5.1.2 Cyclic load of 10 kN (1750 kPa)

Figure 4-41 shows the settlement of the loading bogey under a 10 kN (1750 kPa) cyclic load for the pavement constructed with layerworks at optimum moisture content. Settlement for the same range are shown for the monotonic test. The monotonic load of 10 kN (1750 kPa) resulted in more settlement than the first three applications of a cyclic load of 10 kN. The settlement under a monotonic load of 20 kN (3500 kPa) was the same as the settlement experienced by the pavement after 15 000 cycles when the cyclic test was ended. Settlement appeared to increase approximately linearly with the logarithm of the number of load cycles and did not show the acceleration in settlement observed for the 14 kN (2450 kPa) cyclic load.
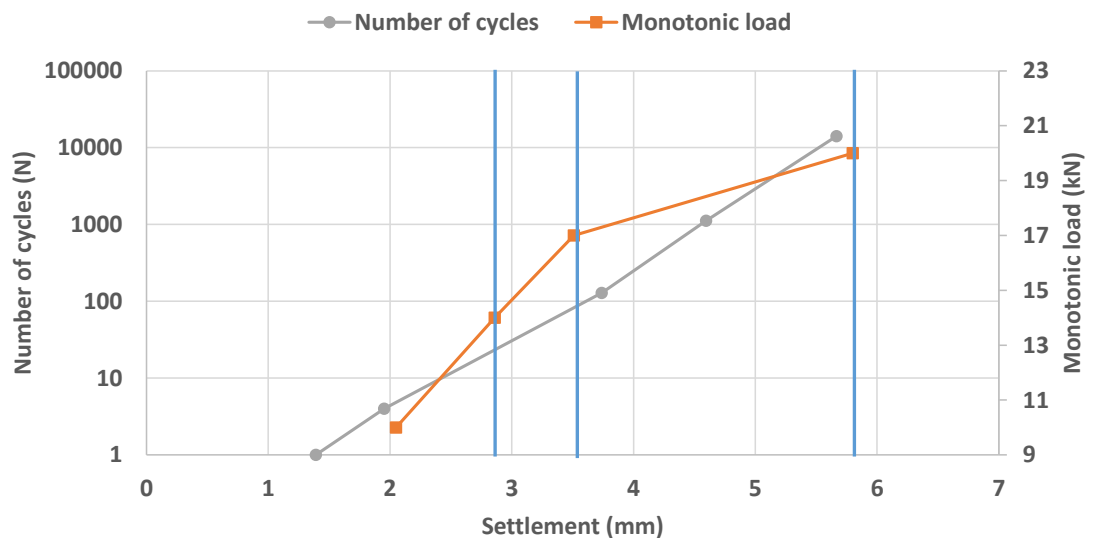
Figure 4-41: Cyclic load test performed at 10 kN (1750 kPa) on fine silica sand layerworks at optimum moisture content with identified settlements

Figure 4-42 shows the shear strains at stages during the cyclic load. At 2.86 mm of settlement, a wider shear zone can be seen for the cyclic load than for the monotonic load. At 3.51 mm settlement, an approximately similarly shaped mechanism can be identified. The slip plane in the monotonic load is more clearly evident than for the cyclic load and showed higher strain intensity. The slip zone which developed in the cyclic test was more widespread. The same can be said of the last row which represents the mechanisms for 5.8 mm of settlement.

Figure 4-42: Comparison of shear strain development for 10 kN (1750 kPa) cyclic load against result from monotonic test at specific settlement magnitudes for fine silica sand layerworks at optimum moisture (legend shows maximum shear strain percentage)

4.5.1.3 Cyclic load of 3 kN (525 kPa)

Figure 4-43 shows the settlement behaviour of the loading bogey under a repetitive load of 3 kN. The load-settlement behaviour under monotonic loading is also shown for the same range of settlement. It can be noted that, unlike with the cyclic loads of 14 kN (2450 kPa) and 10 kN (1750 kPa), the first application of 3 kN (525 kPa) during cyclic loading resulted in larger settlement than the settlement for 3 kN under monotonic loading. This could be due to the bedding error being larger for the cyclic loading than for the monotonic loading or difficulty in controlling the cyclic load application at small loads. The difference in settlement is 0.17 mm. Three stages during the cyclic load test were identified for which DIC was performed. For the same magnitudes of settlement, DIC was performed on the monotonic test and are indicated by the blue lines in Figure 4-43. The slope change at approximately 7000 cycles is believed to be related to problems associated with the control of the small cyclic loads. This is attributed to limitations of the press used.
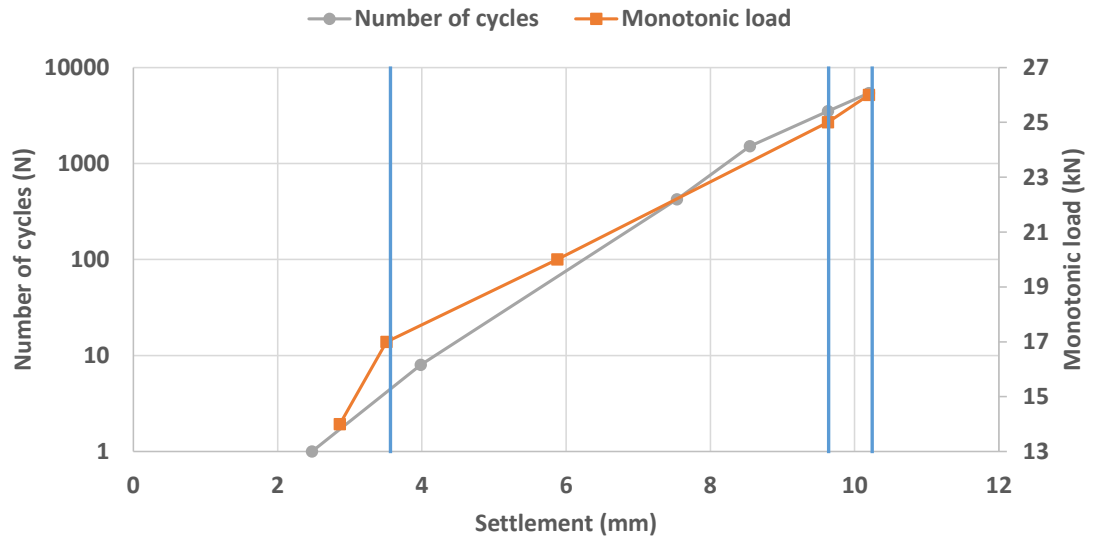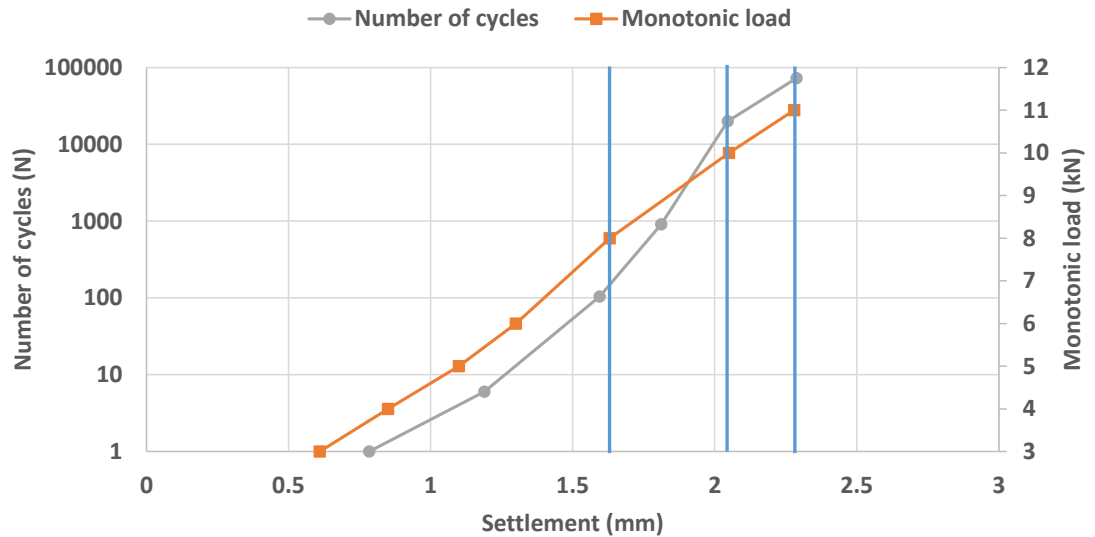
Figure 4-43: Cyclic load test performed at 3 kN (525 kPa) on fine silica sand layerworks at optimum moisture content with identified settlements

In Figure 4-44, the results from the DIC analysis can be seen. The maximum shear strain development in the right half of the model is shown for the cyclic and monotonic loads. The strains were small for the selected settlements and therefore had to be magnified. All the rows show a more intense shear strain zone immediately below the contact point of the loading bogey for the cyclic load test than for the monotonic test. The load intensity in the monotonic test was more severe than in the cyclic test to cause the same amount of settlement. This is opposite to what was seen for the previous results described for Figure 4-40 Figure 4-41. As mentioned for Figure 4-43, this could be due to the bedding error being larger for the cyclic test than for the monotonic test. Due to poor bedding in of the slab, it is expected that the shear strains would be located closer to the point of contact than being spread out to a greater depth in the soil. For the monotonic test, it can be seen that the shear bulb is not symmetrical below the point of contact of the loading bogey. This was due to the interference of the adjacent strip load on the left hand side (not shown due as only half of the model being analysed). This only became apparent in the cyclic test after 75 000 cycles. The depth of the shear strain bulb below the point of contact after 75 000 cycles matches the depth of the shear zone in the monotonic test. This could be that, due to the low magnitude of the load, it took a large number of cycles before the slab had settled in such a way as to overcome the initial bedding error and to transfer the load to the soil in the same way as the slab in the monotonic test.
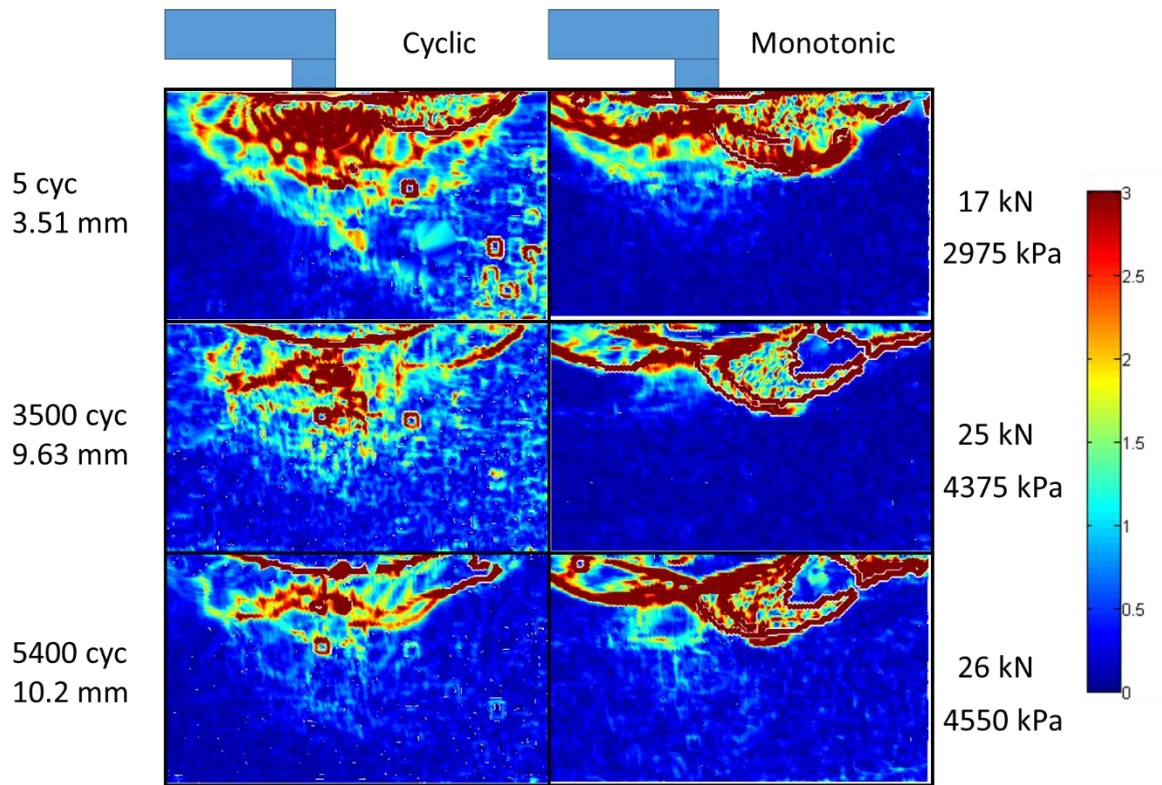
Figure 4-44: Comparison of shear strain development for 3 kN (525 kPa) cyclic load against result from monotonic test at specific settlement magnitudes for fine silica sand layerworks at optimum moisture (legend shows maximum shear strain percentage)

4.5.2 Silica sand layerworks under saturated conditions

A monotonic load test was done on a pavement in which the layerworks were constructed of fine silica sand which was compacted at optimum moisture content to 95% MOD AASHTO dry density and then saturated overnight. Cyclic load test were performed at loads of 14 kN (2450 kPa) as well as 10 kN (1750 kPa) on models with the same properties as the one used for the monotonic load test. It was decided not to carry out tests at 3 kN (525 kPa) due to difficulty to accurately control the load press at small loads. Deformation mechanisms observed during the cyclic load tests were again compared to mechanisms in the monotonic load test at specific settlement magnitudes.

4.5.2.1 Cyclic load of 14 kN (2450 kPa)

Figure 4-45 shows the settlement during the cyclic test in which a repeated load of 14 kN was applied to the model. Also shown is the load-settlement behaviour during the monotonic test for the same settlement range. Similar to what was seen for the layerworks at optimum moisture content (Section 4.5.1.1), settlement appeared to increase approximately linearly

with the logarithm of the number of load cycles but showed an acceleration beyond approximately 1100 cycles. The settlement magnitude in the latter test was however greater.
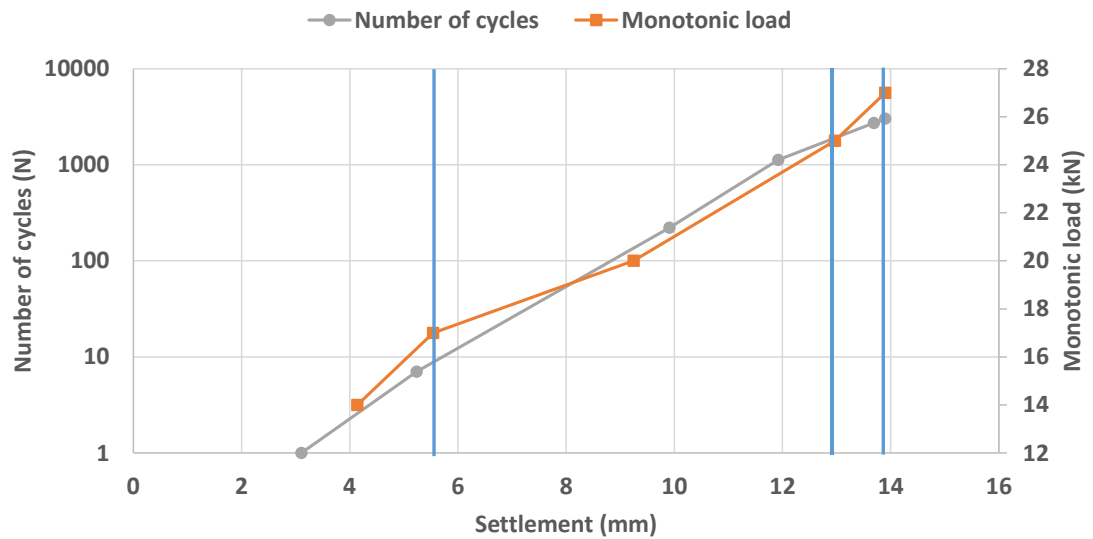
Figure 4-45: Cyclic load test performed at 14 kN (2450 kPa) on fine silica sand under saturated conditions with identified settlements

Figure 4-46 shows the maximum shear strain development at the same settlement magnitudes from the cyclic and monotonic test. At 5.54 mm settlement (9 cycles / 17 kN monotonic), the mechanisms had a similar shape, but the shear zone was slightly deeper for the cyclic load than for the monotonic load. At 13 mm settlement (2115 cycles / 25 kN monotonic), the apparent slip zone was wider for the cyclic loading than for the monotonic load. The shape and depth of the shear zone and slip plane for both the cyclic and monotonic loads were the same at 13.9 mm settlement (3100 cycles / 27 kN monotonic).

For both the monotonic and cyclic tests, the non-symmetrical shear behaviour about the contact point is evident. As explained before, this was due to the interference of the left hand strip load. The slip plane was also deeper for the cyclic load of 14 kN for saturated conditions than for the pavement constructed at optimum moisture content (shown in Figure 4-40).

In the case of the cyclic loading, strains seem to have been more uniformly distributed throughout the failure zone, while under monotonically applied load, deformation concentrated along failure planes, with limited deformation occurring inside the failure zone.

It is interesting to note greater similarity between the deformation mechanisms in the saturated material compared to the model at optimum moisture content (Section 4.5.1.1). Saturated material is less compressible than unsaturated material. The similarity in cyclic to

monotonic deformation mechanisms suggest that it may be valid to model cyclic loading of saturated materials by means of a monotonically applied load.
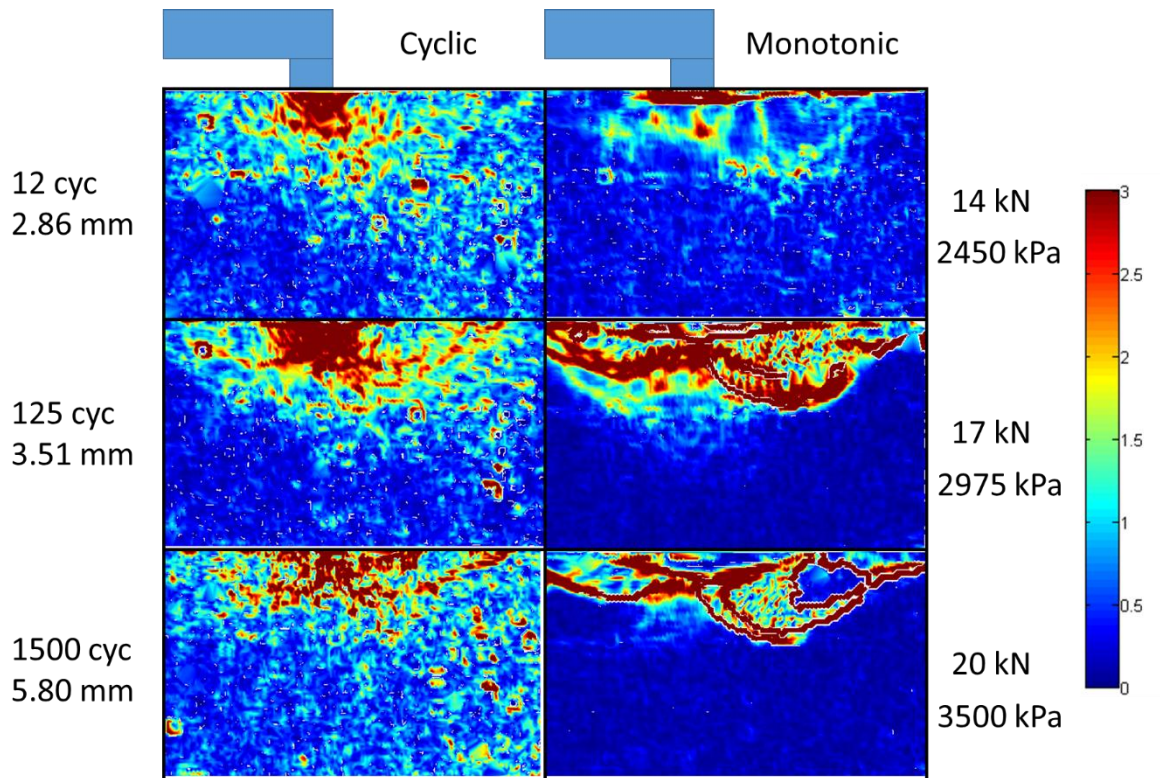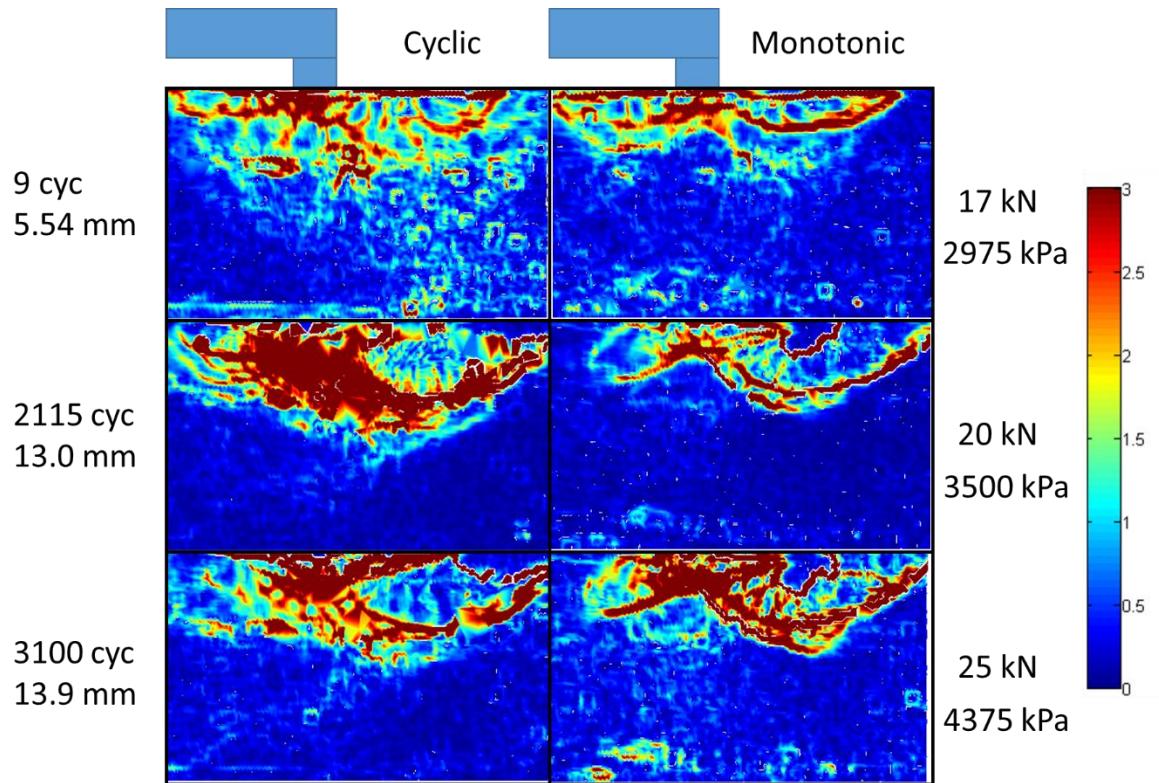

Figure 4-46: Comparison of shear strain development for 14 kN (2450 kPa) cyclic load against result from monotonic test at specific settlement magnitudes for saturated fine silica sand layerworks (legend shows maximum shear strain percentage)

4.5.2.2 Cyclic load of 10 kN (1750 kPa)

In Figure 4-47, the settlement behaviour of the pavement under a cyclic load of 10 kN is shown for a pavement tested under saturated conditions. The monotonic load-settlement behaviour is also shown for the same range of settlements. The settlement under a monotonic load of 10 kN was larger than the first two applications of 10 kN under cyclic loading. This could be due to a difference in bedding errors or due to the monotonic load being applied more gradually. Three positions during the cyclic load test were identified for DIC analysis and are indicated by the blue line in Figure 4-47. The test was concluded after 11 900 cycles of 10 kN had been applied to the pavement. In general, settlement appeared to increase approximately linearly with the logarithm of the number of cycles, but accelerated beyond 1000 cycles while it remained constant in the case of the test at optimum moisture content (Section 4.5.1.2). This deterioration is related to the build-up of positive pore pressure during cyclic loading (Mamou et al., 2017).
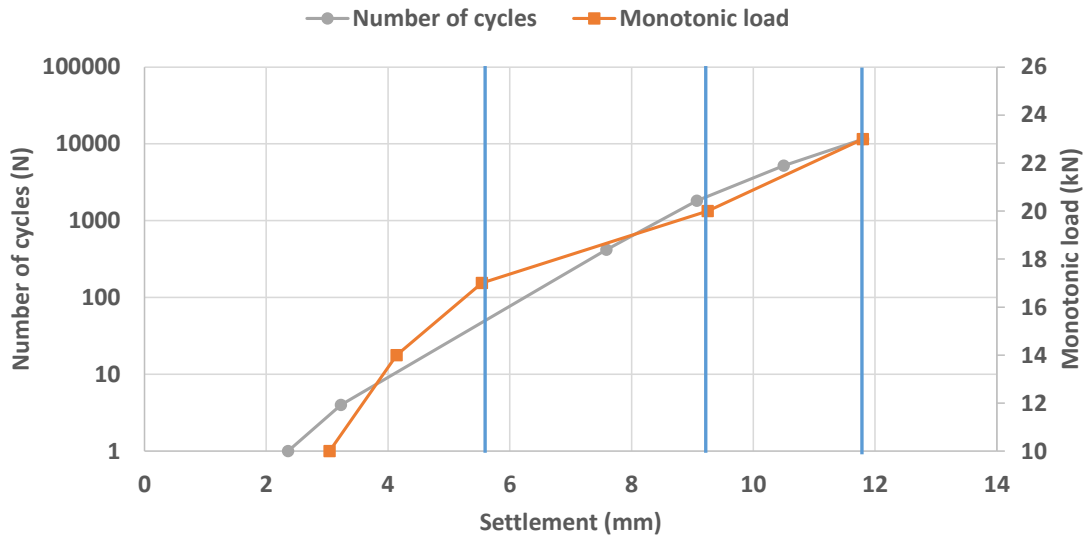
Figure 4-47: Cyclic load test performed at 10 kN (1750 kPa) on fine silica sand under saturated conditions with identified settlements

Figure 4-48 shows the maximum shear strain development. The depth of the shear zone for 5.54 mm settlement (14 cycles / 17 kN monotonic) is deeper for the cyclic load condition than during the monotonic test. The shape of the slip plane, which becomes evident for both the cyclic and monotonic test, was very similar for the cyclic and monotonic tests. There did, however, seem to be more interference from the adjacent strip load for the cyclic test than for the monotonic test. The shear strain mechanisms are also very similar for the cyclic test performed at 10 kN to those performed at 14 kN (shown in Figure 4-46) for the same settlement magnitude.

When compared to testing at optimum moisture content, the failure mechanisms for the two methods of testing (monotonic and cyclic) were more similar in the tests at optimum moisture content. This could be due to the incompressibility of the saturated material so that, under cyclic loading, the pavement tends to behave similar to testing under static load.
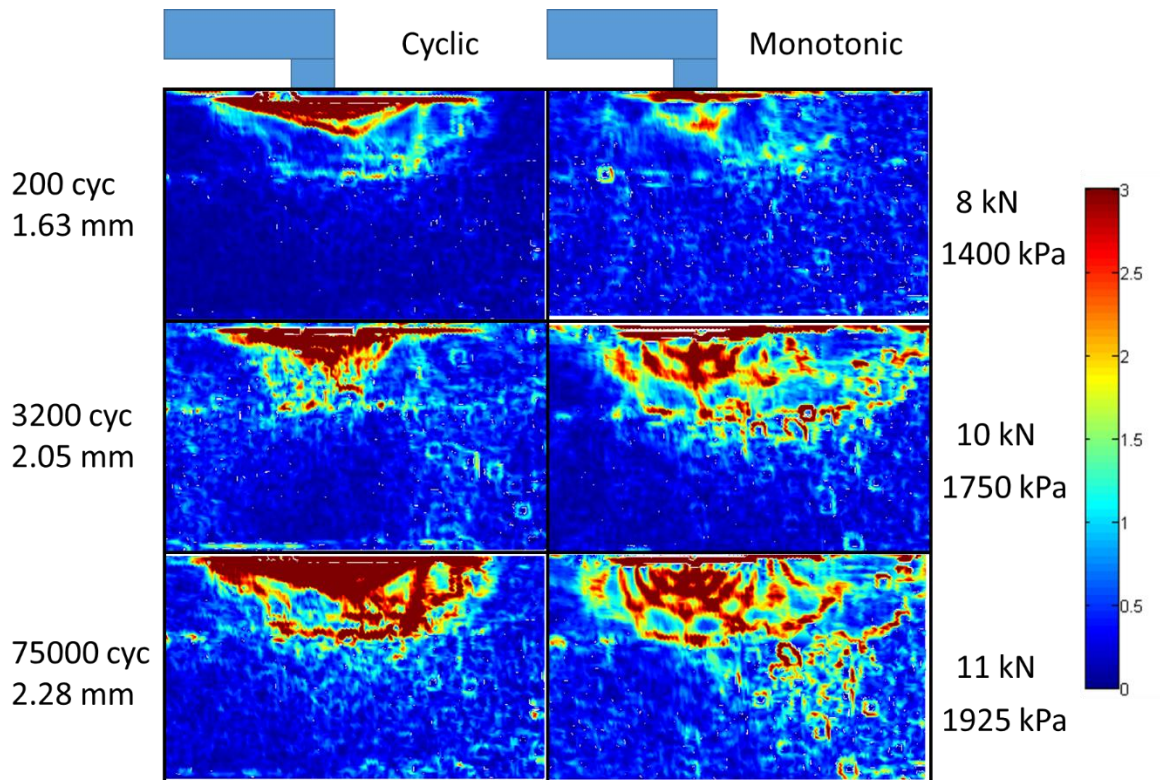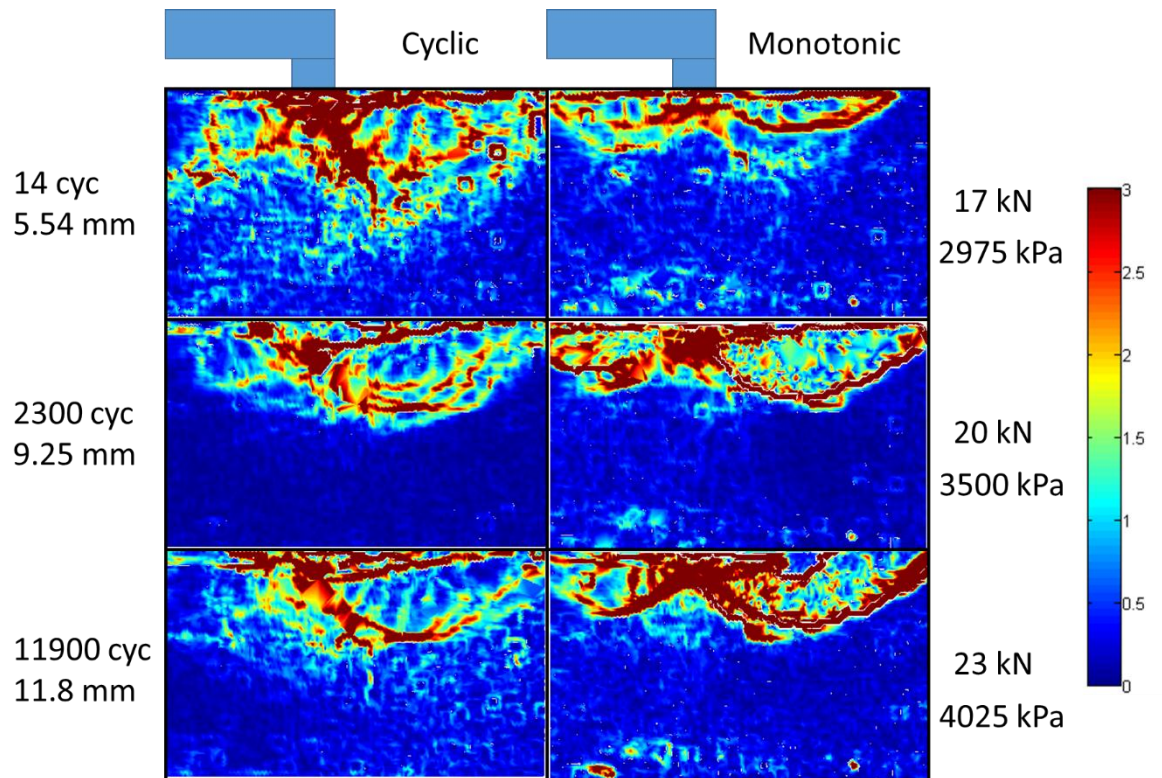
Figure 4-48: Comparison of shear strain development for 10 kN (1750 kPa) cyclic load against result from monotonic test at specific settlement magnitudes for saturated fine silica sand layerworks (legend shows maximum shear strain percentage)

4.5.3 Graded gravel layerworks at optimum moisture content

A monotonic load test was done on a pavement in which the base layers were constructed of a graded gravel which was compacted at optimum moisture content to 95% MOD AASHTO dry density. Cyclic load test were performed at loads of 20 kN, 14 kN, 10 kN as well as 3 kN on models with the same properties as the one used for the monotonic load test. The loads result in pressures in the strips below the loading bogey of 3500, 2450, 1750 and 525 kPa respectively.

4.5.3.1 Cyclic load of 20 kN (3500 kPa)

Figure 4-49 shows the idealised settlement for a cyclic test during which a repetitive load was applied of 20 kN to the pavement. Also shown is the monotonic load-settlement behaviour for the same settlement range. The first application of 20 kN during the cyclic tests resulted in a little more than 5 mm of settlement, while 20 kN during the monotonic test resulted in 6 mm of settlement. The loading rate during the cyclic test is higher than for the monotonic test, and therefore it can be expected that the settlement will be less. Settlements of 7.68, 9.38 and

11.1 mm were chosen for DIC analysis in both the cyclic and monotonic tests. These settlement values are indicated by the blue lines in Figure 4-49.

Figure 4-49: Cyclic load test performed at 20 kN (3500 kPa) on the graded gravel layerworks at optimum moisture with identified settlements

Figure 4-50 shows the maximum shear strain development for both the cyclic and monotonic tests compared for specific settlement values. Unlike the DIC performed on the tests in which the fine silica sand was used, the left half of the model was chosen for the DIC analysis in this case. For all settlement magnitudes in Figure 4-50, the shear zone during cyclic loading extended somewhat deeper into the pavement structure than for the same settlement magnitudes during the monotonic loads. This indicates that the cyclic application of the relatively high load resulted in some compaction at depth. It can be argued that whether cyclic or dynamic compaction occurs is not only frequency dependent (as described by Peralta (2010) in Table 2-1), but also the loading magnitude. It is therefore the rate of load application which determines the threshold at which dynamic compaction occurs. The shear zones for the monotonic tests appear to end at the interface between the base layers and the subgrade layer. The shear zone also seems to be fully developed within 10 cycles, as the shape, depth and magnitude of the shear remains very similar after 14 000 cycles to what it does after 10 cycles.

Figure 4-50: Shear strain development for 20 kN (3500 kPa) cyclic and monotonic test on the graded gravel layerworks at optimum moisture at specific settlement magnitudes (legend shows maximum shear strain percentage)

4.5.3.2 Cyclic load of 14 kN (2450 kPa)

Figure 4-51 shows the settlement under an idealised cyclic load of 14 kN and the monotonic load-settlement behaviour for the same settlement range. It can be observed that the initial settlement due to a cyclic load is lower than the settlement due to 14 kN during monotonic testing. This could be due to the rate at which the load is applied. The initial high rate of settlement during the cyclic tests could be due to bedding in, which something to be expected of the gravel. Thereafter, the rate plotted against log of number of cycles appears to be constant. Settlements of 5.11, 6.0 and 6.9 mm were chosen for DIC analysis and these are indicated by the blue lines in Figure 4-51.

Figure 4-51: Cyclic load test performed at 14 kN (2450 kPa) on the graded gravel layerworks at optimum moisture with identified settlements

The maximum shear strain development for the cyclic load is shown in Figure 4-52 on the left hand column and for the monotonic load on the right. The maximum shear strain distribution for 5.11 mm settlement (5 cycles / 17 kN monotonic) was very similar for the two loading conditions. The depth to which the shear strain occurs seems to be almost the same for both tests and was limited to the base layers. For 6 mm settlement (123 cycles / 20 kN monotonic), the shear depth in the cyclic load test was slightly deeper than in the monotonic load test. It still seemed to be largely limited to the base layers, with some minimal shear strain occurring in the top part of the subgrade. For 6.9 mm settlement (25000 cycles / 23 kN monotonic), the shear strain in the cyclic test is to a much shallower depth than for the monotonic test. The interface between the subgrade and base layers is still clearly visible for both. When compared to the sand, the strain seems to be less concentrated along shear bands, with strain occurring more uniformly and is distributed throughout the gravel layers. This may indicate poor compaction. This is not unlikely, as the gravel layerworks had to be compacted on a subgrade of sand which had a much lower density than the gravel. The density of the gravel could therefore have been at a density lower than the maximum dry density it was indented to be at.

Figure 4-52: Shear strain development for 14 kN (2450 kPa) cyclic and monotonic test on the graded gravel layerworks at optimum moisture at specific settlement magnitudes (legend shows maximum shear strain percentage)

4.5.3.3 Cyclic load of 10 kN (1750 kPa)

In Figure 4-53, the idealised settlement of the pavement under a cyclic load of 10 kN can be seen. The same range of settlements for the load-settlement behaviour during monotonic testing is also shown. It can again be seen, as for the cyclic test conducted at 14 kN on the graded gravel, that the initial slope of the settlement graph is high. This is due to poor bedding which can be attributed to poor compaction of the gravel due to the difference in densities of the graded gravel layerworks and the sand subgrade below. The settlement, due to the lower loading rate, is higher for the monotonic test at 10 kN than for the first load application of 10 kN during the cyclic test.
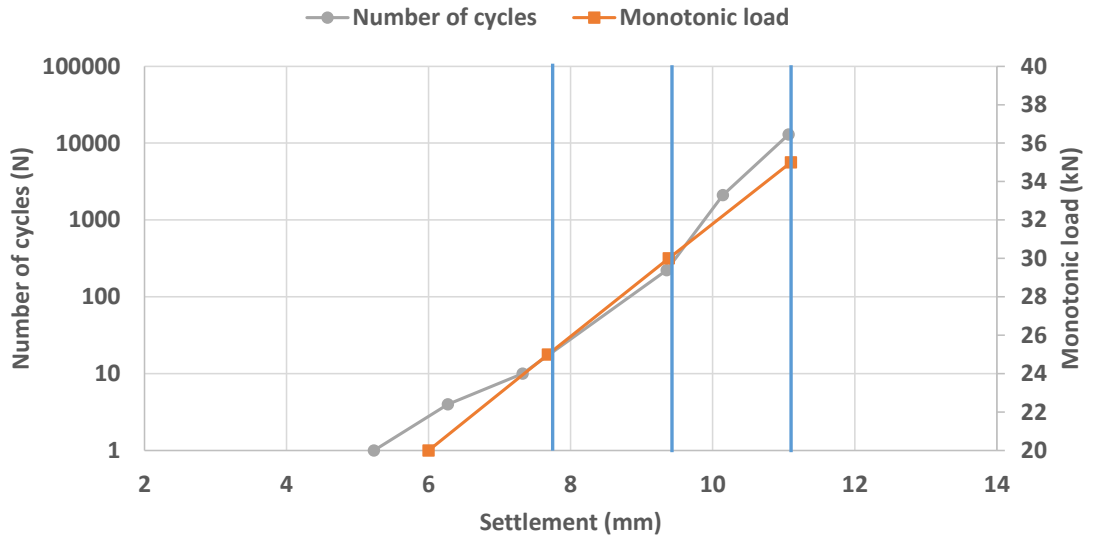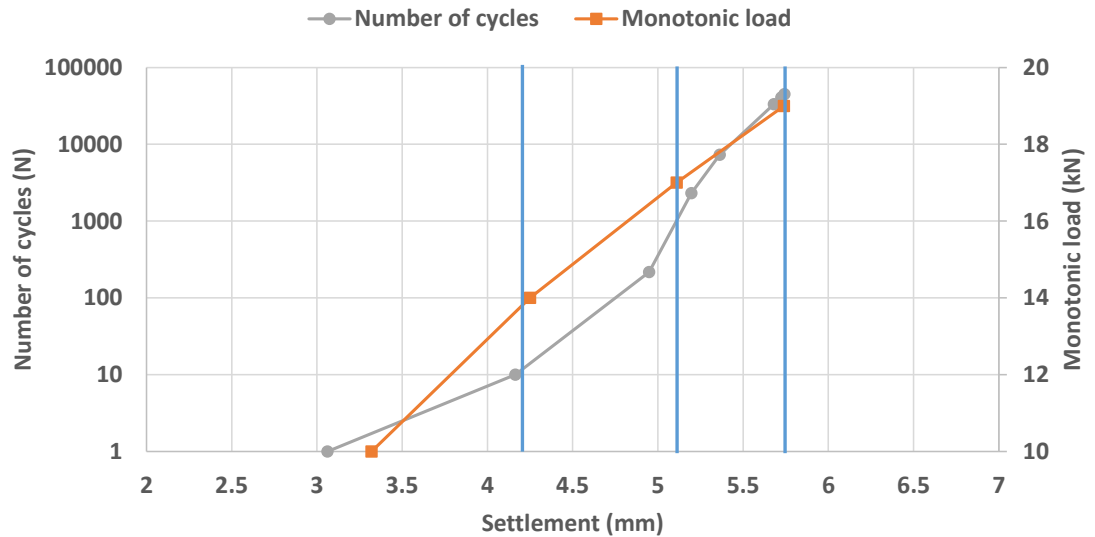
Figure 4-53: Cyclic load test performed at 10 kN (1750 kPa) on the graded gravel layerworks at optimum moisture with identified settlements

Settlement values of 4.2, 5.11 and 5.74 mm were identified for DIC analysis in both the cyclic and monotonic tests. These are shown as the blue lines in Figure 4-53. The results of the DIC analysis, in terms of maximum shear strain, are shown in Figure 4-54. The strain intensity and spread was greater for the monotonic test (on the right in the figure) than for the cyclic test (on the left in the figure). This is similar to what was seen for the test conducted on fine silica sand at a very low load magnitude (Figure 4-44). This may be due to poorer bedding in for the model tested under monotonic loading conditions. The settlement values that were chosen are very close together – ranging from 4.2 mm to 5.7 mm. This may be the reason for the shear zone and intensity being largely unchanged for the three chosen settlement values during the cyclic test.
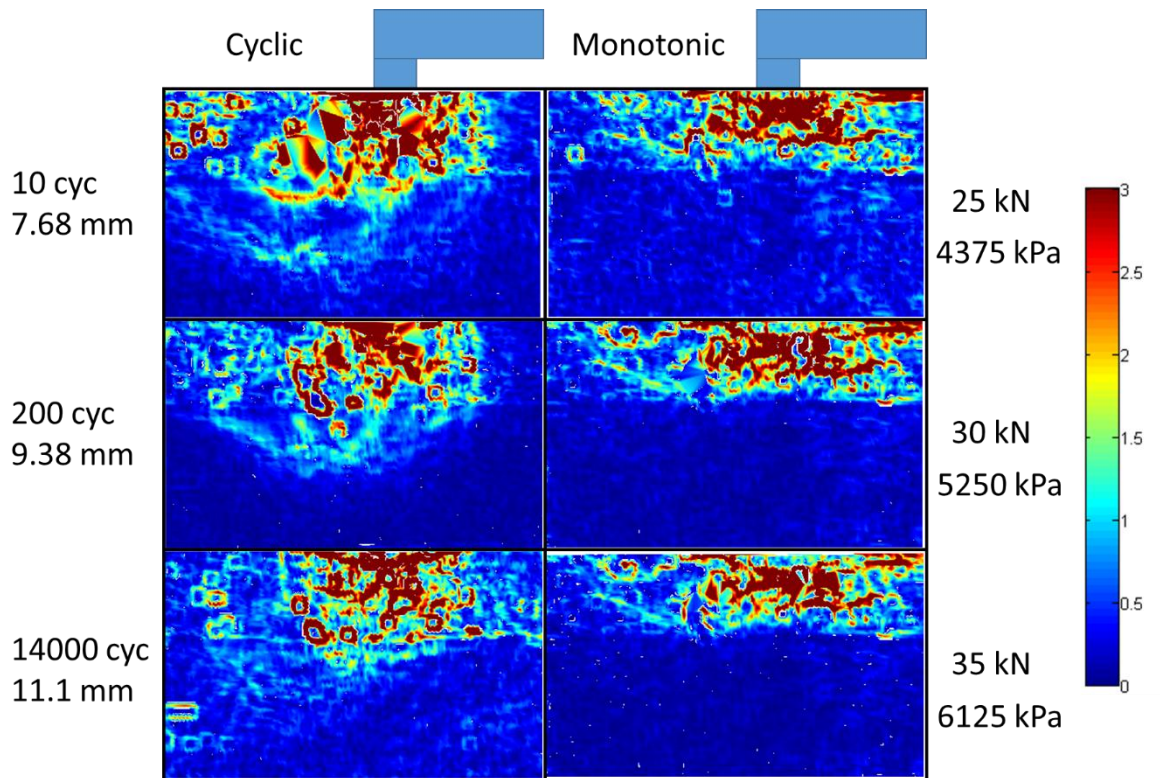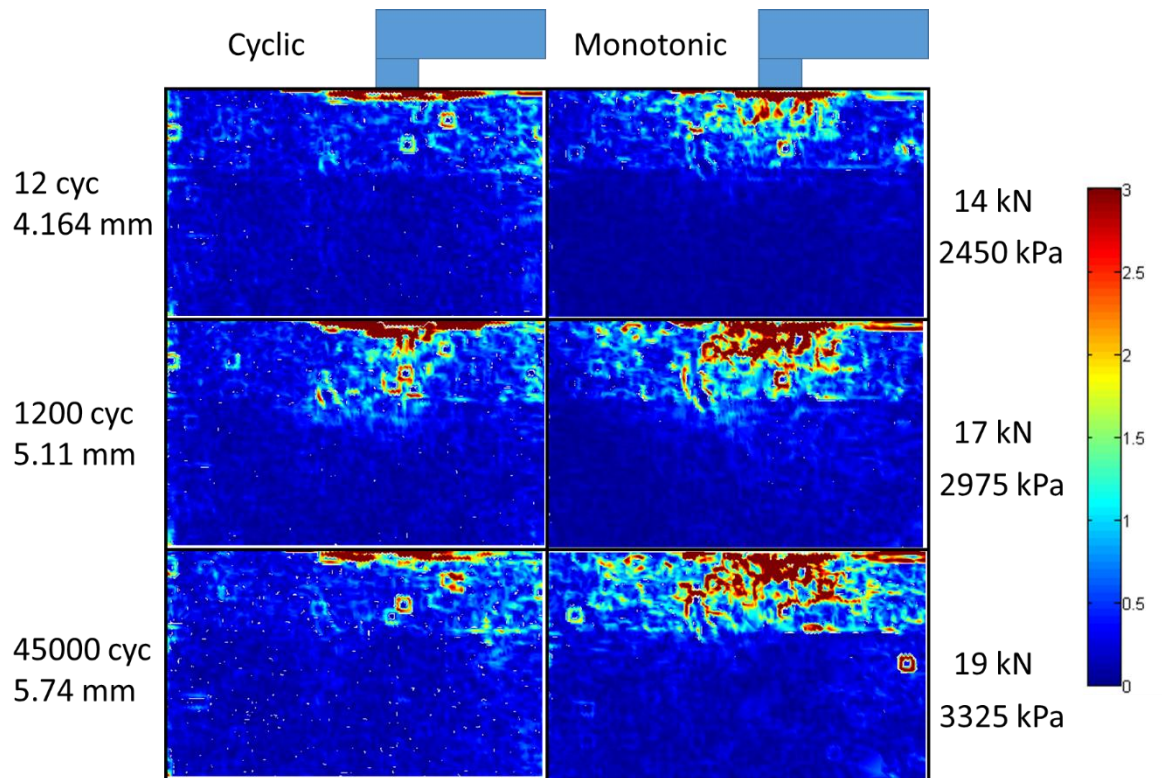
Figure 4-54: Shear strain development for 10 kN (1750 kPa) cyclic and monotonic test on the graded gravel layerworks at optimum moisture at specific settlement magnitudes (legend shows maximum shear strain percentage)

4.5.3.4 Cyclic load of 3 kN (525 kPa)

Figure 4-55 shows the idealised settlement behaviour of a pavement tested at a cyclic load magnitude of 3 kN. Also shown is the monotonic load-settlement behaviour for the same range of settlements. The rapid settlement towards the beginning of the cyclic test is probably associated with the initial setting in. Thereafter, the settlement trend with the log of the number of cycles appears to be constant up to about 10 000 cycles. After 10 000 cycles the settlement rate begins to accelerate again. Three settlement values, were selected for comparison of deformation mechanisms in the cyclic and monotonic test. These are 1.25, 1.50 and 1.80 mm and are indicated by the blue lines in Figure 4-56. For 1.25 mm settlement, 10 cycles of 3 kN (525 kPa) need to be applied or 4 kN (700 kPa) needs to be applied monotonically. To get 0.25 mm more settlement (1.50 mm), the load has to be increased to 5 kN (875 kPa). To get 1.80 mm settlement, numerous cycles of 3 kN (525 kPa) need to be applied or a monotonic load of 6 kN needs to be applied.
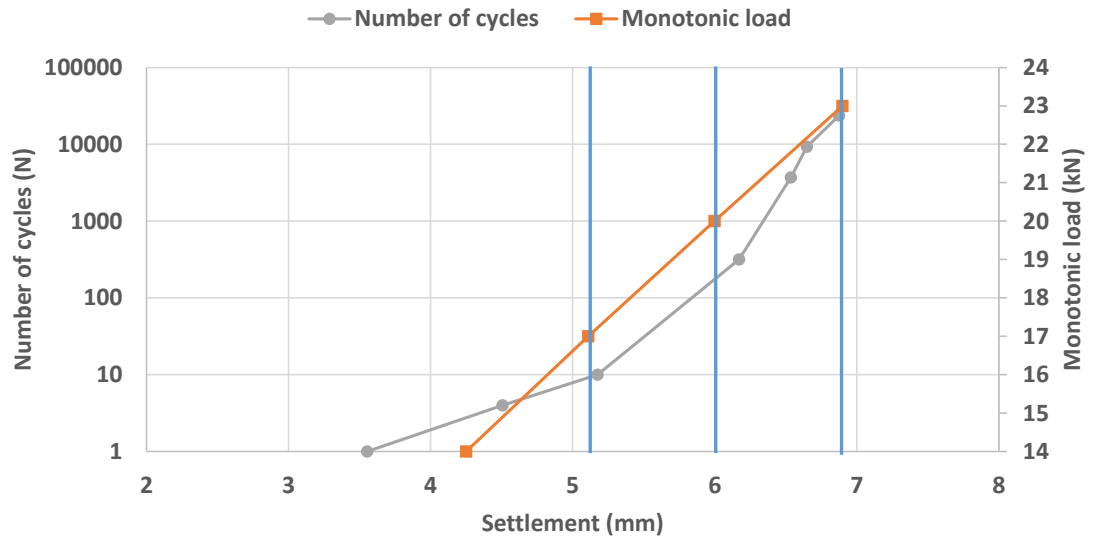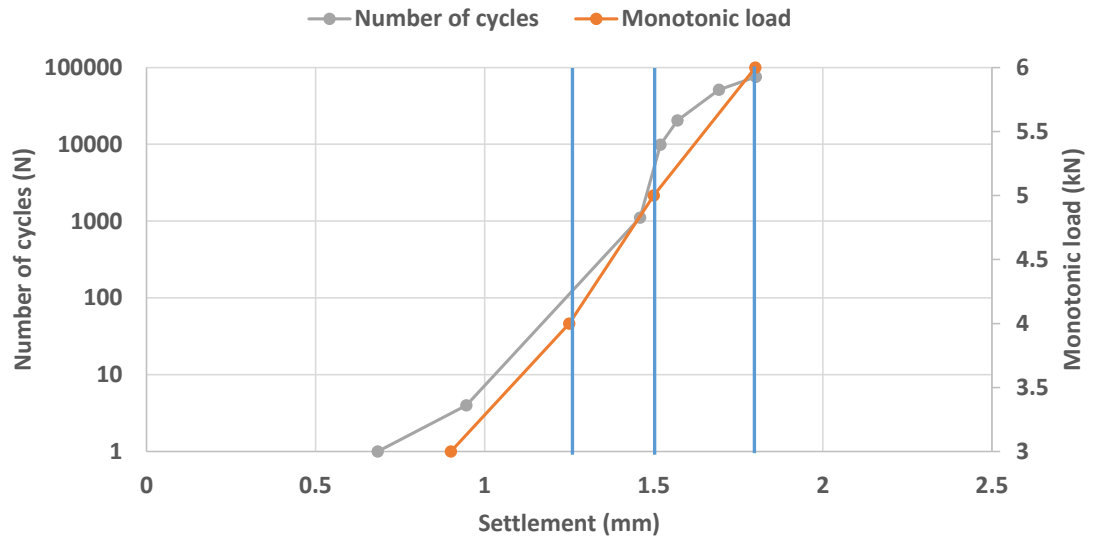
Figure 4-55: **Cyclic load test performed at 3 kN (525 kPa) on the graded gravel layerworks at optimum moisture with identified settlements**

Figure 4-56 shows the maximum shear strain development for the predetermined settlements shown in Figure 4-55. It appears that, for all three stages, proper bedding had not yet been achieved in the monotonic test. This is shown by the relative shallowness of the shear strain in the monotonic test. In the cyclic test, the load is transferred deeper into the pavement structure than for the monotonic test, indicating that better bedding had been achieved. For both the monotonic and cyclic load tests, the maximum shear strain is confined to the layerworks above the subgrade. As mentioned earlier, this could be due to the poor compaction of the layerworks that had to be compacted on a subgrade of sand that had a lower density. The gravel could therefore not be compacted to the desired density. The gravel therefore behaved in a softer manner than expected. This observation, if true for the cyclic test performed at a load of 3 kN, then also applied to all tests performed on the gravel, as the same compaction procedure was used for all of them.
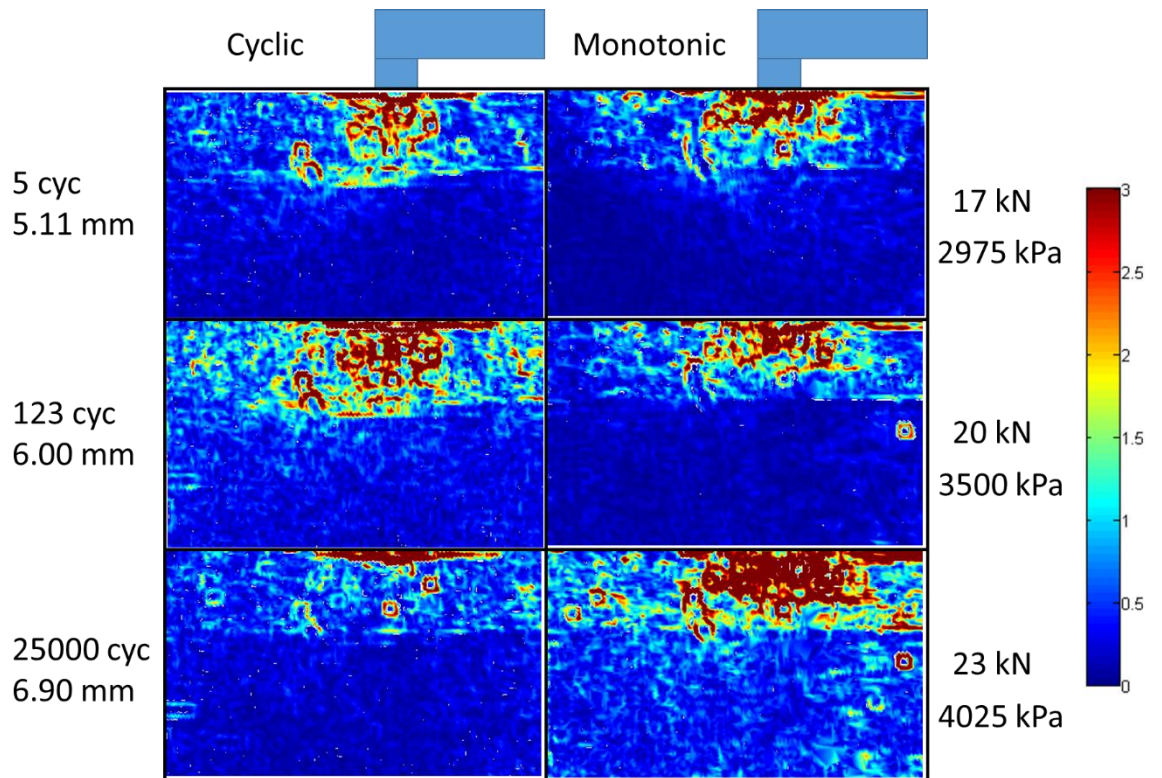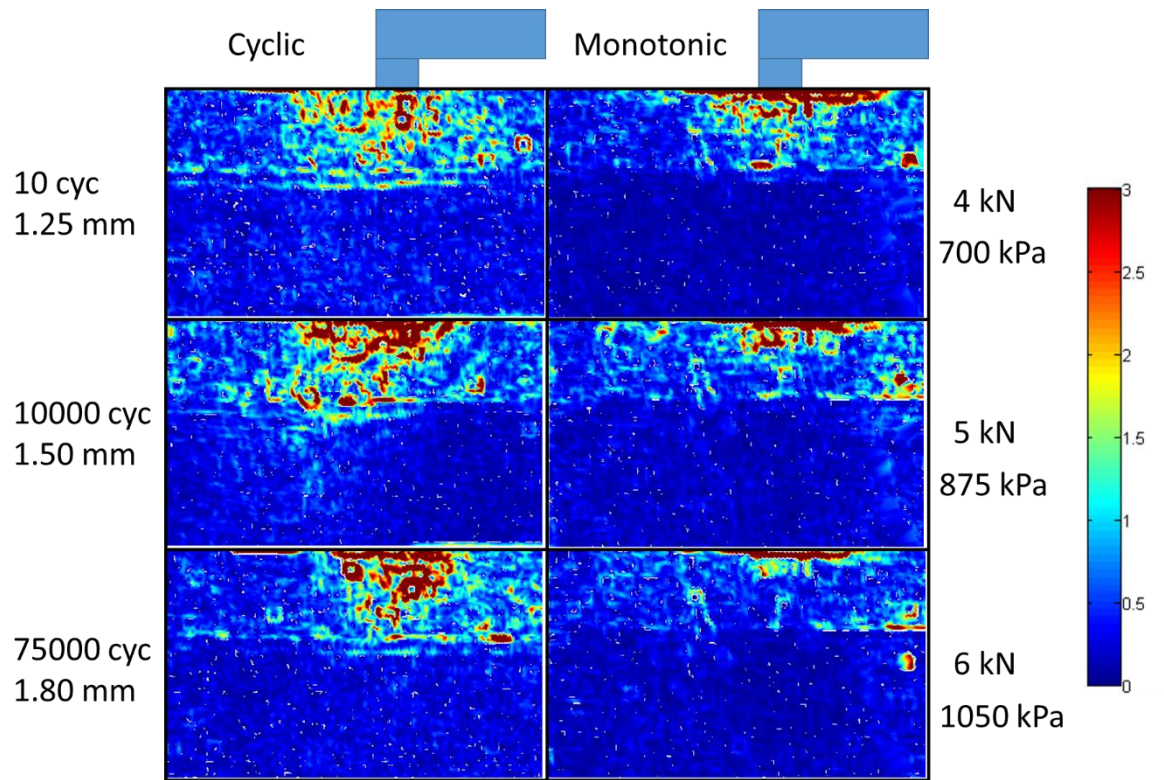
Figure 4-56: Shear strain development for 3 kN (525 kPa) cyclic and monotonic test on the graded gravel layerworks at optimum moisture at specific settlement magnitudes (legend shows maximum shear strain percentage)

5 CONCLUSIONS AND RECOMMENDATIONS

Advances in soil mechanics, particularly in the field of unsaturated soil mechanics, have allowed for a better understanding of the behaviour of soil under monotonic and cyclic loading that can occur in road pavements. The field of pavement engineering would benefit from this due to the nature of the materials and the loading regimes found in typical road pavements. The analysis and design of Ultra-Thin Continuously Reinforced Concrete Pavements (UTCRCP) can benefit from a mechanistic approach which realistically captures the failure mechanisms mobilising in these pavements during extended use.

This chapter presents the conclusions reached from testing scaled-down UTCRCP on two base material types under saturated and unsaturated conditions during which monotonic and cyclic load tests were performed. Recommendations are also given for further research and implementation of findings from this study.

5.1 CONCLUSIONS

The conclusions of this study are presented with reference to the objectives which are set out in Section 1.2. The purpose of this study was to determine whether, and to what extent, plane-strain monotonic loading of a road pavement could be used as an accelerated test method of imposing the damage accumulation that would result under numerous cyclic load applications in model pavements. This was done for UTCRCP road layerworks of two material types and at two degrees of saturation.

The hypothesis that an accelerated test, involving only the application of monotonic loading, can be used to replicate the behaviour of UTCRCP for a predetermined degree of rutting is rejected for UTCRCP on compacted layerworks at optimum moisture content. It is, however, partially accepted for UTCRCP on compacted layerworks that are saturated.

5.1.1 Monotonic loading

Four monotonic tests were done on two material types under saturated and unsaturated conditions. The settlement of the pavement was recorded and the deformation mechanisms were observed. The failure load for each test setup was also determined.

It was found that the initial stiffness of the pavement models constructed entirely of fine silica sand was higher than the initial stiffness of the models constructed with the graded gravel. The unsaturated samples showed a stiffer response to loading that the saturated samples for both material types. This is due to the generation of excess pore water pressures under

numerous cycles in the saturated models. This buildup of excess pore pressure reduced the effective stress in the soil and thus reduced the stiffness response.

Both models constructed of fine silica sand exhibited clear failure at a load of 17 kN (2975 kPa). The load-settlement behaviour of the models constructed of the graded gravel was linear throughout the tests and therefore a settlement criterion had to be applied to define failure.

The silica sand could exhibit a failure point with a clear failure mechanism. The graded gravel represented a more realistic road pavement material, but the point at which failure occurred was not as clear as in the case of the sand. The deformation mechanisms only became traceable at high loads.

5.2 Settlement response under cyclic loading

Cyclic loads amounting to various percentages of the monotonic failure loads were applied to each model setup. During this cyclic loading, the settlement response was initially linear with the log of the number of cycles, but then accelerated beyond a certain number of cycles. The energy absorbed by the pavements was initially higher, for models at both saturated moisture content and optimum moisture content, and then became constant with increasing number of cycles.

For the samples tested at optimum moisture conditions, the settlement was higher for the models constructed with fine silica sand than those constructed with the graded gravel. The settlement was also directly related to the applied cyclic load magnitude for both material types. For a load of 525 kPa, which results in a typical standard axle on the loading bogey, the settlement reached a stable value for both material types under applied cyclic load. At higher cyclic loads, the settlement rate appeared to be stable until a threshold was reached when the settlement rate increased with further load cycles.

5.3 Monotonic and cyclic deformation mechanisms

The deformation mechanisms were compared for monotonic and cyclic loading at the same settlement magnitudes. For the pavements constructed with fine silica sand and graded gravel and tested under unsaturated conditions, the slip zone comprised of a wider shear band for the cyclic tests than for the monotonic test. For the tests conducted on fine silica sand which was fully saturated, the slip mechanisms were very similar for both monotonic and cyclic loading. Monotonic testing can therefore be done on saturated pavements to simulate the damage

accumulation under cyclic loading. Cyclic tests have to be done for unsaturated materials to simulate damage accumulation.

5.4   RECOMMENDATIONS

The following recommendations are made for future research:

- Moving wheel loads, instead of strip loads, should be used so that the principle of stress rotation can be preserved and a more realistic loading regime can be applied to the pavement structure.

- A study should be done to compare loading of soil using strip loads, point loads and moving wheel loads (that result in cyclic stress rotation). The cyclic loads using strip loads are expected to result in higher deformations than point loads due to the greater stress intensity of a strip load when compared to a point load. In a similar fashion, moving wheel loads are expected to result in higher settlements than point loads due to the effect of principal stress rotation. In this way, it can be determined whether or not strip loads could be used to model moving wheel loads.

- Tests should be conducted at a wider variety of degrees of saturation to better understand the effect of moisture on UTCRCP. It is suggested that this can also be used to determine whether pavements should be constructed at optimum moisture content or at some lower degree of saturation where the maximum tensile strength gain is possible due to matric suctions in the soil.

- Instrumentation should be incorporated into the tests so that the pore water pressure response during cyclic and monotonic loading can be monitored and better understood. This could be done for both saturated and unsaturated materials.

- A graded gravel should be used that has a better colour texture than the one used for the purpose of this study. This would yield clearer results from the DIC analysis. Although the fine silica sand used in the experiment was fit for DIC analysis, the behaviour of this material does not adequately represent the behaviour of a typical road construction material.

- Further cyclic testing should be done at the lower load magnitudes that are typically expected from traffic. This should be done using equipment that can apply the number of cycles expected to be experienced by the road. This would reveal whether failure of the pavement can occur even though it seemed that settlement had reached a stable value.

- The influence of load and rest times on the pavement deterioration under numerous cycles can also be investigated. The load and rest times can be calibrated to real traffic conditions.

- The scaling influence should be considered and the testing should ideally be done in a geotechnical centrifuge. Full scale testing could also be done to calibrate the centrifuge tests.

The following recommendations are made regarding the findings of this study:

- It is important to ensure that an adequate bond is achieved between the concrete slab and the soil layers below. Due to flexibility and the relatively low mass of the concrete slab, the slab has the tendency of debonding from the soil on either side of the wheel paths as it curves.

- Moisture should not be allowed to penetrate into the soil below the pavement surface. This results in a loss of matric suction causing the rapid deterioration of the pavement structure.

6 REFERENCES

American Association of State Highway and Transportation Officials Guide for Design of Pavement Structures, 1996. *Guide for design of pavement structures*. Washington, DC: American Association of State Highway and Transport Officials (AASHTO).

Aitchison, G.D. 1961. Relationship of moisture stress and effective stress functions in unsaturated soils. *Pore pressure and suction in soils.* London: Butterworths, pp 47-52.

Alonso, E.E., Gens, A. & Josa, A. 1990. A constitutive model for partially saturated soils. *Géotechnique*, 40 (3), pp.405-430.

Bishop, A.W. 1959. The principle of effective stress. *Teknisk Ukeblad*, pp. 859-863.

Bolton, M.D. 1986. The strength and dilatancy of sands. *Géotechnique,* 36 (1), pp. 65-78.

Boyce, J.R. 1976. The behaviour of granular material under repeated loading. *PhD Thesis*, University of Nottingham, Nottingham, U.K.

Briggs, M.A., Adrian, T. & Arun, J.V. 2015. Behaviour of fibre-reinforced concrete beams on grade. *International Journal of Physical Modelling in Geotechnics*, 16 (4), pp. 152-159.

Brown, S.F. 1996. Soil mechanics in pavement engineering, Géotechnique, 46 (3), pp. 383-426.

Brown, S.F & Brodrick, B.V. 1999. 25 years' experience with the pilot-scale Nottingham pavement test facility. *Proceedings of the International Conference on Accelerated Pavement Testing*, Reno, Nevada.

Brown, S.F. and Bush, D.I. 1972. Dynamic response of model pavement structure. *Journal of Transportation Engineering, American Society of Civil Engineers*, 98, TE4, pp. 1005-1022.

Brown, S.F., Austin, G. & Overy, R.F. 1980. An instrumented triaxial cell for cyclcic loading of clays. *Geotechnical Testing Journal of the ASTM*, Vol. 3, pp.145-152.

Brown, S.F., Loach, S.C. & O'Reilly, M.P. 1987. Repeated loading of fine grained soils. *Contractor Report 72, Transportation Research Laboratory*.

Brunton, J.M. and Akroyde, P.M. 1990. Monitoring the performance of a full-scale experimental pavement. *Proceedings of the 3rd International Conference of the Bearing Capacity of Roads and Airfields*, Trondheim, pp. 585-594.

Buchanan, S. 2007. Resilient modulus: What, why and how. *Vulcan Materials Company*. August 2007.

Buitelaar, P., 2004. Heavy reinforced ultra high performance concrete. *Proceedings of the International Symposium on Ultra High Performance Concrete*. Kassel, Germany.

Burmister, D.M. 1943. The theory of stresses and displacements in layered systems and application to the design of airport runways. *Proceedings, Highway Research Board, National Research Council*, Vol. 23, pp.126-144, Washington DC.

Caicedo, B., Coronado, O., Fleureau, J.M. & Correia, A.G. 2009. Resilient behaviour of non-standard unbound granular materials. *Road Materials Pavement Design*, 10 (2), pp. 287-312.

Cary, C.E. & Zapata, C.E. 2011. Resilient modulus for unsaturated unbound materials. *Road Materials and Pavement Design*, 12 (3), pp.615-638.

Cary, C.E. & Zapata, C.E. 2016. Pore water pressure response of soil subjected to dynamic loading under saturated and unsaturated conditions. *International Journal of Geomechanics*, 16 (6), pp. unknown.

Ceratti, J.A., Gehling, W.Y.Y & Nunez, W.P. 2004. Seasonal variations of a subgrade soil resilient modulus in southern Brazil. *Transport Research Record 1874*, Transportation Research Board, Washington, DC, pp. 165-173.

Chan, F.W.K. 1990. Permanent deformation resistance of granular layers in pavements, *PhD Thesis*, University of Nottingham.

Chan, W.K. & Brown, S.F. 1991. Granular bases for heavily loaded pavements. *Technical Report Number PR91019*, Department of Civil Engineering, University of Nottingham, Nottingham, U.K.

Chandler, R.J. and Gutierrez, C.I. 1986. The filter paper method of suction measurement. *Géotechnique*, 36 (2), pp. 265-268.

Charlier, R. Hornych, P., Srsen, M., Hermannsson, A., Bjaarnason, G., Erlingsson, S. & Pavsic, P. 2008. Water influence on bearing capacity and pavement performance: field

observations. *In* Water in road structures: movement, drainage and effects. *Edited by* A. Dawson. Springer, pp. 175-214.

Cheung, L.W. 1994. Laboratory assessment of pavement foundation materials. *PhD Thesis*, University of Nottingham, Nottingham, U.K.

Clayton, C.R.I. 2011. Stiffness at small strain: research and practice. *Géotechnique*, 61 (1), pp. 5-37.

Clayton, C.R.I. and Heymann, G. 2001. Stiffness of geomaterials at very small strains. *Géotechnique*, 51 (3), pp. 245-255.

COLTO, 1998. Standard specifications for road a bridge works for state road authorities. Pretoria. *South African Institution of Civil Engineers*

Croney, D. and Coleman, J.D. 1948. Soil thermos-dynamics applied to the movement of moisture in road foundations. *Proceedings of the 7th International Conference on Applied Mechanics*, London, 3, pp. 163-177.

CSIR, 2011. Guidelines for the construction of 50 mm thick ultra-thin reinforced concrete pavement (50 mm UTRCP). *Prepared for Gauteng Department of Public Transport and Roads Works*. CSIR, Pretoria.

Dawson, A.R. and Plaistow, L. 1993. Parametric study – flexible pavements. *Flexible Pavements*, Balkema, pp. 229-237.

De Beer, M. 1994. The evaluation, analysis and rehabilitation design of roads. *Report IR 93/296. South African Roads Board*, Department of Transport, Pretoria, South Africa.

De Jong, J.T., Randolph, M.F. & White, D.J. 2003. Interface load transfer degradation during cyclic loading: a microscale investigations. *Soils and Foundations, Japanese Geotechnical Society*, 43 (4), pp. 81-83.

Denneman, E., Kearsley. E.P. & Visser, A.T. 2010 Size effect in high performance concrete road pavement materials. In G.P.A.G. van Zijl & W.P. Boshoff (Eds), *Advanced Concrete Materials, Proceedings of the International Conference*, Stellenbosch, South Africa, 17-19 Novemeber 2009: 53-58. Leiden: CRC Press/Balkema.

Denneman, E. & Du Plessis, L. 2012. Ulta-thin concrete pavements addressing the design issues. *CSIR International Publication Technical Report CSIR/BE/IE/IR/2012/0006/C*, DWDMS No: 214762, CSIR, March 2012.

Denneman, E., Kearsley. E.P. & Visser, A.T. 2012. Definition and application of a cohesive crack model allowing improved prediction of the flexural capacity of high performance fibre reinforced concrete pavement materials. *Journal of the South African Institution of Civil Engineering*, 54 (2), pp.101-111.

Du Plessis, J.L., Coetzee, N.F., Hoover, T.P., Harvey, J.T. & Monismith, C.L. 2006. Three decades of development and achievements: The heavy vehicle simulator in accelerated pavement testing. *Geotechnical Special Publication*, 154, Geo Institute, ASCE.

Edil, T.B. & Motan, S.E. 1978. Soil-water potential and resilient behaviour of subgrade soils, (Unknown source), pp. 54-63.

Erlingsson, S. 2010. Impact of water on the response and performance of a pavement structure in an accelerated test. *Road Materials and Pavement Design*, 11 (4), pp.863-880.

Erlingsson, S. & Rahman, M.S. 2013. Evaluation of permanent deformation characteristics of unbound granular materials by means of multistage repeated-load triaxial tests. *Transportation Research Record: Journal of the Transportation Research Board*, No. 2369, Washington DC, pp. 11-19.

Falkner, H., Huang, Z. & Teutsch, M. 1995. Comparitive study of plain and steel fibre reinforced concrete ground slabs. *Concrete International*, 17 (1), pp. 45-51.

Fredlund, D.G, Morgernsten, N.R. & Widger, R.A. 1978. The shear strength of unsaturated soils. *Canadian Geotechnical Journal*, 15, pp. 313-321.

Freeme, C.R. 1983. Evalluation of pavement behaviour for major rehabilitation of roads. Technical Report RP/19/83, *National Institute for Transport and Roads Research*. CSIR, South Africa.

Freeme, C.R. & Marais, C.P. 1974. Traffic load associated cracking of asphalt pavements. *Proceedings of the 2nd Conference on Asphalt Pavements in South Africa*, Durban, South Africa.

Freeme, C.R., Servas, V.P. & Walker, R.M. 1986. Pavement behaviour as determined by HVS testing. International Conference on Bearing Capacity of Roads and Airfields.

Grabe, P.J. & Clayton, C.R.I. 2009. Effects of principal stress rotation on resilient behaviour in rail track foundations, *Journal of Geotechnical and Geoenvironmental Engineering*, 135 (4), pp.?

Hamblin, A.P. 1981. Filter-paper method for routine measurement of field water potential. *Journal of Hydrology*, 53(3), pp.355-360.

Han, Z. and Vanapalli, S.K. 2016. State-of-the-art: prediction of resilient modulus of unsaturated subgrade soils. *International journal of Geomechanics*, 16 (4), pp. unknown

Han, Z. & Vanapalli, S.K. 2016. Stiffness and shear strength of unsaturated soils in relation to soil-water characteristic curve. *Géotechnique*, (8), pp.1-21.

Heath, A.C., Pestana, J.M., Harvey, J.T. & Bejerano, M.O. 2004. Normalising behaviour of unsaturated granular pavement materials. *Journal of Geotechnical and Geoenvironmental* Engineering, 130 (9), pp.896-904.

Hight, D.W. and Stevens, M.G.H. 1982. An analysis of the California Bearing Ratio test in saturated clays. Géotechnique, 32 (4), pp. 315-322.

Hveem, F.N. 1955. Pavement deflections and fatigue failure, *Highway Research Board Bulletin 114*, Highway Research Board, National Academy of Sciences, Washington, DC, pp. 43-48.

Hveem, F.N. and Sherman, G.B. 1962. California method for the structural design of flexible pavements. *Proceedings of the International Conference on the Structural Design of Asphalt Pavements*, Ann Arbour, Michigan, pp. 851-866.

Ioannides, A.M. 1991. Subgrade characterisation for Portland cement concrete pavements. *Proceedings of the International Conference on Geotechnical Engineering for Coastal Development – Theory and Practice*, Port and Harbour Institute, Ministry of Transport, Yokohama 3 – 6, Japan, pp.809-840.

Ioannides, A.M. 2006. Concrete pavement analysis: the first eighty years. *International Journal of Pavement Engineering*. 7 (4). Taylor and Francis, pp. 233-249.

Ishihara, K. and Towhata, I. 1983. Sand response to cyclic rotation of principal stress directions as induced by wave loads. *Soils and Foundations, Japanese Society of Soil Mechanics and Foundation Engineering*, 23 (4), pp. 12-26.

Irving, J.A. 1999. Soil structure interaction of fibre reinforced concrete floor slabs on grade. *MScE Thesis*, Department of Civil Engineering, University of New Brunswick, Fredericton, New Brunswick, Canada.

Jansen Van Rensberg, F. 2013. Ultra-thin reinforced concrete pavement: benefiting South Africa. *SATC*, July 2013.

Jennings, J.E. 1961. A revised effective stress law for use in the prediction of the behaviour of unsaturated soils. *Pore Pressure and Suction in Soils*. London: Butterworths, pp.26-30.

Jennings, J.E. and Burland, J.B. 1962. Limitations to the use of effective stresses in partly saturated soils. *Géotechnique*, 12 (2), pp. 125-144.

Jordaan, G.J. 1993. User's manual for the South African mechanistic pavement rehabilitation design method. *Report IR91\242. South African Roads Board*, Department of Transport, South Africa.

Khalil, N., Habte, M. & Zargarbashi, S. 2008. A fully coupled flow deformation model or cyclic analysis of unsaturated soils including hydraulic and mechanical hysteresis. *Computers and Geotechnics*, 35 (6), pp. 872-889.

Kannemeyer, L., Perrie, B.D., Strauss, P.J. & Du Plessis, L. 2007. Ultra-thin continuously reinforced concrete pavement development in South Africa. *Proceedings of the 9th International Conference on Concrete Pavements*. San Francisco, USA.

Kearsley, E.P., Steyn, W.J.vdM. & Jacobsz, S.W. 2014. Centrifuge modelling of ultra thin continuously reinforced concrete pavements, *Proceedings of the 8th International Conference on Physical Modelling in Geotechnics 2014 (ICPMG2014)*, Perth, Australia, 14 – 17 January 2014.

Kearsley, E.P. & Mostert, H.F. 2009. Enabling the use of high performance fibre reinforced concrete in infrastructure. *Proceedings of the International Conference on Advanced Concrete Materials*, November 2009, Stellenbosch, South Africa, pp. 287-295.

Klomp, A.J.G. and Niesman, Th. W. 1967. Observed and calculated strains at various depths in asphalt pavements. *Proceedings of the 2nd International Conference on the Structural Design of Asphalt Pavements*, Ann Arbour, Michigan, pp. 114-136.

Knappet, J.A. & Craig, R.F. 2012. *Craig's Soil Mechanics* 8th ed. Oxon: Spon Press

Lambe, T.W. 1960. A mechanistic picture of shear strength in clay. *Proceedings of the ASCE Research Conference on Shear Strength of Cohesive Soils*. Colorado, Boulder, pp. 555-580.

Lashine, A.K. 1971. Some aspects of the characteristics of keuper and marl under repeated loading. *Doctoral Dissertation*, University of Nottingham, Nottingham, U.K.

Lee, Y. 1986. Strength and deformation characteristics of rockfill. *PhD Thesis*, Asian Institute of Technology.

Lekarp, F., Isacsson, U. & Dawson, A. 2000. State of the art II: Permanent strain response of unbound aggregates. *Journal of Transportation Engineering*. 126 (1), pp.76-83.

Li, D. & Selig, E.T. 1996. Cumulative plastic deformation for fine grained subgrade soils. *Journal of Geotechnical Engineering*, 122 (12), pp. 1006-1013.

Lister, N.W. 1972. The transient and long term performance of pavements in relation to temperature. *Proceedings of the 3rd International Conference on the Structural Design of Asphalt Pavements*, Ann Arbour, Michigan, pp. 42-51.

Loach, S.C. 1987. Repeated loading of fine-grained soils for pavement design. *Ph.D. Thesis*, University of Nottingham.

Lu, N., Wu, B. & Tan, C.P. 2007. Tensile strength characteristics of unsaturated sands. *Journal of Geotechnical and Geoenvironmental Engineering*, 132 (2), pp. 131-142.

Lu, N. & Likos, W. 2004. *Unsaturated Soil Mechanics*, Hoboken, New Jersey: John Wiley & Sons, Inc.

Mamou, A., Powrie, W., Priest, J.A. % Clayton, C. 2017. The effects of drainage on the behaviour on railway track foundation materials during cyclic loading. *Géotechnique*, 67 (10), pp. 845-854.

Maree, J.H. 1978. Design parameters for crushed stone in pavements (in Afrikaans). *Master's Thesis*, University of Pretoria, South Africa.

Maree, J.H. & Freeme, C.R. 1981. The mechanistic design method used to evaluate the pavement structures in the catalogue of the draft TRH4 1980. *Technical Report RP/2/81. The National Institute for Transport and Road Research*, CSIR, South Africa.

Minh Thu, T., Rahardjo, H. & Leong, E. 2006. Shear strength and pore-water pressure characteristics during constant water triaxial tests. *Journal of Geotechnical and Environmental Engineering*, 132 (3), pp. 441-419.

Mukandila, M., Milne, T. & Horak, E. 2009. Constructability aspects of ulta thin continuously reinforced concrete pavement. *28ᵗʰ South African Transportation Conference*, Pretoria, pp. 234-244.

NCHRP 1-37A. 2004. Guide for mechanistic-empirical design of new and rehabilitated pavement structures, *Transportation Research Board: National Cooperative Highway Research Program*.

Ng, C.W.W., Zhou, C., Yuan, Q. & Xu, J. 2013. Resilient modulus of unsaturated subgrade soil: Experimental and theoretical investigations. *Canadian Geotechnical Journal*, 50 (2), pp. 223-232.

Ng, C.W.W. and Menzies, B. 2007. *Advanced unsaturated soil mechanics and engineering*. Tylor & Francis, New York, U.S.A.

Nutt, J.L. 1982. Finite element modelling of partially saturated soils for a study of the California Bearing Ratio test. *MSc Thesis*, Imperial College, University of London, U.K.

Otte, E. 1972. The stress-strain properties of cement-stabilised materials. *Master's Thesis*. University of Pretoria, South Africa.

Otte, E. 1974. The stress-strain curve for cement-and lime-treated materials. *Proceedings of the 2nd Conference on Asphalt Pavements in South Africa*, Durban, South Africa.

Otte, E. 1977. Structural design procedure for cement-treated layers in pavements. *Ph.D. Thesis*. University of Pretoria, South Africa.

Pappin, J.W. 1979. Characteristics of a granular material for pavement design. *PhD Thesis*, University of Nottingham, Nottingham, U.K.

Peralta, P.K. 2010. Investigations on the behaviour of large diameter plies under long-term lateral cyclic loading in cohesionless soil. *Dissertation*.

Powell, W.D., Potter, J.F., Mayhew, H.C. & Nunn, M. E. 1984. The structural design of bituminous roads. *Laboratory Report 1132*, TRRL.

Ramsamooj, D.V., Majidzadeh, K. & Kauffmann, E.M. 1972. The analysis and design of the flexibility of pavements. *Proceedings of the 3ʳᵈ International Conference on the Structural Design of Asphalt Pavements*, London, pp. 692-704.

Raybould, M.R. 1992. The response of silty-clay mixtures to cyclic loading. *PhD Thesis*, University of Nottingham, Nottingham, U.K.

Richards, B.G. 1966. The significance of moisture flow and equilibria in unsaturated soils in relation to the design of engineering structures built on shallow foundations in Australia. *Symposium on Permeability and Capillarity*, American Society for Testing and Materials, Atlantic City, New Jersey, U.S.A.

Roesler, J.R., Lange, D.A., Altoubat, S.A., Reider, K.A. & Ulreich, G.R. 2004. Fracture of plain and fibre-reinforced concrete slabs under monotonic loading. *Journal of Materials in Civil Engineering*, 16 (5), pp. 452-460.

Saad, B. 2014. Analysis of excess water impact on the structural performance of flexible pavements. *International Journal of Pavement Engineering*. 15(5), pp. 409-426.

Saarenketo, T. and Aho, S. 2005. Managing spring thaw weakening on low volume rods: problem desription, load restriction, policies, monitoring and rehabilitation. *The ROADEX II*, Northern Periphery.

Salour, F. & Erlingsson, S. 2017. Permanent deformation characteristics of silty sand subgrades from multistage RLT tests. *International Journal of Pavement Engineering*, 18 (3), pp.236-246.

Salour, F. Erlingsson, S. & Zapata, C.E. 2014. Modelling resilience modulus seasonal variation of silty sand subgrade soils with matric suction control. *Canadian Geotechnical Journal*, 51 (12), pp. 1413-1422.

Schofield, A.N. 1980. Cambridge geotechnical centrifuge operations. *Géotechnique*. 2 (1), pp. 227-268.

Seed, H.B., Chan, C.K. & Monismith, C.L. 1955. Effects of repeated loading on the strength and deformation of compacted clay, *Proceedings from the Highway Resource Record*, Vol. 34, pp. 541-558.

Seed, H.B., Chan, C.K. & Lee, C.E. 1962. Resilience characteristics of subgrade soils and their relation to fatigue failures in asphalt pavement. *Proceedings of the Conference on the Structural Design of Asphalt Pavements*, University of Michigan, Ann Arbor, Michigan, pp.611-636.

Sheng, D., Sloan, S.W. & Gens, A. 2004. A constitutive model for unsaturated soils: thermomechanical and computational aspects. Computational Mechanics, 27 (9), pp. 453-465.

Sivakumar, V., Kodikara, J., O'Hagan, R., Hughes, D., Cairns, P. & McKinley, J.D. 2013. Effects of confining pressure and water content on performance of unsaturated compacted clay under repeated loading. *Géotechnique*, 63 (8), pp. 628-640.

Stanier, S. and White D. 2013. Improved image-based deformation measurement in the centrifuge environment. *Geotechnical Testing Journal*, 36 (6), pp. 1-14.

Steyn, W.J., DeBeer, M. & Du Preez, W. 1999. Simulation of dynamic traffic loading for use in accelerated pavement testing (APT), *Proceedings of the First International Conference on APT*. Reno, California, USA.

Strauss, P.J., Slavik, M. & Perrie, B.D. 2001. A mechanistically and risk-based designed method for concrete pavements in South Africa. *Proceedings of the 7th International Conference on Concrete Pavements*. Orlando, California, USA.

Thyse, H.L, De Beer, M., Prozzi, J. & Semmelink, C.J. 1995. TRH4 revision 1995. Phase I: Updating the transfer functions for the South African mechanistic pavement design method, *Division of Roads and Transport Technology, CSIR*, Pretoria, South Africa.

Thyse, H.L., De Beer, M. & Rust, F.C. 1996. Overview of South African mechanistic pavement design method. *Transportation Research Record*, CSIR, Pretoria.

Toll, D.G. 2012. The behaviour of unsaturated soils. *Handbook of Tropical and Residual Soils Engineering*. Ed. By B.B.K. Huat, D.G. Toll &A. Prasad. London: Taylor & Francis.

TRH4, 1985. The structural design of interurban and rural road pavements. *Committee of State Road Authorities. Department of Transport*, Pretoria, South Africa.

Turnbull, W.J. 1950. Appraisal of the CBR method, Development of CBR flexible pavement design method for airfields – a symposium, *Transportation, American Society of Civil Engineers*, pp. 547-554.

Vanapalli, S.K. Fredlund, D.G., Pufahl, D.E. & Clifton, A.W. 1996. Model for the prediction of shear strength with respect to soil suction. *Canadian Geotechnical Journal*, 33 (3), pp. 379-392.

Verdugo, R., Gesche, S. & De La Hoz, K. 2003. Metodologia de evaluacion de parametros de Resistencia al corte de suelos gruesos. *XII Panamarecian Conference on Soil Mechanics and Foundations Engineering*, MIT. USA. Vol. 1, pp. 691-696.

Walker, R.N. 1985. The South African Heavy Vehicle Simulator. *Accelerated Testing of Pavements*, CSIR, Pretoria, South Africa.

Werkmeister, S., Dawson, A.R. & Wellner, F. 2004. Pavement design model for unbound granular materials, *Journal of Transportation Engineering*. 130 (5), pp.665-674.

Westergaard, H.M. 1926. Stresses in concrete pavements computed by theoretical analysis. *Public Roads*, 7 (2), pp.25-35.

White, D.J., Take, W.A. & Bolton, M.D. 2003. Soil deformation measurement using particle image velocimetry (PIV) and photogrammetry. *Géotechnique*, 53(7), pp.619-631.

Yang, S., Lin, H., Kung, J.H.S. and Huang, W. 2008. Suction-controlled laboratory tests o resilient modulus of unsaturated compacted subgrade soils. *Journal of Geotechnical and Environmental Engineering*, 134 (9), pp. 1375-184.

Yang, C., Cui, Y.J., Pereira, J.M. & Huang, M.S. 2008. A constitutive model for unsaturated cemented soils under cyclic loading. *Computers and Geotechnics*, 35, pp. 853-859.

Zaman, M., Solanki, P., Ebrahimi, A & White, L. 2010. Neutral network modelling of resilient modulus using routine subgrade soil properties. *International Journal of Geomechanics*, 10 (1), pp, 1-12.

Zapata, C.E., Andrei, D., Witczak, M.W. & Houston, W.N. 2007. Incorporation of environmental effects in pavement engineering. *Road Materials Pavement Design*, 8(4), pp. 667-693.

Zhou, C. and Ng, C.W.W. 2016. Simulating the cyclic behaviour of unsaturated soil at various temperatures using a bounding surface model. Géotechnique, 66 (4), pp. 344-350.